

AD A 056857

UDC FILE COPY

AFFDL-TR-77-135

LEVEL

A041536

III

2  
Sc

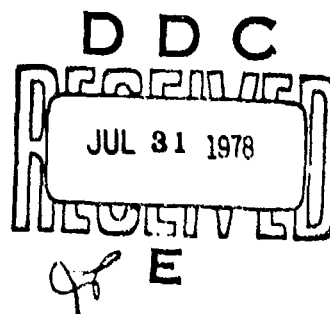
**PRIMARY ADHESIVELY BONDED STRUCTURE  
TECHNOLOGY (PABST)**

**Phase II: Detail Design**

DOUGLAS AIRCRAFT COMPANY  
McDONNELL DOUGLAS CORPORATION  
LONG BEACH, CALIFORNIA 90846

AUGUST 1977

TECHNICAL REPORT AFFDL-TR-77-135  
Final Report September 1976 - May 1977



Approved for public release; distribution unlimited.

AIR FORCE FLIGHT DYNAMICS LABORATORY  
AIR FORCE WRIGHT AERONAUTICAL LABORATORIES  
AIR FORCE SYSTEMS COMMAND  
WRIGHT-PATTERSON AIR FORCE BASE, OHIO 45433

78 07 21 021


NOTICE

When Government drawings, specifications, or other data are used for any purpose other than in connection with a definitely related Government procurement operation, the United States Government thereby incurs no responsibility nor any obligation whatsoever; and the fact that the government may have formulated, furnished, or in any way supplied the said drawings, specifications, or other data, is not to be regarded by implication or otherwise as in any manner licensing the holder or any other person or corporation, or conveying any rights or permission to manufacture, use, or sell any patented invention that may in any way be related thereto.

This report has been reviewed by the Information Office (OI) and is releasable to the National Technical Information Service (NTIS). At NTIS, it will be available to the general public, including foreign nations.

This technical report has been reviewed and is approved for publication.

  
JAMIE M. FLORENCE  
Project Engineer

  
WILLIAM R. JOHNSTON  
Actg Prog Mgr, AMS Program Office  
Structural Mechanics Division

FOR THE COMMANDER

  
HOLLAND B. LOWNDES  
Acting Chief  
Structural Mechanics Division

"If your address has changed, if you wish to be removed from our mailing list, or if the addressee is no longer employed by your organization please notify AFEDL/FBA, W-PAFB, OH 45433 to help us maintain a current mailing list".

Copies of this report should not be returned unless return is required by security considerations, contractual obligations, or notice on a specific document.

SECURITY CLASSIFICATION OF THIS PAGE (When Data Entered)

<b>REPORT DOCUMENTATION PAGE</b>		<b>READ INSTRUCTIONS BEFORE COMPLETING FORM</b>	
1. REPORT NUMBER AFFDL-TR-77-135		2. GOVT ACCESSION NO.	
3. TITLE (and Subtitle) PRIMARY ADHESIVELY BONDED STRUCTURE TECHNOLOGY (PABST). PHASE II, Detail Design.		4. TYPE OF REPORT & PERIOD COVERED Final rept. September 1976-December 1977.	
5. AUTHOR(s)		6. CONTRACT OR GRANT NUMBER(s) F33615-75-C-3016	
9. PERFORMING ORGANIZATION NAME AND ADDRESS Douglas Aircraft Company McDonnell Douglas Corporation Long Beach, California 90846		10. PROGRAM ELEMENT, PROJECT, TASK AREA & WORK UNIT NUMBERS 486U0404	
11. CONTROLLING OFFICE NAME AND ADDRESS Air Force Flight Dynamics Laboratory (AFFDL/FBA) Air Force Wright Aeronautical Laboratories AFSC, Wright-Patterson AFB, OH 45433		12. REPORT DATE December 1977	
14. MONITORING AGENCY NAME & ADDRESS (if different from Controlling Office) (12) 342p.		13. SECURITY CLASS. (of this report) Unclassified	
15a. DECLASSIFICATION/DOWNGRADING SCHEDULE			
16. DISTRIBUTION STATEMENT (of this Report) Approved for public release; distribution unlimited			
17. DISTRIBUTION STATEMENT (of the abstract entered in Block 20, if different from Report)			
18. SUPPLEMENTARY NOTES			
19. KEY WORDS (Continue on reverse side if necessary and identify by block number) Bonded Structure, spectra, damage tolerance, Criteria-adhesive bonds, da/dN material data			
20. ABSTRACT (Continue on reverse side if necessary and identify by block number) This report covers the design, analysis, and trade studies conducted during Phase II, Detail Design of the Primary Adhesively Bonded Structure Technology (PABST) Program.  During this Phase, drawings were made and released to Manufacturing for the construction of a 42 foot long test component simulating the forward fuselage of the C-15 airplane. The design concept, selected at the completion of			

DD FORM 1 JAN 73 1473 EDITION OF 1 NOV 68 IS OBSOLETE

SECURITY CLASSIFICATION OF THIS PAGE (When Data Entered)

11640088 07 21 0000 LB

SECURITY CLASSIFICATION OF THIS PAGE(When Data Entered)

Phase Ib-Preliminary Design consisted of wide spaced/close spaced internal longerons in the upper fuselage and external longerons in the lower (bilge area) fuselage.

External loads were developed for both fatigue and ultimate loading conditions in conformance with the military specifications. The external shears and bending moments were matched to the Full Scale Demonstration Component test curves, adjusted for the actual test fixture loading points.

Internal loads were generated and static, damage tolerance and fatigue analyses were performed on the Full Scale Demonstration Component. A spectra was developed based on a statistical analysis of information accumulated from Air Force operations and used for the fatigue and damage tolerance analyses.

## FOREWORD

This report presents the results of the detail design (Phase II) of the Primary Adhesively Bonded Structure (PABST) program, Contract F33615-75-C-3016. The effort described herein was performed by the Douglas Aircraft Company, Long Beach, California, a division of the McDonnell Douglas Aircraft Corporation, with Mr. E. W. Thrall, Jr., as the Program Manager.

This work was sponsored by the Air Force Flight Dynamics Laboratory (AFFDL) under joint management and technical direction of AFFDL and the Air Force Materials Laboratory (AFML), Wright-Patterson Air Force Base, Ohio. This contract is administered as a part of the Advanced Metallic Structures, Advanced Development Programs (AMS ADP), Program Element Number 63211F, Project 486U. Mr. William R. Johnson is the Acting Program Manager and Mr. Jamie M. Florence is the Project Engineer (AFFDL/FBA) for the PABST program.

This work was performed during the period 15 October 1976 to May 1977. Acknowledgment and appreciation is given to Lt. Col. Joseph S. Ford who served as the ADP Manager for this program during this period.

ACCESSION FOR	
NTIS	White Section <input checked="" type="checkbox"/>
DOC	Dist Section <input type="checkbox"/>
UNANNOUNCED	<input type="checkbox"/>
JUSTIFICATION	
BY	
DISTRIBUTION AVAILABILITY CODES	
Dist.	Avail. and Special
A	

## TABLE OF CONTENTS

	<u>Page</u>
INTRODUCTION	1
DESIGN CRITERIA	3
Fatigue and Damage Tolerance Criteria-Metallic Structure	5
Damage Tolerance Criteria-Adhesive Bond Areas	9
FULL-SCALE DEMONSTRATION COMPONENT	11
DETAIL DESIGN	21
Skin Splices	23
Longerons	33
Frames	35
Frame and Longeron Intersections	39
Intercostals	47
Tear Stoppers	55
PANEL DESIGN	57
Constant Section Panels	59
Non-Constant Section Panels	67
NON-PARTICIPATING STRUCTURE	79
Door Installation	81
Wing Box	85
Floor structure	89
LOADS	93
External Loads	95
Internal Loads	101
ANALYSIS	115
Static Analysis	117
Spectrum Analysis	123
Damage Tolerance	149
Adhesive Bonded Joint Analysis	187
TRADE STUDIES	189
Stiffener Flange Shape Study	191
Damage Tolerance Parametric Studies	197

## TABLE OF CONTENTS (Continued)

SUMMARY	<u>Page</u> 227
CONCLUSIONS	229
APPENDIX A	231
APPENDIX B	249
APPENDIX C	263
REFERENCES	299

## LIST OF FIGURES

<u>Figure</u>		<u>Page</u>
1	Full-Scale Demonstration Component	11
2	Typical Constant Section Frame	12
3	Perspective of Full-Scale Demonstration Component	13
4	Skin Panel for Full-Scale Demonstration Component	14
5	Simulated Wing Assembly And Fuselage Interface	15
6	Forward FSDC Attachment to Pressure Bulkhead	17
7	Typical FSDC to Aft Fixture Attach	18
8	Typical Longerons to Aft Fixture Attach	19
9	Floor Beam to Aft Test Fixture Attach	20
10	Typical Mechanical Lap Splice	25
11	Typical Mechanical Double Strap Butt Splice	27
12	Circumferential Mechanical Splice	28
13	Longitudinal and Circumferential Bonded Butt Splice	31
14	Internal and External Longerons	34
15	Typical Frames	36
16	Front Spar Frame Segment - Sta. 703.000	38
17	Typical Frame/Longeron Intersection	41
18	Typical Longerons and Intermediate Frame Intersection	42
19	Typical Nose Frame and Internal Longeron Intersection	43
20	Typical Nose Frame and Bonded Skin Splice Intersection	45
21	Intercostal Locations	49
22	Frame Stabilization Intercostal	50
23	Frame Stabilization Intercostal	51

<u>Figure</u>	LIST OF FIGURES (Continued)	<u>Page</u>
24	Intercostals Forward of Station 439	52
25	Floor to Fuselage Intercostal	53
26	Door Jamb Intercostals	54
27	Bonded Tear Stoppers	56
28	Panel Locations	58
29	Constant Section Close-Spaced Internal Longerons Panel	60
30	Photograph of Constant Section Close-Spaced Internal Longerons Panel	61
31	Constant Section Close-Spaced External Longerons Skin Panel	63
32	Photograph of Constant Section Close-Spaced External Longerons Skin Panel	64
33	Constant Section Wide-Spaced Longerons Panel	65
34	Photograph of Constant Section Wide-Spaced Longerons Panel	66
35	Nonconstant Section Close-Spaced Internal Longerons Panel	69
36	Photograph of Nonconstant Section Close-Spaced Internal Longerons Panel	70
37	Nonconstant Section External Longerons Panel	71
38	Photograph of Nonconstant Section External Longerons Panel	72
39	Nonconstant Section Side Panel With Wide-Spaced Longerons	73
40	Photograph of Nonconstant Section Side Panel With Wide-Spaced Longerons	74
41	Nonconstant Section Left Side Panel With Door Cutout and Jamb	75
42	Photograph of Non Constant Section Left Side Panel With Door Cutout and Jamb	76
43	Door Corner Doublers (Looking Inboard)	77
44	Heavy Skin Longitudinal Bonded Splice	78
45	End of L-11 at Station 439	78
46	Door Panel and Installation	82

<u>Figure</u>	LIST OF FIGURES (Continued)	<u>Page</u>
47	Door Assembly	83
48	Wing/Fuselage Interface	85
49	Cargo Floor Assembly	90
50	Typical Extruded Floor Plank	90
51	Floor Support Bulkhead	91
52	PABST Demonstration Component Test Setup	96
53	Cargo Floor Loading Linkage - Fatigue Test	97
54	Cargo Floor Loading Linkage - Ultimate Test	98
55	Structure Idealization	102
56	Definition of Output Terms	103
57	PABST Fuselage Test Specimen - Left Side Upper Section - Panel	108
58	PABST Fuselage Test Specimen - Left Side Upper Section - Bar	109
59	Cross Section of Frame Through Longeron Cutout	112
60	Frame Bending Test (Specimen 23)	113
61	PABST Runway Roughness Data	125
62	Typical Mission Stress Cycle	133
63	Schematic of the Distributed AMST Payloads External Loads Analysis for PABST	135
64	Damage Tolerance Analysis Check Points	137
65	Damage Tolerance Analysis Flow Chart for Metal Structure	150
66	Effects of Pressure Pillowing in a Stiffened Cylinder	152
67	Nonuniform Stress Distribution Factor	153
68	Curves of $da/dN$ versus $\Delta K$ for 2024-T3 Bare Sheet - Preliminary	156
69	Curves of $da/dN$ versus $\Delta K$ for 7075-T6 Clad Sheet - Preliminary	157

<u>Figure</u>	LIST OF FIGURES (Continued)	<u>Page</u>
70	Curves of $da/dN$ versus $\Delta K$ for 2024-T3 Bare Sheet - Final	158
71	Curves of $da/dN$ versus $\Delta K$ for 7075-T6 Clad Sheet - Final	159
72	Crack Growth Time History for Checkpoint E with Preliminary Loads	161
73	Residual Strength for Checkpoint E with Preliminary Load	162
74	Crack Growth Time History for Checkpoint H with Preliminary Load	164
75	Residual Strength for Checkpoint H with Preliminary Load	165
76	Three-Mass/Three-Spring Model for Check Point D	169
77	7075-T6 Extrusion Elastic-Plastic Model - Checkpoint D	170
78	7075-T6 Clad Sheet Elastic-Plastic Model - Checkpoint D	171
79	FM73 Adhesive Load - Deflection Model - Check Point D	172
80	Rivet Load - Deflection Model - Check Point D	172
81	Effect of Considering a Multimass/Multispring Model at Check Point D	174
82	7475-T761 Sheet Elastic - Plastic Model - Check Point A	175
83	FM73 Adhesive Load - Deflection Model-Check Point A	176
84	Effect of Considering Plasticity and a Multimass/Multi-spring Model at Check Point A	177
85	Transverse Riveted Splice Specimen (ZJ197656-1)	178
86	Analysis-Test Correlation for the Transverse Riveted Splice Specimen	180
87	Crack Locations on Left Side of Shear Panel	181
88	Crack Locations on Right Side of Shear Panel	182
89	Shear Interaction Test Specimen Spectra	183

<u>Figure</u>	LIST OF FIGURES (Continued)	<u>Page</u>
90	Crack Growth Time History of Shear Interaction Panel Crack No. 4	183
91	Residual Strength Diagram for Shear Interaction Panel Crack No. 5	184
92	Crack Locations on Test Panel with Door	185
93	Crack Growth Time History of Curved Panel Crack No. 4	186
94	Crack Growth Time History of Curved Panel Crack No. 5	186
95	Residual Strength Diagram for Curved Panel Crack RS2	186
96	Typical Extrusion (Simulated) on Skin Panel	194
97	Typical "Heavy" Extrusion (Simulated) on Skin Panel	195
98	Simulated Extrusion With Skin and Doubler	196
99	Damage Tolerance Study Locations	197
100	The Effect of Variation in Aircraft Usage on Life Prediction	202
101	Curves of DA/DN versus $\Delta K$ for 7475-T761 Bare Sheet - Preliminary	203
102	Lower end of Curves Shifted to $\Delta K = 3000$ at $DA/DN = 10^{-8}$	204
103	Lower End of Curves Shifted to $\Delta K = 1350$ at $DA/DN = 10^{-8}$	205
104	Entire Curve Shifted Laterally Such That $\Delta K = 3000$ at $DA/DN = 10^{-8}$	206
105	Entire Curve Shifted Laterally Such that $\Delta K = 1350$ at $DA/DN = 10^{-8}$	207
106	Effect of Varying Material Properties on a Circumferential Crack	209
107	Effect of Varying Material Properties on a Longitudinal Crack	210

<u>Figure</u>	LIST OF FIGURES (Continued)	<u>Page</u>
108	Effect of Initial Flaw Size Variation on Life	211
109	Crack Growth Time History for $A = 0.237$ , $t = 0.04$ , Spacing = 16.16	213
110	Residual Strength for $A = 0.237$ , $t = 0.04$ , Spacing = 16.16	214
111	Summary of Sensitivity of Life to Geometry Variation	215
112	Spectra Initial Stress Value versus Life	216
113	Effect on Life of Varying Tear Strap Spacing for a 0.213-SQ-IN. Strap	219
114	Residual Strength for One Strap With Area = 0.213 SQ IN. and 39.4 IN. Spacing	220
115	Residual Strength for Two Straps With Area = 0.213 SQ IN. and 26.3 IN. Spacing	221
116	Residual Strength for Three Straps With Area = 0.213 SQ IN. and 19.7 IN. Spacing	222
117	Residual Strength for Four Straps With Area = 0.213 SQ IN. and 15.76 IN. Spacing	223
118	Residual Strength for Five Straps With Area = 0.213 SQ IN. and 13.16 IN. Spacing	224
119	Residual Strength for Five Straps With Area = 0.142 SQ IN. and 13.16-IN. Spacing	225
120	Effect of Strap Area Variation on Residual Strength for Two Straps	226
C1	Vertical Bending Moment - PABST Max-Min Ultimate	264
C2	Vertical Shear - PABST Max-Min Ultimate	265
C3	Vertical Shear - Condition 15 FG (2) Fatigue Condition (Limit)	266
C4	Vertical Bending Moment - Condition 15 FG (2) Fatigue Condition (Limit)	267
C5	Vertical Shear - Condition 16 FG (3) Fatigue Condition (Limit)	268

<u>Figure</u>	LIST OF FIGURES (Continued)	<u>Page</u>
C6	Vertical Bending Moment - Condition 16 FG (3) Condition (Limit)	269
C7	Vertical Shear - Condition 19 FG (4) Fatigue Condition (Limit)	270
C8	Vertical Bending Moment - Condition 19 FG (4) Fatigue Condition (Limit)	271
C9	Vertical Shear - Condition 20 FG (5) Fatigue Condition (Limit)	272
C10	Vertical Bending Moment - Condition 20 FG (5) Fatigue Condition (Limit)	273
C11	Vertical Shear - Condition 27 FG (6) Fatigue Condition (Limit)	274
C12	Vertical Bending Moment - Condition 27 FG (6) Fatigue Condition (Limit)	275
C13	Vertical Shear - Condition 28 FG (7) Fatigue Condition (Limit)	276
C14	Vertical Bending Moment - Condition 28 FG (7) Fatigue Condition (Limit)	277
C15	Vertical Shear-Condition 39FG (8) Fatigue Condition (Limit)	278
C16	Vertical Bending Moment - Condition 39 FG (8) Fatigue Condition (Limit)	279
C17	Vertical Shear - Condition 40 FG (9) Fatigue Condition (Limit)	280
C18	Vertical Bending Moment - Condition 40 FG (9) Fatigue Condition (Limit)	281
C19	Vertical Shear - Condition 1 FG (10) Fatigue Condition (Limit)	282
C20	Vertical Bending Moment - Condition 1 FG (10) Fatigue Condition (Limit)	283
C21	Vertical Shear - Condition 3 FG (11) Fatigue Condition (Limit)	284
C22	Vertical Bending Moment - Condition 3 FG (11) Fatigue Condition (Limit)	285
C23	Vertical Shear - Condition 11 FG (12) Fatigue Condition (Limit)	286
C24	Vertical Bending Moment - Condition 11 FG (12) Fatigue Condition (Limit)	287
C25	Vertical Shear - Condition 7 FG (13) Fatigue Condition (Limit)	288

LIST OF FIGURES (Continued)		
<u>Figure</u>		<u>Page</u>
C26	Vertical Bending Moment - Condition 7 FG (13) Fatigue Condition (Limit)	289
C27	Vertical Shear - Condition F525.119 (14) Ultimate	290
C28	Vertical Bending Moment - Condition F525.119 (14) Ultimate	291
C29	Vertical Shear Condition 2262 GD (15) Ultimate	292
C30	Vertical Bending Moment - Condition 2262 GD (15) Ultimate	293
C31	Vertical Shear - Condition 2513 VH (16 and 17) Ultimate	294
C32	Vertical Bending Moment - Condition 2513 VH (16 and 17) Ultimate	295
C33	Vertical Shear - Condition 2059 BM (18 and 19) Ultimate	296
C34	Vertical Bending Moment - Condition 2059 BM (18 and 19) Ultimate	297

## LIST OF TABLES

<u>Table</u>	<u>Page</u>
1 PABST Utilization	7
2 External Loads and Conditions for Format Solutions	99
3 Shear Panels, Max/Min	104
4 Shear Panels	105
5 Bar Elements	106
6 Bar Elements, Max/Min	107
7 Shear - Compression/Tension Interaction Static Test Panel	110
8 Shear Static Test Panel	111
9 Tension Tee Test	114
10 Example Output-Loading Condition 20	119
11 Example Output-Max/Min Search for Frame and Skin	120
12 Example Output-Loading Condition 15	121
13 Example Output-Max/Min Search for Interaction	122
14 PABST Runway Roughness Spectra	124
15 PABST Landing Impact Spectrum	127
16 PABST Atmospheric Turbulence Parameters	129
17 Low Level Penetration Gust Plus Maneuver Spectrum	130
18 Maneuver Load Spectra for Airplane CG Vertical Load Factors	131
19 External Load Conditions for Development of Stress Spectra	136
20 Locations and Longitudinal Stress of the Analysis Elements	138
21 Stress Spectrum for Check Point A (90 Repetitions of the Spectrum Represent One Lifetime)	141
22 Summary of the Damage Tolerance Analysis of the FSuC Checkpoints	166
23 Summary of Tapered Flange versus Constant with Edge Chamfer	193

# LIST OF TABLES (Continued)

<u>Table</u>		<u>Page</u>
24	Structural Geometry for Studies	199
25	Utilizations for the Sensitivity Studies	201
26	Skin Thickness, Longeron Area and Spacing Variations Studied	212
27	Tear Strap Geometries and Residual Strength Results	218
A1	Stress Spectra for Studies No. 2 and No. 4 One Spectra Represents 1000 Hours	232
A2	Stress Spectra for Studies No. 1, No. 3, and No. 5 One Spectra Represents 333.3 Hours	234
A3	Stress Spectra with Utilization 2 for Study No. 1 One Spectra Represents 333.3 Hours	236
A4	Stress Spectra with Utilization 3 for Study No. 1 One Spectra Represents 333.3 Hours	239
A5	Stress Spectra with Utilization 4 for Study No. 1 One Spectra Represents 333.3 Hours	242
A6	Stress Spectra with Utilization 5 for Study No. 1 One Spectra Represents 333.3 Hours	245
B1	Basic Flight Profile 1-1 (Outbound)	250
B2	Basic Flight Profile 1-1 (Touch and Go)	251
B3	Basic Flight Profile 1-1 (Return)	252
B4	Basic Flight Profile 1-2 (Outbound)	253
B5	Basic Flight Profile 1-2 (Return)	254
B6	Training Flight Profile 2-1 (Outbound)	255
B7	Training Flight Profile 2-1 (6 Touch and Go's)	256
B8	Training Flight Profile 2-1 (Return)	257
B9	Training Flight Profile 2-2 (Outbound)	258
B10	Training Flight Profile 2-2 (6 Touch and Go's)	259
B11	Training Flight Profile 2-2 (Return)	260
B12	Low-Altitude Resupply Flight Profile 3-1	261
B13	Low-Altitude Resupply Flight Profile 3-2	262

## LIST OF SYMBOLS

AMST	-	Advanced Medium STOL Transport
a	-	half crack length - inch
$\bar{C}$	-	center line
CTOL	-	Conventional Take Off and Landing
c	-	material constant
c.g.	-	center of gravity
DBLR	-	doubler
DT	-	damage tolerance, damage tolerance flaw
da/DN	-	crack propagation rate - inches/cycle
FSDC	-	Full Scale Demonstration Component
$F_{TU}$	-	ultimate tensile strength
$I_{N.A.}$	-	area moment of inertia about the neutral axis
IRAD	-	Independent Research and Development
K	-	crack tip stress intensity factor - ksi $\sqrt{\text{in}}$
ksi	-	1000 pounds per square inch
L	-	longeron
LL	-	loft line
l	-	bonded overlap distance
MAC	-	mean aerodynamic chord
N	-	cycles
NDI	-	non-destructive inspection
$n_x$	-	lateral load factor
$n_y$	-	longitudinal load factor
$n_z$	-	vertical load factor
O.T.	-	one time
OWE	-	operator's weight empty
PLCS	-	places
P	-	pressure
p	-	material constant
psi	-	pounds per square inch
R	-	min stress/max stress

RS - residual strength, or residual strength flaw  
 STA - fuselage station  
 STOL - Short Take Off and Landing  
 TYP - typical  
 TOGW - take off gross weight  
 t - thickness  
 $\gamma$  - effect of stiffness on a crack grown in the attached sheet  
 $\gamma$  - adhesive strain  
 $\Delta K$  - difference in stress intensity  
 $\Delta n_z$  - runway incremental load factor  
 $\delta$  - deflection - inches  
 $\epsilon$  - unit deformation or strain - inch/inch  
 $\xi$  - non-uniform stress distribution factor  
 $\sigma_{O.T.}$  - one time stress - psi  
 $\sigma_{PRIN.}$  - principal stress - psi  
 $\phi 1B$  - PABST phase 1B  
 $\phi 2$  - PABST phase 2

## INTRODUCTION

The use of adhesive bonding in components of aircraft structure has increased dramatically over the last 15 years to the point where most aircraft delivered today utilize some degree of adhesive bonding. However, these applications have been confined primarily to secondary structure where the adhesive bond stress is a low percentage of the adhesive shear strength. This experience with secondary structure had led to the recognition that problems with adhesive bond durability, inspection and the effects of defects must be solved prior to the extensive use of adhesive bonding on primary structure.

Extensive government and industry exploratory development programs over the past few years have resulted in improved adhesives, primers and surface preparation, as well as improved laboratory test techniques that can closely simulate the type and nature of service experience. In addition, non-destructive inspection techniques for adhesive bonds have been vastly improved. These developments have provided confidence that a final validation program should be pursued to prove the adequacy of adhesive bonding for primary structure.

A series of interrelated Air Force sponsored programs have been constructed to obtain additional bond durability data on coupons and components, provide data on sonic fatigue resistance of bonded structure and develop the necessary manufacturing, field and depot repair methods, and the verification of bondline defects.

In February of 1975 the Douglas Aircraft Company, under contract to the Air Force, initiated a technology validation program for primary adhesive bonded structures (PABST). This program was to perform a preliminary design, perform detail design, fabricate test articles and perform coupon, component and full scale fatigue, static and damage tolerance testing. The objective of PABST was to validate that application of adhesive bonding could result in substantial cost and weight savings when compared to conventional fabrication techniques, while providing significant improvements in structural

safety and durability. The results of the Phase Ib Preliminary Design effort are documented in Reference 1. This report documents the Phase II effort of the detail design and analysis of a forty-two (42) foot forward fuselage section of a Full Scale Demonstration Component (FSDC) that simulates the configuration of the next generation of Air Force aircraft.

## DESIGN CRITERIA

The criteria for the PABST Program contain the requirements of the applicable military aircraft specifications with appropriate modifications consistent with the scope of the PABST Program. These specifications include the MIL-A-008860 series, MIL-STD-1530(USAF) and MIL-A-83444 (USAF) documents. The intent is that the implementation of this criteria in the bonded fuselage design will result in a structural integrity equivalent to that required for airworthiness. The implementation will be demonstrated by test and analysis.

The criteria data are based on the projected C-15 STOL aircraft. The basic design parameters and weights are documented in detail in Reference 1, pages 59 through 65.

Specific criteria for fatigue and damage tolerance are presented in the following section. Included are residual strength requirements written to supplement the slow crack growth criteria of MIL-A-83444 (USAF) for the PABST metal structure and complete criteria for adhesive bonded areas developed during Phase Ib.

Fatigue and Damage Tolerance Criteria - For Full Scale  
Demonstration Component (FSDC) - Metallic Structure

Applicable Documents. - The following documents apply to the extent specified: MIL-STD-1530(USAF) "Aircraft Structural Integrity Program, Airplane Requirements" (1 September 1972) except for sections: 4.2d, 4.2e, 5.1.1, 5.2.3, 5.2.7, 5.2.8, 5.2.9, 5.2.10, 5.2.11, 5.3.1.2, 5.3.4, 5.3.4.1, 5.3.4.2, 5.3.5, 5.3.5.1, 5.3.5.2, 5.3.5.3, 5.3.5.4, 5.3.6, 5.3.6.1, 5.3.6.3, 5.3.7, 5.3.8, 5.3.8.1, 5.3.8.2, 5.4 and its subsections and 5.5 and its subsections.

MIL-A-83444 "Airplane Damage Tolerance Requirements" except for Sections 3.1.1.1b, 3.1.1.3 and its subsections, 3.1.3 paragraph on fail safe structure, 3.2.2 and its subsections, and 3.2.3 and its subsections.

MIL-A-008866A "Airplane Strength and Rigidity, Ground Tests" except for Sections: 3.6 (except as modified for STOL aircraft), 3.10, 3.11, 3.12, 3.13, 4.3.

MIL-A-008867A "Airplane Strength and Rigidity, Reliability Requirements, Repeated Loads and Fatigue" except for Sections: 3.2.3f, 3.2.3g, 3.3.4.1c except for environment, 3.3.4.2 environmental effects, 3.4.1.1, 3.4.4.2, 3.4.5.2, 3.4.5.3, 3.4.5.5 except real time and environment, 3.4.5.6, 3.4.5.9, 3.5.3, 3.7, 3.7.1, and 3.8.

Fatigue Criteria. - The PABST fatigue criteria shall incorporate a utilization model considering all pertinent loadings arising from preflight taxi, post-flight taxi including effects of reverse thrust, landing impact, vertical and horizontal gusts, flight maneuvers, pressurization, thermal loads, ground handling loads and the influence of the environment on the strengths of the various materials.

Service Life. - The design service life and design usage of PABST are shown exclusive of scatter factor.

Flight Service Life	30,000 Hours, 12,507 Flights and 46,194 Landings
Pressurizations	19,014

Landings, Full Stop	29,977
Touch and Go's	16, 127

The projected equivalent utilization for fatigue analysis of the PABST FSDC structure is given in Table 1 .

Design Fatigue Life. - The design fatigue life is the service life defined above multiplied by a scatter factor of 4.0.

Service Loads and Environment Spectra. - The basic inputs to define the cyclic loads spectra shall be as defined in MIL-A-008861A and MIL-A-008866A modified to incorporate the higher sink rates associated with STOL type aircraft. For the metal FSDC structure, the environment used was room temperature and laboratory air.

Slow Crack Growth Damage Tolerance Criteria - Metallic Structure. - PABST safety of flight structure shall be qualified as slow crack growth under the appropriate sections of MIL-A-83444 and shall be designed so the possibility of catastrophic failure will be extremely remote. Compliance with these criteria shall involve residual strength and crack growth analysis and/or tests. In addition, the structural design and analysis shall account for the fail safe criteria in the following paragraph.

Fail Safe Criteria - Metallic Structure. - The PABST FSDC structure shall have a fail safe capability comparable to that of commercial airplane fuselages, as defined in Federal Aviation Regulation 25. The fail safe requirements of MIL-A-83444 Section 3.1.1.1b, 3.1.1.3, 3.1.3, 3.2.2, 3.2.3 and their subsections will not be met since slow crack growth was used.

The structure shall be capable of withstanding (1) limit load with a two bay crack and (2) the maximum average internal member load occurring in 20 lifetimes, or limit load whichever is less, for foreign object damage as specified in the following subsections.

TABLE 1  
PABST UTILIZATION

FLIGHT NUMBER	DESCRIPTION	MISSION LENGTH		LANDINGS PER MISSION			HOURS PER LANDING	SERVICE LIFE				PAYLOAD LBS.	
		FLIGHT HOURS	MI	STOL	CTOL	TOUCH & GO		FLIGHT HOURS	% TOTAL FLIGHT HOURS	STOL	CTOL	LANDINGS TOUCH & GO	NUMBER OF MISSIONS
1-1	BASIC	2.76	524	1	1	1	0.92	20007	66.7	7236	7236	7236	7236
1-2		2.0	715		1	1	1.0	1894	6.3		947	947	947
								21901	73.0	7236	8183	8183	8183
2-1	BASIC TRAINING	1.6	394	1	1	6	0.2	1974	6.6	1234	1234	7404	1234
2-2		1.4	370	1	1	6	0.2	126	0.4	90	90	540	90
								2100	7.0	1324	1324	7944	1324
3-1	LOW ALTITUDE RESUPPLY	2.0	582	3	1		0.5	3000	10.0	4500	1500		1500
3-2		2.0	573		4		0.5	3000	10.0		6000	6000	1500
								6000	20.0	4500	7500	12000	3000
								30001	100.0	13060	17007	16127	12507
												46194	100.0

2(8183) = 16366 FULL PRESSURE CYCLES  
2(1324) = 2648 PARTIAL PRESSURE CYCLES

19014 PRESSURE CYCLES (ACTUAL UTILIZATION HAS 17150 PRESSURE CYCLES)

Longitudinal Cracks: - The structure with a longitudinal crack shall be able to withstand (1) a two-bay skin crack or a skin-to-longeron disbond and the center frame (or splice) intact, and (2) a 15 inch long foreign object damage skin crack with both the center frame (or splice) and crack arrest member (if present) failed. For the first requirement, at least the skin crack adjacent to a frame (or splice), where high stresses are induced from frame bending and pressure, shall be considered. All cracks considered shall be assumed to propagate in both directions.

Circumferential Cracks: - The structure with a circumferential crack shall be able to withstand (1) a two-bay crack with the center longeron (or splice) intact, and (2) a 15 inch long foreign object damage crack with the longeron or splice and crack arrest member (if present) failed. All flaws shall propagate in both directions.

## Damage Tolerance Criteria - Adhesive Bond Areas

General Requirements. - The requirements of MIL-A-83444, for metal and mechanically joined elements shall be supplemented with the following requirements for the design of adhesive bonds joining two or more elements of the structure. Compliance with these criteria shall be developed by analysis and/or test. The analytical damage tolerance assessment shall be confined to residual strength estimates. The analyses shall assume the presence of flaws in the bond placed in the most unfavorable location and orientation with respect to applied stress and material properties. The experimental investigation shall be limited to distinguishing between flaws which grow and those which do not. Thermal and humidity effects shall be accounted for.

Entire panels or parts which are improperly processed; i.e., parts with global damage, shall be rejected. Parts with local contamination or flaws shall be reworked to a quality in which the flaws shall not grow to unacceptable sizes within two airframe lifetimes.

Initial Flaw Sizes: - An initial flaw shall be assumed to exist in each and every bond in its most critical location including those highly stressed areas resulting from variable bondline thickness. The size of the flaw shall be the greater of (1) the minimum detectable size for the NDI technique used on the bond, or (2) the smallest flaw remaining after a larger flaw has been repaired. Each flaw shall be analyzed for residual strength independently of all other flaws, either in the bond or metal. Initial flaws shall be located so there is no interaction between them.

Bond Inspectability: - The detail design shall minimize the use of uninspectable bonds and, wherever practical, shall be such as to force the first evidence of failure into a visible or easily inspectable area. Techniques, such as staggering the ends of the overlaps, shall be used to facilitate inspection of the bonds. Each uninspectable bond shall be limited in extent to a subcritical size.

Flaw Growth in Bonds: - Flaws in bonds induced in service shall not grow from initial sizes defined above to critical size within two airframe lifetimes. All flaws large enough to grow in service shall be repaired prior to delivery of an aircraft to preclude corrosion. In addition, bonds which contain sub-critical flaws in areas subject to corrosion shall be sealed to provide environmental resistance.

Fail Safe Capability: - The fail safe capability of the bonded structure shall be demonstrated by test and/or analysis. The structure shall be capable of withstanding (1) limit load with each of the following two-bay disbond configurations:

- (a) a two bay disbond in only one side of a double strap butt splice,
- (b) a two bay disbond in a single strap butt splice, or single lap splice,
- (c) a two bay longeron-to-skin disbond, and
- (d) a two bay shear-clip-to-skin or crack-arrest-member-to-skin disbond;

and (2) the maximum average internal member load occurring in 20 lifetimes, but less than limit load, for impact or the foreign object damage specified as:

- (a) a 15" disbond on both sides of a splice, and
- (b) a 15" long foreign object damage skin crack with both the center frame (or splice) and the crack arrest member failed or with both the longeron (or splice) and crack arrest member failed as applicable.

## FULL-SCALE DEMONSTRATION COMPONENT

The Full Scale Demonstration Component (FSDC) simulates the forward section of the C-15 airplane fuselage from station 367 to 871. The entire FSDC will be cantilevered from the aft test fixture. The FSDC general arrangement is shown in Figures 1 through 5.

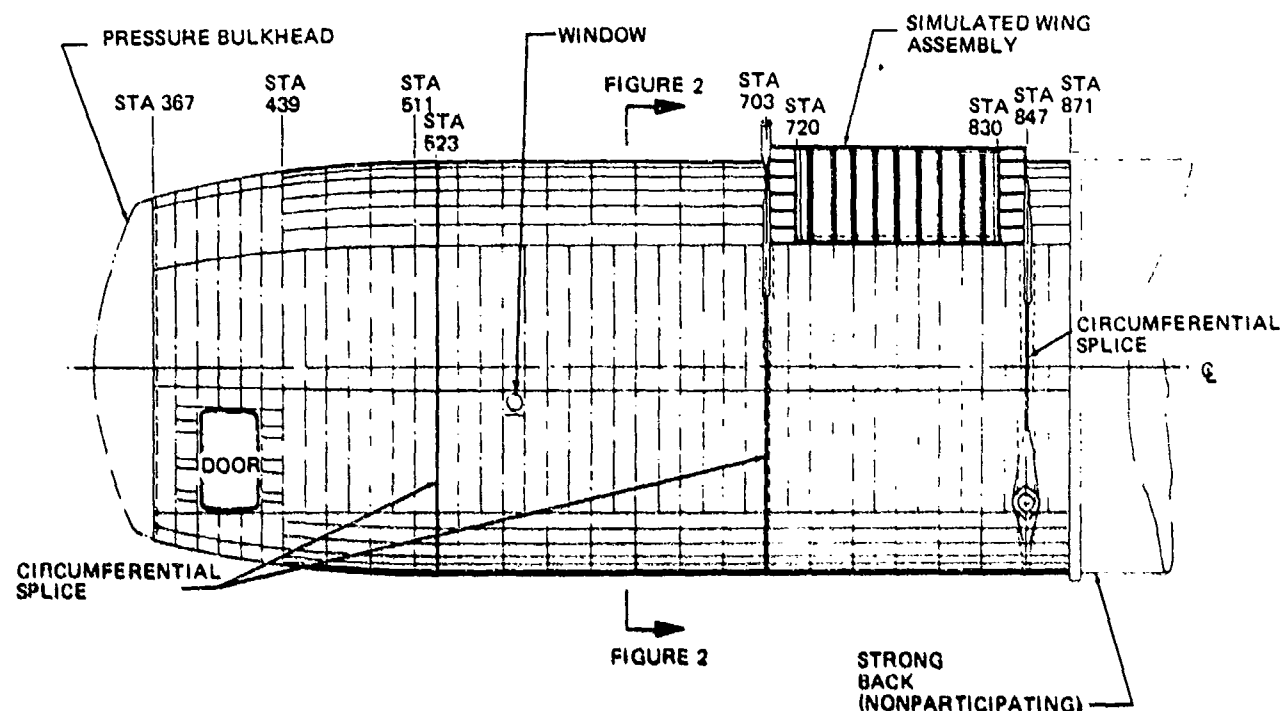


**FIGURE 1. FULL-SCALE DEMONSTRATION COMPONENT  
(LEFT SIDE VIEW)**

The FSDC is a 42 foot long test component consisting of a nose section, forward of station 439, and a cargo compartment section, aft of station 439. Most of the fuselage shell is cylindrical with a constant 108 inch radius circular cross section starting from station 516 and extending aft to station 871. Forward of station 516 to station 367, the shell is circular in cross-sectional shape, while the lofted shape from station 367 to station 516 is a circular arc.



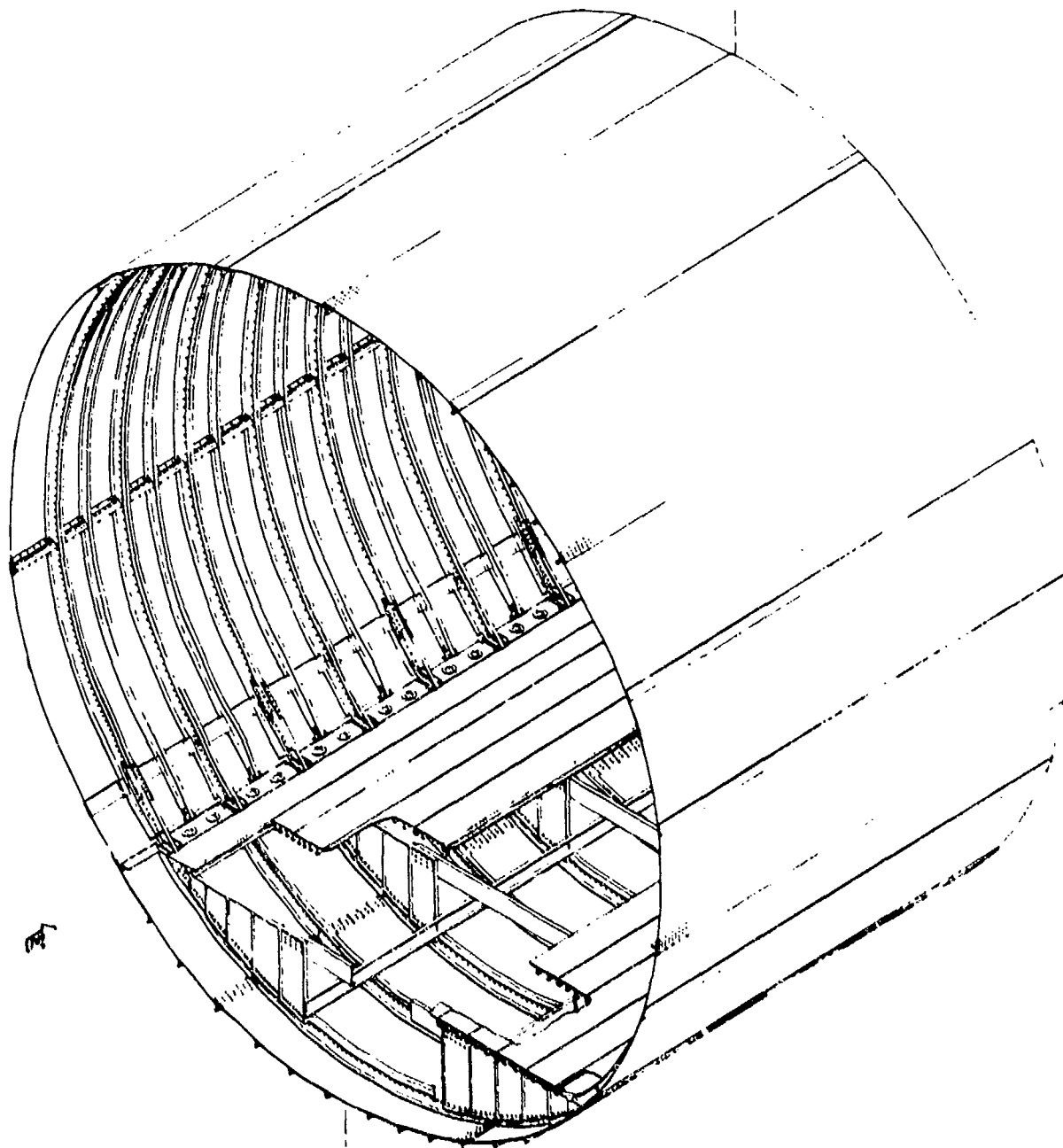
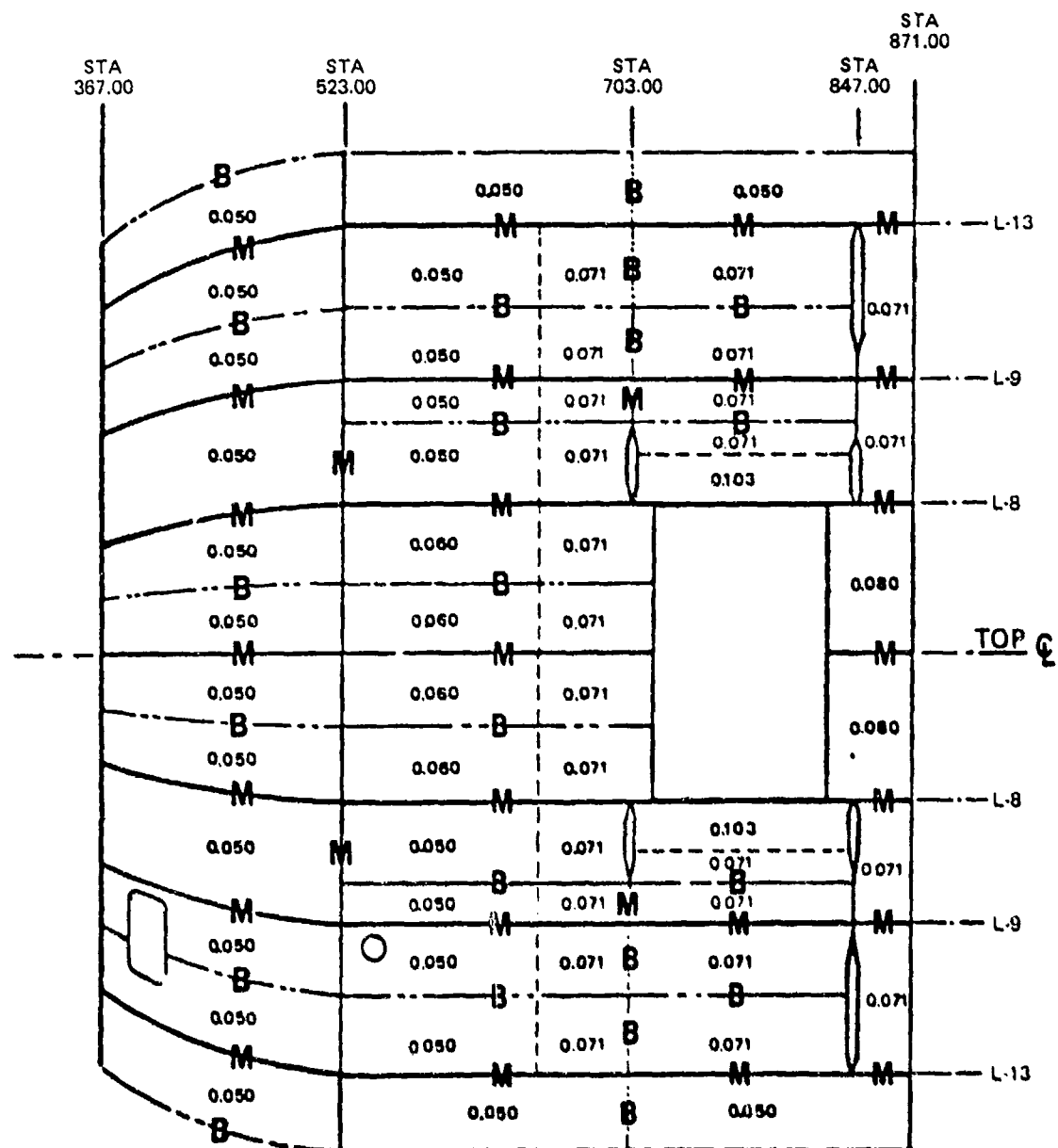


FIGURE 3. PERSPECTIVE OF FULL-SCALE DEMONSTRATION COMPONENT



NOTE:

1. ALL SKINS ARE 2024-T3
2. **B** = BONDED JOINT
3. **M** = MECHANICALLY ATTACHED JOINT

FIGURE 4. SKIN PANELS FOR FULL-SCALE DEMONSTRATION COMPONENT

Figure 5 shows the simulated wing to fuselage connection. The simulated wing is basically a box comprised of front and rear spar assemblies, a lower skin panel, and end bulkheads. The wing box is open on top with axial load carrying members (links) to transmit loads in longerons 1 and 4 across the wing.

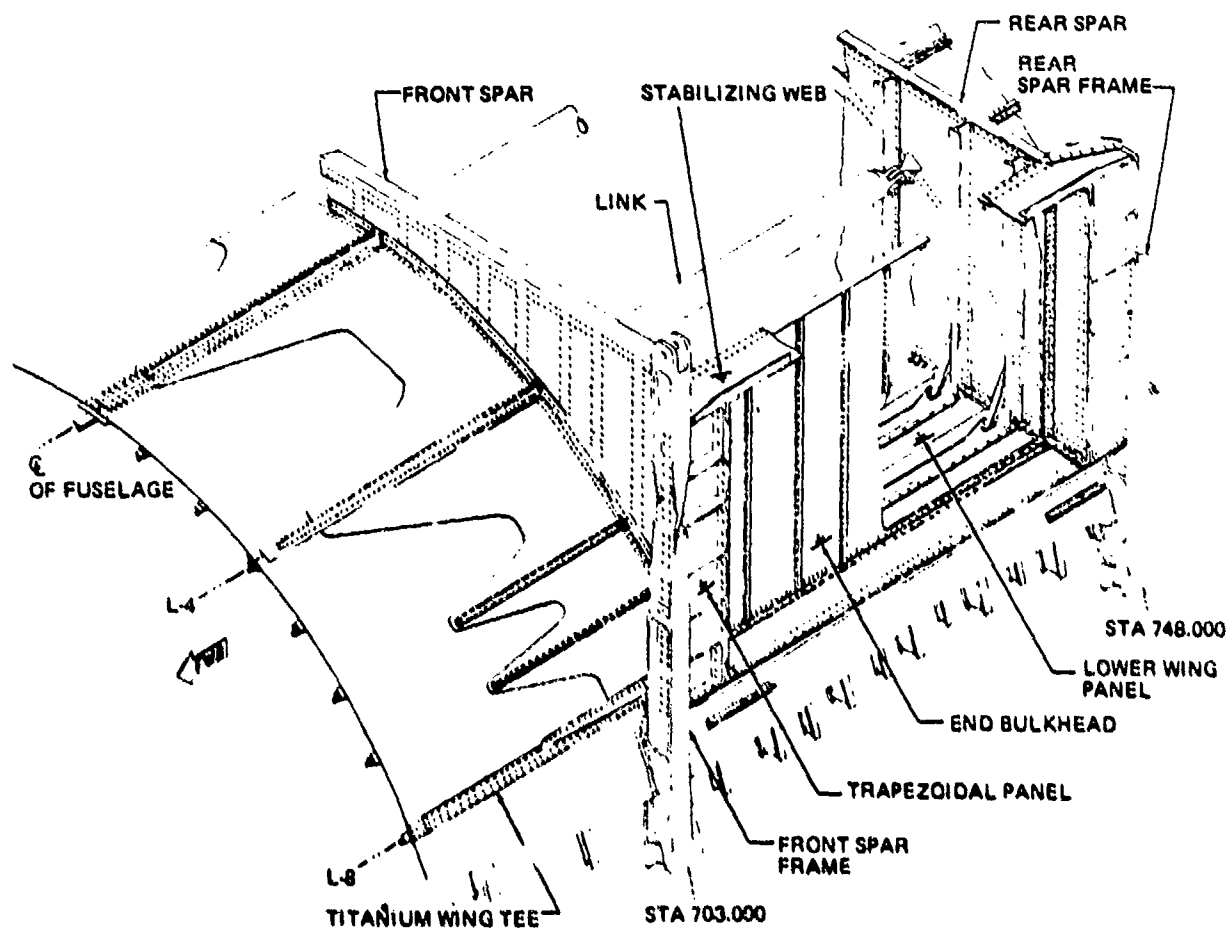


FIGURE 5. SIMULATED WING ASSEMBLY AND WING/FUSELAGE INTERFACE

The forward end of the FSDC is attached to a steel dome shaped pressure bulkhead. The bulkhead is counterbalanced and contains a hatch for entering the FSDC for inspection. The fuselage is joined mechanically to the bulkhead with a double lap splice as shown in Figure 6. Doublers are bonded to the skins to make a total thickness of 0.35 plus bondlines. The fatigue stress level (typically about 1100 PSI) at the joint to the forward pressure bulkhead is one seventh that in the participating test structure. The design of the joint is similar to that used on preceding aircraft test articles which successfully withstood a greater number of fatigue cycles without the additional benefit of bonded doublers in addition to the mechanical fasteners. The joint at the aft end of the FSDC has similar integrity. Shims are added to the pressure bulkhead on assembly in order to match the bulkhead to the fuselage. Intercostals, also shown in Figure 6, provide stabilization for the frame at station 367. They are located at the bottom centerline, tear stopper 2, tear stopper 3 (right side), splice 13 (left side), and at longerons (longs.) 1, 4, 8 and 9.

The aft end of the FSDC is supported by the test fixture at station 871. Circumferentially, the fuselage skin and doublers pick up two formed angles which are secured to the test fixture by two rows of 1/4" attachments, in Figure 7. Additional support of the FSDC at the test fixture is provided by machined supports at longeron locations and intermediate locations, as shown in Figure 8. The FSDC floor planks pick up a horizontal beam located at floor level in the test fixture as shown in Figure 9. The cargo compartment floor extends aft from station 367 to station 875 at a constant height,  $Z = -75.654$ . The floor planks are omitted two feet from each side of the centerline for the full length of the fuselage; i.e., the extruded floor planks extend from  $X = \pm 25$  to the side of the fuselage. This open area located at the fuselage centerline provides easy access to the under floor area for manufacturing, inspection, engineering and test personnel. Keel members (extruded channels) are located below the cargo floor and mechanically fastened to the web of the frame at  $X = \pm 25$  through shear clips.

A plug type, honeycomb, crew entrance door is located on the left

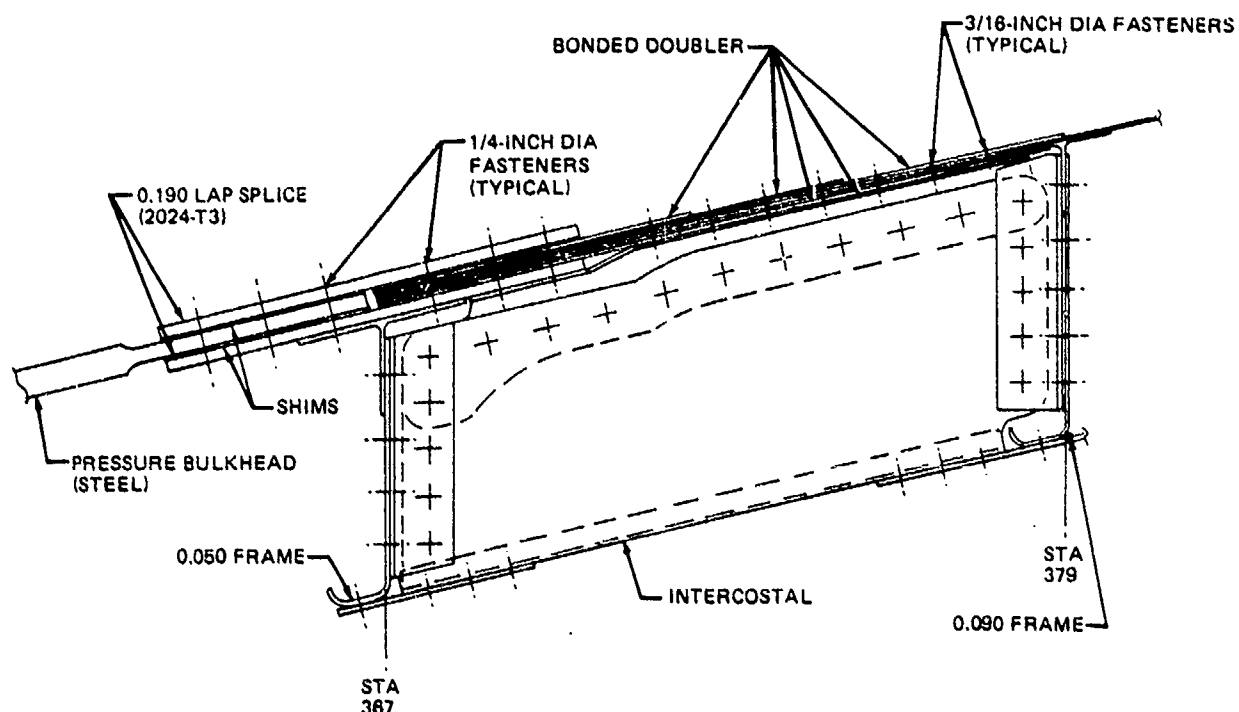


FIGURE 6. FORWARD FSDC ATTACHMENT TO PRESSURE BULKHEAD

side between the cargo compartment floor and longeron 9 in the nose section between stations 391 and 427.

A nonstressed window installation is provided on the left side of the fuselage just below longeron 9 between stations 559 and 571. The "window" is a cutout (8.50 inch dia.) in the skin with an aluminum sheet simulating the clear plexiglas window.

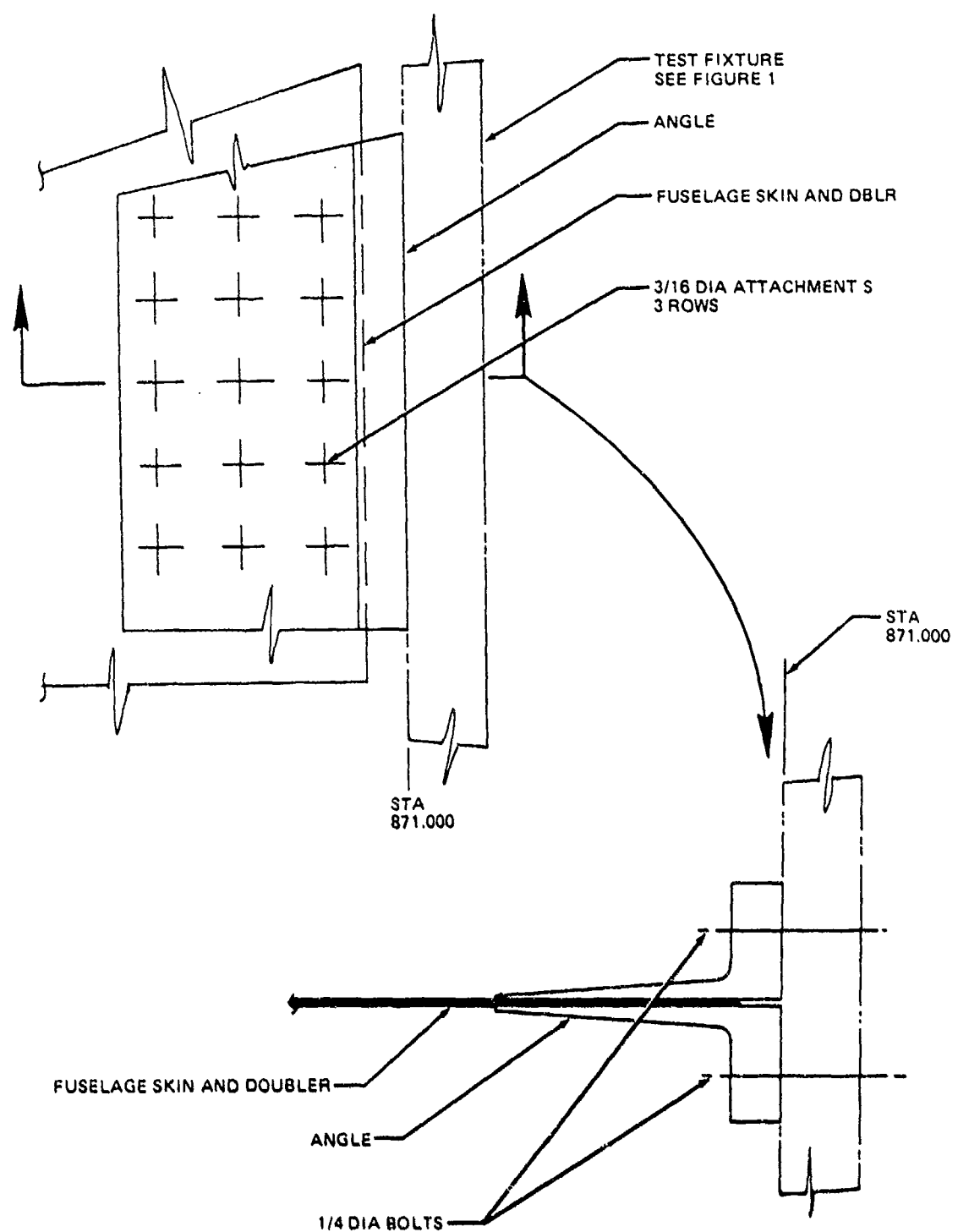


FIGURE 7. TYPICAL FSDC TO AFT FIXTURE ATTACH

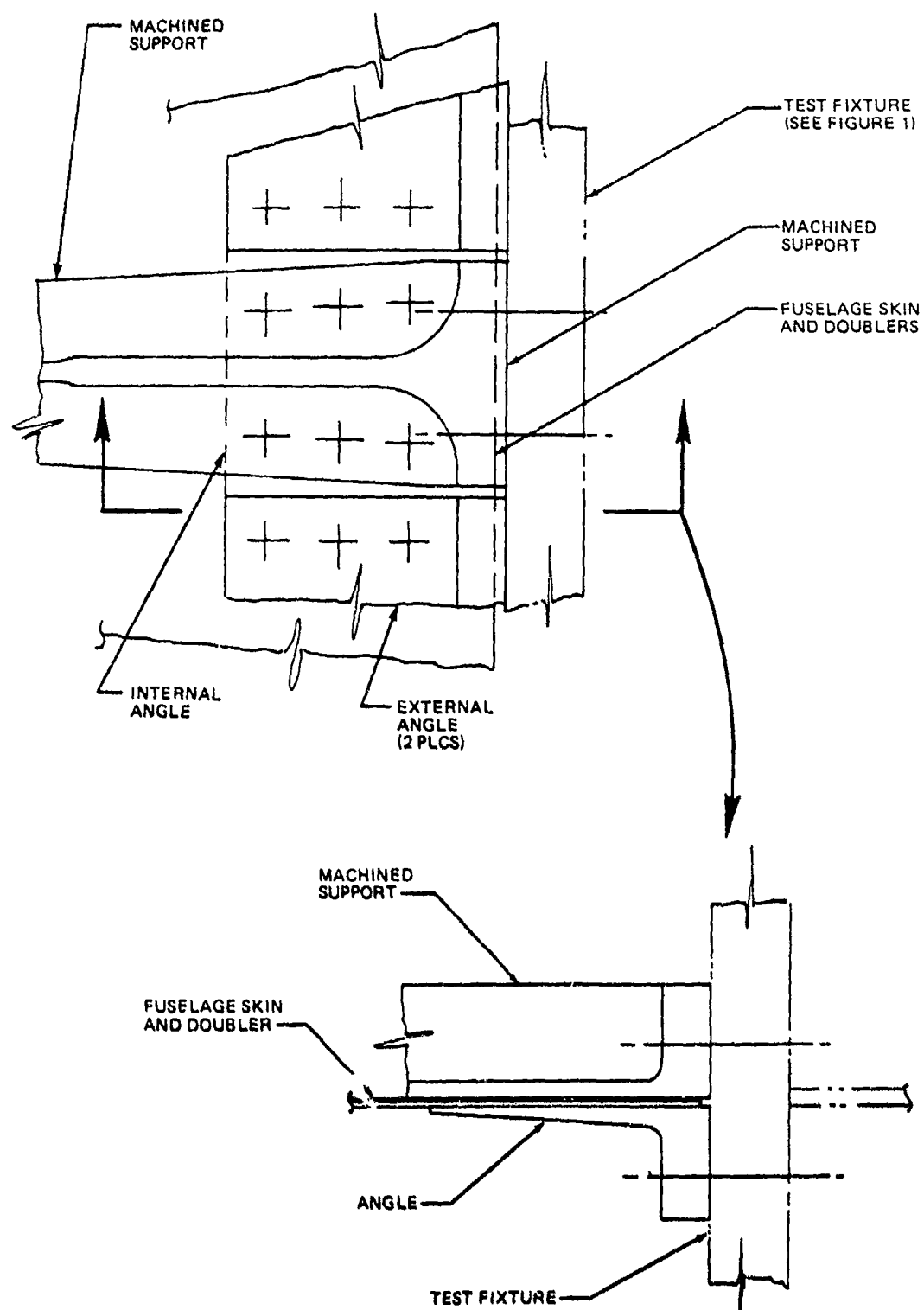


FIGURE 8. TYPICAL LONGERON TO AFT FIXTURE ATTACH

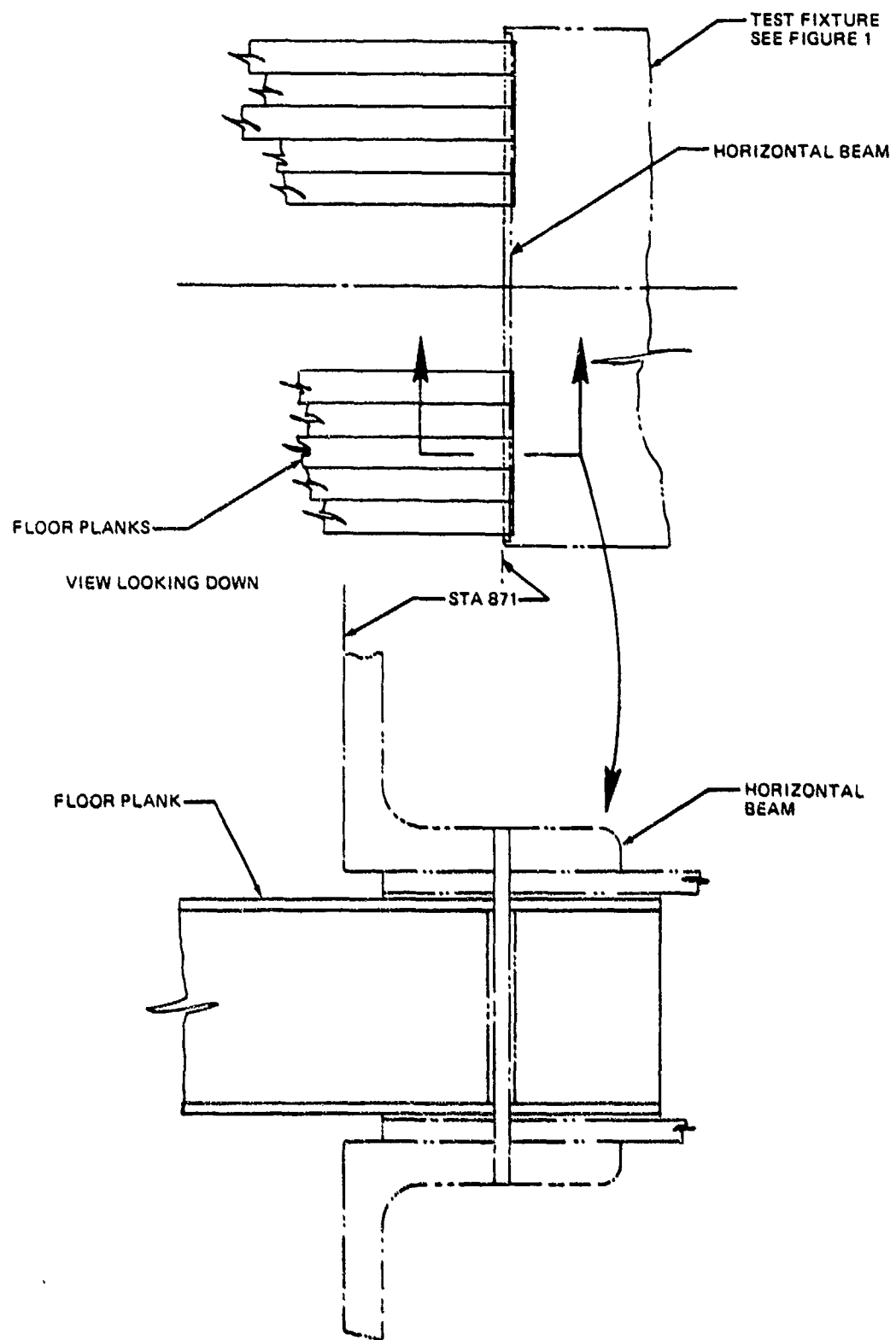


FIGURE 9. FLOOR BEAM TO AFT TEST FIXTURE ATTACH

## DETAIL DESIGN

The structural members and assemblies that make up the Full Scale Demonstration Component (FSDC) were designed to the static, fatigue and damage tolerance criteria established during the preliminary design phase. Since minimum cost was a PABST goal, the frames and longerons were sized to carry the design loads with the least number of different extrusion shapes. Mechanical fastening was kept to a minimum within the limitations of manufacturing capability and the availability of sheet stock. The mechanical splices were designed and tested early in the program to the Full Scale Demonstration Component (FSDC) stress levels and demonstrated that they exceeded the four lives of fatigue and the damage tolerance criteria of MIL-A-83446. The strength criteria and the ease of assembly determined the type of splice selected. Intercostals were added to stabilize all frames and to provide axial load capability to the nose section.

## Skin Splices

The FSDC has both mechanical and bonded skin splices in the longitudinal and circumferential directions. The splices were designed to meet the static ultimate loads and the fatigue and damage tolerance criteria described in the Design Criteria Section.

All fasteners that penetrated an adhesive bond line on an exterior skin were installed with wet sealant and the faying surfaces sealed with MIL-S-81733 sealant. This procedure ensured a pressure seal and protected the joint from moisture intrusion.

Mechanical Skin Splices. - The FSDC bonded panel assemblies were sized to minimize the number of mechanical splices. The primary constraint was the maximum circumferential panel assembly dimension that could be bonded in the PABST autoclave. In addition to the facility limitations, the consideration of manufacturing "breaks" for a production fuselage was included.

As a cost reduction, the longitudinal skin splices were all single overlap designs except for the top centerline splice at longeron 1 that was a symmetrical double lap butt configuration. The butt splice selection was based primarily on reducing cost by providing a panel assembly that was symmetrical about the FSDC centerline.

Designs were evaluated to determine the most efficient longitudinal mechanical splice configuration. The factors considered were cost, structural efficiency, inspectability, and ease of assembly. All of the FSDC mechanical splices in the study used a combination of .188" diameter mechanical fasteners and MIL-S-81733 Type IV-12 (PR 1431G) sealant on the faying surface of the skins to prevent moisture entrapment and corrosion as well as for pressure sealing.

For the longitudinal splices between bonded subassemblies, possible configurations included: (1) conventional symmetrical multi-row double-strap

mechanical butt splices (2) single-lap purely mechanical splices (3) single-lap splices with fasteners and hot-bonded doublers for the reinforcement of the most highly loaded rivet holes, and (4) variations of these cases. These options were reduced to a single lap unsymmetrical mechanical splice and a symmetrical double strap splice for the FSDC.

Longitudinal Single Lap Unsymmetrical Splice: - Typical FSLC single lap mechanical splice designs are shown in Figure 10. In all three examples, the fasteners through the stiffener are 3/16 inch bolts while the upper and lower rows contain half as many fasteners and they are 3/16 inch rivets. Longerons 8 is bonded to the lower skin as shown in the Figure, and a bonded doubler is used to improve the life of the splice. The doubler is external so that the skins make direct contact with each other in order to minimize load path eccentricity. The methods of minimizing the induced bending stresses due to load path eccentricities are discussed in the section on Adhesive Bonded Joint Analyses. The upper three rows of fasteners are countersunk into the doubler, while the lower row is countersunk into the .050 skin. The net section stress in the skin is lowest there and the countersunk skin does not become the weak link. Reinforcing the skin there with the doubler would attract more load to that row of rivets and cause the lower skin to fail there at a reduced number of cycles. Countersinking the .050 skin at the upper row of rivets would also have caused early failure since the upper skin has the highest net section and bending stresses at this point.

The splice at long.9 is similar to that just discussed except that it is not necessary to reinforce the upper skin at the upper row of rivets since the skin thickness is .071 there. Also, the heavier longeron is not bonded to the lower skin.

At long.13 the external longeron is bonded to the upper skin and the reinforcing doubler is bonded to the lower skin. This splice uses three rows of fasteners, the lower row being a half row of rivets as shown in the figure. The longeron reinforces the first row of bolts where the net section stress is the highest. This produces a modest gain in life over the other splices, however the life of the other splices is 5.2 times better than the required design life, based on test.



Longitudinal Symmetrical Double Strap Butt Splice: - The double strap butt splice is shown in Figure 11. A 0.040 x 4.00 doubler of 2024-T3 was installed on the inside surface of the upper skin where the two full rows of attachments were located in order to increase the skin bearing allowable. The doubler also acted as a reinforcing member for the skin where the shear tees stopped short of the longeron and created stress risers locally in the skin. The splice consisted of four full rows of steel huck bolts and two half rows of rivets with the manufactured head on the inboard side of the skins and an 82° countersink on the exterior surface of the skins.

For maximum efficiency with the protruding head fasteners of the double strap joint, each strap should have half the extensional stiffness of the skins being joined. However, this requirement was incompatible with the need to avoid knife-edging the fastener holes in the outer strap for flush fasteners. Therefore, the load between the fastener rows was shared unequally by thickening the outer strap for countersinking.

Circumferential Single Lap Butt Splice: - The circumferential skin splices were designed to provide a flush exterior for aerodynamic considerations as shown in Figure 12. An 0.016 2024-T3 doubler was bonded to the inside of the 0.050 skin to permit flush fasteners above the cargo floor. Two full rows of lockbolts on each side of the butt splice pass through an 0.071 splice plate, an 0.032 splice plate and the outer skin. The inner row of lockbolts also attaches the circumferential frame and provides additional transition of the butt splice load. Like the longitudinal single lap splice, the outer riveted row contains only half as many as were in the inner riveted rows.

FSDC Splice Selection: - The single lap splice was found to be superior to the symmetrical double strap butt splice from design, strength and manufacturing considerations as follows:

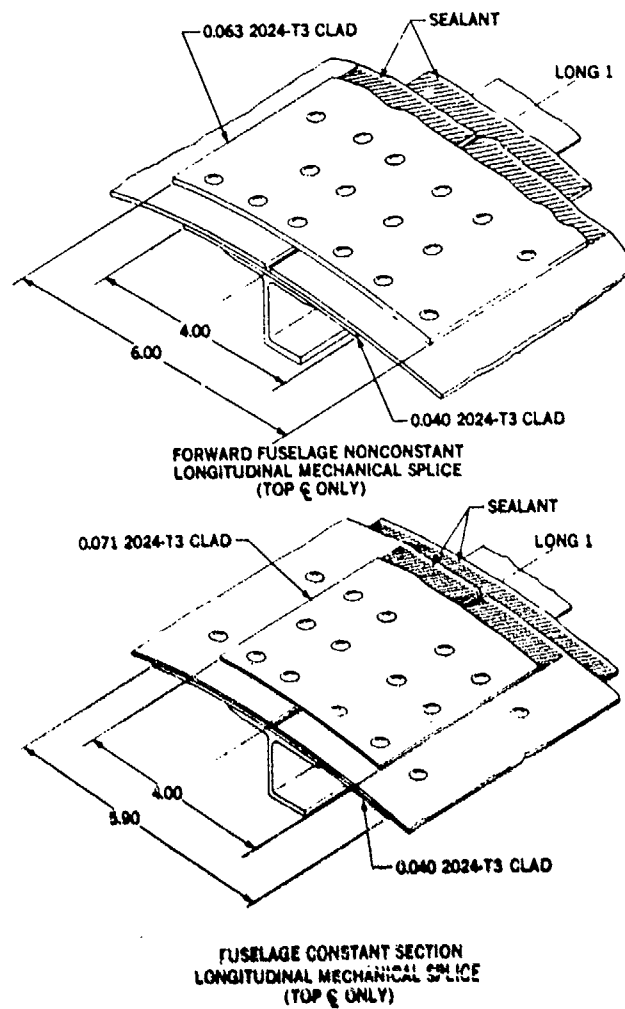
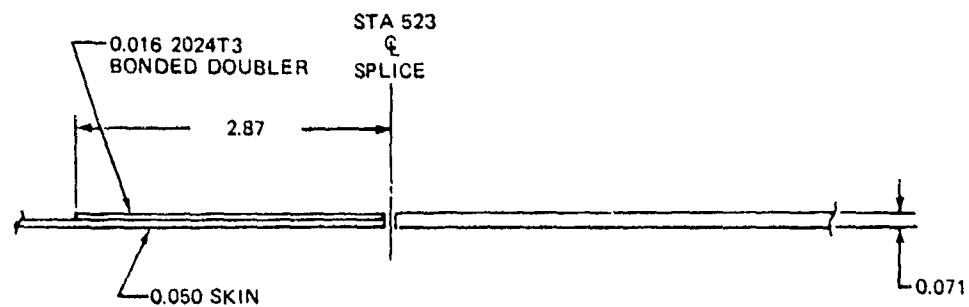
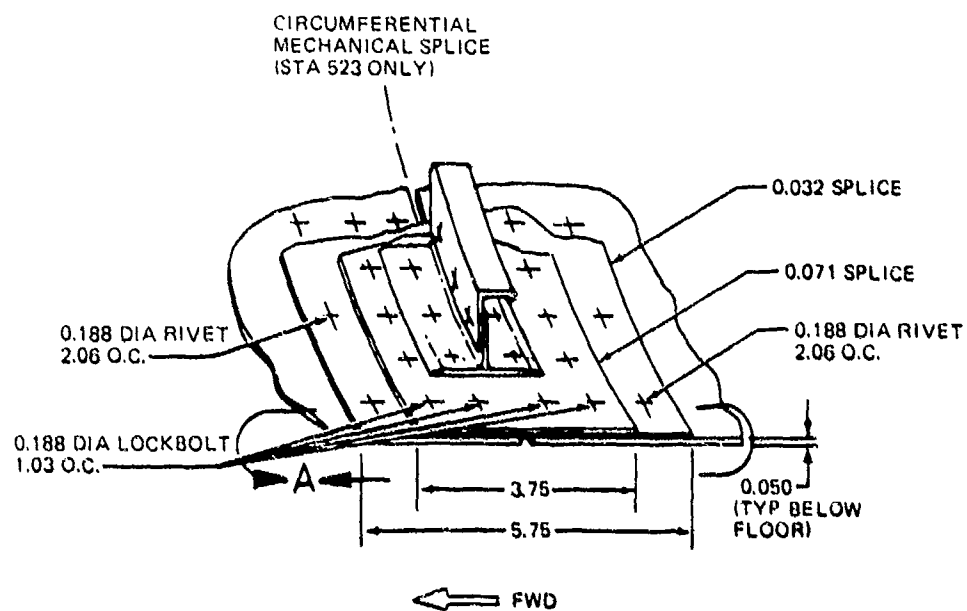


FIGURE 11. TYPICAL MECHANICAL DOUBLE STRAP BUTT SPLICE



VIEW A

TYPICAL ABOVE FLOOR FOR FLUSH FASTENER  
(SKIN AND DOUBLER ONLY SHOWN)



NOTE FASTENERS ARE FLUSH ABOVE THE CARGO FLOOR (LONGERON 10) AND PRO-  
TRUDING HEAD BELOW FLOOR IN THE EXTERNAL LONGERON REGION.

FIGURE 12. CIRCUMFERENTIAL MECHANICAL SPLICE

(1) For the static load case, the attachments in the single lap splice were capable of carrying approximately 3500 #/in. while those in the double strap splice were good for only 1800 #/in. in the 0.050 gage skin.

(2) For the fatigue loads, a single lap test specimen, representative of a current Douglas commercial airplane, lasted 500,000 cycles at 14,000 psi skin stress.

(3) Only half as many fasteners were needed since the connection was direct instead of through intermediate members.

(4) The single lap splice was much easier to assemble and did not need as many straps.

(5) The single overlap eliminated the need for trimming on assembly which was required by the butting of the skins in the double strap splice. This resulted in the removal of the protective anodize and primer on the skins in the double strap configuration.

(6) The single lap splice permitted easier countersinking of the flush fasteners.

(7) The single lap splice was relatively simple to inspect in comparison with the double strap splice.

The only disadvantage of the single lap splice was the load path eccentricity discussed previously in this report. A generous overlap distance of 4.25 inches (85t) was used for the 0.050 inch skin to minimize the problem. Consequently the single overlap splice is slightly heavier than a double strap joint of equivalent life.

In summary, the single-lap splice employed at the manufacturing breaks of the PABST FSDC was cheaper than the conventional symmetrical double strap butt splice with two rows and two half rows of fasteners instead of four and four half rows. It was also more resistant to corrosion since all faying surfaces were sealed with hot bond or PR1431G sealant. No anodized/primed

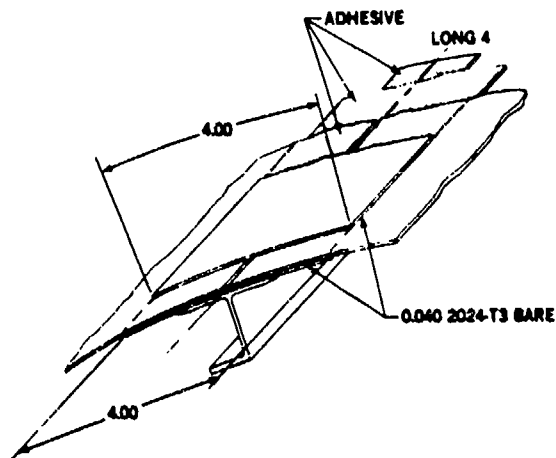
areas were trimmed on assembly. In addition, this design had more than adequate life.

A conventional symmetrical double-strap butt splice was used at the top center of the fuselage to make the design symmetric. There was no need for breaking the protective BR127 primer for this particular splice by trimming on assembly since the tolerances could be absorbed at the adjacent single-lap splices in the FSDC.

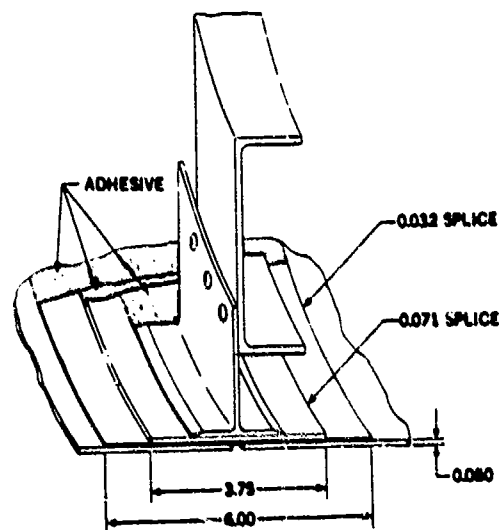
Bonded Skin Splices. - The PABST design employed one or more bonded splices within each subassembly, the number and location depending on the availability of the skin stock. As stated in the previous subsection, the skin was broken up into the minimum number of segments compatible with the size of the autoclave.

The bonded splices included: (1) double-strap longitudinal butt splices (inner and outer) straps) in Figure 13, and (2) flush single-strap circumferential butt splices with laminated inner straps only as shown in Figure 13. The designs were based on both elastic-plastic analysis and on test data.

To obtain maximum bond strength of the double-strap butt splice, the inner and outer straps should be half the skin thickness of the panels being joined. The mechanical testing of such splices in the PABST program confirmed there would not be any bond failures for environmentally resistant adhesives. However, the splice strap failed consistently by metal fatigue, although the skin and strap membrane stresses were nominally the same. To improve splice efficiency for the skin gages of interest (i.e., less than 0.1 inch thick), splice straps were thickened by one gage above the ideal half-skin-thickness value. The overlap was designed to provide sufficient plastic zones in the adhesive at the overlap ends to utilize the full metal strength to transfer the load. The middle elastic trough inherent in the adhesive bonded joint was designed to be long enough to ensure that this middle section of the adhesive would resist creep by remaining unloaded. The total overlap distance was then set as the sum of the two plastic end



**LONGITUDINAL BONDED SPLICE**



**CIRCUMFERENTIAL BONDED SPLICE  
(STA 703 ONLY)**

**FIGURE 13. LONGITUDINAL AND CIRCUMFERENTIAL BONDED BUTT SPLICE**

zones and the elastic trough in the middle, see Reference 1. A typical bonded longitudinal splice is shown in Figure 13.

Figure 13 also shows a typical bonded circumferential splice. The analysis capability for such a splice is not as comprehensive as for the longitudinal splices due to the non-linearities induced by load path eccentricity. However, the available analyses satisfactorily predicted the bending stresses in the strap where the skins butt together and in the skins where the splice ends. The associated adhesive peel stresses at the same locations were also obtained. The analyses showed that these splices were very sensitive to  $l/t$  ratio. A spliced panel was tested having the same  $l/t$  ratio of 33:1 as for an equivalent mechanical splice, Reference 1 page 185. The test confirmed the high induced bending stresses predicted by analysis. This high stress was the result of the splice being forced to bend sharply where the skins were butted together. It should be noted that in an equivalent mechanical splice, the splice can deflect smoothly over the gap between the inner row of fasteners thus reducing the bending.

The test panel sustained the loads for the required life but the failure was catastrophic and without warning. The splice plate fractured where the skins butted together and the two longerons disbonded. Failure initiated at an 0.4 inch fatigue crack on the visible side of the splice and at an 0.7 inch crack on the opposite side under the adhesive. As a result of this test, the PABST  $l/t$  ratio was increased to 50:1 to reduce the bending stresses. In addition, the splice plate was laminated instead of being tapered from thicker stock. Aerodynamic drag considerations precluded use of the stronger double strap joint with a transverse external strap. The basic problem with flush joint is that increased reinforcement also causes greater load path eccentricity.

Coupon testing during the PABST development phase showed that adhesive bonds fail progressively if the attached metal is maintained at, or in excess of, the yield stress. It should be noted that this is a sustained load problem. The same joint could withstand loads up to the metals ultimate strength if the load is applied rapidly. This phenomenon must be accounted for in the design of bonded splices for production aircraft by using the metal yield strength as the design allowable strength.

## Longerons

Two basic longeron cross sections were used for the FSDC. The internal longeron shape is a J-section and the external longeron shape is a bulb tee.

The J-section was selected in preference to the more efficient (in compression) Z-section since it was better suited for the bonding process adopted for the PABST Program. The bonding pressure applied to the outstanding flange of the J-section produces a more uniform bonding surface pressure when the flange against the skin is symmetrical with respect to the upstanding web. See Figure 14 for the detailed cross sectional shape. In addition, the symmetrical constant thickness flange with a chamfered edge provides the necessary flexibility at the edge to minimize peel action while providing the right angle intersection of the upstanding leg and flange for the mechanical splice of the longeron. The constant thickness was preferred for NDI for ease of inspection. The height of the longeron was selected on the basis of the minimum required for the splice and for adequate section properties. For additional details on the selection of the J-section see Reference 1.

The bulb T-section was selected over the other candidate shapes for the external longeron because it possessed more desirable features, including aerodynamic properties, than the other shapes while having a compression allowable strength nearly equal to the J-section. The cross sections were evaluated for ease of manufacture, assembly, repair, inspection and simplicity of design. For additional information see Reference 1.

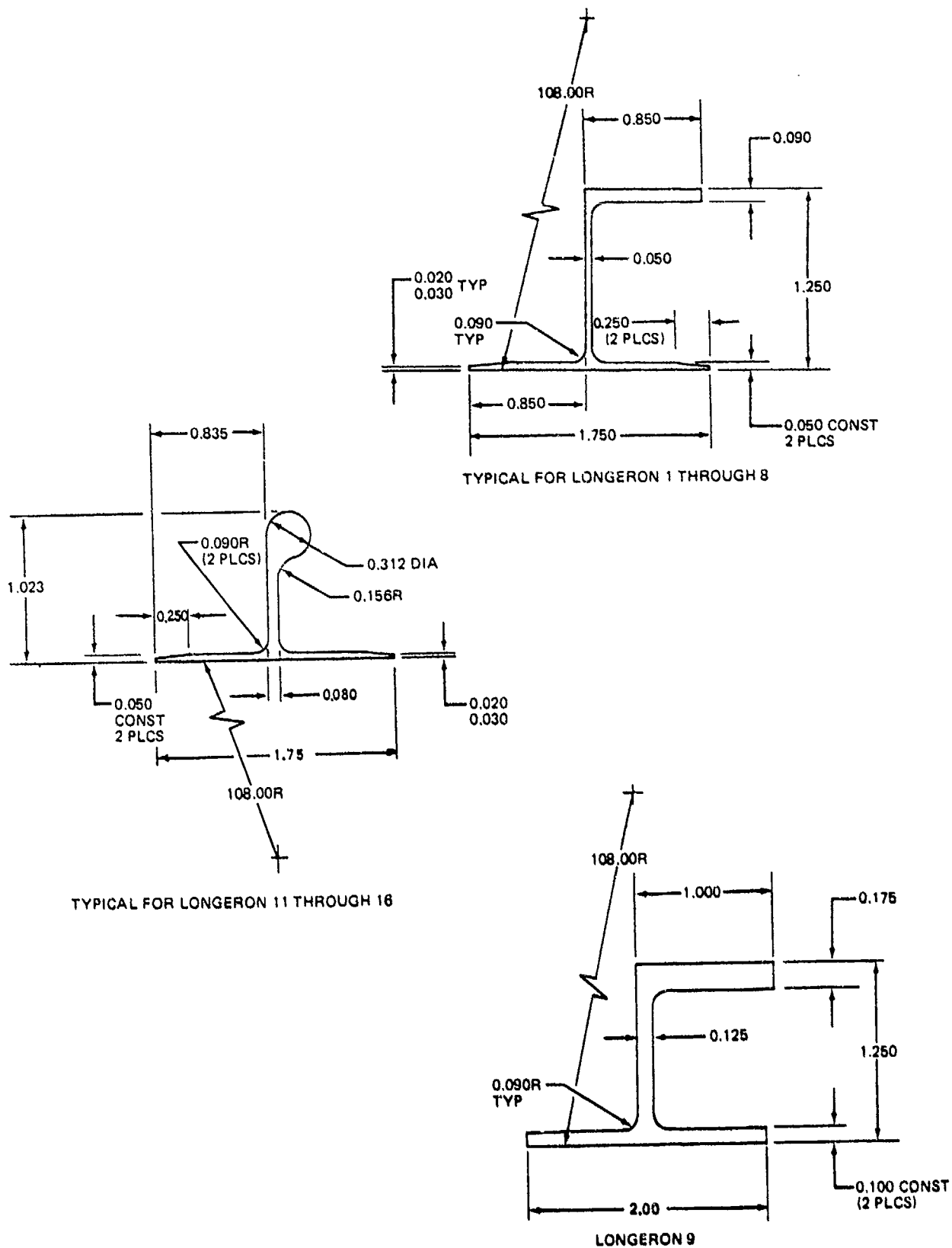


FIGURE 14. INTERNAL AND EXTERNAL LONGERONS

## Frames

Frames are required for circumferential stiffening of the fuselage shell. Spacing of the standard frames for the PABST FSDC is 24 inches. This spacing was that of the Baseline fuselage design, Reference 1. It did not appear possible to obtain a single optimum frame spacing for both the wide spaced and the close spaced longeron regions. The intermediate frames on the side panels are located mid way between the standard frames; i.e., 12 inches.

Typical Frames. - The typical frame cross section as selected for the FSDC and shown in Figure 15, was tailored to provide an acceptable structural section at minimum cost. The preliminary loads which were available at the beginning of the Detail Design Phase indicated that an overall frame height (skin inner surface to inner cap of the frame) could be 4.95 inches. However, the use of a new sheet metal frame cross section would have meant new stretch form dies with attendant high tooling costs and adverse schedules impact. The selected frame for the FSDC measures 5.78 inches in overall height. This dimension was chosen so that existing tooling used to stretch form sheet aluminum frame details for the YC-15 fuselage could be utilized.

A frame tee with cutouts to provide longeron continuity is bonded to the skin. A Z-section frame is attached to this shear tee by means of 0.188 inch diameter rivets spaced about 1.0 inches on center. Mechanical splices for the frames are staggered with respect to skin splices as shown in Figure 2. Frame/shear tee height is 4.95 inch in the nose section and 5.78 inch in the cargo compartment section as shown in Figure 15. In the nose section the frame thickness is 0.050 inch and 0.063 inch in the cargo compartment except under the wing where it is 0.080 inch. The frames are rolled 7075-T6 material. The floor support bulkhead frames are extruded 7075-T6 channel sections. The frame shear tees are 7075-T6 extruded T-sections.

Front and Rear Spar Frame Segments. - The fuselage frames at station 703 and station 847 are integrally stiffened numerically machined frames. They are

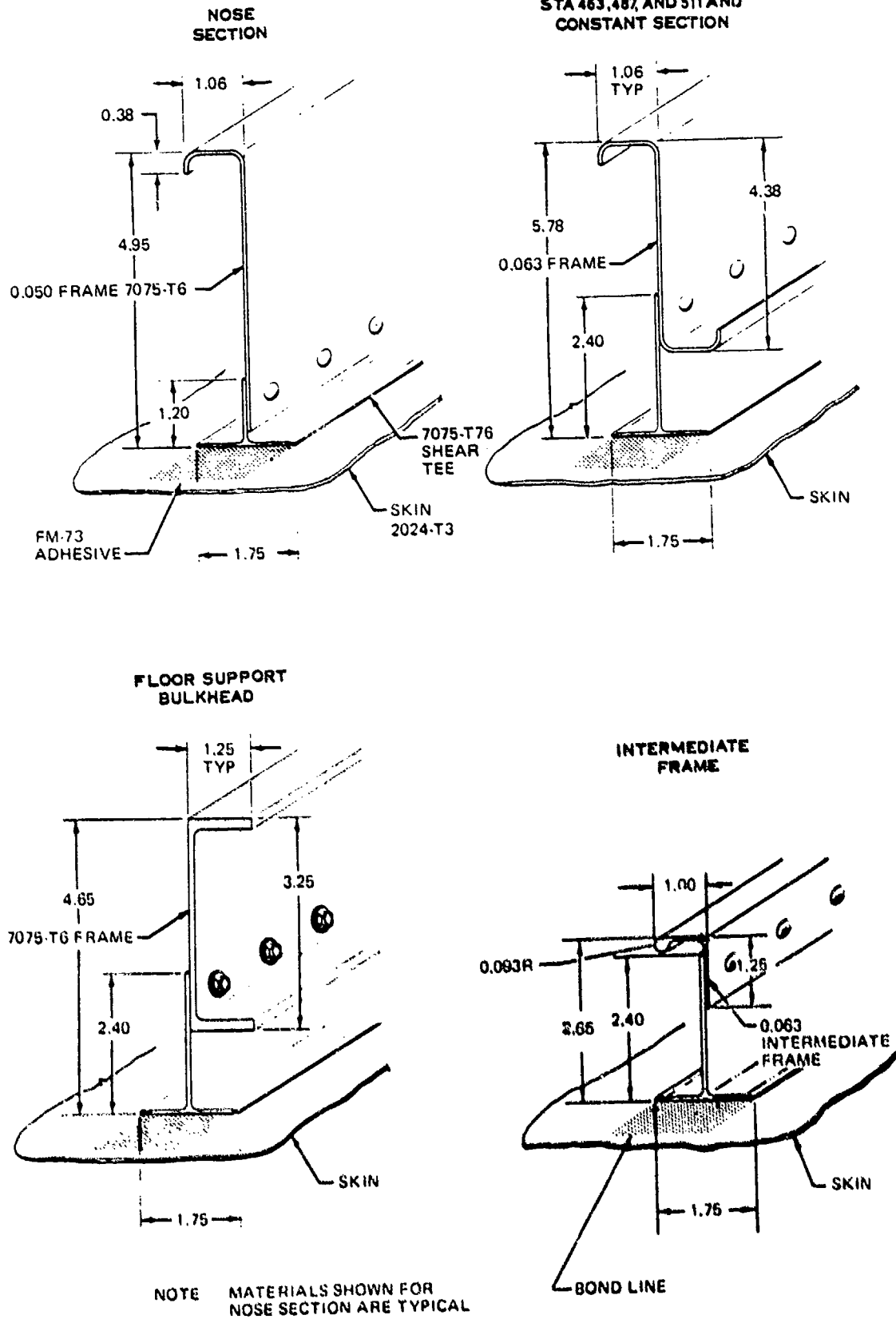


FIGURE 15. TYPICAL FRAMES

shown in Figure 16. These 7075-T411 frames are milled from 8.50 x 60 x 200 inch aluminum hand forgings and subsequently heat treated to a 7075-T73 condition.

Vertical loads from the wing front and rear spars were introduced into these frames and eventually sheared out into the fuselage side panels, Figure 5. On the Full Scale Demonstration Component, a vertical load simulating the wing aerodynamic lifting reaction was applied directly to the frame post at station 703. This procedure greatly simplified the design and construction of the wing assembly without adding extra design requirements to the frame.

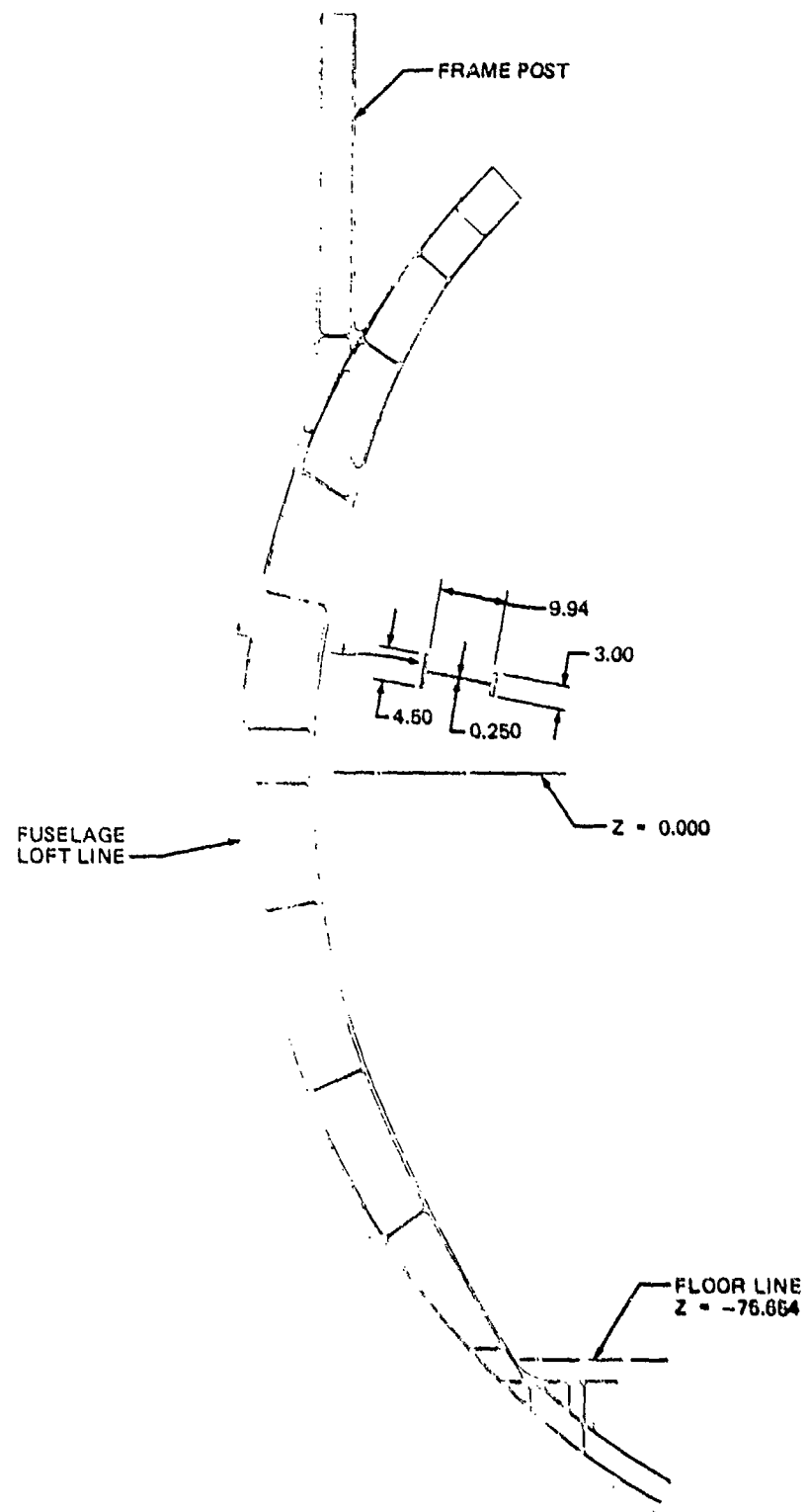


FIGURE 16. FRONT SPAR FRAME SEGMENT - STA 703.000

## Frame and Longeron Intersections

PABST panel tests have demonstrated that the design of the frame-longeron intersections is of major importance for all load conditions. The most critical FSDC design problem is where the frame shear tees are notched to permit the internal longerons to pass through uninterrupted.

Two notched shear tee designs for the internal longeron region were fatigue tested using stiffened flat panels (Reference 1, page 194). One design had the interrupted shear clips terminating on the skin. Fatigue cracks initiated at each frame/longeron intersection, grew together rapidly, and failed the panel. An artificially induced crack next to the longeron and halfway between the frames grew slowly by comparison and did not attain critical length. The second design had the shear tee notches terminating on a splice doubler instead of the skin alone. No fatigue cracks initiated.

The frame-bending test panel (Reference 1) developed adequate strength - but failed by crippling the outer frame flange over the longeron as soon as the skin to shear clip bond had begun to fail. A much lighter panel could have been made to withstand those same loads by improving the continuity of load path at that intersection.

Significantly higher shear and compression allowables were developed in test panels with external longerons; i.e., un-notched shear tees, than for internal longeron reinforced panels. The shear panel test results of Reference 1 show that for the same skin thickness the shear allowable was 18 percent higher for the external longeron. The allowable shear stresses for the external and internal longeron stiffened panels were 30,700 psi and 25,300 psi respectively.

The detail design of a notched frame shear tee should, therefore, minimize: (1) the crippling of the unreinforced outer flange of the frame at the intersection, and (2) the transfer of tensile load from the notched shear clip into the skin to prevent fatigue cracking next to the longeron. In addition, the cross sectional area of the interrupted stiffener must be

accounted for in determining the required bond width to preclude disbonding. In short, the panel strength of a bonded stiffened panel is even more critically dependent upon the details of the stiffener intersections than is the case for riveted construction.

The notched shear tees of the FSDC were designed with bonded doublers under the internal longerons or bonded doublers on the exterior of the skin to minimize skin cracking. However, the frame outer flanges were not reinforced. The general PABST design philosophy has been one of minimum reinforcement of known deficiencies only.

The weight of the fuselage shell structure design could be reduced by reinforcing the interrupted stiffeners to be equal in strength to the unnotched basic structure and then lightening the remaining structure to the requirements of the next lower failure mode.

Intersections. - A typical intersection in the cargo compartment for frames and internal longerons is shown in Figure 17. A 2024-T3 aluminum tear stopper is bonded under the longeron. The frame tee is cutout at this intersection to allow for the longeron. It is joggled to fit on top of the tear stopper to ensure that a continuous load path is attained across the cutout. A mechanically fastened shear tee ties the longeron to the frame to provide rolling stability.

On the sides of the fuselage shell where the longerons are wide spaced, intermediate frames are provided between the 24 inch spaced frames. These intermediate frames run from longeron 8 to longeron 10 (cargo floor plane). A typical intersection for an intermediate frame at longeron 8 is shown in Figure 18. The internal mechanical splice plate at longeron 8 is cutout to fit over the intermediate frame tee when the skin panels are mechanically joined together. Two back-to-back splice angles tie the intermediate frame and the longeron 8 flange together with 0.188 inch diameter lockbolts.

A typical intersection for the nose frame and longeron is shown in Figure 19. The tear stopper ends at the base of the frame tee and the longeron extends over and is bonded to the base of the frame tee. In addition, two

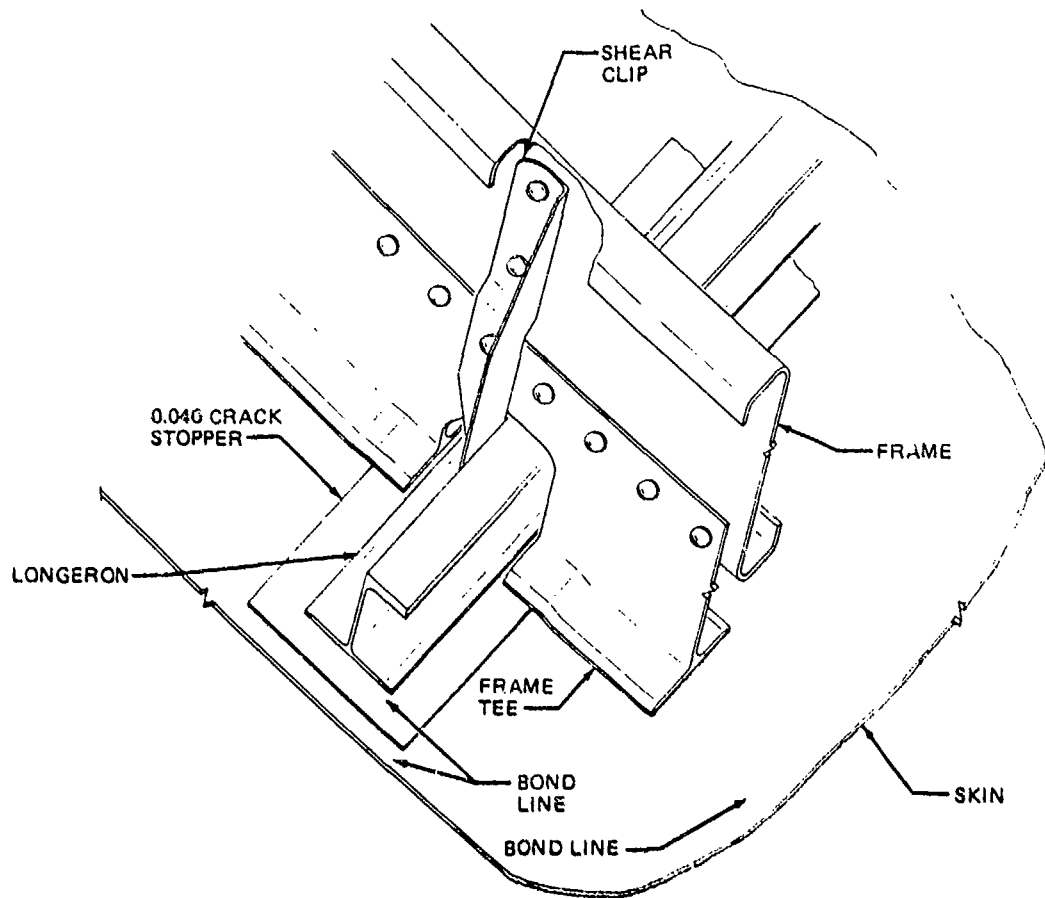


FIGURE 17. TYPICAL FRAME/LONGERON INTERSECTION

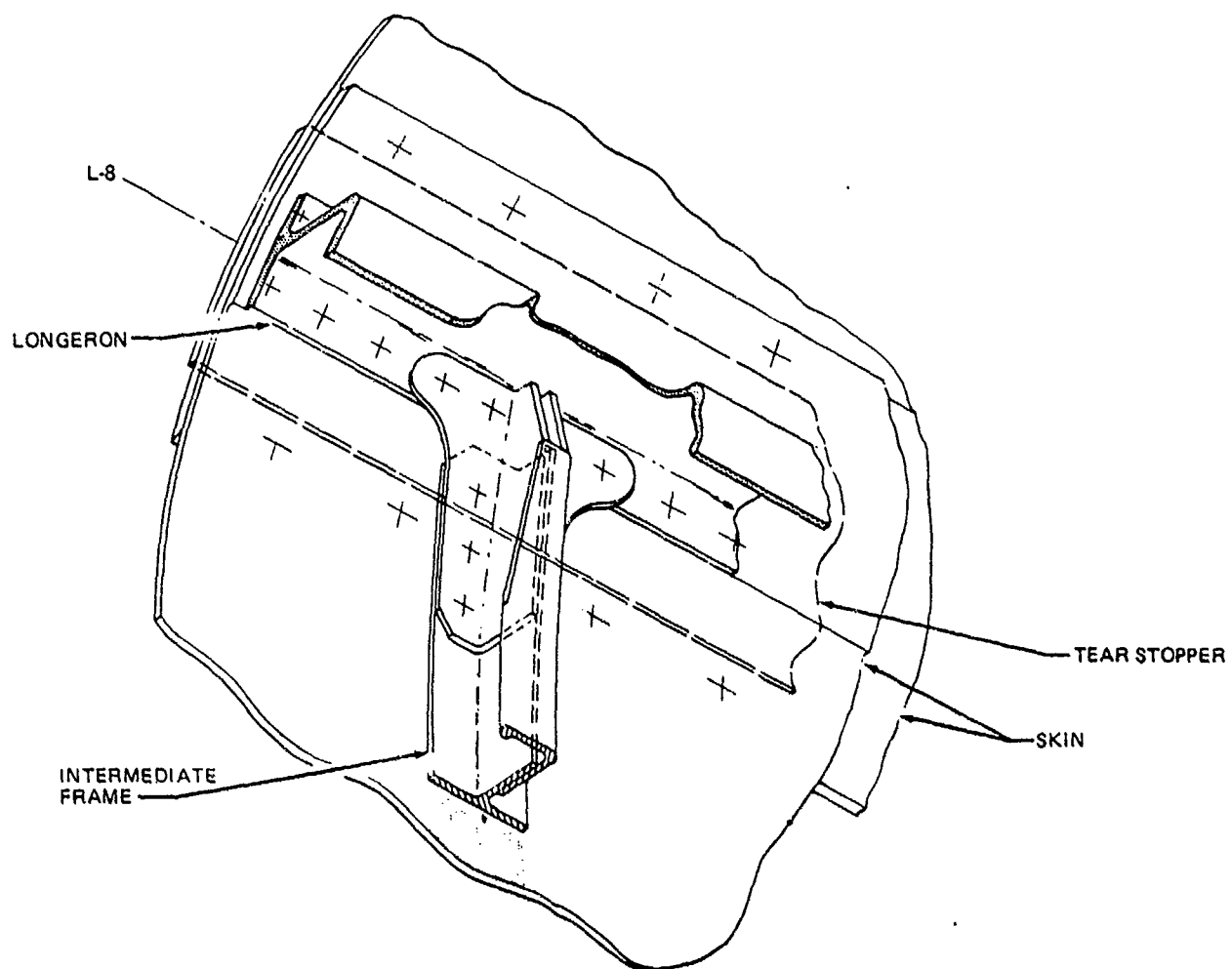


FIGURE 18. TYPICAL LONGERONS AND INTERMEDIATE FRAME INTERSECTION

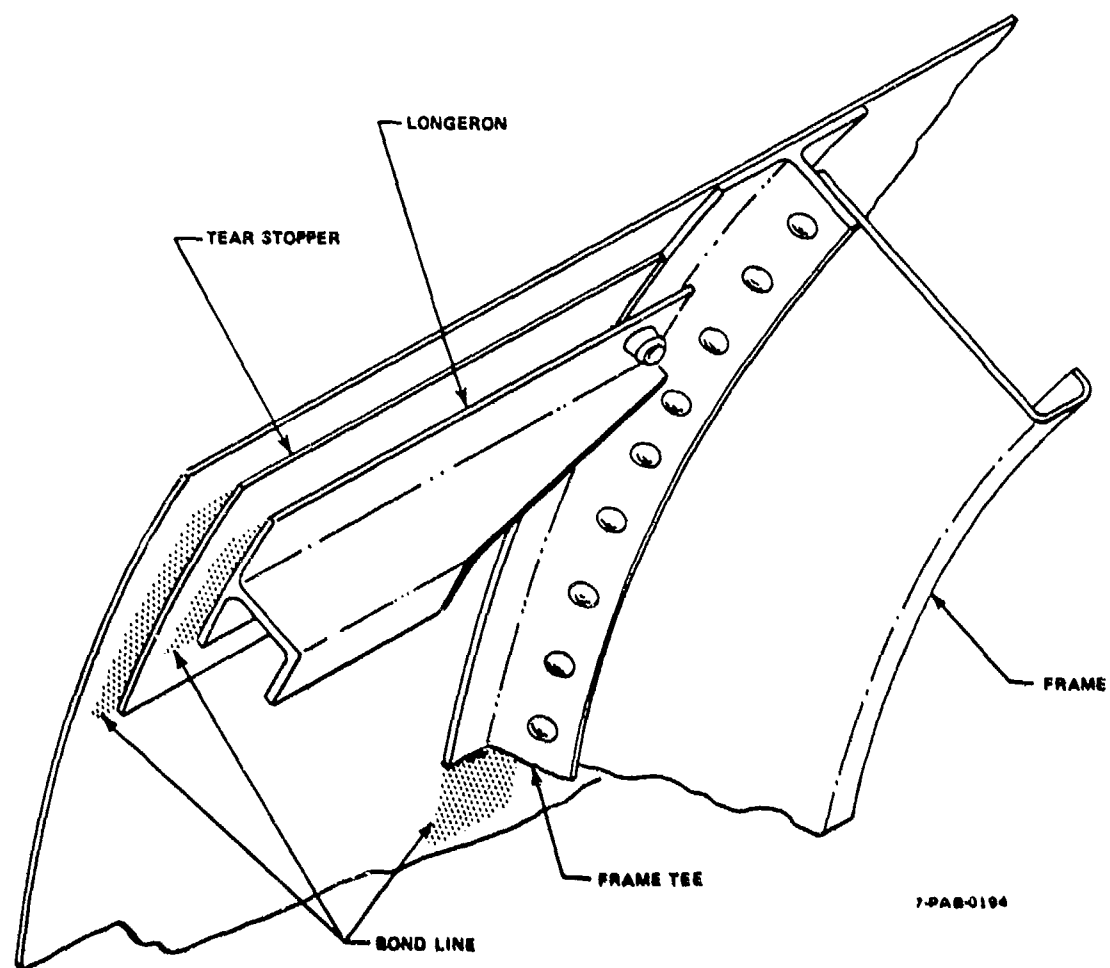


FIGURE 19. TYPICAL NOSE FRAME AND INTERNAL LONGERON INTERSECTION

steel bolts fasten the longeron, frame tee and skin together. After the assembly is hot bonded the frame is mechanically fastened to the frame tee with aluminum rivets.

A typical intersection for the nose frame and bonded skin splice is shown in Figure 20. The nose frame tee stops short of the skin doublers. The skin, skin doublers, and frame tee are hot bonded together. After bonding the frame is installed with aluminum rivets. Two back-to-back angles and a filler plate are used to splice the frame tee across the bonded skin splice. Flush 0.188 inch diameter lockbolts tie the angles to the frame tee, skin, and skin doublers. Aluminum rivets tie the angles and filler plate to the vertical frame tee and frame web.

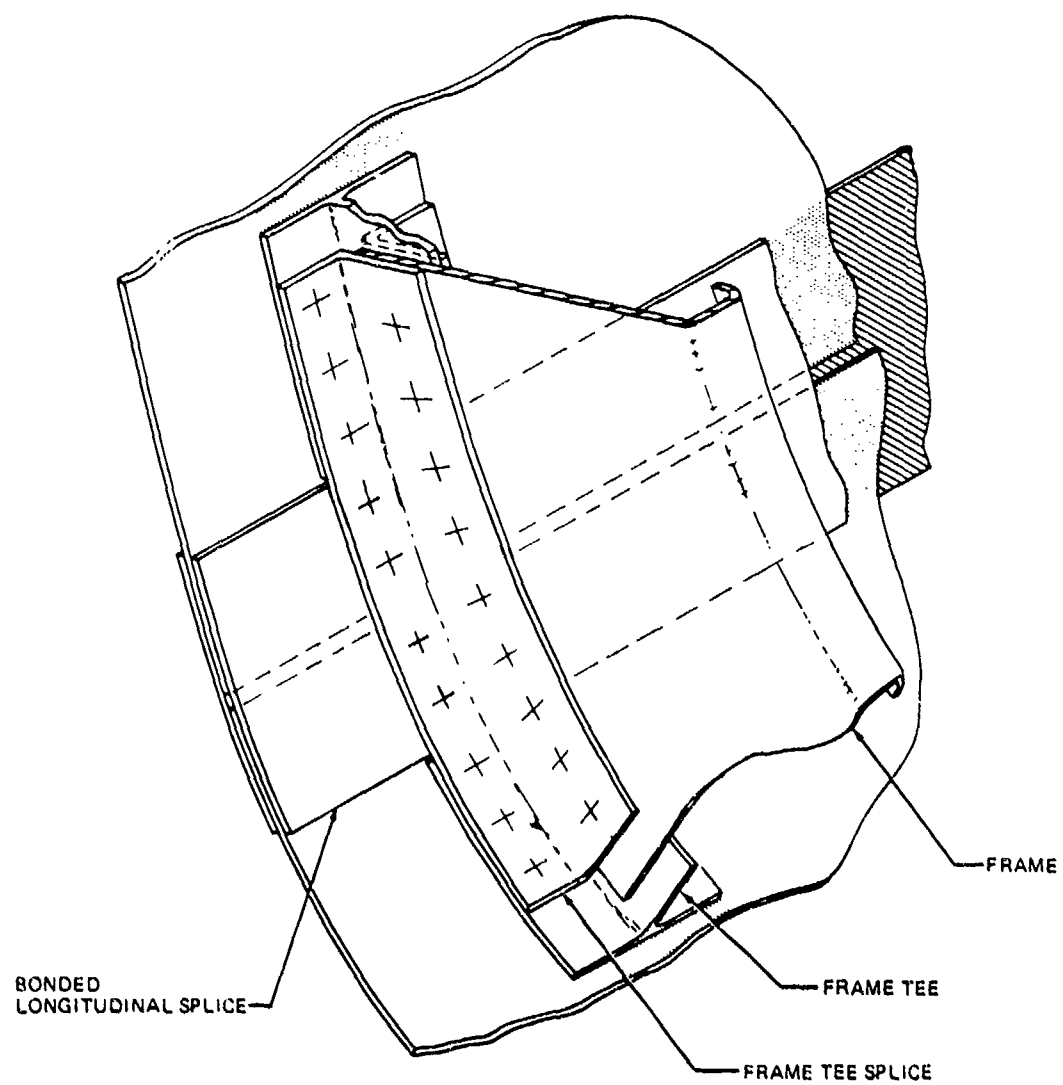


FIGURE 20. TYPICAL NOSE FRAME AND BONDED SKIN SPLICE INTERSECTION

## Intercostals

The intercostals are installed in various locations throughout the FSDC as shown in Figure 21. They were physically designed to function as frame stabilizing members (Figures 22 & 23), axial load carrying members (Figure 24), floor-to-fuselage shell shear tie members (Figure 25), and door jamb stabilizing members (Figure 26).

The frame stabilizing intercostals are located (a) in every other bay in areas where the frames are full depth (Figure 22) and (b) in areas where the shallower depth intermediate frames are installed (Figure 23), and (c) also located between every frame from station 679.000 to station 847.000 and positioned below the lower wing skin. These intercostals function as closing members for the under wing doubler. They also provide a reaction point for the frame stabilizing channel located forward of station 679.

The design of the frame stabilizing channels was straight forward with a minimum number of intercostal parts thereby reducing costs and weight. This design can only be applied where the eccentric load transmitted to the channel is held to a minimum. This is only found in the constant section of the FSDC where it is an inline longitudinal configuration.

Axial load carrying intercostals (Figure 24) were located between stations 367 thru 451 in the non-constant section where longerons were not present to carry axial loads. Obviously, these intercostals also function as frame stabilizers.

The floor intercostals were provided to transmit the floor shear loads into the fuselage shell as shown in Figure 25. For a further discussion, see the section on floors.

Door jamb intercostals (Figure 26) located around the door cutout are designed to give a solid reaction point for the door stop from the load transmitted by the door. The intercostals also stabilize the adjacent door

jams and jamb frames.

In the area between stations 439 thru 871 and bounded by longeron 8 on the left side and longeron 8 on the right side, the longeron frame attach clips stabilize the frame, consequently no intercostals were required as shown in Figure 21. Below the floor and between stations 439 and 871, longeron 13 left side and longeron 13 right side, a channel member (keel) stabilizes the frames.

The structural arrangement of all intercostals is basically the same. They are made up of (1) clips that attach to the frames, (2) a tee that is bonded to the skin and attached to the clips, (3) an intercostal angle that is mechanically fastened to the tee and clips, (4) a gusset attaching the intercostal angle to the frame, and (5) a filler.

The fillers occupy the gaps under the tees which allows the tees to be made in straight pieces without joggles to reduce manufacturing costs. The fillers are designed to overlap on the skin approximately 1/2 inch beyond each side of the tees to simplify and aid inspection. Skins that required chem-milling for doublers, etc., also utilized the extra available skin thickness to provide chem-milled steps where the filler would normally be placed under the tees. Consequently, separate bonded fillers were unnecessary on these panels.

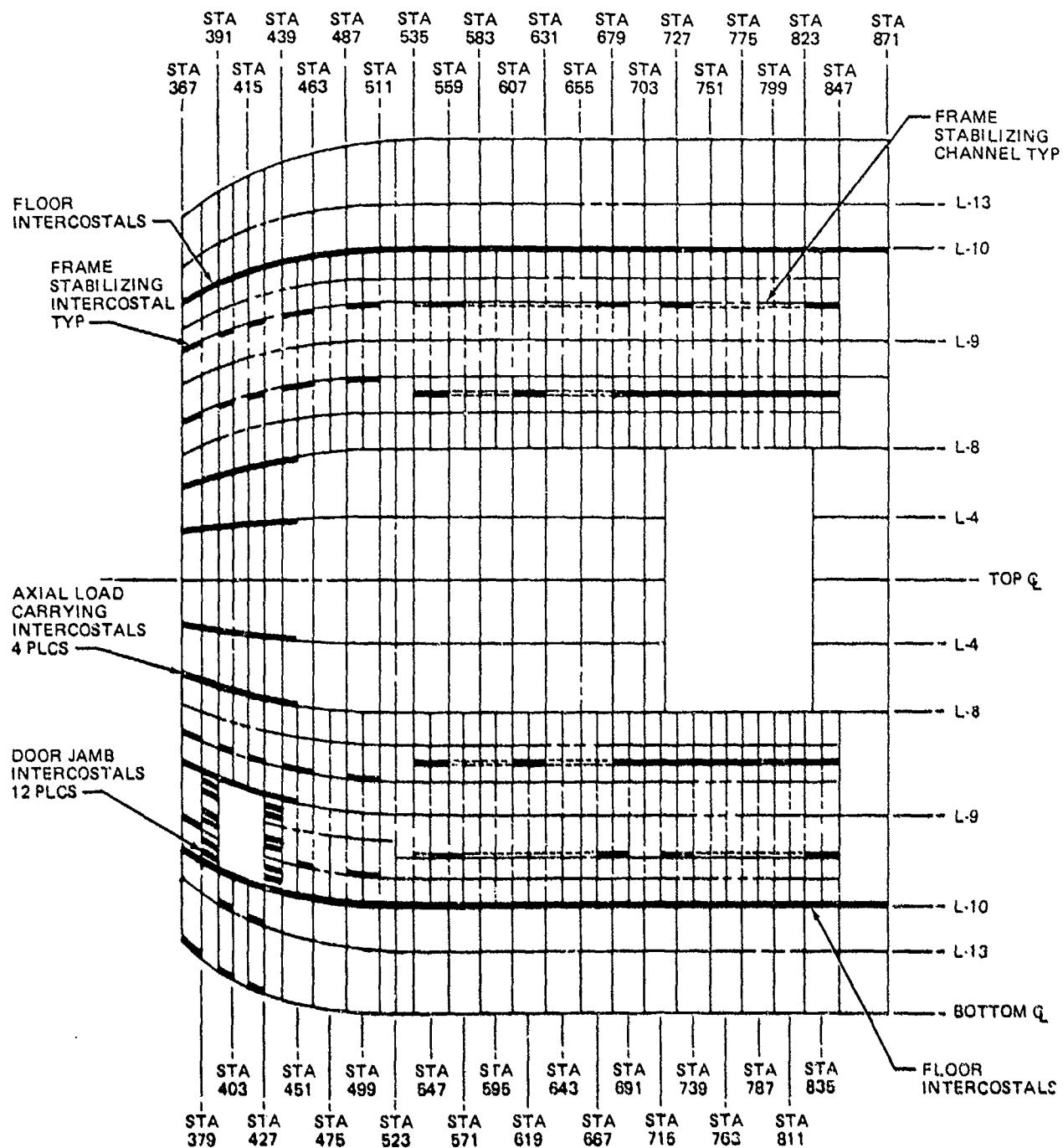


FIGURE 21. INTERCOSTAL LOCATIONS

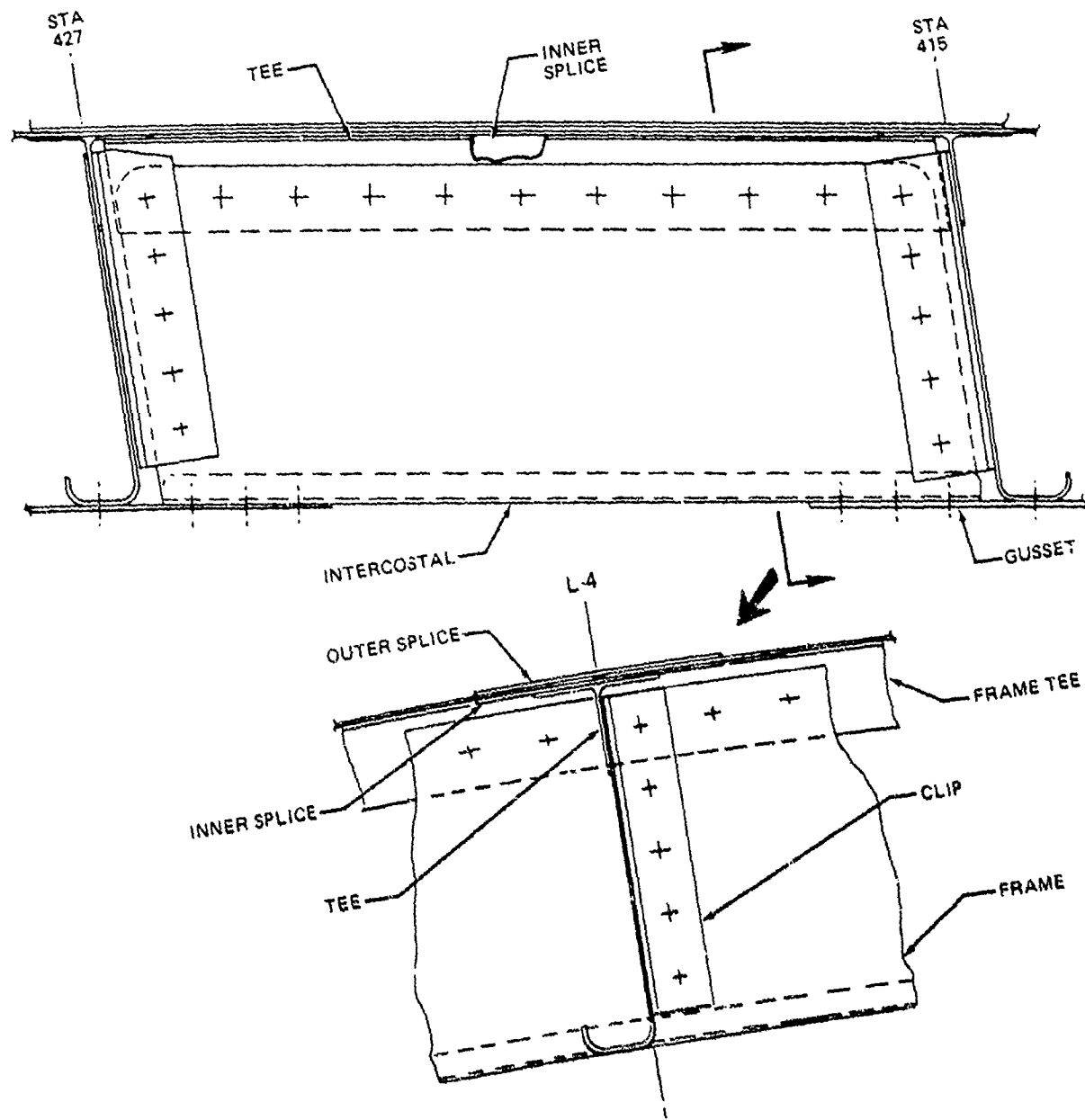


FIGURE 22. FRAME STABILIZATION INTERCOSTAL

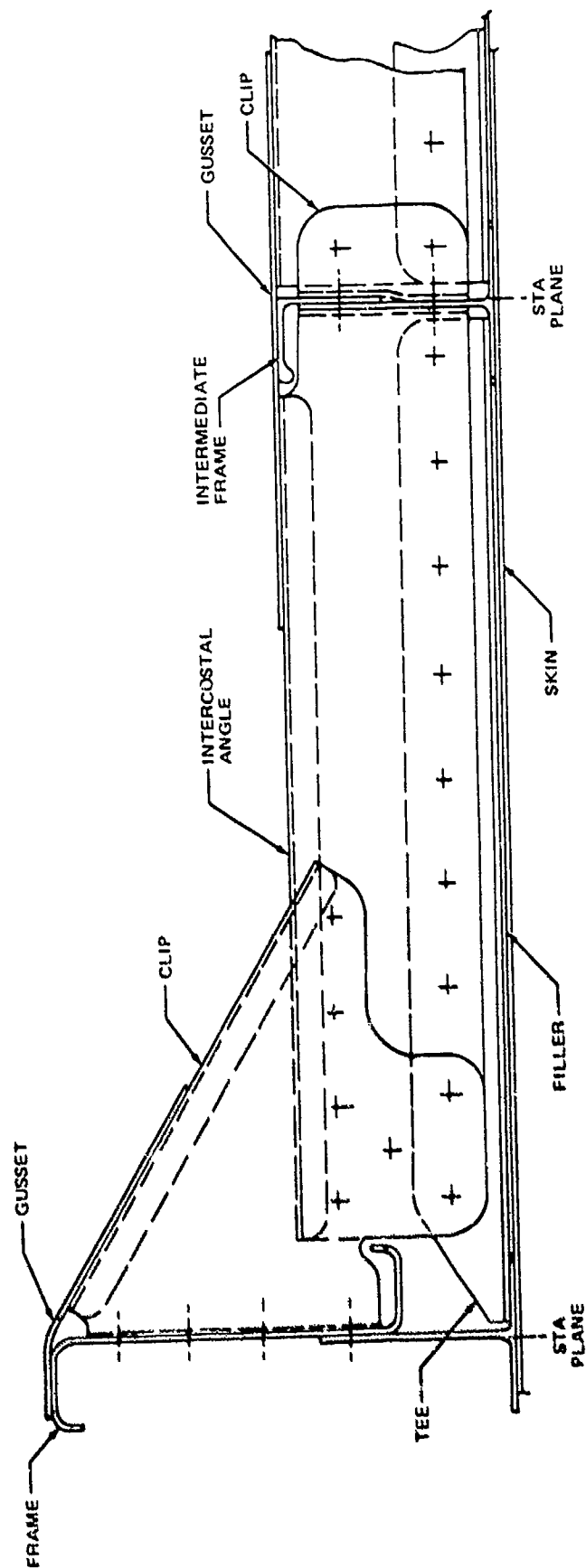


FIGURE 23. FRAME STABILIZATION INTERCOSTAL

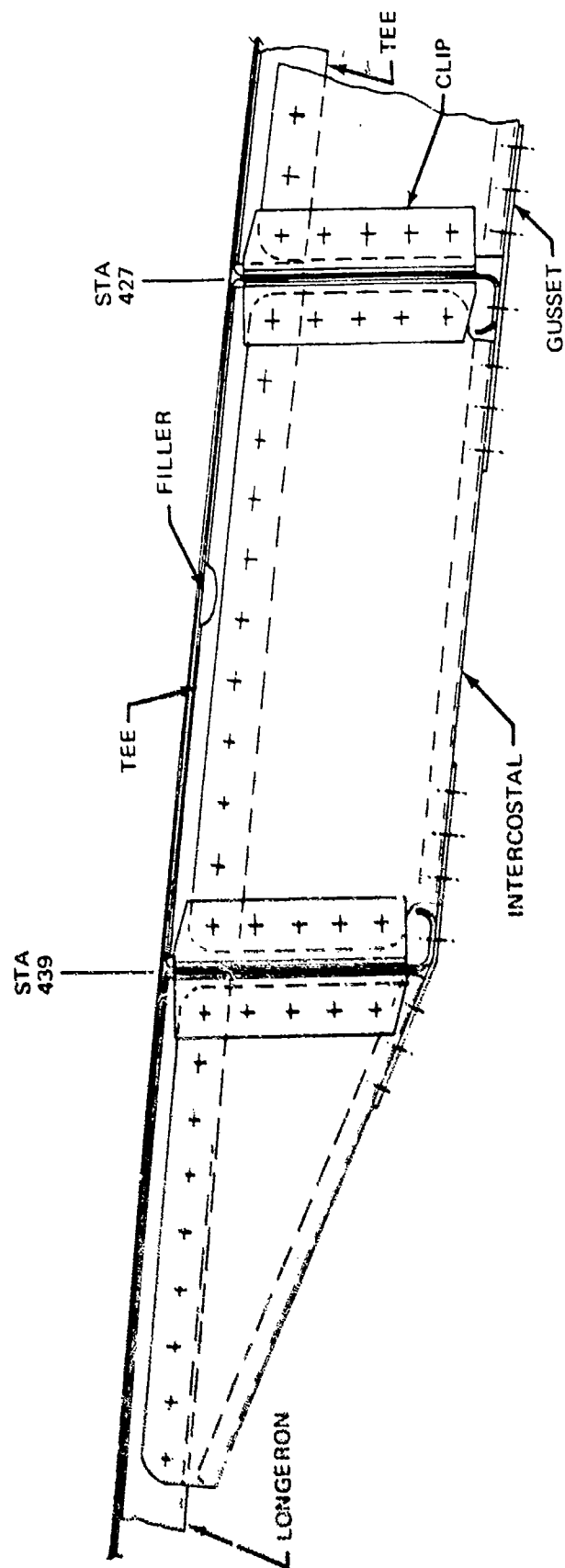


FIGURE 24. INTERCOSTALS FORWARD OF STATION 439

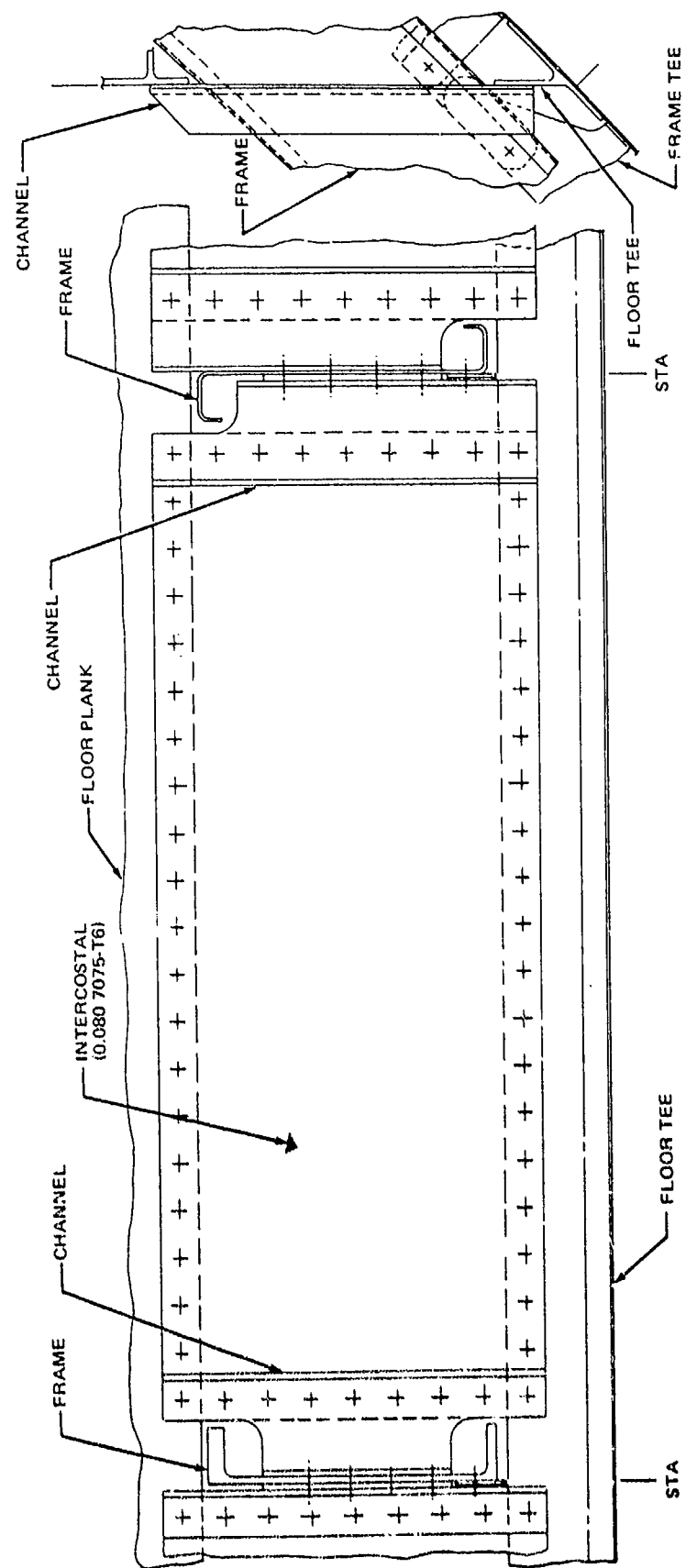


FIGURE 25. FLOOR TO FUSELAGE INTERCOSTAL

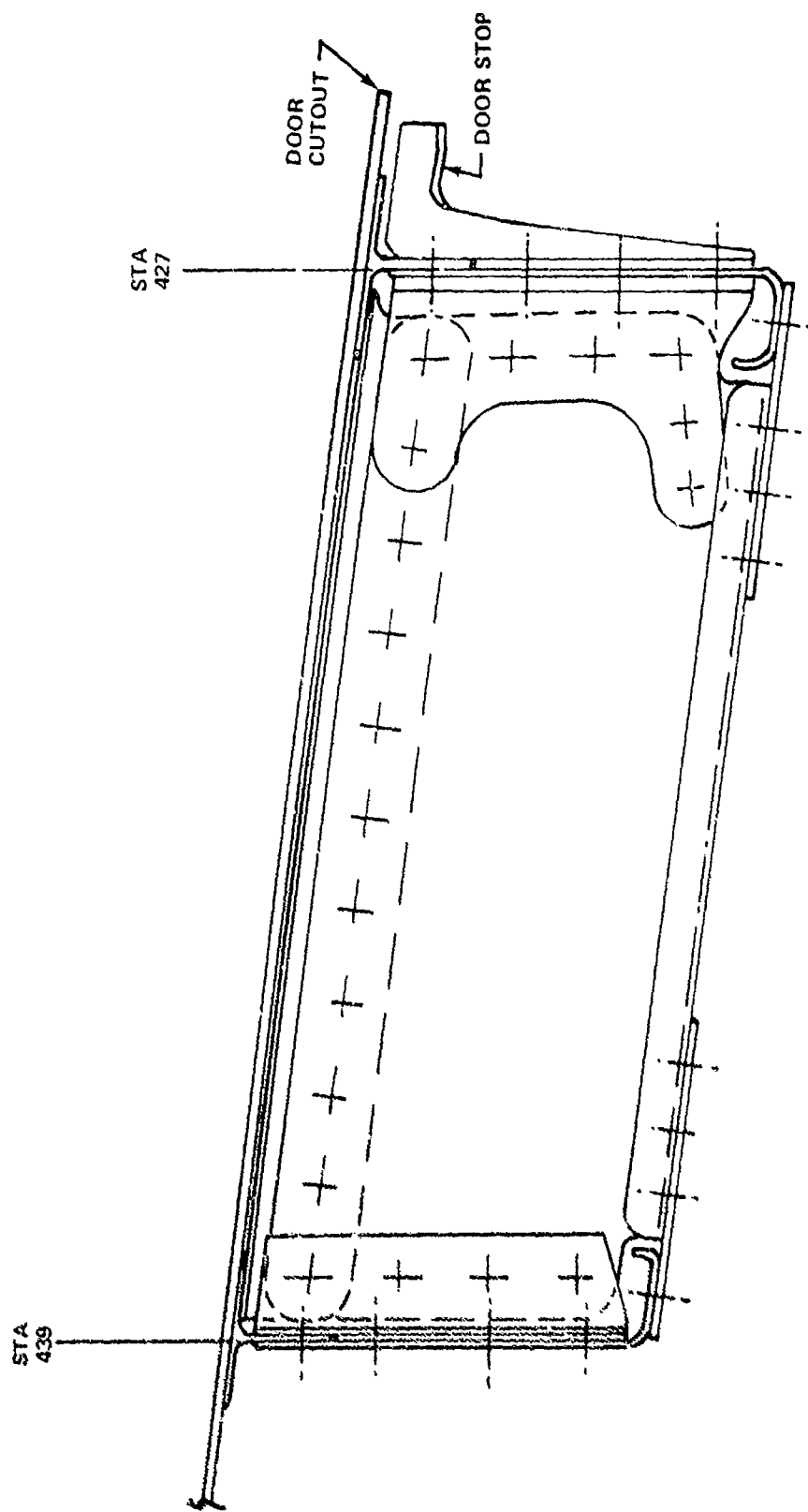
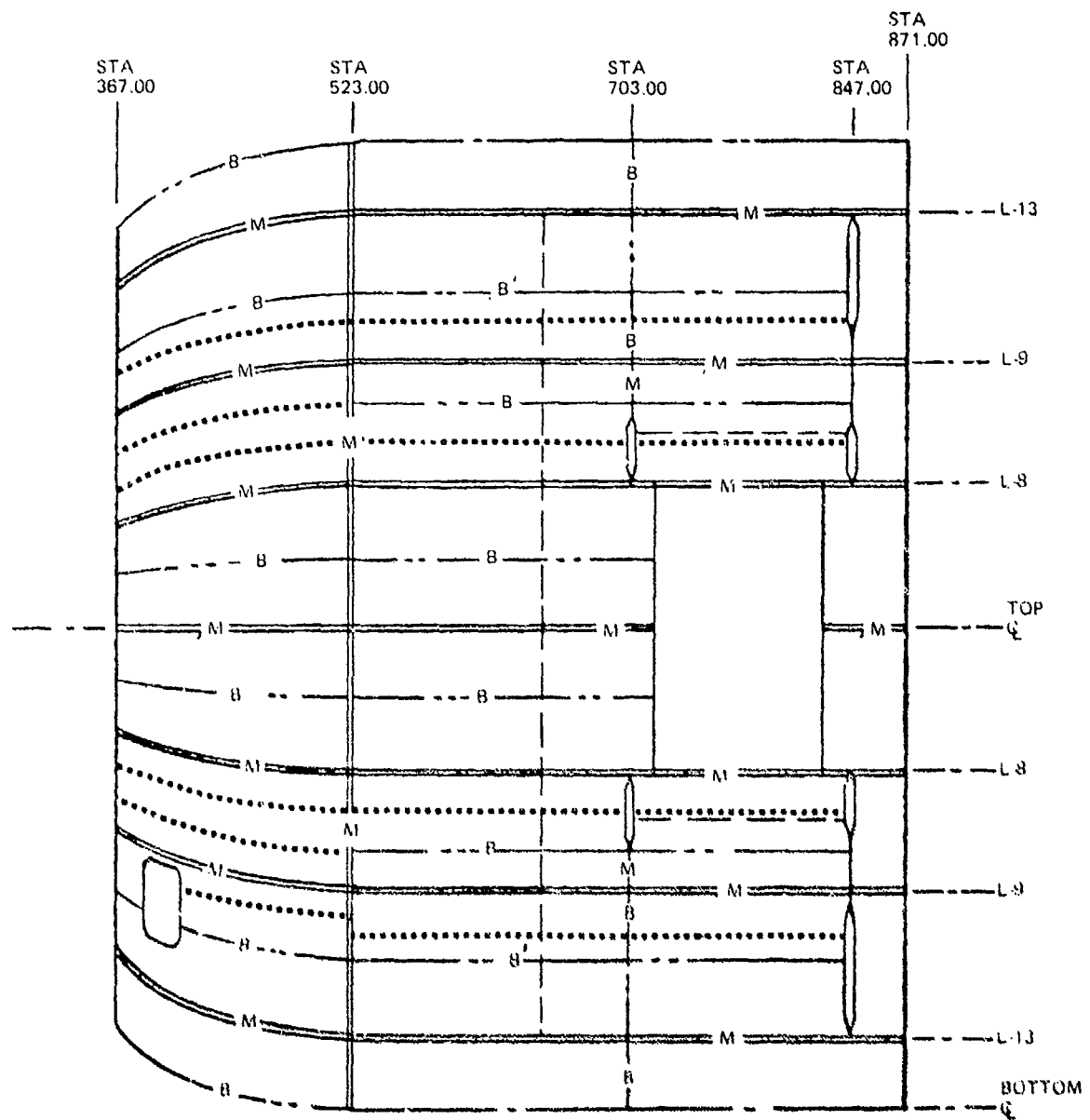


FIGURE 26. DOOR JAMB INTERCOSTALS

## Tear Stoppers

Tear stoppers were located around the fuselage in a longitudinal orientation to satisfy the slow crack growth and residual strength requirements per MIL-A-83444 "Airplane Damage Tolerance Requirements." Fail safe capability is equivalent to Douglas commercial airplanes currently in service. Tear stoppers were required in the wide spaced longeron side panels only. The close spaced longeron upper and lower skin panels did not require tear stoppers because the panel dimensions were such that the criteria flaw did not attain critical dimensions in the transverse direction. Cracks in the longitudinal direction were effectively stopped by the bonded frame shear tees. Tear stoppers are discussed in detail in the Damage Tolerance section of this report.

Three 7475-T761 bonded longitudinal tear stoppers, 0.071 in. x 3 in., are provided externally on the side where the longerons are wide spaced in the forward fuselage as shown in Figure 27). Two tear stoppers, approximately 27 inch spacing, are located between longerons 8 and 9. The panel assembly between longerons 9 and 10 has one tear stopper below longeron 9, approximately 30 inch spacing, and a bonded longitudinal splice which functions as a tear stopper located close to longeron 10. The constant section of the fuselage has two 7475-T761 bonded tear stoppers located on the wide spaced side panels. The panel assembly between longerons 8 and 9 has one tear stopper plus a bonded longitudinal skin splice which functions as a tear stopper. The panel assembly between longerons 9 and 10 is similar to the previously described panel between longerons 8 and 9. For additional information see the discussion on tear stoppers in the Trade Studies Section titled Damage Tolerance Parametric Studies.



NOTE: .... DENOTES 0.071 x 3 x 7475-T761 TEAR STOPPER

FIGURE 27. BONDED TEAR STOPPERS

## PANEL DESIGN

There are three different types of skin panel designs on the FSDC. These are the internal close spaced longeron panels located at the upper half of the fuselage, the external closed spaced longeron panels located in the lower section of the fuselage and last the wide spaced longeron panel located at the fuselage sides. Figure 28 shows the locations of all panel boundaries as well as their relationship with one another.

Panel boundaries were situated at the maximum dimensions based on manufacturing and tooling constraints, existing autoclave size limiting panel arc length to 113 inches, the fuselage configuration requirements and vendor manufacturing constraints based on the skin width of 94 inches for 0.050 inch thick skin. These limitations are best represented by the following panels. Panel 5A and 14A, first panels installed in the fuselage assembly fixture, were designed to be cradled in this fixture thus eliminating the bottom center line splice and therefore simplifying tooling. The panel width constraint was thus based on the maximum skin width of 94 inches. Due to autoclave width limitations and a natural manufacturing break at longeron 8, panels 1A, 1B, 9A, 9B were butt spliced at the top center line of the fuselage. 3A panel had special constraints imposed on it. Besides limiting its size to the autoclave dimensions a large door was designed into this panel of sufficient size to allow for the passage of an integrally bonded upper jamb header. A circumferential mechanical splice was provided at the boundary between the constant section and the double contoured nonconstant section to simplify tooling requirements as well as to simulate an actual manufacturing break that normally would be required for a production fuselage. Due to the massive loads introduced from the wing and main landing gear it was necessary to allow for the continuation of the one piece hand forged frame segments to pass through the fuselage skin panels. Therefore a panel boundary was designed at station 703 and station 847.

The minimum skin thickness over the entire fuselage was set at 0.050 inch based on foreign object damage criteria. To satisfy fatigue criteria for the

FSDC, 2024-T3 bare aluminum alloy was chosen for all skins and doublers. The skin thickness ranges from a minimum of 0.050 inch in the area forward of the wing to a maximum of 0.10 inch near the rear spar frame where shears are high due to the landing loads induced by the main landing gear and to the flight loads induced by the wing.

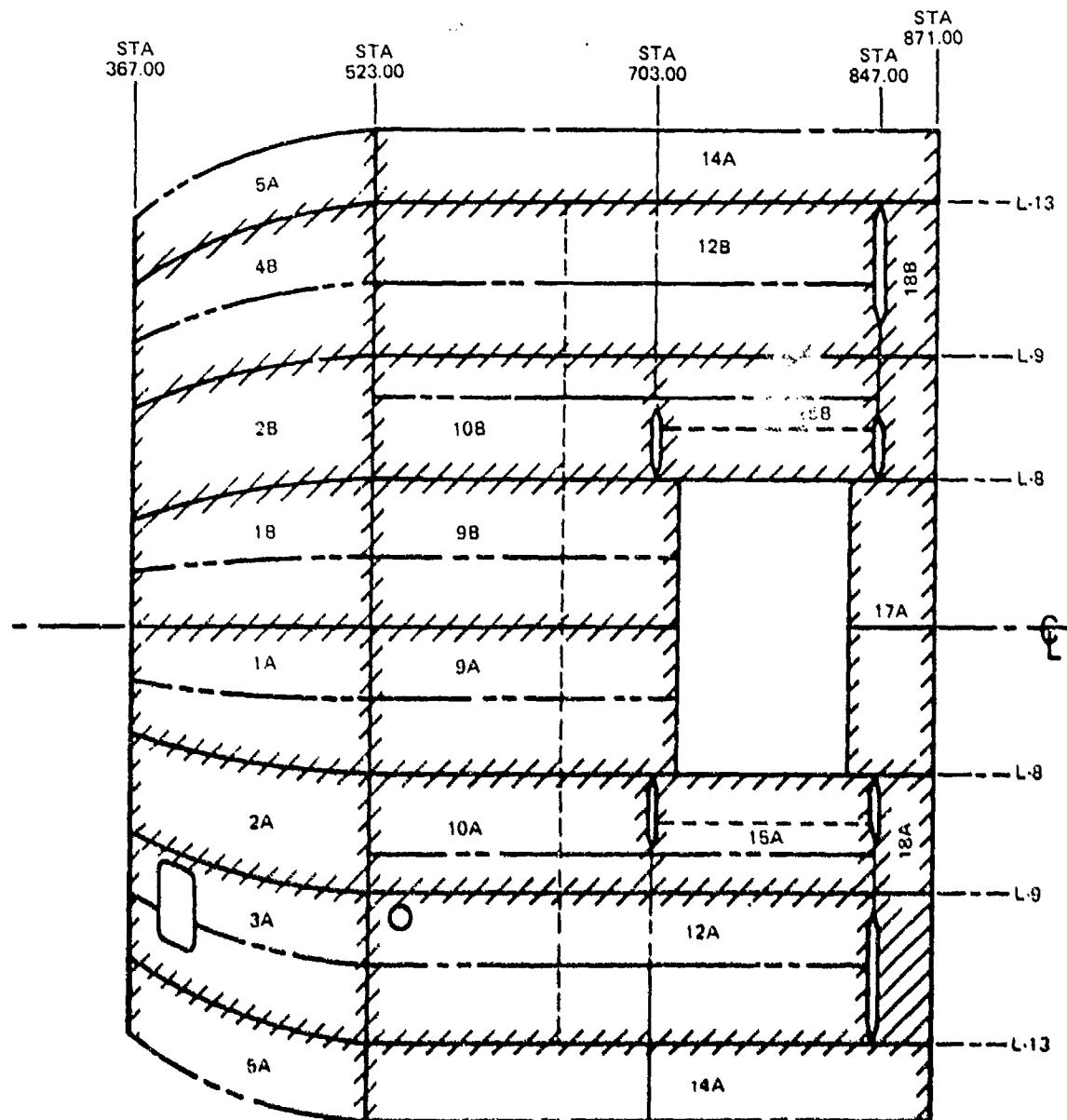


FIGURE 28. PANEL LOCATION

## Constant Section Panels

The constant section extends from station 523 to 871 at the strong back test fixture as shown in Figure 28. All longerons and frames are continuous to station 871 except at the interface of the simulated wing assembly and fuselage. Longitudinal mechanical splices are positioned at longerons 1, 8, 9 and 13. At station 523 the constant section panels are butt spliced to the non-constant section with mechanical fasteners.

Internal Longeron Panels. - A typical close spaced internal longeron panel assembly 9A, is shown in Figures 29 and 30. The panels extend from station 523 to station 720 and from longerons L-8 left to L-8 right. The panels consist of left and right bonded assemblies and are joined mechanically at longeron 1. Each bonded assembly is stiffened longitudinally by extruded J-section longerons and bonded internally with tear-stoppers under each longeron for failsafe requirements. These 7075-T6511 extruded aluminum longerons are spaced approximately 15 inches on center. Typical dimensions for the internal J-section longerons are shown in Figure 14. Due to the size of the panel a longitudinal bonded skin splice is provided at L-4. The basic skin thickness is 0.071 that is chem-milled to 0.060 inches between longerons in the forward half of the panel where skin shears and axial loads in the longerons are relatively low. Additional doublers are bonded externally to the aft end of the panel to carry the high shear load induced from the front spar. Machined fittings in longerons 1 and 4 are transferring loads from the links across wing cavity to the fuselage shell are installed mechanically as shown in Figure 29. Frame tees spaced 24 inches from station 535 are bonded to the skin. They are locally cut out for each longeron and are joggled on top of the tear-stoppers to minimize fatigue problems in the skin. A typical frame tee and internal longeron intersection is shown in Figure 17.

External Longeron Panel. - A typical close spaced external longeron panel assembly 14A, is shown in Figures 31 and 32. This panel extends from station 523 to station 871 and from longeron 13 left to L-13 right. It measures approximately 8 ft wide x 29 ft long. The longerons are bulb T-sections that were

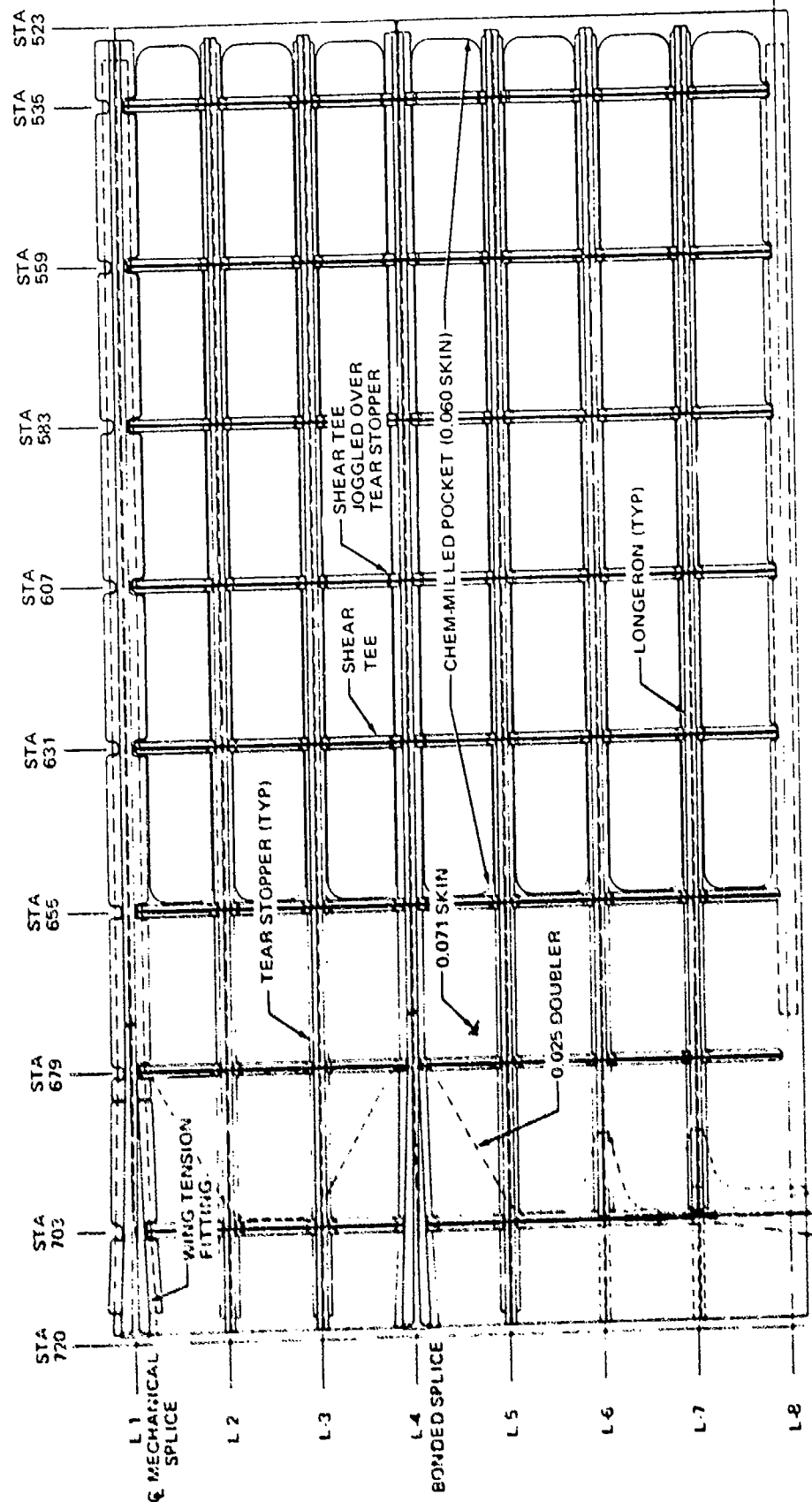


FIGURE 29. CONSTANT SECTION CLOSE-SPACED INTERNAL LONGERON PANEL

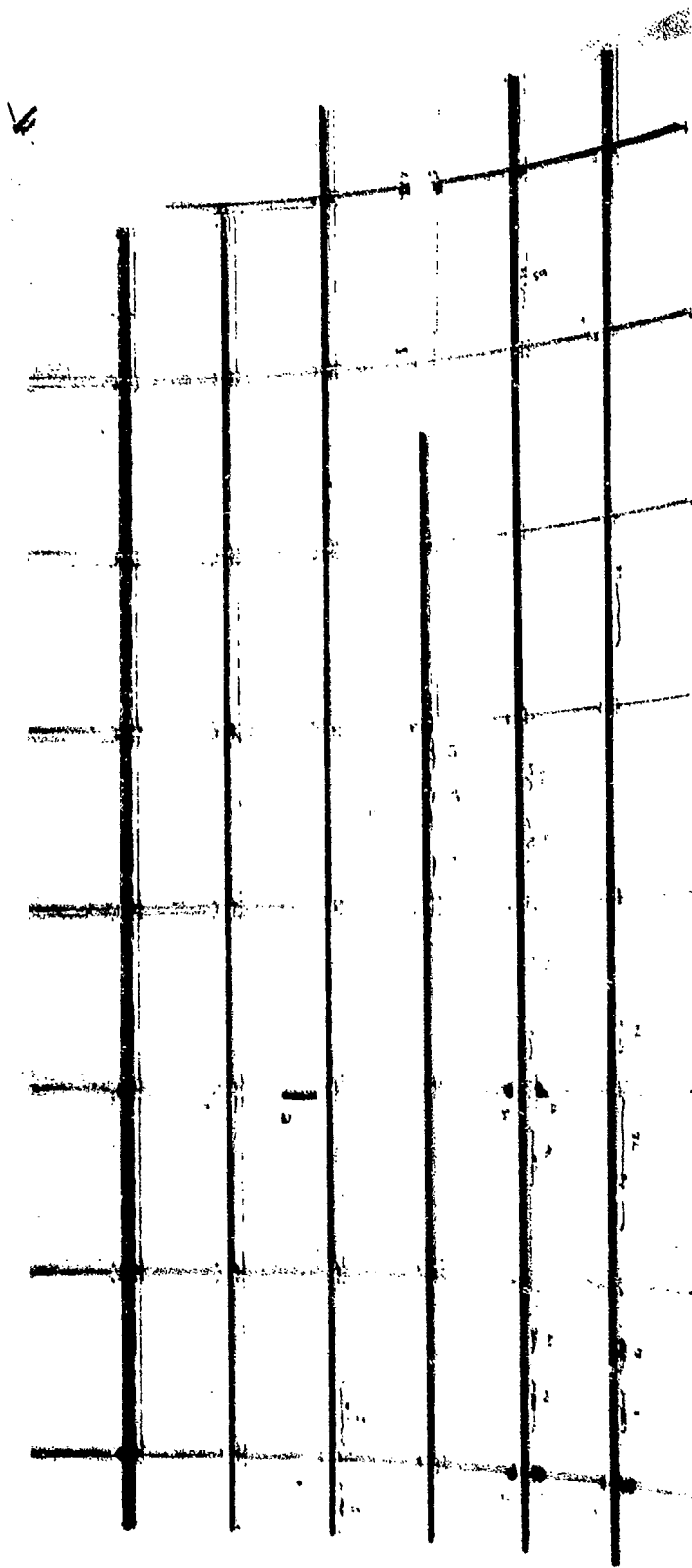


FIGURE 30. PHOTOGRAPH OF CONSTANT SECTION CLOSE-SPACED INTERNAL LONGERON PANEL

previously discussed. Typical dimensions for a basic external longeron are shown in Figure 14. The longerons were spaced approximately 13.5 inches on center except additional external longerons were added at the end of the panel to carry the high compressive axial loads induced by the test external load conditions. Internal and external doublers are bonded to the aft section of the panel to provide an interface with the strong back test fixture. Due to the excessive length of the panel, a transverse bonded skin splice was located at station 703 as shown in Figure 13. The longitudinal mechanical skin splice at L-13 was previously discussed and shown in Figure 10. Cutouts are not required in the bonded frame tees due to the external location of the longerons. This eliminates a chronic problem that arises at the frame-longeron intersection with internal longeron panels.

The external longeron panel also has a 0.375 inch diameter hole in every bay to provide drainage for water or bilge fluid that may accumulate in the bottom of the fuselage.

Wide Space Longeron Panels. - A typical side panel 12A, with wide-spaced longerons is shown in Figure 33 and 34. All the side panels are similar to one another in their structural arrangement. Longerons are wide spaced from L-8 to L-9 and from L-9 to L-10. In the longitudinal bonded skin splice, the external splice doubler is uninterrupted over the entire length of the panel while internal splice doublers are interrupted and joggled on top of frame tees. 7475-T761 external tear-stoppers, 0.071 x 3.00 wide, are bonded longitudinally to provide added fail-safe capability in these panels. Additional frame tees and light frames between full depth frames are also provided in order to increase the initial buckling strength of the skin. Intercostals and straps are located between longerons to stabilize each frame.

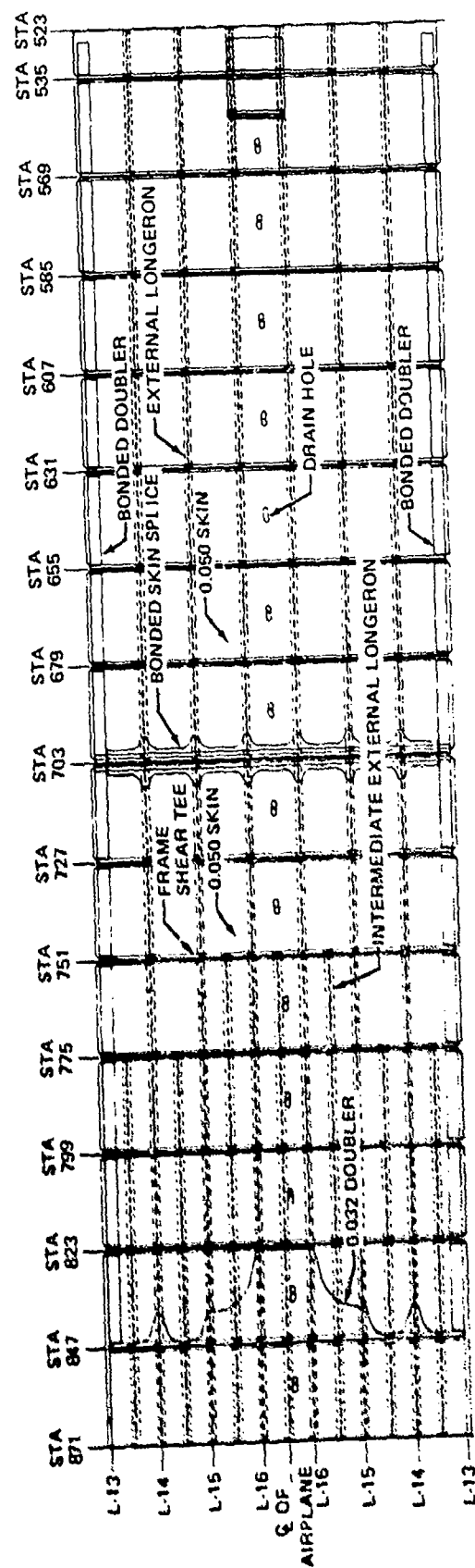


FIGURE 31. CONSTANT SECTION CLOSE-SPACED EXTERNAL LONGERON SKIN PANEL

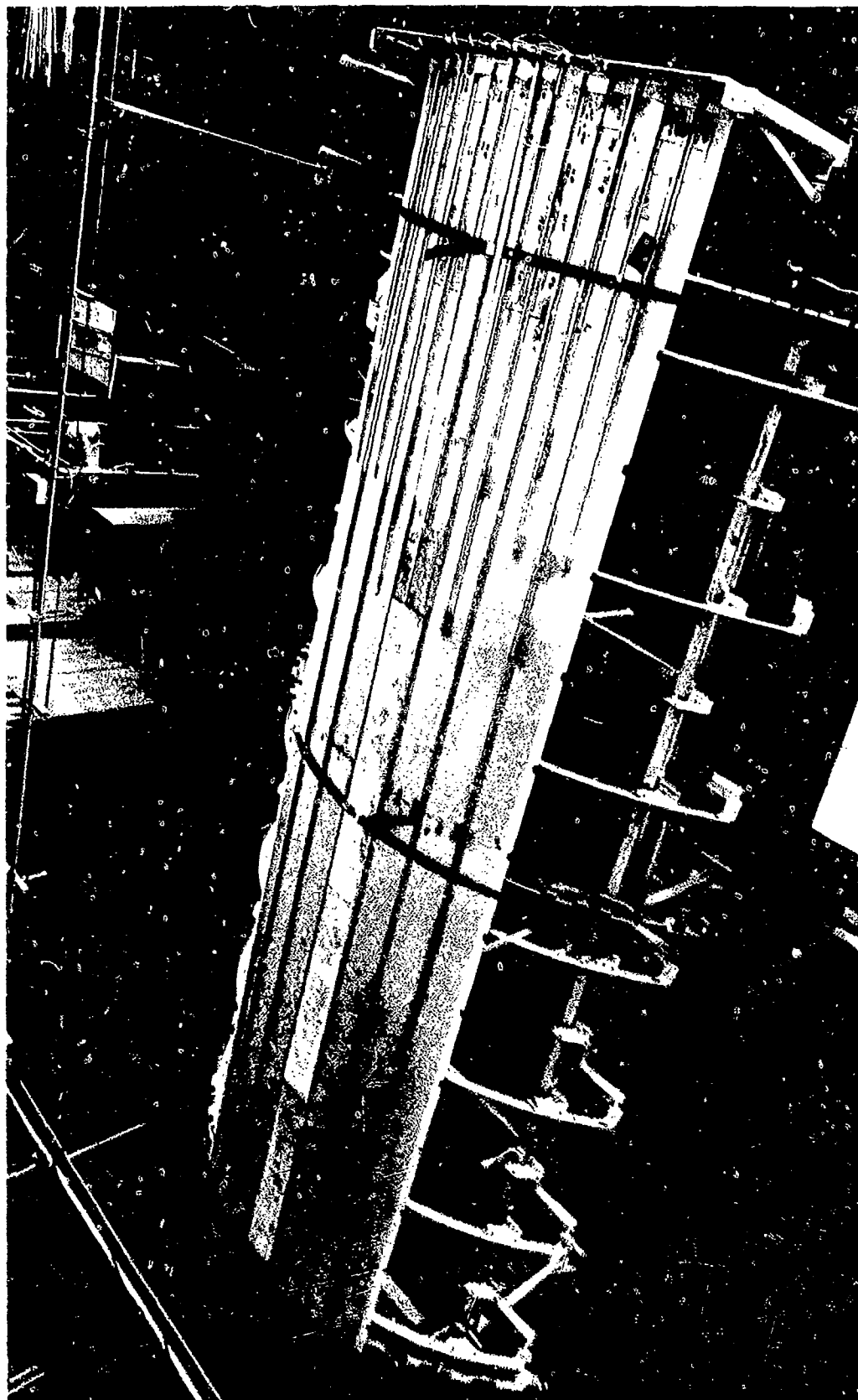


FIGURE 32. PHOTOGRAPH OF CONSTANT SECTION CLOSE-SPACED EXTERNAL LONGERON SKIN PANEL



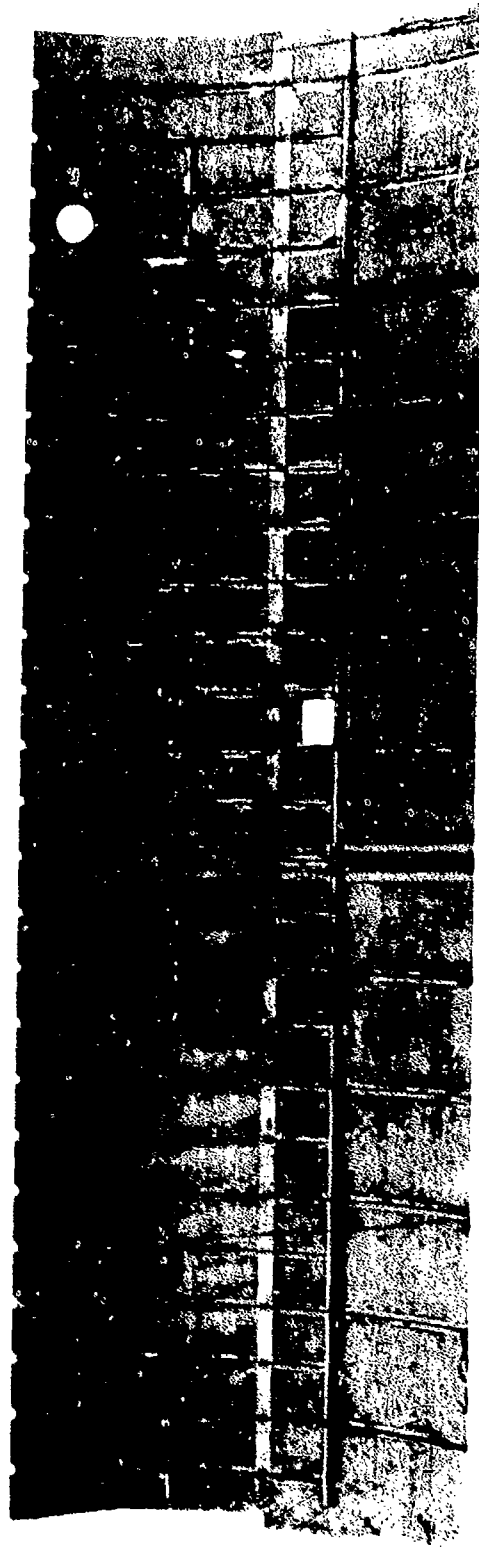


FIGURE 34 PHOTOGRAPH OF CONSTANT SECTION WIDE-SPACED LONGERON PANEL

## Non-Constant Section Panels

All longerons and frames aft of and including station 439 are identical and/or similar to the constant section panels. All the longerons end at station 439. Forward of station 439 at longerons 1, 4, 8 and 9, full depth intercostals provide axial load capability for the panel (see Figure 21). The frames aft of station 439 are similar to the constant section frames in size and spacing. The frames at station 439 and forward are full depth as shown in Figure 9 and are spaced at 12 inch intervals.

Internal Longeron Panel. - A typical close spaced internal longeron panel assembly, 1A, is shown in Figures 35 and 36. The bonded assembly shown and its opposite assembly are joined mechanically at longeron 1. This assembled internal longeron panel section extends from station 523 forward to station 367 and from L-8 left to L-8 right. The bonded skin splice at L-4 forward of station 439 contains a continuous 2024-T3 external splice, .050 x 3.50 inches, and a discontinuous internal splice of the same dimensions. The internal splice is located between the frame tees and is also used as a filler as shown in Figure 35, for the intercostal tee that is bonded across the frame tees. The mechanical splice at L-1 forward of station 439 is shown in Figure 11.

External Longeron Panel. - A typical external longeron panel assembly, 5A, is shown in Figures 37 and 38. This panel extends from station 367 to 523 and from L-13 left to L-13 right. It is similar to the upper panel except that the longerons are bonded on the outside surface of the skin. The longerons are bulb T-sections identical in cross section to the external longerons used in the constant section. The frame shear tees are continuous without interruption. This panel has 0.375 inch diameter holes near the bottom centerline in every bay to provide drainage for water or bilge fluid that may accumulate in the bottom of the fuselage.

Wide Space Longeron Panel. - A typical side panel with wide spaced longerons 2A, is shown in Figures 39 and 40. This panel extends from station 523 to 367 and from bonded longeron 8 to mechanically fastener longeron 9. The

one piece skin is 0.050 inch 2024-T3 bare aluminum alloy. The two 7475-T761 tear stoppers shown in Figure 27 are 0.071 inch thick by 3 inch wide. Intercostals are located at tear stopper #2 in every other bay in order to stabilize the frames. Doublers, 0.016 inch thick, have been added near station 523 in order to effectively increase the skin thickness to 0.066 inch where countersunk fasteners are to be installed.

Door Jamb Panel. - The wide spaced longeron left side panel with simulated crew entrance door, 3A, shown in Figures 41 and 42, is located between stations 523 and 367 from Longerons L-9 to L-13. It contains a 32 inch by 60 inch cut-out for the entrance door. The 2024-T3 skins are chem-milled to provide a 0.050 inch thick skin aft of station 439 and a 0.125 inch thick skin around the door corners. All chem-milled steps are external as shown in Figure 41. The door corner doublers, shown in Figure 43 are also chem-milled and bonded to the skin. There are two bonded longitudinal skin splices on the panel. One is at mid-door level and the other is at longeron 12. The 0.050 skins are spliced with an inner and outer bonded splice member as shown in Figure 13. Where the thicker skins are spliced, the double lap bonded splice has been modified in order to reduce the shear stress in the adhesive (see Figure 44). The thick skins are chem-milled at the splice and a third splice member is added between the skin and outer splice. As shown in Figure 45 longerons 11 and 12 terminate at station 439. Bonded straps are added to protect the skin from cracking adjacent to the end of the longeron. The door jamb frames, at stations 427 and 391, are 0.090 inch thick. Sheet metal intercostals are added mechanically to form the door jamb structure as shown in Figure 26. On the fuselage skin side the intercostal picks up a tee that is bonded to the skin.

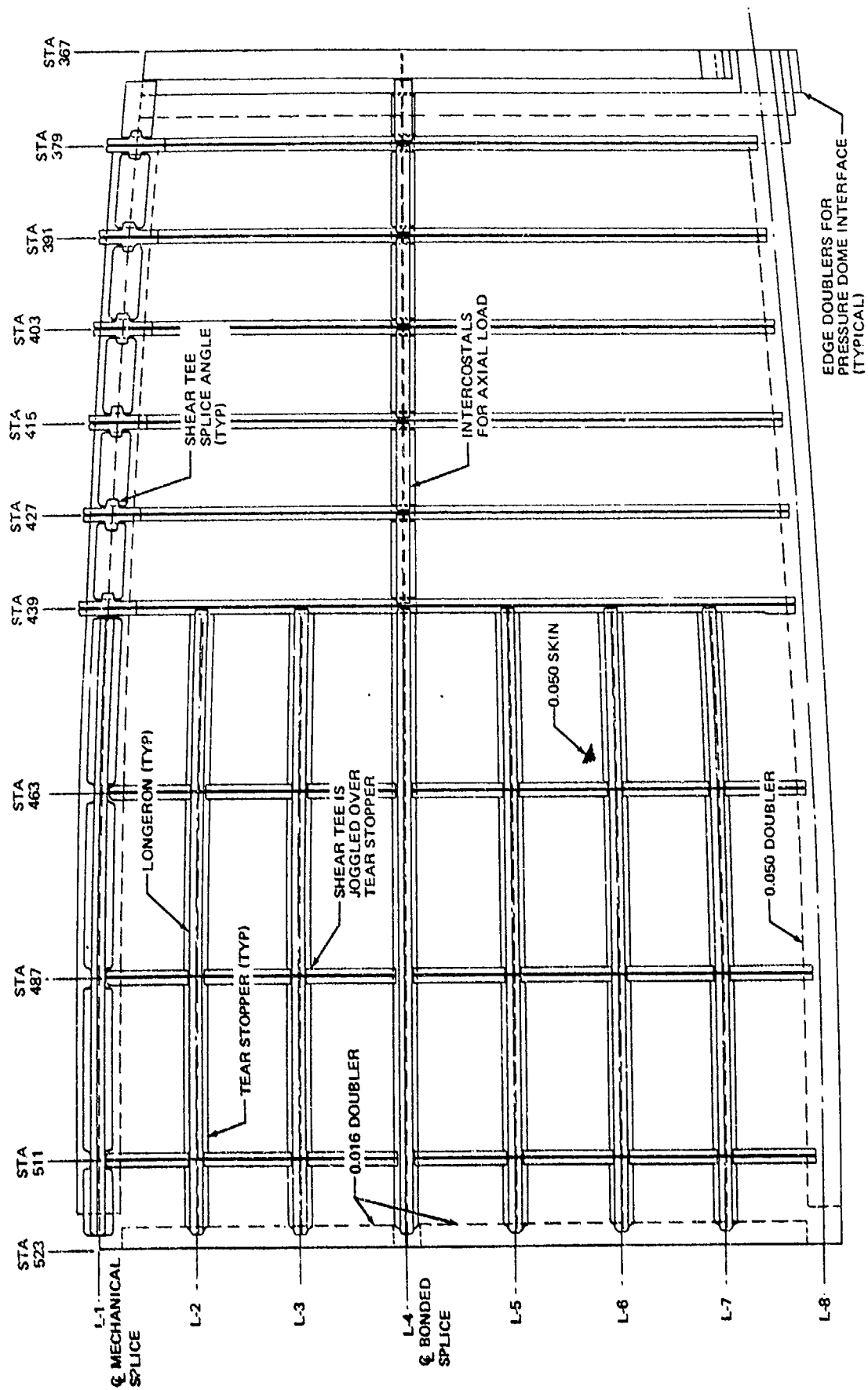


FIGURE 35. NONCONSTANT SECTION CLOSE-SPACED INTERNAL LONGERON PANEL

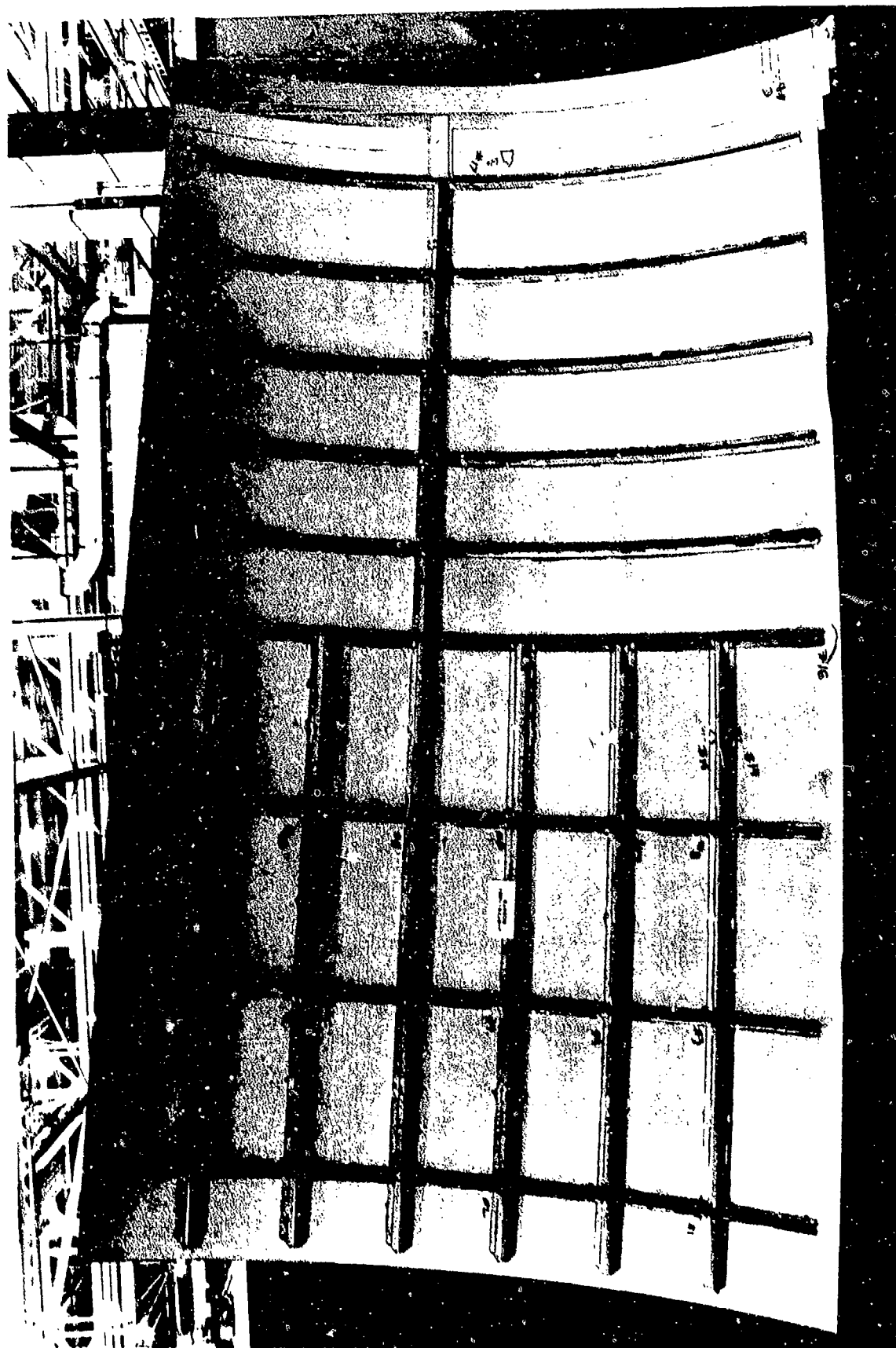


FIGURE 36. PHOTOGRAPH OF NONCONSTANT SECTION  
CLOSE-SPACED INTERNAL LONGERON PANEL

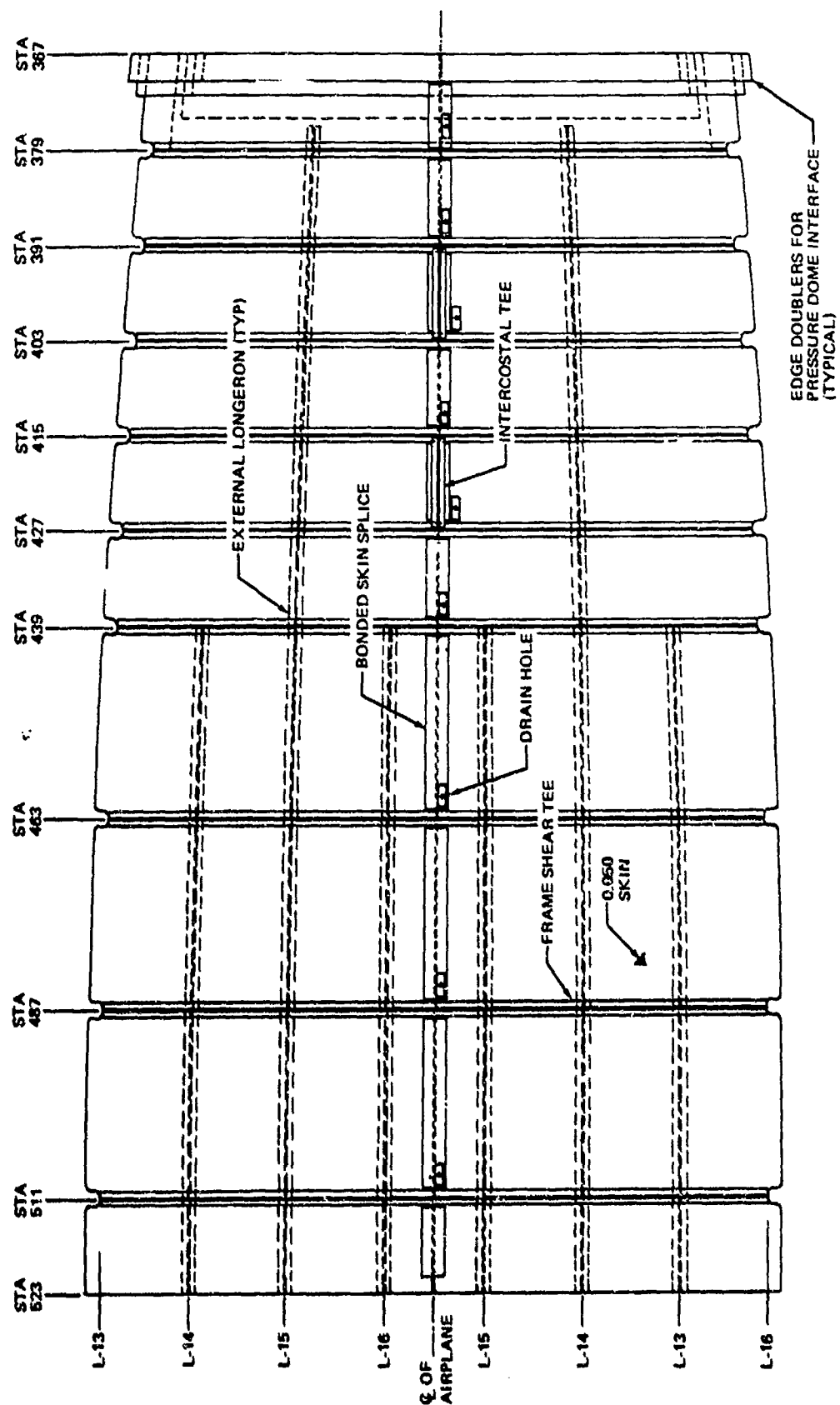


FIGURE 37. NONCONSTANT SECTION EXTERNAL LONGERON PANEL



FIGURE 38. PHOTOGRAPH OF NONCONSTANT SECTION EXTERNAL LONGERON PANEL

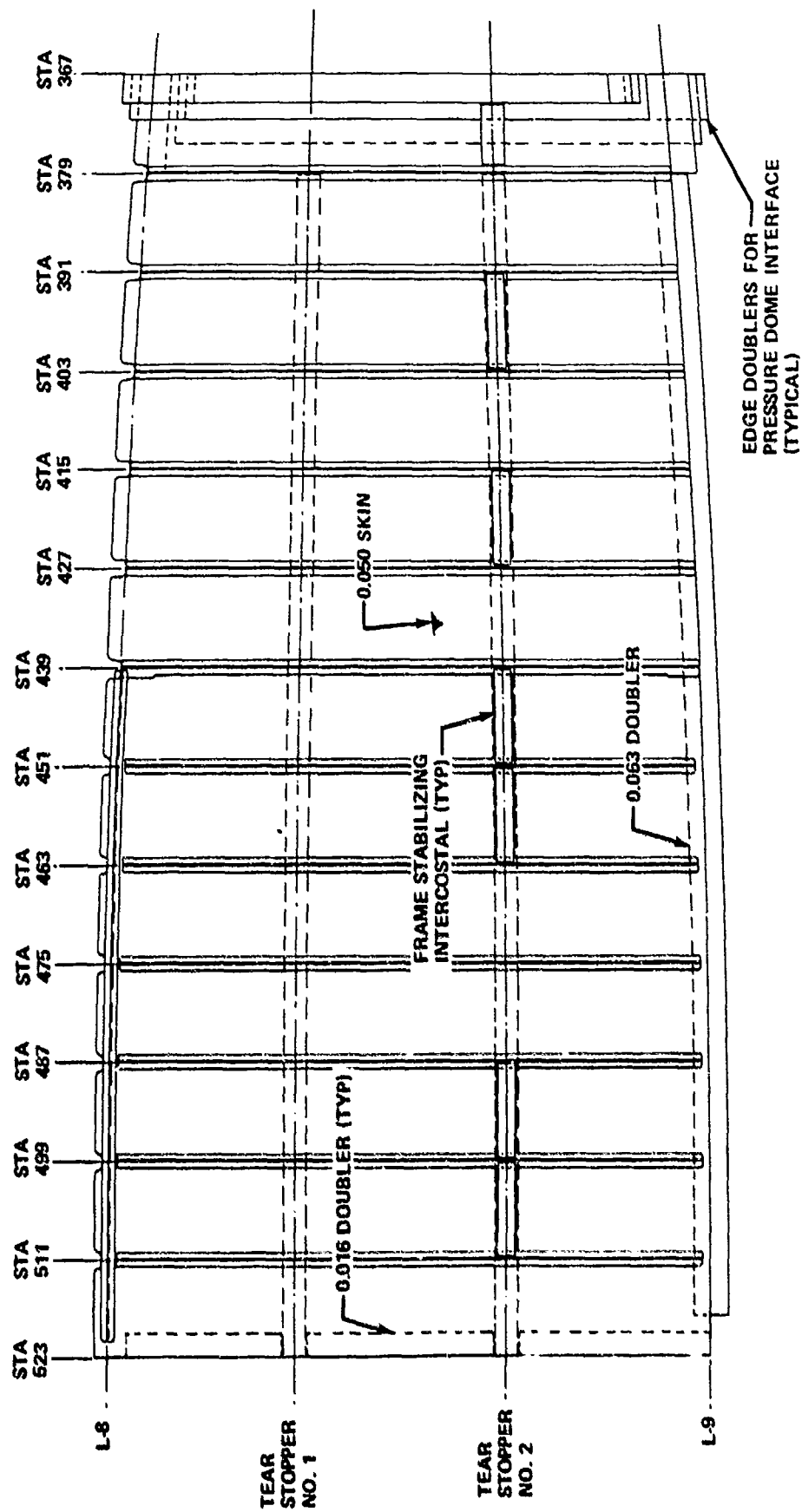


FIGURE 39. NONCONSTANT SECTION SIDE PANEL WITH WIDE-SPACED LONGERONS

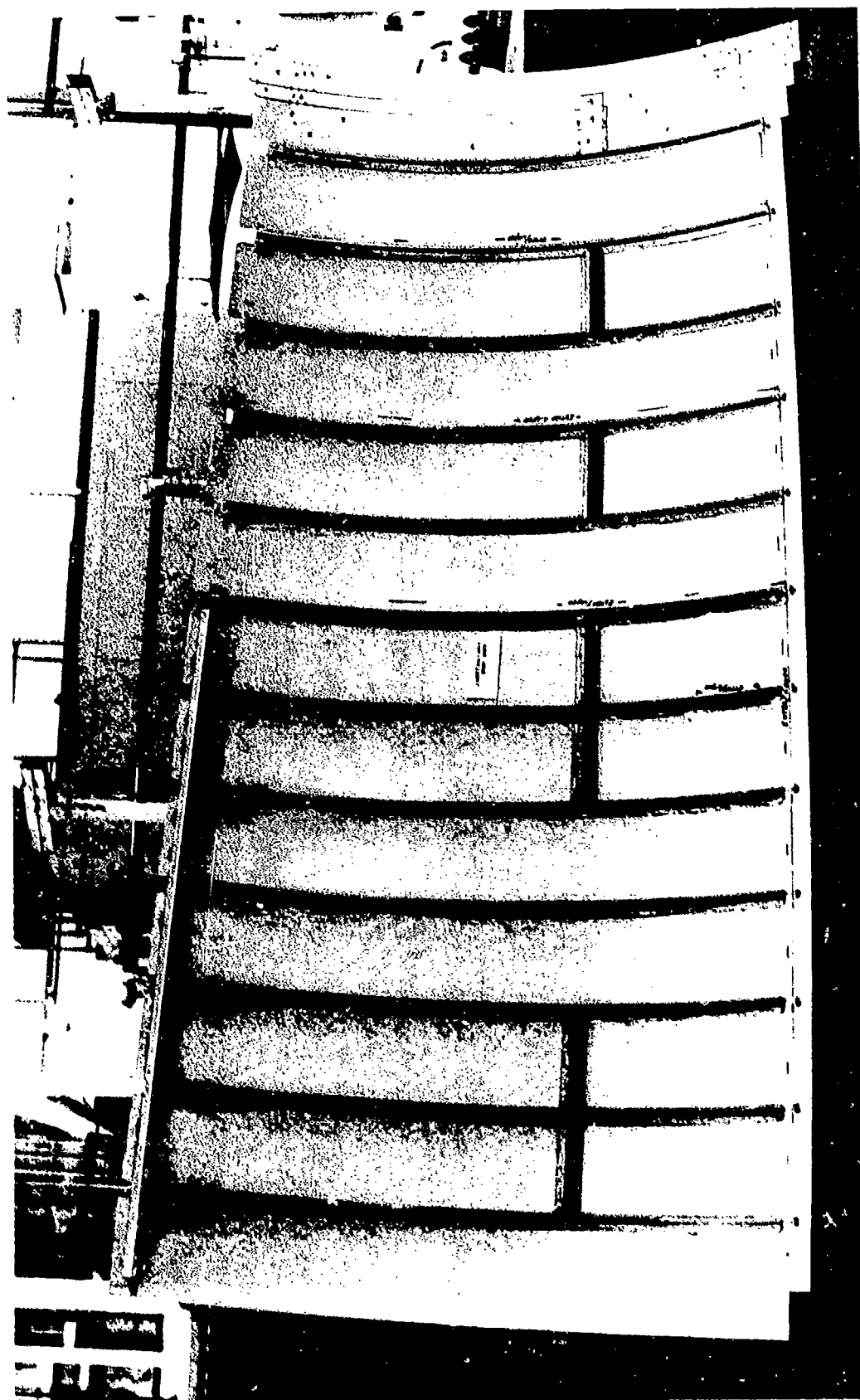


FIGURE 40. PHOTOGRAPH OF NONCONSTANT SECTION  
SIDE PANEL WITH WIDE-SPACED LONGERON



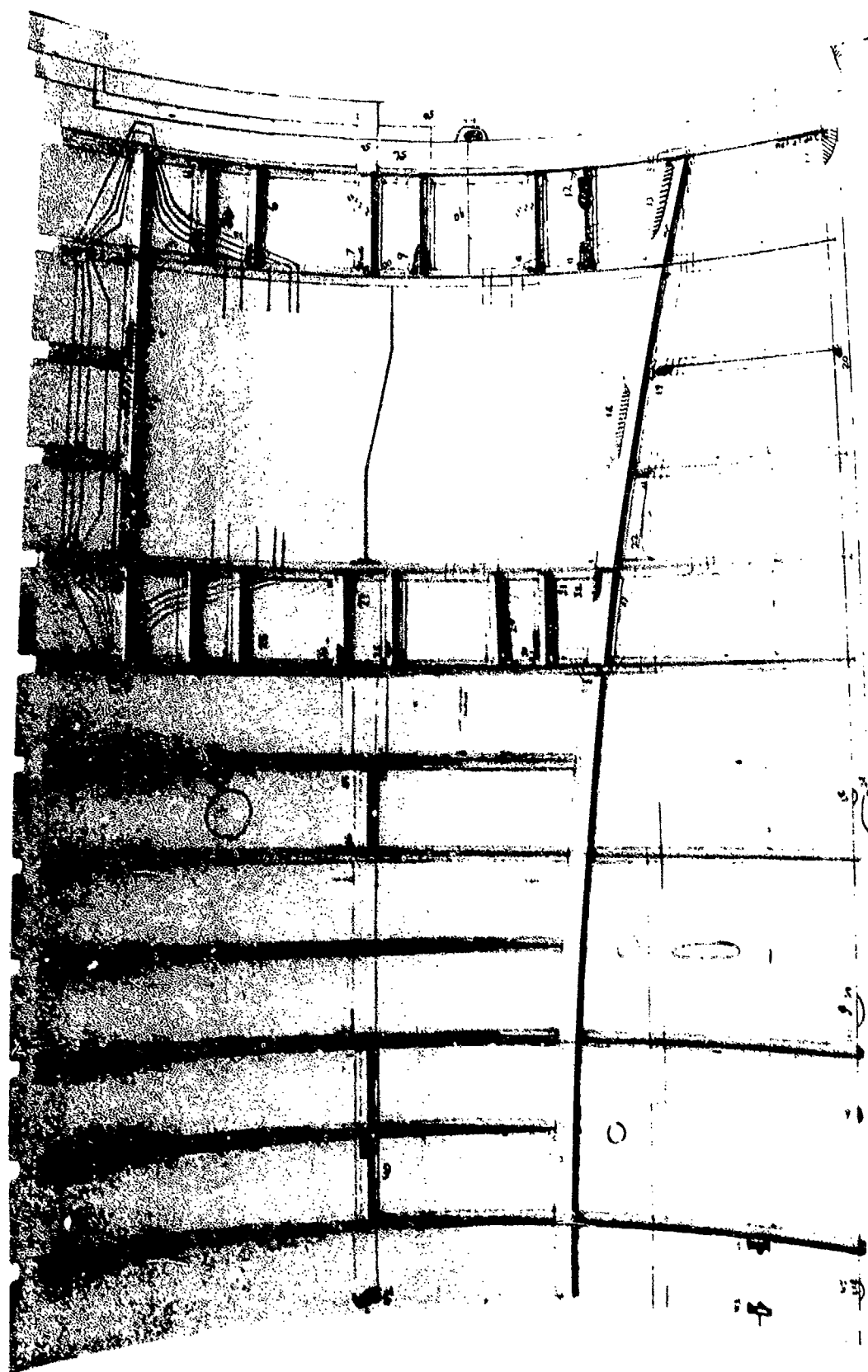


FIGURE 42. PHOTOGRAPH OF NONCONSTANT SECTION LEFT SIDE PANEL WITH DOOR CUTOUT AND JAMB

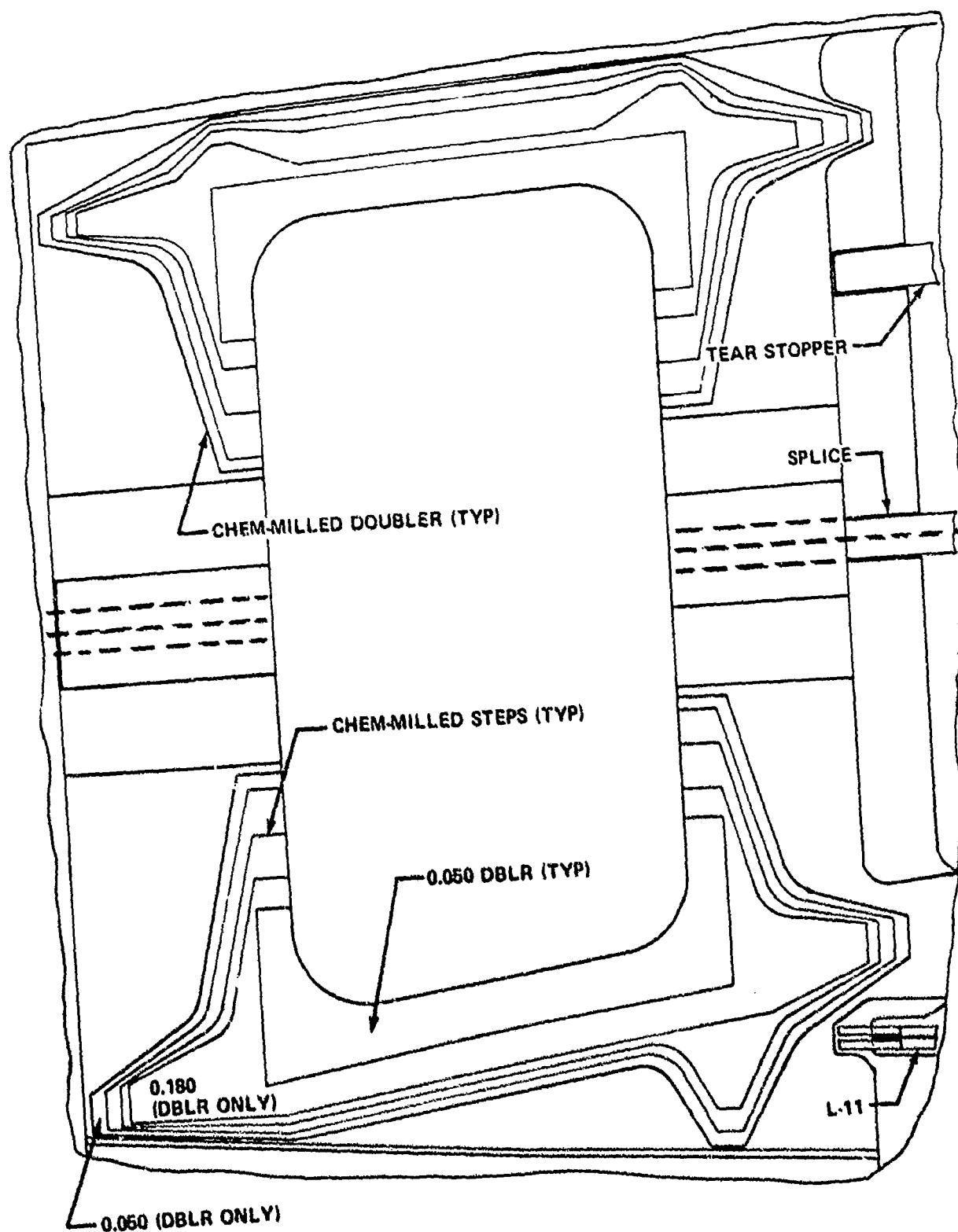
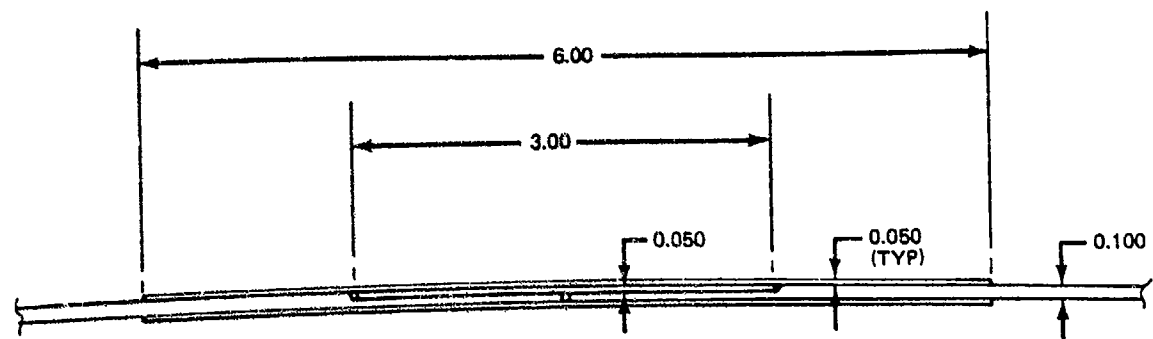


FIGURE 43. DOOR CORNER DOUBLERS (LOOKING INBOARD)



NOTE: TYPICAL FORWARD AND AFT OF CREW ENTRANCE DOOR

FIGURE 44. HEAVY SKIN LONGITUDINAL BONDED SPLICE

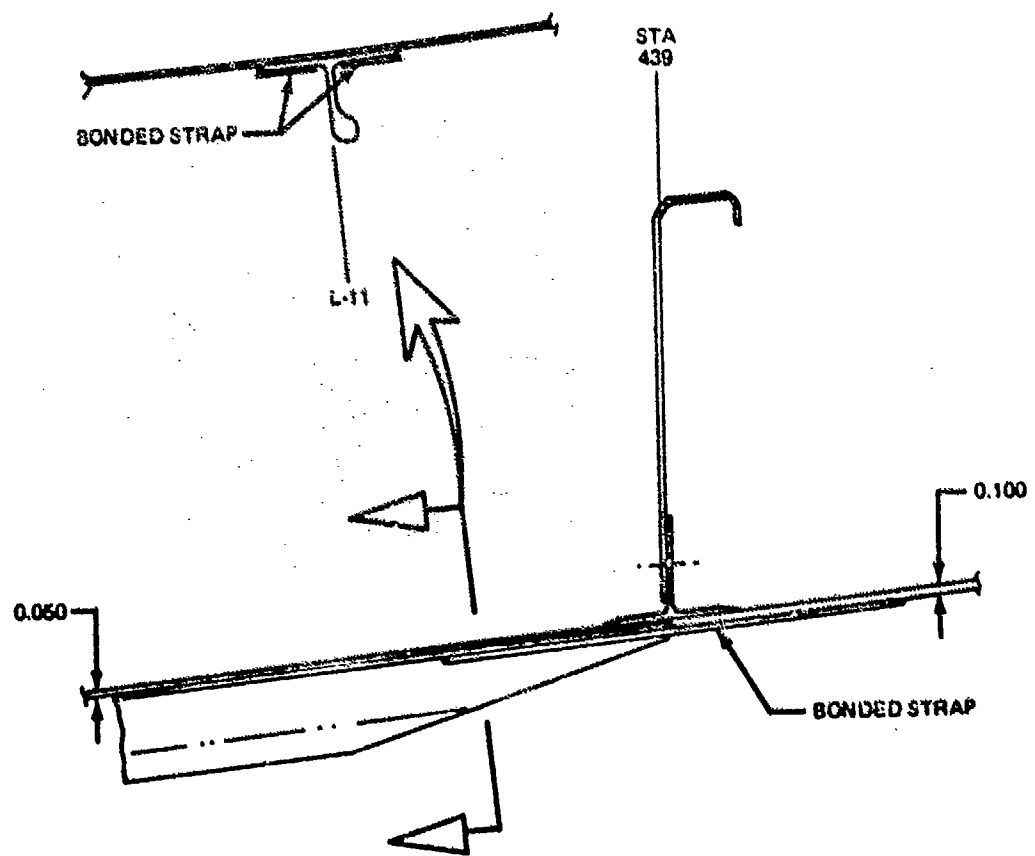


FIGURE 45. END OF L-11 AT STATION 439

## NON-PARTICIPATING STRUCTURE

The door, wing and floor assembly design emphasis was placed on the introduction of loads, boundary restraints and configuration constraints to the test fuselage. Design simplicity and thus a substantial cost saving was the result. The door is a simple plug type door of honeycomb construction that introduces equivalent loads on the fuselage jamb as would be encountered by an actual flight article. The wing box structural assembly is rectangular box shaped with identical front and rear spars. This wing simulates the interaction that would result between an actual aerodynamically designed wing and the fuselage. To minimize cost and provide access to the bottom interior of the fuselage, the floor structure was constructed of C-15 type non-machined plank extrusions that extended approximately one third of the distance across each side of the fuselage.

## Door Installation

The door installation, considered to be "non-participating structure" in the FSDC is located in the nose section on the left side between station planes 391 and 415. This location is in the compound curved area of the fuselage.

The door is basically a plug-type door and is designed to simulate the proposed C-15 door, as shown in Figure 46. The loads and end moments at the door jamb stops are essentially a representation of the C-15 loading.

Design Consideration. - The door was designed to be less stiff than the door jamb in order to assure an even distribution of loads at the jamb stops when the door deflects under pressure loads. This stiffness relationship is standard design practice and is intended to keep the door jamb stops from being overloaded. The ultimate design load condition for the door is 2P pressure (14.3 psi). The load generated from this condition is 2400 lbs at each door jamb stop. The critical design condition that generates the maximum load at the door stops is the failsafe condition. At 1P pressure, 7.15 psi, with either end beam out, the maximum load at a door jamb stop is 2900 lbs with a resulting end moment of 3626 in-lbs. These loads were the design loads for the door and door jamb.

Door Description. - Since the door is non-participating structure, the use of honeycomb construction was chosen. Basically, the door is made up of an inner and outer skin, bare 2024-T3 aluminum sheet, with a Flex Core aluminum honeycomb (5.7 pcf) sandwiched in between and edges with blocks of 7075-T73 aluminum plate and a 2024-T3 bare aluminum sheet around the periphery of the panel as shown in Figure 47. The six beams attached to the blocks, filler and skins transfer the pressure loads from the door to the door jamb stops. A simple synthetic rubber flap seal, Neoprene-50 shore hardness is bonded around the periphery of the door. The filler and skins are stretch formed. The blocks along the station planes, as well as the bottom and top edges of the door, are rolled. These are the only door installation parts requiring forming. The Flex-Core

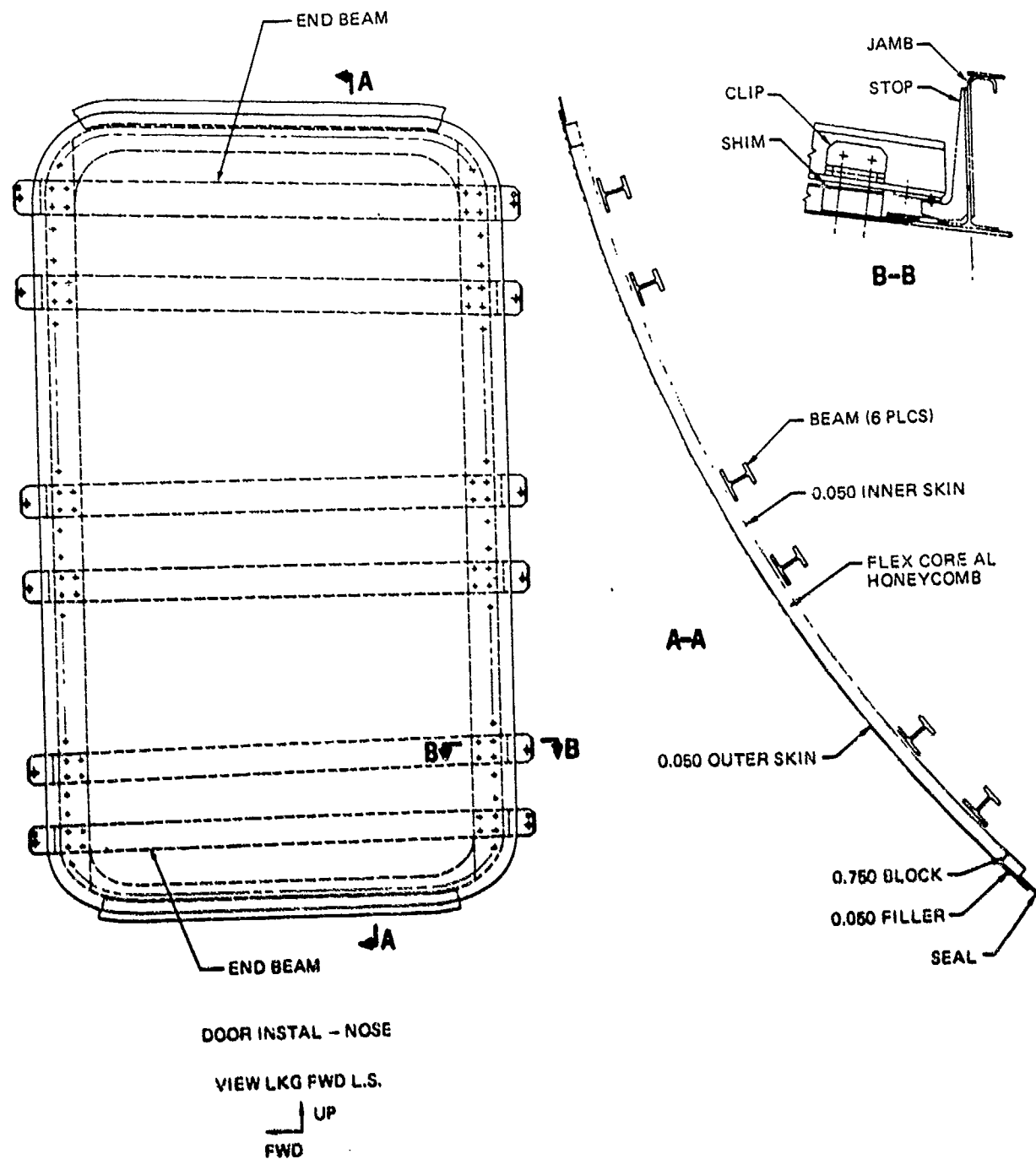


FIGURE 46. DOOR PANEL AND INSTALLATION

honeycomb easily molds into the compound curved area of the panel while the six beams are cut in straight pieces. Clips and tapered shims are used where the beams are attached to the blocks. The clips provide necessary durability when transferring load from the door to the beams, while the tapered shims allow the beams to be made in straight pieces without forming. Attachments along the periphery of the door eliminate any potential adhesive peel problem.

The door is non-functional and is bolted in place from inside the fuselage with a total of four bolts, one in each of the end beam corners. If required the door may be easily removed for additional access inside the fuselage in conjunction with the primary Access Door located in the front pressure bulkhead once the test program is implemented.

Summary. - The structural integrity and useful life for an adhesively bonded honeycomb door structure will be demonstrated in the FSDC test program. The results could establish that honeycomb construction should be considered for future door designs.

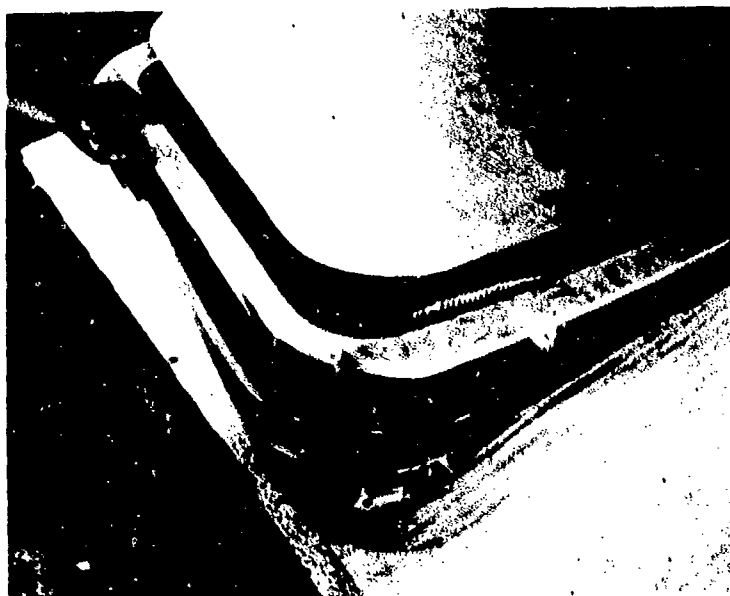


FIGURE 47. DOOR ASSEMBLY

## Wing Box

The wing is a five sided rectangular box shape with the upper wing skin panel omitted as shown in Figures 5 and 48. This wing is attached to the fuselage by means of a titanium tee under the wing, aluminum tees at the front and rear spars and trapezoidal panels connecting the spars to the spar frame segments.

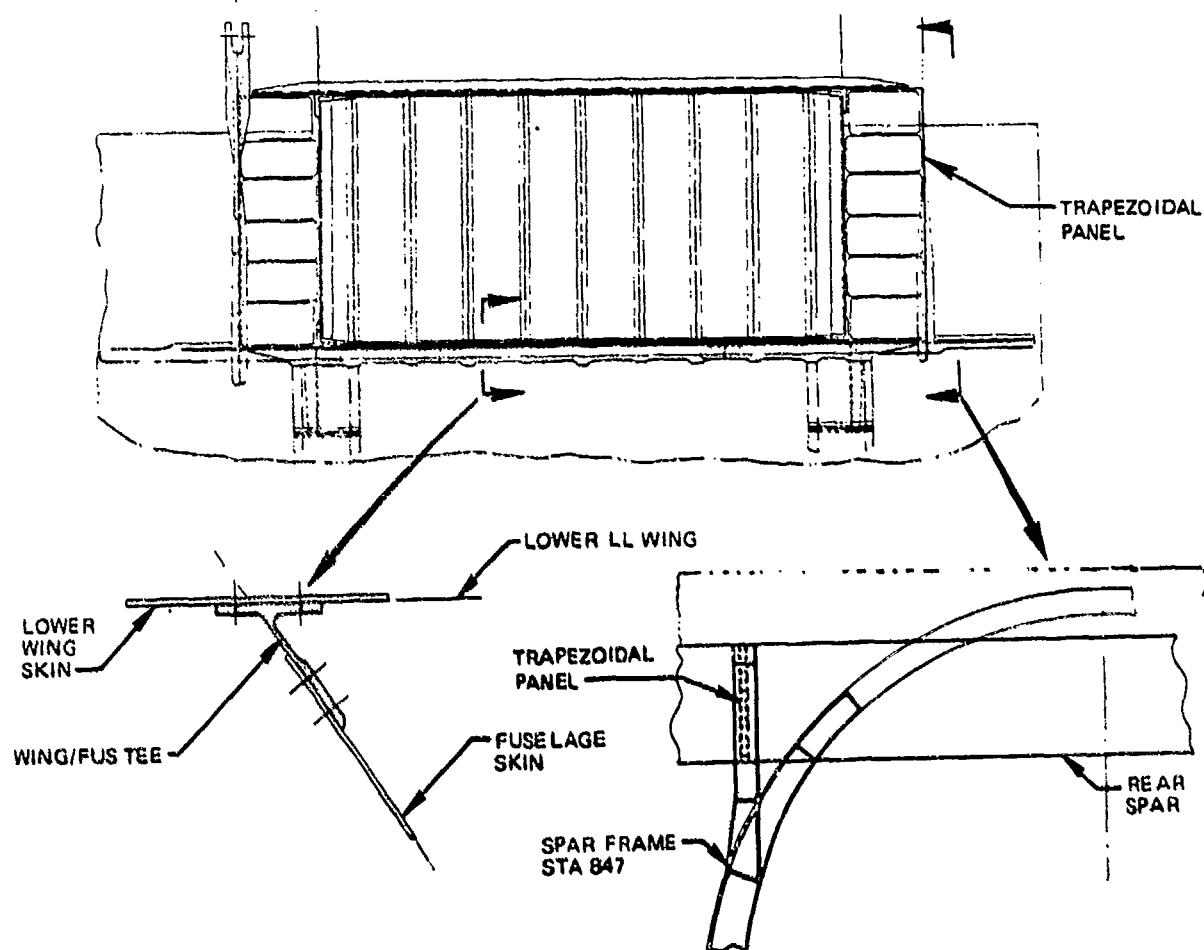


FIGURE 48. WING/FUSELAGE INTERFACE

The function of the wing in the FSDC is to simulate a typical wing to fuselage interaction, to provide a pressure barrier and to assure a major discontinuity in the upper half of the fuselage. To simplify the wing design, only vertical wing loads are applied to the front spar frame. Simplification is also achieved by eliminating aerodynamic consideration. In addition, (1) replacing the upper wing skin with links, (2) making the front and rear spars identical and (3) eliminating all internal bulkheads reduced assembly and installation time.

Lower Wing Panel. - The panel was designed with a 0.250 inch thick 2024-T351 aluminum plate, 110 x 200 inches and stiffened by 16 6061-T6 aluminum 10-inch deep I-beams. This panel is a pressure barrier which beams out this load to the front and rear spars.

Front and Rear Spar. - The spars were 0.250 inch thick 2024-T351 aluminum plates, 55 x 200 inches, and stiffened by 16 five inch deep 6061-T6 aluminum I-beams. They function as a pressure barrier as well as a member to redistribute the load from the bottom wing panel through the trapezoidal panel to the spar frames.

End Bulkheads. - The end bulkheads carry part of the hoop load introduced by the underwing fuselage skin panels. These bulkheads redistribute this load into the spar frames by way of the trapezoidal panels. These bulkheads also stabilize the front and rear spar. They are composed of 0.125 thick 2024-T3 aluminum sheet stiffened with tee shaped 7075-T6 extrusions. To provide stability to the bulkhead, a web on top of the wing and extending from the front to the rear spar ties in the upper bulkhead cap.

Titanium Wing Tee. - The wing tee is a flexible joint which transfers the fuselage hoop loads from the underwing fuselage skin panel into the bottom wing panel and wing end bulkhead. This joint isolates the fuselage panel so that the bending loads are not transmitted into the wing structure. Fuselage axial loads are transferred around the wing cavity by way of the wing tee. The tee is 100 percent machined from 6Al - 4V titanium extrusion and assembled from three sections.

Link Assembly. - Three steel tubular members located at longerons 1 and 4 transfer loads from the upper half of fuselage across the wing cavity.

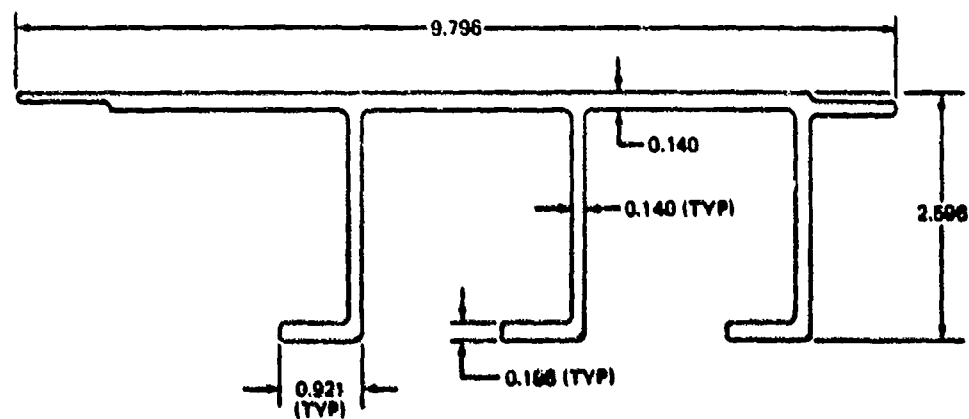
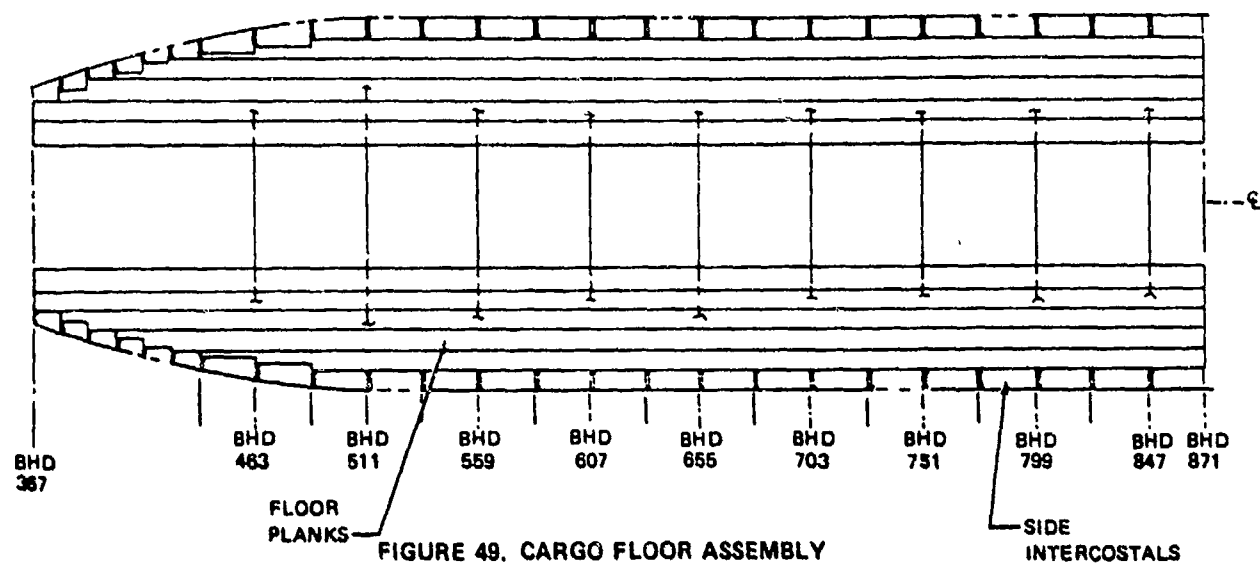
## Floor Structure

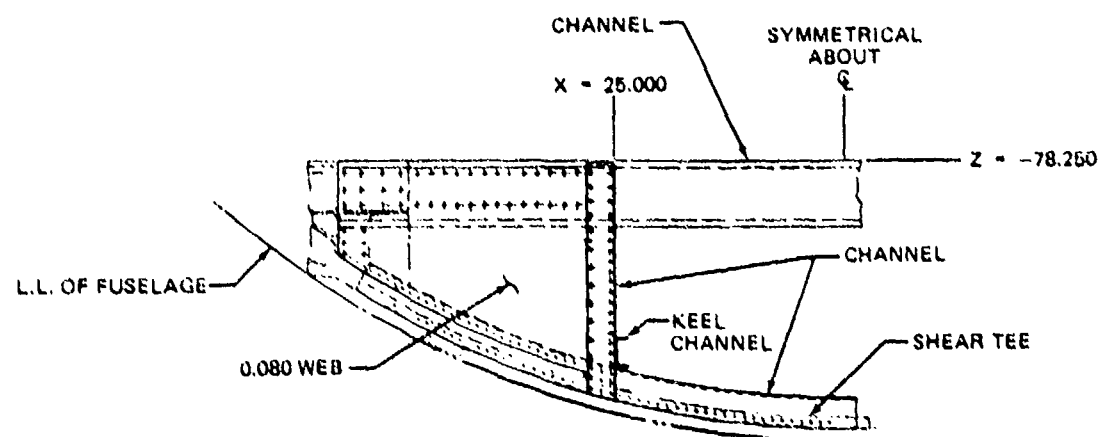
The floor structure used for the FSDC is based on a YC-15 floor structure design philosophy. It is comprised of three basic sections: floor planks, side intercostals, and bulkheads as shown in Figure 49. The floor extends aft from station 367 to the test fixture at station 871.

Floor Planking. - The planking used for the FSDC floor is a C-15 type extrusion sized to carry the required floor loads imposed by various floor loading conditions; e.g., trucks, tank, pallets, as shown in Figure 50. To minimize the cost impact on the PABST program, the floor planks have been used as extruded and only a minimum amount of machining has been used. The floor planks are mechanically fastened together with attachments 2 inches on center to form an assembly of approximately 45 inches wide on each side of the fuselage, leaving an open section of approximately 50 inches in the center of the fuselage for easy access to the under-floor area. The amount of planking installed is sufficient to provide the necessary load paths and stiffness requirements for the fuselage shell.

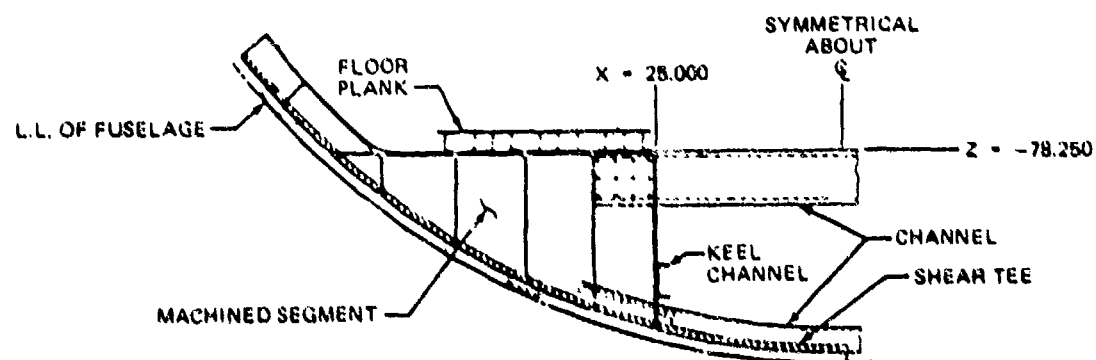
Floor Intercostal. - The floor intercostals for the FSDC, as shown in Figure 25, are sheet-metal mechanically-fastened members similar to the YC-15 floor intercostals except that lighting holes have been eliminated to minimize cost. The floor intercostals extend the full length of the FSDC and attach the floor plank assembly to the bonded fuselage side skin panels.

Bulkheads. - The FSDC bulkheads are mechanically fastened assemblies, 48 inches on center, consisting basically of two configurations. At stations 703 and 847, the bulkheads are built up sheet metal, which are similar to the YC-15 bulkheads. The bulkhead at station 463 and the constant section bulkheads at stations 511, 559, 607, 655, 751, and 799 as shown in Figure 51, are integral stiffened machined segments that are machined from plate stock to minimize cost.





FLOOR SUPPORT BULKHEAD AT STA 703 AND 847



FLOOR SUPPORT BULKHEAD AT STA 463, 511, 559, 607, 655, 751 AND 799

FIGURE 51. FLOOR SUPPORT BULKHEAD

## LOADS

The loads used for design of the Full Scale Demonstration Component are based on the YC-15 AMST Aircraft program. The external aircraft loads were derived from the YC-15 design parameters for flight (gust and maneuver) and ground (taxi, landing, towing and jacking) conditions. The most critical of these conditions were used to derive the internal loads for each structural member of the Full Scale Demonstration Component. The development for both external and internal loads is included in the section that follows.

## External Loads

Flight and ground external loads were developed for both ultimate and fatigue loading conditions in conformance with the military specifications noted in the criteria. A complete set of external loads sufficient to design a full scale bonded aircraft fuselage were developed during the PABST Phase Ib (Reference 1). A study was conducted of these conditions and the most critical for structural sizing were selected for design of the FSDC (Table 2 ).

The external ultimate shears and bending moment curves for each of these design conditions were matched by a similar FSDC test curve based on the actual test fixture loading points. The test fixture loading points are shown in Figures 52, 53, and 54. The critical ultimate design and unit fatigue test load curves are shown in Figures C1 through C34 in Appendix C.

The external load conditions for fatigue and damage tolerance spectrum generation are shown in Table 2. These unit conditions are used to generate internal loads which are subsequently factored by a computer program to arrive at the analysis spectrum and the accumulated fatigue damage and damage tolerance crack propagation. A comparison of analysis external unit fatigue conditions with FSDC test conditions for the actual test fixture loading points is shown in Figures C3 through C26 in Appendix C.

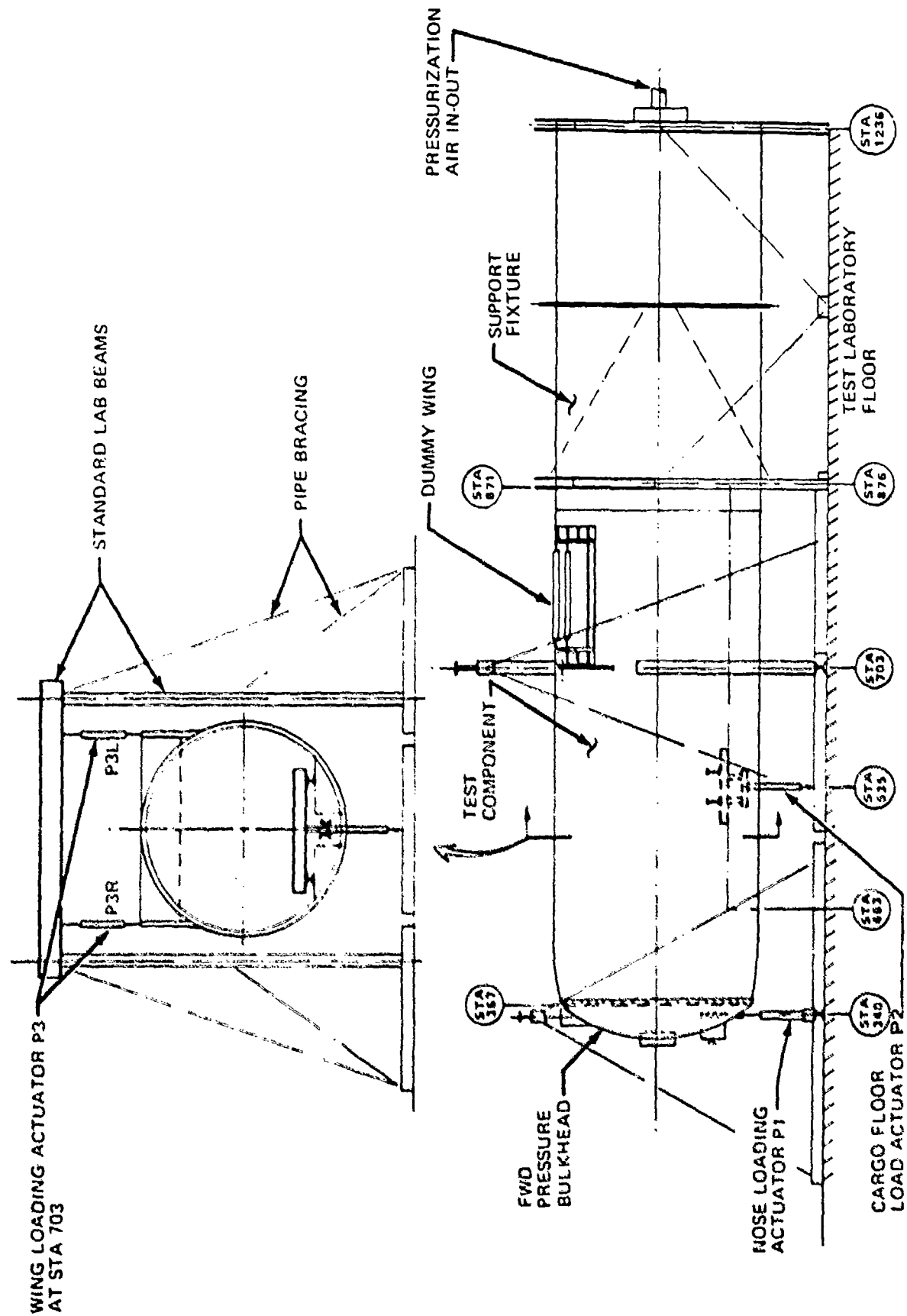


FIGURE 52. PABST DEMONSTRATION COMPONENT TEST SETUP



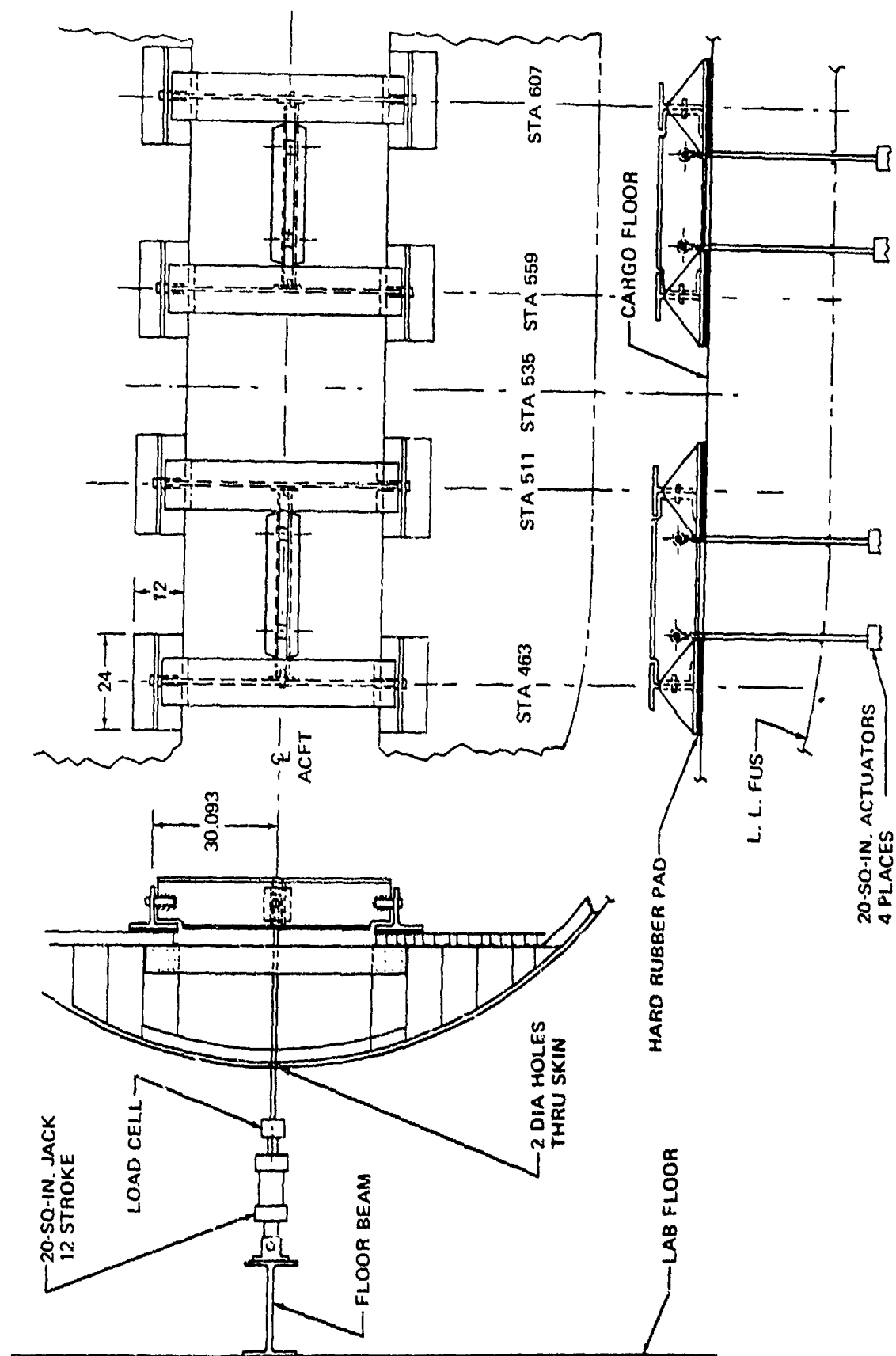


FIGURE 54. CARGO FLOOR LOADING LINKAGE -- ULTIMATE TEST

TABLE 2  
EXTERNAL LOADS AND CONDITIONS FOR FORMAT SOLUTIONS

Cond. No.	Ext. Load No.	Description	Vert. Acc., N <sub>z</sub>	Payload	Cabin Press. (psi)	P <sub>1</sub> (lb)	P <sub>2</sub> (lb)	P <sub>3</sub> Total of 2 Jacks (lb)
UNIT FATIGUE CONDITIONS								
1	----	1P, Cabin Pressure (7.15 psi)	0	0	7.15	0	0	0
2	15 FG	Typ. STOL Flt. Cruise	1	20,250	7.15	-6,427	-13,231	18,993
3	16 FG	Typ. STOL Flt. Cruise	1.77	20,250	7.15	-8,885	-23,433	47,709
4	19 FG	Typ. CTOL Flt. Cruise	1	54,250	7.15	-5,420	-24,147	32,388
5	20 FG	Typ. CTOL Flt. Cruise	1.75	54,250	7.15	-6,530	-42,173	74,568
6	27 FG	Low Alt. STOL Cruise	1	27,000	0	-7,630	-15,737	9,534
7	28 FG	Low Alt. STOL Cruise	2	27,000	0	-11,802	-32,673	52,223
8	39 FG	Low Alt. CTOL Cruise	1	62,000	0	-7,731	-26,386	28,920
9	40 FG	Low Alt. CTOL Cruise	1.99	62,000	0	-11,744	-53,552	90,250
10	1 FG	Typ. STOL Flt. Taxi	1	20,250	0	10,849	-19,855	-37,958
11	3 FG	Typ. CTOL Flt. Taxi	1	54,250	0	17,095	-32,379	-35,111
12	11 FG	Low Alt. CTOL Resupply Taxi	1	62,000	0	24,184	-35,932	-47,762
13	7 FG	Low Alt. STOL Resupply Taxi	1	27,000	0	13,041	-22,833	-37,996
ULTIMATE CONDITIONS								
14	F525.19	2 Pt. Landing Spring Back	Varies	27,000	0	-116,641	-120,359	-68,698
15	2262 GD	Braked Roll	Varies	31,100	0	167,532	-86,303	-85,268
16	2513 VH	CTOL Gust	Varies	62,000	0	-12,737	-180,975	114,413
17	2513 VH	CTOL Gust	Varies	62,000	10.725	-12,737	-180,975	114,413
18	2059 BM	2G Bal. Maneuver	2	62,000	0	-15,608	-14,476	245,647
19	2059 BM	2G Bal. Maneuver	2	62,000	10.725	-15,608	-14,476	245,647
20	----	2P, Cabin Pressure (14.3 psi)	0	0	14.3	0	0	0

## Internal Loads

The FSDC fuselage is modeled in three joined sections as shown in Figure 55. The modeling technique employed is based on the lumped parameter element; bars to carry axial, bending, and torsional loads, and panels to carry shear loads. Detail areas of bars and panels were varied to properly represent the design and configuration. The internal load generation method of analysis for the model members employs the FORMAT computer program which combines the characteristics of the force method with the solution algorithm characteristics of the displacement method.

The simultaneous solution from the three joined sections with previously defined applied external critical design loads, results in the output data printed in the form of bar and panel loads and nodal deflections. A maximum-minimum sort of loads for each element and selected conditions are printed in total. These printouts are used for the detail structural integrity calculations.

The structural idealized model is shown in Figure 55. An example of the output for an individual load condition and the max./min. for all conditions is shown in Tables 3, 4, 5 and 6 for a selected area shown in Figure 56 (shear panels) and Figure 57 (longeron and frame bars). In Table 3, for example, the highest absolute shear for all load conditions for panel 62 is -300 lbs/in. for load condition 14, acting in the negative sense and along the PS and RQ edges relative to the conventions defined in Figure 56. Table 4 is a typical output for all panels and for load condition 14 only. A complete set of internal loads output is available for reference.

Additionally, a computer automated stress analysis is performed on the modeled elements. This phase of the format program computes combined axial and bending stresses, principal stresses, and combined shear and axial stresses, and the individual type stress margin of safety. The computer program also summarizes the most critical margins of safety for each type of stress at each node point and identifies the loading condition. This data provides rapid quantitative data for assessing areas for structural adequacy.

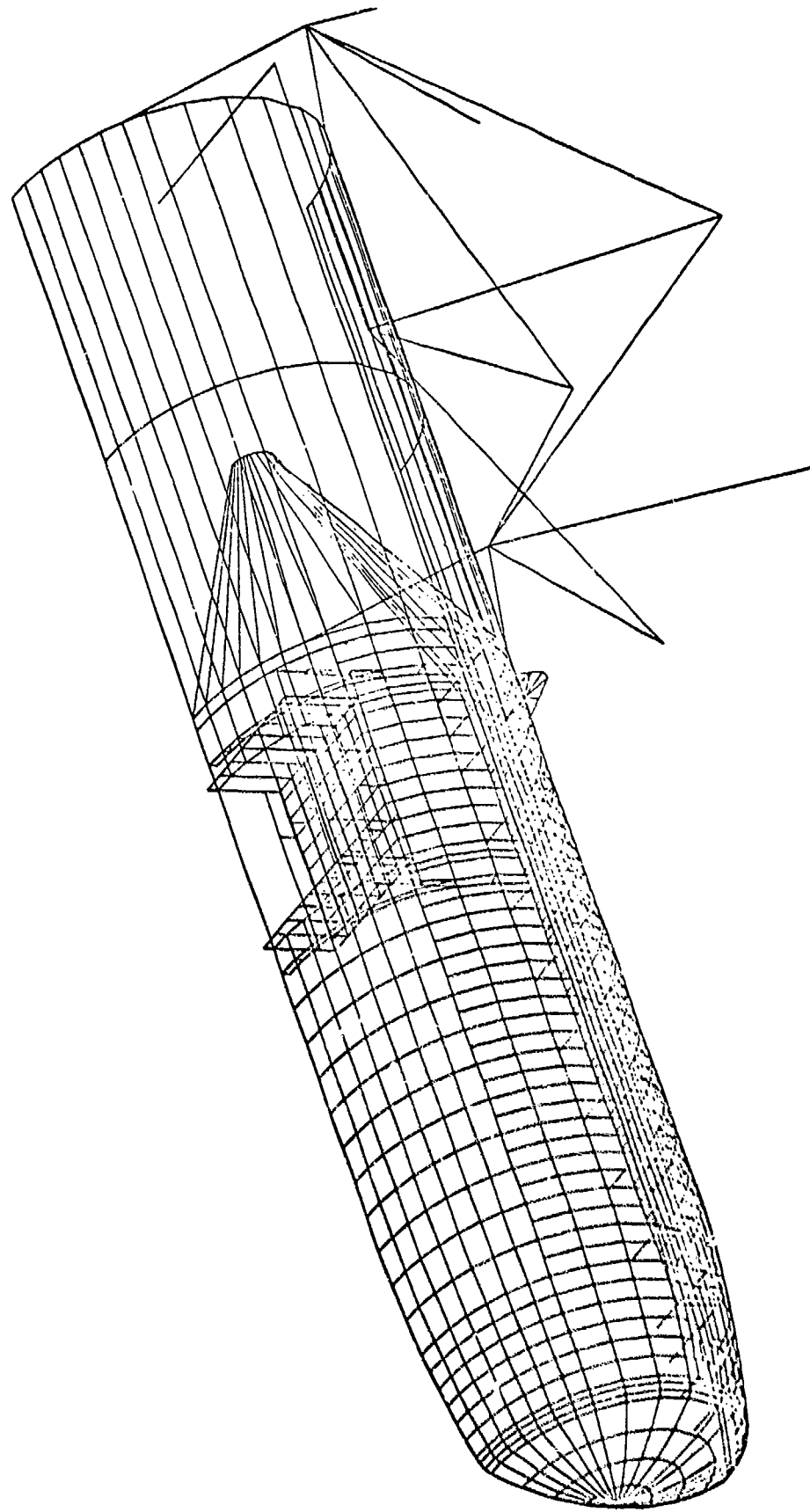
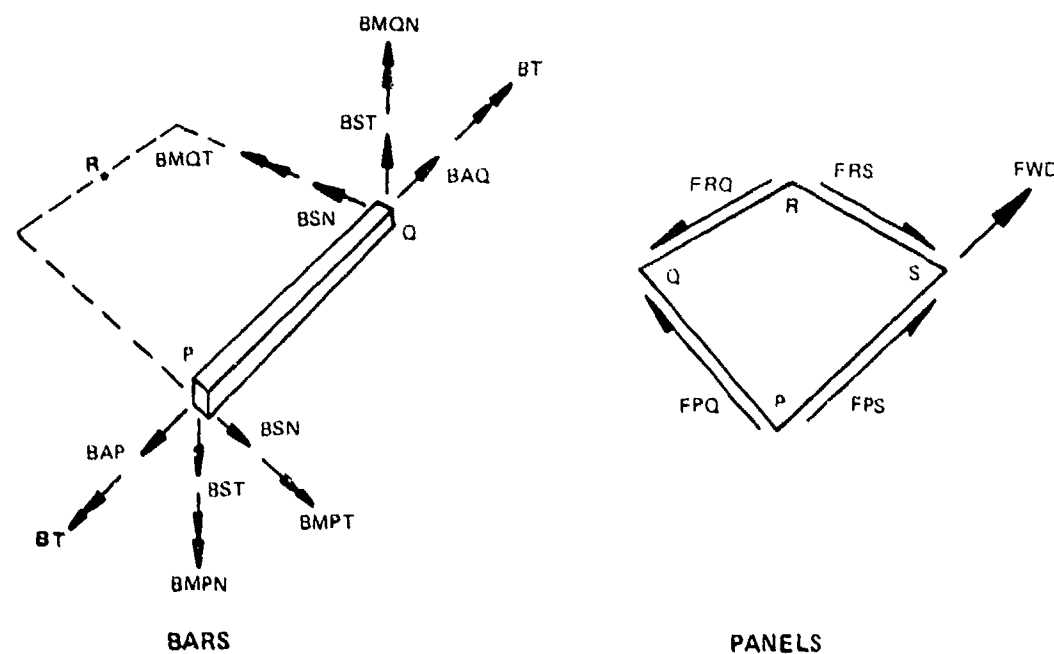


FIGURE 55. STRUCTURE IDEALIZATION



Note: Sign Convention - all forces are positive when acting as shown.

- BMQN - Bending moment at the Q end of the bar about an axis normal to the PQR plane (lbs)
- BMPN - Bending moment at the P end of the bar about an axis normal to the PQR plane (lbs)
- BSN - Bar shear acting in the PQR plane (lbs)
- BT - Bar torque acting about the bar axis (lbs)
- BAP - Bar axial load at the P end (lbs)
- BAQ - Bar axial load at the Q end (lbs)
- FRS - Panel shear load acting on the RS side (lbs), QRS (lbs/in.)
- FRQ - Panel shear load acting on the RQ side (lbs), QRS (lbs/in.)
- FPQ - Panel shear load acting on the PQ side (lbs), QPC (lbs/in.)
- FPS - Panel shear load acting on the PS side (lbs), QPC (lbs/in.)

FIGURE 66. DEFINITION OF OUTPUT TERMS



TABLE 4  
SHEAR PANELS

SHEAR NO.	CONDITION P	PANELS Q	COLUMN R	DOUGLAS AIRCRAFT COMPANY INTERNAL LOADS FS25.119 14. MATPFX PFORCE FRQ	TWO PT. LANDING * 0.100000E FRS	SPRING BACK AND PSTRES * OPQ	0.100000E ORQ	OL CASE QRS	PARC DI OPS
48	161	137	138	-3396	-3319	-3108	-255	-249	-255
49	137	137	138	-3396	-3326	-3034	-249	-244	-249
50	137	137	138	-3356	-3298	-3034	-249	-244	-249
51	137	137	138	-3356	-3298	-3034	-249	-244	-249
52	137	137	138	-3356	-3298	-3034	-249	-244	-249
53	137	137	138	-3356	-3298	-3034	-249	-244	-249
54	137	137	138	-3356	-3298	-3034	-249	-244	-249
55	137	137	138	-3356	-3298	-3034	-249	-244	-249
56	137	137	138	-3356	-3298	-3034	-249	-244	-249
57	137	137	138	-3356	-3298	-3034	-249	-244	-249
58	137	137	138	-3356	-3298	-3034	-249	-244	-249
59	137	137	138	-3356	-3298	-3034	-249	-244	-249
60	137	137	138	-3356	-3298	-3034	-249	-244	-249
61	137	137	138	-3356	-3298	-3034	-249	-244	-249
62	137	137	138	-3356	-3298	-3034	-249	-244	-249
63	137	137	138	-3356	-3298	-3034	-249	-244	-249
64	137	137	138	-3356	-3298	-3034	-249	-244	-249
65	137	137	138	-3356	-3298	-3034	-249	-244	-249
66	137	137	138	-3356	-3298	-3034	-249	-244	-249
67	137	137	138	-3356	-3298	-3034	-249	-244	-249
68	137	137	138	-3356	-3298	-3034	-249	-244	-249
69	137	137	138	-3356	-3298	-3034	-249	-244	-249
70	137	137	138	-3356	-3298	-3034	-249	-244	-249
71	137	137	138	-3356	-3298	-3034	-249	-244	-249
72	137	137	138	-3356	-3298	-3034	-249	-244	-249
73	137	137	138	-3356	-3298	-3034	-249	-244	-249
74	137	137	138	-3356	-3298	-3034	-249	-244	-249
75	137	137	138	-3356	-3298	-3034	-249	-244	-249
76	137	137	138	-3356	-3298	-3034	-249	-244	-249
77	137	137	138	-3356	-3298	-3034	-249	-244	-249
78	137	137	138	-3356	-3298	-3034	-249	-244	-249
79	137	137	138	-3356	-3298	-3034	-249	-244	-249
80	137	137	138	-3356	-3298	-3034	-249	-244	-249
81	137	137	138	-3356	-3298	-3034	-249	-244	-249
82	137	137	138	-3356	-3298	-3034	-249	-244	-249
83	137	137	138	-3356	-3298	-3034	-249	-244	-249
84	137	137	138	-3356	-3298	-3034	-249	-244	-249
85	137	137	138	-3356	-3298	-3034	-249	-244	-249
86	137	137	138	-3356	-3298	-3034	-249	-244	-249
87	137	137	138	-3356	-3298	-3034	-249	-244	-249
88	137	137	138	-3356	-3298	-3034	-249	-244	-249
89	137	137	138	-3356	-3298	-3034	-249	-244	-249
90	137	137	138	-3356	-3298	-3034	-249	-244	-249
91	137	137	138	-3356	-3298	-3034	-249	-244	-249
92	137	137	138	-3356	-3298	-3034	-249	-244	-249
93	137	137	138	-3356	-3298	-3034	-249	-244	-249
94	137	137	138	-3356	-3298	-3034	-249	-244	-249
95	137	137	138	-3356	-3298	-3034	-249	-244	-249
96	137	137	138	-3356	-3298	-3034	-249	-244	-249
97	137	137	138	-3356	-3298	-3034	-249	-244	-249
98	137	137	138	-3356	-3298	-3034	-249	-244	-249
99	137	137	138	-3356	-3298	-3034	-249	-244	-249
100	137	137	138	-3356	-3298	-3034	-249	-244	-249

DOUGLAS AIRCRAFT COMPANY  
PARIST INTERNAL LOADS

THIS PAGE IS BEST QUALITY PRACTICABLE  
FROM COPY FURNISHED TO DDC

TABLE 6  
BAR ELEMENTS, MAX/MIN

DOUGLAS AIRCRAFT COMPANY  
PABST INTERNAL LOADS

BAR NO.	ELEMENTS, MAX/MIN, /	PABST	INTERNAL	LOADS	PAQ	SARS	BSN	0.100000F	BMNP	OL	CASE	PABCDI	BST	BMTD	BMTD	BMTD	BT
463	137 138 153	15004	15845	15845	15845	15845	-12	866	1410	1410	0*	0*	0*	0*	0*	0*	0*
		20*	20*	20*	20*	20*	15*	17*	17*	17*	0*	0*	0*	0*	0*	0*	0*
		-613	-538	-538	-538	-538	-41	131	317	317	0*	0*	0*	0*	0*	0*	0*
		14*	14*	14*	14*	14*	17*	20*	14*	14*	0*	0*	0*	0*	0*	0*	0*
464	133 133 153	15844	15812	15812	15812	15812	3	1410	1515	1515	0*	0*	0*	0*	0*	0*	0*
		20*	20*	20*	20*	20*	20*	17*	17*	17*	0*	0*	0*	0*	0*	0*	0*
		-540	-456	-456	-456	-456	-12	317	410	410	0*	0*	0*	0*	0*	0*	0*
		14*	14*	14*	14*	14*	14*	14*	20*	20*	0*	0*	0*	0*	0*	0*	0*
465	139 143 153	15815	15825	15825	15825	15825	38	1515	1074	1074	0*	0*	0*	0*	0*	0*	0*
		20*	20*	20*	20*	20*	19*	17*	16*	16*	0*	0*	0*	0*	0*	0*	0*
		-457	-375	-375	-375	-375	-11	410	-75	-75	0*	0*	0*	0*	0*	0*	0*
		14*	14*	14*	14*	14*	14*	20*	20*	20*	0*	0*	0*	0*	0*	0*	0*
466	140 141 153	15832	15905	15905	15905	15905	86	1074	737	737	0*	0*	0*	0*	0*	0*	0*
		20*	20*	20*	20*	20*	17*	16*	14*	14*	0*	0*	0*	0*	0*	0*	0*
		-276	-298	-298	-298	-298	-4	-75	-983	-983	0*	0*	0*	0*	0*	0*	0*
		14*	14*	14*	14*	14*	14*	20*	20*	20*	0*	0*	0*	0*	0*	0*	0*
467	141 142 153	15841	16101	16101	16101	16101	98	737	656	656	0*	0*	0*	0*	0*	0*	0*
		20*	20*	20*	20*	20*	17*	14*	14*	14*	0*	0*	0*	0*	0*	0*	0*
		-293	-145	-145	-145	-145	4	-983	-2305	-2305	0*	0*	0*	0*	0*	0*	0*
		14*	14*	14*	14*	14*	14*	20*	17*	17*	0*	0*	0*	0*	0*	0*	0*
468	142 143 153	16089	15585	15585	15585	15585	90	656	-321	-321	0*	0*	0*	0*	0*	0*	0*
		20*	20*	20*	20*	20*	17*	14*	14*	14*	0*	0*	0*	0*	0*	0*	0*
		-139	252	252	252	252	0	-2305	-4577	-4577	0*	0*	0*	0*	0*	0*	0*
		14*	14*	14*	14*	14*	0	17*	17*	17*	0*	0*	0*	0*	0*	0*	0*
469	143 144 153	15611	16797	16797	16797	16797	151	-321	1248	1248	0*	0*	0*	0*	0*	0*	0*
		20*	20*	20*	20*	20*	20*	14*	15*	15*	0*	0*	0*	0*	0*	0*	0*
		262	-1049	-1049	-1049	-1049	-128	-4507	-7170	-7170	0*	0*	0*	0*	0*	0*	0*
		14*	14*	14*	14*	14*	15*	17*	20*	20*	0*	0*	0*	0*	0*	0*	0*
470	144 145 153	10884	940	940	940	940	134	1248	0	0	0*	0*	0*	0*	0*	0*	0*
		20*	20*	20*	20*	20*	15*	15*	0	0	0*	0*	0*	0*	0*	0*	0*
		-1049	-10	-10	-10	-10	-172	-7170	0	0	0*	0*	0*	0*	0*	0*	0*
		15*	15*	15*	15*	15*	20*	20*	0	0	0*	0*	0*	0*	0*	0*	0*
471	146 147 153	223	2054	2054	2054	2054	159	0	2826	2826	0*	0*	0*	0*	0*	0*	0*
		14*	14*	14*	14*	14*	14*	0	0	0	0*	0*	0*	0*	0*	0*	0*
		-5251	-7925	-7925	-7925	-7925	-1637	0	-276	-276	0*	0*	0*	0*	0*	0*	0*
		20*	20*	20*	20*	20*	20*	0	0	0	0*	0*	0*	0*	0*	0*	0*
472	147 148 153	1034	3803	3803	3803	3803	-5	2826	8583	8583	0*	0*	0*	0*	0*	0*	0*
		14*	14*	14*	14*	14*	14*	20*	17*	17*	0*	0*	0*	0*	0*	0*	0*
		-7501	-3934	-3934	-3934	-3934	-487	-276	-213	-213	0*	0*	0*	0*	0*	0*	0*
		17*	17*	17*	17*	17*	17*	14*	14*	14*	0*	0*	0*	0*	0*	0*	0*
473	148 149 153	8809	17695	17695	17695	17695	473	8583	2701	2701	0*	0*	0*	0*	0*	0*	0*
		20*	20*	20*	20*	20*	20*	17*	17*	17*	0*	0*	0*	0*	0*	0*	0*
		-3924	-696	-696	-696	-696	-67	-213	324	324	0*	0*	0*	0*	0*	0*	0*
		15*	14*	14*	14*	14*	14*	14*	15*	15*	0*	0*	0*	0*	0*	0*	0*

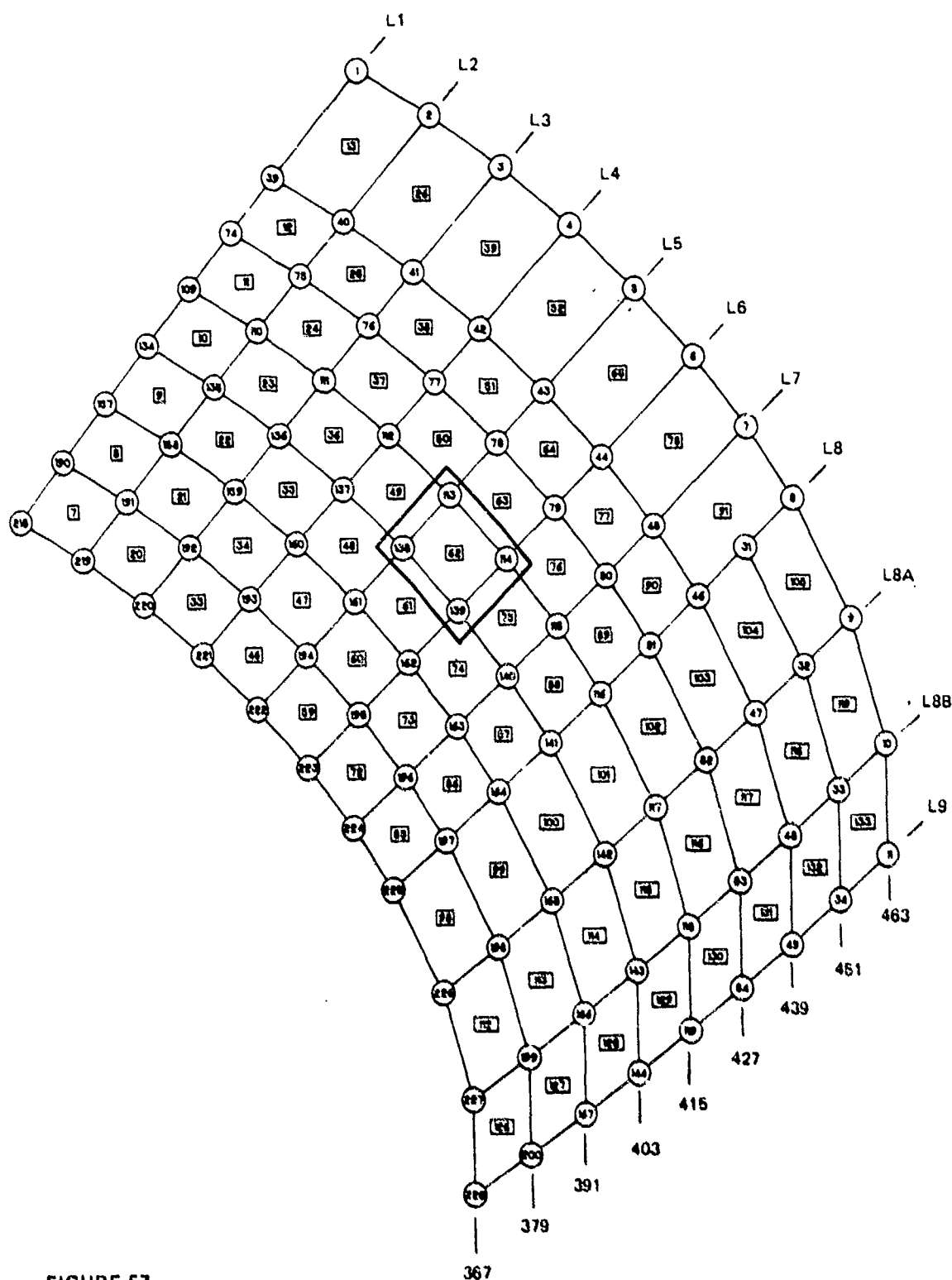


FIGURE 57.

PABST FUSELAGE TEST SPECIMEN - LEFT SIDE UPPER SECTION - PANEL  
FROM STATION 367.0 TO 463.0, REF NODES ON Y-AXIS 30, 38, -, 108, 105,  
156, -, 217, -  
SHOWING POINT NUMBERS AND PANEL NUMBERS

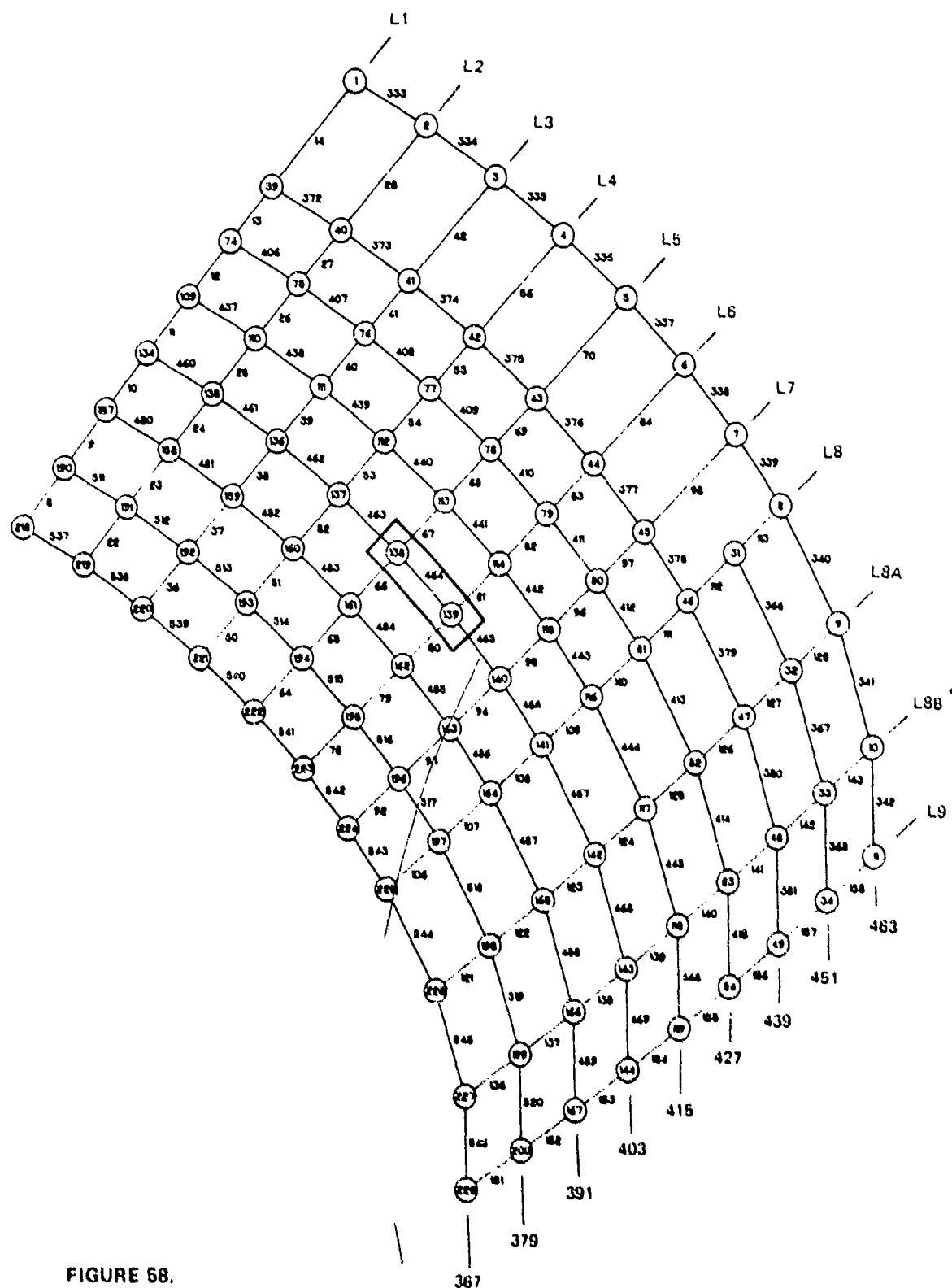






FIGURE 68.

PABST FUSELAGE TEST SPECIMEN - LEFT SIDE UPPER SECTION - BAR  
FROM STATIONS 367.0 TO 463.0, REF NODES ON Y-AXIS 30, 38, -, 108, 106,  
156, -, 217, -  
SHOWING POINT NUMBERS AND BAR NUMBERS

Shear Static Test Panels. - These tests were to determine the static shear and the combined shear plus tension or compression strength of the fuselage shell concept. The test results are shown in Tables 7 and 8. All visible evidence of the test specimens indicated that failures initiated in the metal with occasional secondary adhesive disbond. A significant observation is that, in those specimens having shear tee cutouts at the frame/longeron intersections, failure was initiated by crippling of the Z frame flange closest to the skin. It should be noted also that, in the absence of such cutouts, the shear tee was often ripped along the web/flange intersection, with the flange still bonded securely to the sharply wrinkled skin. For the one skin thickness in Table 8 where the original design shear slightly exceeded the test shear, an additional doubler was added on the FSDC where this design shear occurs.

TABLE 7  
SHEAR - COMPRESSION/TENSION  
INTERACTION STATIC TEST PANEL







ADHESIVE FM73, PRIMER BR127, TEST TEMP = 140°F

SKIN 7075T6	LONGERON	TEST		DESIGN	
		SHEAR (KSI)	AXIAL (KSI)	SHEAR (KSI)	AXIAL (KSI)
0.05		18.1	-29.2	17.8	-14.0
0.05		23.0	56.6	13.4	56.4
0.09	NONE	16.9	-8.7	16.3	-8.4
0.05		30.6	67.9	13.4	55.4
0.05		18.0	-18.2	17.8	-14.0

AXIAL STRESS - - COMPRESSION, + = TENSION

TABLE 8  
SHEAR STATIC TEST PANEL

PRIMER BR127

SKIN 7075T6	LONGERON	ADHESIVE	TEST TEMP	TEST SHEAR (KSI)	DESIGN SHEAR (KSI)	ANALYSIS FAILURE PREDICTION (KSI)
0.04		FM73	-50°F	19.8	13.0	18.3
0.09		RIVETED	R.T.	24.6	20.0	21.8
0.09		FM73	R.T.	26.5	20.0	21.8
0.04		M1133	-50°F	27.5	13.0	18.3
0.04		M1133	140°F	25.3	13.0	18.3
0.09	NONE	FM73	140°F	19.6	20.0	10.6
0.09*	NONE	FM73	140°F	23.8	20.0	12.6
0.0434		FM73	140°F	30.7	13.0	23.3

\*12 IN. FRAME  
SPACING

Frame Bending Test. - These tests determine the static strength of a typical frame-longeron-skin combination under pure bending in the frame. The frame section properties and test setup are shown in Figures 59 and 60 respectively. The test results are shown in Figure 60. Initial failure occurred along a one-inch length in the bond between the skin and frame tie shear clip, starting at the edge of the shear clip cutout for the longeron, followed by complete disbond between longerons and subsequent frame crippling.

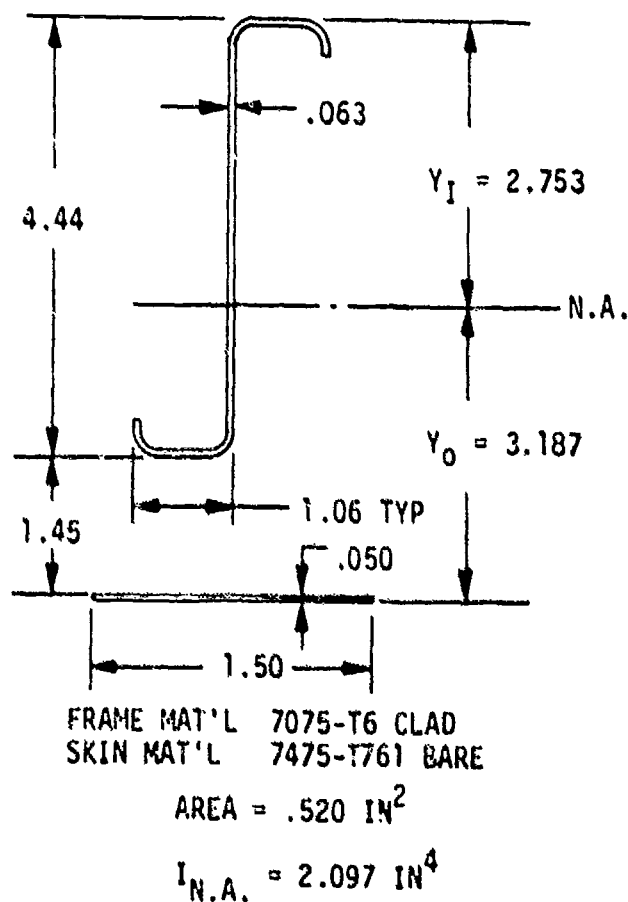


FIGURE 59. CROSS SECTION OF FRAME THROUGH LONGERON CUTOUT

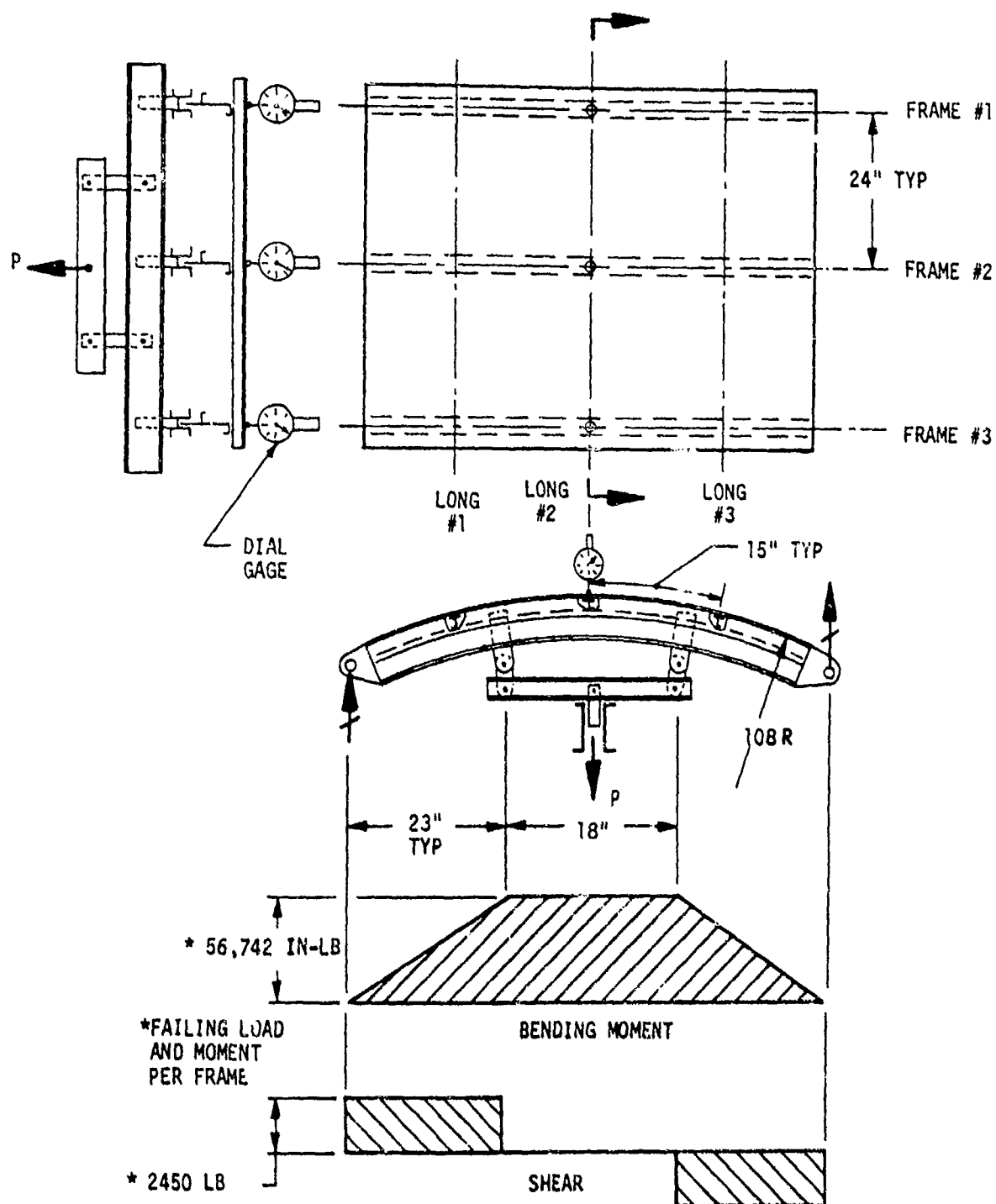
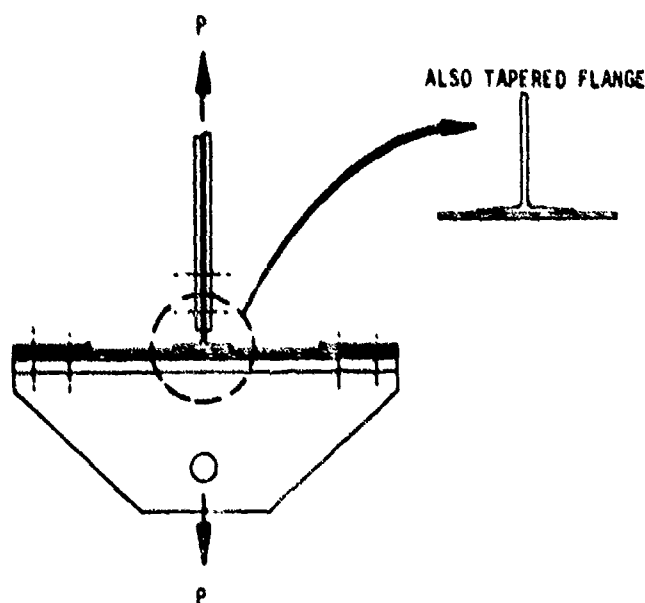


FIGURE 60. FRAME BENDING TEST (SPECIMEN 23) AND RESULTS

Tension Tee Static Tests. - These tests were made to determine the joint static strength between the frame tee shear clip and the skin under the simulated cabin pressure (14.3 psi ult) load. The test results are summarized in Table 9. All failures in Table 9 were in the bond and generally of the cohesive type failure.

TABLE 9  
TENSION TEE TEST

SKIN	ADHESIVE	PRIMER	FAILURE LOAD TEST TEMP			DESIGN LOAD
			-50 ± 5°F	R.T.	140 ± 5°F	-50°F
0.090 7075-T6	FM 73	BR 127	1740 LB			249 LB
0.040 7075-T6	FM 73	BR 127	1595 LB			389 LB
0.090 7075-T6	AF 55	XA 3950			4000 LB	249 LB
0.090 7075-T6	M 1133	BR 127	2170 LB			249 LB
0.090 7075-T6	AF 55	XA 3950	5910 LB	5050 LB	5075 LB	249 LB
0.090 7075-T6	M 1133	BR 127	2640 LB	4650 LB		249 LB
0.040 7075-T6	AF 55	XA 3950	1670 LB	3700 LB	4220 LB	389 LB
0.040 7075-T6	M 1133	BR 127	2105 LB	3275 LB	3358 LB	389 LB



## ANALYSIS

This section contains the analysis of the Full Scale Development Component for static, damage tolerance, fatigue, and bonded joint strength. Additionally, the spectra is developed for the fatigue and damage tolerance loading.

## Static Analysis

The critical static metal failure modes for the FSDC structural arrangement are identified from previous aircraft experiences as being:

1. Skin to stiffening element joint failure due to cabin pressure pulling the skin away from the stiffening members.
2. Skin to stiffening element joint failure due to "tension field" skin shear wrinkling.
3. Primary frame bending failure when the skin fails to continue acting as part of the frame/skin bending action due to attachment failure between the skin and frame resulting from the skin wrinkle prying action.

In order to determine the design static allowable for each of these failure modes, tests were run as described in Tables 7, 8, 9 and Figure 60.

From these test results, allowable load for each of the critical failure modes were derived. Allowable loads for material strength and fasteners were taken from MIL-HDBK-5.

The load allowable data for failure modes 2 and 3 along with MIL-HDBK-5 material strength data was input to the C9BA computer stress program. The resulting output lists stresses and margins of safety for each structural member (see Tables 10 through 13 for example output and Figure 57 and 58 in the Internal Load section for location of this example). The margin of safety in the Tables noted is the quotient of the allowable stress divided by the design stress. Tables 10 through 13 are examples of the output from the C9BA computer stress program used to determine stresses and margins of safety for frame flange, longeron crosssection, skin shear and principal stress, and the interaction strength of skin shear stress acting with longeron axial stress ("tension field" effects). The computer program derives these stresses for each loading condition (see Tables 10 and 12), and then searches out the most critical conditions by the lowest three margins of safety (Tables 11 and 13) Node 139 from the computer idealized model (sta 403, longeron 6) in Figure 57

is taken as an example. The max/min search of failure modes shown in Table 11 shows the lowest margin of safety 2.38 occurs in the frame outer flange for condition 20, and for the failure mode in Table 13 the lowest margin of safety is 2.31 for condition 15. In Table 10, at node 139, the upper row of values in the axial stress in the frame inner and outer flanges, longeron crosssection, skin in plane shear, skin in plane principal stresses respectively, all at the frame 403, longeron 6 intersections. The second row of values is the margin of safety, which is the quotient of the allowable stress divided by the design stress associated with the appropriate member and mode of loading.

TABLE 10

## EXAMPLE OUTPUT - LOADING CONDITION 20

DOUGLAS AIRCRAFT COMPANY  
PART FULL SCALE DEMONSTRATION COMPONENT

MODE	*** INNER PSI	FRAME OUTER PSI	***** INNER PSI	LONGERON OUTER PSI	*** SHEAR STRESS PSI	*** PRINCIPAL SIGMA MAX	*** PRINCIPAL SIGMA MIN	*** TAU MAX	DESCRIPTION
179 STRESS MARGIN	11381 5.59	14146 2.68		6596 8.25	2182	14732 3.14	6011	4360 7.71	SHELL SSI STA 391 LONG 14
180 STRESS MARGIN	3423 HIGH	17560 1.96		9973 5.12	236	17567 2.47	9966	3800 9.00	SHELL SSI STA 391 LONG 15
181 STRESS MARGIN	-119 HIGH	19239 1.70		13296 3.59	1589	19637 2.11	12897	3370 HIGH	SHELL SSI STA 391 LONG 16
182 STRESS MARGIN	-969 HIGH	19077 1.73		15533 2.93	1589	19686 2.10	14924	2381 HIGH	SHELL SSI STA 391 LONG 16A
134 STRESS MARGIN	15143 3.95	15217 2.39		10819 4.64	370	15347 2.97	10780	2279 HIGH	SHELL SSI STA 403 LONG 1
135 STRESS MARGIN	14931 4.01	15386 2.37		9871 5.18	370	15411 2.96	9847	2782 HIGH	SHELL SSI STA 403 LONG 2
136 STRESS MARGIN	14920 4.03	15383 2.37		9788 5.23	247	15394 2.96	9777	2808 HIGH	SHELL SSI STA 403 LONG 3
137 STRESS MARGIN	15035 3.99	15278 2.40		10074 5.05	595	15366 2.97	10007	2669 HIGH	SHELL SSI STA 403 LONG 4
138 STRESS MARGIN	14561 4.15	15401 2.37		9658 5.32	595	15462 2.95	9597	2932 HIGH	SHELL SSI STA 403 LONG 5
139 STRESS MARGIN	14587 4.14	15348 2.38		9563 5.38	568	15403 2.96	9508	2948 HIGH	SHELL SSI STA 403 LONG 6
140 STRESS MARGIN	15218 3.92	15016 2.44		9523 5.41	607	15132 3.03	9457	2837 HIGH	SHELL SSI STA 403 LONG 7
141 STRESS MARGIN	16563 3.53	14293 2.78	9527 5.40	9692 5.29	852	14446 3.22	9539	2453 HIGH	SHELL SSI STA 403 LONG 8
142 STRESS MARGIN	18184 3.12	13517 2.99		10044 5.07	852	13715 3.45	9846	1934 HIGH	SHELL SSI STA 403 LONG 8A
143 STRESS MARGIN	19696 2.81	11719 3.61		12182 4.01	2388	14351 3.25	9551	2399 HIGH	SHELL SSI STA 403 LONG 8B
144 STRESS MARGIN	20226 2.71	3669 HIGH	7076 7.62	17627 2.46	7067	20581 1.96	716	9932 2.83	SHELL SSI STA 403 LONG 9

TABLE 11

EXAMPLE OUTPUT - MAX/MIN SEARCH FOR FRAME AND SKIN

DOUGLAS AIRCRAFT COMPANY  
PAIST FULL SCALE DEMONSTRATION COMPONENT

MODE	MINIMUM MARGINS OF SAFETY AND CRITICAL LOAD CONDITIONS										DESCRIPTION
	FRAME *****		LONGERON *****		PRINCIPAL ***		TAU				
	INNER	MARGIN	OUTER	INNER	MARGIN	OUTER	SIGMA	MAX	MIN	MAX	
136	MARGIN	4.03	2.37		5.03		2.96		7.19		SHELL SS1 STA 403 LONG 3
	COND	2.0	2.0		17		2.0		14		
	MARGIN	6.36	3.49		5.21		3.57		HIGH		
	COND	1.9	1.9		15		1.7		HIGH		
137	MARGIN	6.41	3.50		5.23		3.68		20		SHELL SS1 STA 403 LONG 4
	COND	1.7	1.7		2.0		1.9				
	MARGIN	3.59	2.40		5.05		2.97		5.47		
	COND	2.0	2.0		2.0		2.0		14		
138	MARGIN	6.45	3.49		5.09		3.20		7.79		SHELL SS1 STA 403 LONG 5
	COND	1.9	1.7		1.7		1.7		15		
	MARGIN	6.53	3.49		5.26		3.34		9.23		
	COND	1.7	1.9		1.9		1.9		17		
139	MARGIN	4.15	2.37		5.12		2.95		4.74		SHELL SS1 STA 403 LONG 6
	COND	2.0	2.0		2.0		2.0		14		
	MARGIN	6.97	3.38		5.73		3.11		6.65		
	COND	1.9	1.7		1.7		1.7		15		
140	MARGIN	7.13	3.40		5.90		3.25		7.62		SHELL SS1 STA 403 LONG 7
	COND	1.7	1.9		1.9		1.9		17		
	MARGIN	4.14	2.38		5.38		2.96		4.19		
	COND	2.0	2.0		2.0		2.0		14		
141	MARGIN	6.78	3.36		6.39		3.05		5.79		SHELL SS1 STA 403 LONG 8
	COND	1.6	1.7		1.7		1.7		15		
	MARGIN	7.03	3.38		6.51		3.20		6.64		
	COND	1.9	1.9		1.9		1.9		17		
142	MARGIN	3.92	2.44		5.41		3.03		3.88		SHELL SS1 STA 403 LONG 9
	COND	2.0	2.0		2.0		2.0		14		
	MARGIN	6.44	3.43		7.30		3.10		5.23		
	COND	1.9	1.7		1.7		1.7		15		
143	MARGIN	6.63	3.45		7.31		3.25		6.09		SHELL SS1 STA 403 LONG 10
	COND	1.7	1.9		1.9		1.9		17		
	MARGIN	3.53	2.78		5.29		3.21		3.64		
	COND	2.0	2.0		2.0		2.0		14		
144	MARGIN	5.42	3.81		8.19		3.22		4.62		SHELL SS1 STA 403 LONG 11
	COND	1.9	1.7		1.7		1.7		15		
	MARGIN	5.52	3.86		8.23		3.38		5.76		
	COND	1.7	1.9		1.9		1.9		17		

TABLE 12  
EXAMPLE OUTPUT - LOADING CONDITION 15

DOUGLAS AIRCRAFT COMPANY  
PABST FULL SCALE DEMONSTRATION COMPONENT

MODE	**** INNER PSI	FRAME OUTER PSI	***** INNER PSI	LONGERON OUTER PSI	*** PSI	SHEAR STRESS PSI	*** MAX	PRINCIPAL STRESS SIGMA MAX	TAU MAX	DESCRIPTION
178 STRESS MARGIN				-92 HIGH	11184	11184	11138	-11280	11184	SHELL SSI STA397.0 LONG 13
179 STRESS MARGIN				370 HIGH	10752	10752	10939	-10567	10753	SHELL SSI STA397.0 LONG 14
180 STRESS MARGIN				955 HIGH	6053	6053	6549	-5593	6071	SHELL SSI STA397.0 LONG 15
181 STRESS MARGIN				1715 HIGH	3024	3024	4001	-2285	3143	SHELL SSI STA397.0 LONG 16
134 STRESS MARGIN				-3851 3.34	670	670	113	-3964	2039	SHELL SSI STA409.0 LONG 1
135 STRESS MARGIN				-4040 4.15	1551	1551	526	-4567	2547	SHELL SSI STA409.0 LONG 2
136 STRESS MARGIN				-3950 4.25	2442	2442	1164	-5124	3144	SHELL SSI STA409.0 LONG 3
137 STRESS MARGIN				-3767 3.11	3585	3585	2166	-5933	4050	SHELL SSI STA409.0 LONG 4
138 STRESS MARGIN				-3841 4.41	4321	4321	2808	-6649	4729	SHELL SSI STA409.0 LONG 5
139 STRESS MARGIN				-3837 4.42	4918	4918	3360	-7198	5279	SHELL SSI STA409.0 LONG 6
140 STRESS MARGIN				-3832 4.73	5342	5342	3758	-7591	5675	SHELL SSI STA409.0 LONG 7
141 STRESS MARGIN				-3745 4.47	5966	5966	4380	-8126	6253	SHELL SSI STA409.0 LONG 8
144 STRESS MARGIN				1035 HIGH	15208	15208	15735	-14699	15217	SHELL SSI STA409.0 LONG 9
145 STRESS MARGIN			-1751	58 HIGH	10558	10558	10588	-10529	10559	SHELL SSI STA409.0
146 STRESS MARGIN				1864 HIGH	15232	15232	16192	-14328	15260	SHELL SSI STA409.0 LONG 10

THIS PAGE IS BEST QUALITY PRACTICABLE  
FROM COPY FURNISHED TO DDC

TABLE 13

## EXAMPLE OUTPUT - MAX/MIN SEARCH FOR INTERACTION

DOUGLAS AIRCRAFT COMPANY  
PABST FULL SCALE DEMONSTRATION COMPONENT

## MINIMUM MARGINS OF SAFETY AND CRITICAL LOAD CONDITIONS

NODE	*** FRAME MARGIN	***** LONGERON MARGIN	***** OUTER	***** INNER	***** OUTER	***** INNER	PRINCIPAL SIGMA MAX	*** TAU MAX	INTER- ACTION MARGIN	DESCRIPTION
139 MARGIN					4.42	2.31			2.31	SHELL SS1 STA409.0 LONG 6
COND					15	15			15	
MARGIN					5.33	2.73			2.73	
COND					20	14			14	
MARGIN					6.25	3.50			3.50	
COND					17	17			17	
140 MARGIN					4.43	2.17			2.17	SHELL SS1 STA409.0 LONG 7
COND					15	15			15	
MARGIN					5.31	2.48			2.48	
COND					20	14			14	
MARGIN					7.08	3.46			3.46	
COND					17	17			17	
141 MARGIN					4.47	1.99			1.99	SHELL SS1 STA 409.0 LONG 8
COND					15	15			15	
MARGIN					4.87	2.29			2.29	
COND					20	14			14	
MARGIN					7.50	3.42			3.42	
COND					19	17			17	
144 MARGIN					-0.09	-0.21			-0.21	SHELL SS1 STA409.0 LONG 9
COND					14	14			14	
MARGIN					0.10	0.07			0.07	
COND					16	16			16	
MARGIN					0.34	0.31			0.31	
COND					18	18			18	
145 MARGIN					6.67	1.28			1.28	SHELL SS1 STA409.0
COND					20	15			15	
MARGIN					HIGH	3.47			3.47	
COND					19	14			14	
MARGIN					HIGH	5.80			5.80	
COND					16	17			17	

## Spectrum Analysis

Load Sources. - The variable loads encountered by the airplane result from the flight and ground environments in which an airplane must operate. This data results from a statistical analysis of information accumulated from Air Force operations and is normally described in terms of incremental load factor excursions from the one g condition.

Taxi: - This spectrum covers the runway roughness during the pre and post flight taxi, take-off and landing roll. Because of its mission, the C-15 airplane would be called upon to operate out of airfields which range from paved runways to unpaved runways. For purposes of this analysis three grades of runways were considered:

(1) Paved Runways. The data of MIL-A-8866A was used for paved runways. Half the vertical load factor cycles are presumed to occur in the take-off phase and the other half in the landing phase of each mission. For convenience, the data as used in this analysis is included in Table 14.

(2) Semi-prepared Runways. Based on Southeast Asia operations of the C-130 aircraft, the vertical load factor experienced on semi-prepared runways was found to be 1.5 times as severe as that on paved runways. Thus, to obtain the taxi spectrum for semi-prepared runways, the MIL-SPEC spectrum was multiplied by this factor and the data used is presented in Table 14.

(3) Unimproved Runways. For the unimproved runways roughness data, recourse was again made to C-130 Southeast Asia operations experience. It was found that at a frequency of one per ten landings, the incremental load factor for unimproved runways was 1.37 times that for semi-prepared runways. This point is shown in Figure 61. At higher incremental load factors and corresponding lower frequencies the data was extrapolated by drawing a line parallel to that for semi-prepared runways. Table 14 has, for the three categories of runways, the frequency at specified incremental load factor levels.

Landing Impact: - The airplane sink rate depends in a large measure on the landing mode. In conventional landings where adequate runways are available, the sink rate at touchdown will be much less severe than those encountered under short field landing conditions. For short field landings, the

TABLE 14  
PABST RUNWAY ROUGHNESS SPECTRA

$\pm \Delta n_z$	Cumulative Occurrences/1,000 Landings		
	Paved Runways MIL-A-8866A Spec.	Semi-Prepared Runways	Unimproved Runways
.1	194,094	280,000	280,000
.2	29,094	100,000	210,000
.3	2,094	30,000	130,000
.4	94.155	5,000	68,000
.5	4.155	750	22,000
.6	.155	100	5,300
.7	.005	15	900
.8		2	130
.9		.3	20
1.0		.05	3
1.1			.5

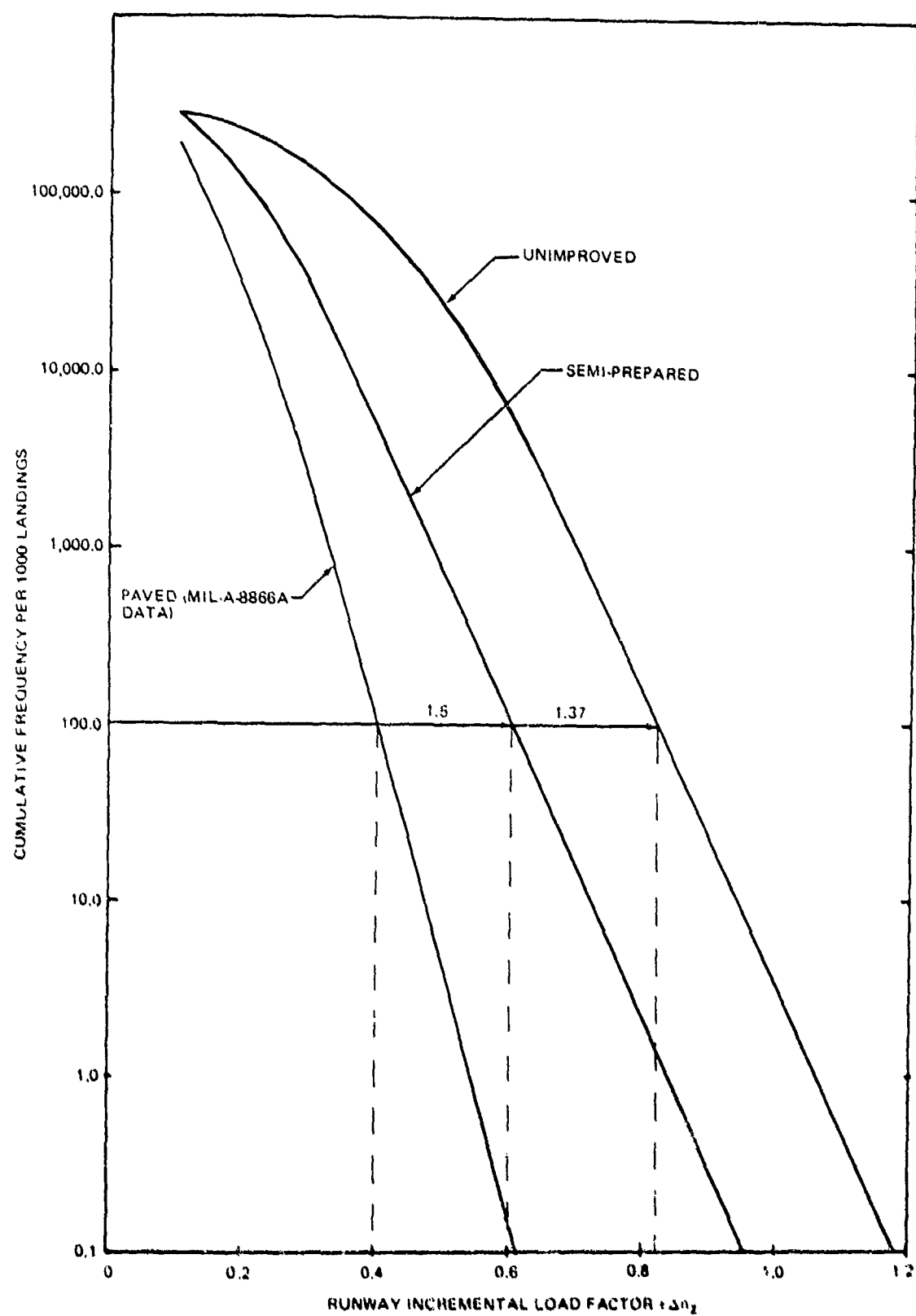


FIGURE 61. PABST RUNWAY ROUGHNESS DATA

gross weights at touchdown are significant to the rate of sink spectrum. These parameters were considered in developing the landing impact spectra used in the PABST analysis. For the PABST analysis the following equations were used to convert landing sink speed to airplane center of gravity load factor.

$$\Delta n_z = 0.2 + 0.0113 (V_s - 2)^2 \quad \text{for } V_s \geq 2 \text{ ft./sec.}$$

$$\Delta n_z = 0.1 V_s \quad \text{for } V_s \leq 2 \text{ ft./sec.}$$

where  $\Delta n_z$  = vertical load factor, g's.

and  $V_s$  = sink rate, ft./sec.

Conventional (CTOL) Landings:- The data used was that in Table IX of MIL-A-8866A converted to airplane center of gravity load factor using the above equations. The data is presented in Table 15.

Short Field (STOL) Landings:- Short field landings were considered at high and low gross weight landings. The dividing line was  $GW = 153,000\#$ . At higher gross weights the design sink speed was lower and the corresponding load factors were lower. The data are based on C-130 and Breguet 941 landings. The data as used in this analysis are presented in Table 15.

Gust: - The gust spectrum experienced for the PABST analysis was established as follows:

$$\Sigma N = \left[ N_{o1} P_1 e^{-\Delta g/b_1 \bar{A}} + N_{o2} P_2 e^{-\Delta g/b_2 \bar{A}} \right] T$$

Where

$N_{o1}$  = 10 cumulative occurrences/stat. mile

$N_{o2}$  = 7.5 cumulative occurrences/stat. mile

$\bar{A}$  = Airplane Center of Gravity Load Factor Unit Response

$P_1, P_2, b_1$  and  $b_2$  are Turbulence Parameters, Functions of Altitude

$\Sigma N$  = cumulative occurrences

TABLE 15  
PABST LANDING IMPACT SPECTRUM

$\Delta n_z$	Cumulative Occurrences/1,000 Landings		
	Conventional (CTOL) Landings	Short Field (STOL) Landings	
		G.W. > 153,000#	G.W. < 153,000#
.1			
.2	530	800	900
.3	50	290	600
.4	9	160	450
.5	4.3	94	320
.6	2.2	60	250
.7	1.3	39	210
.8	.65	25	163
.9		14	133
1.0		11	110
1.2		4.6	70
1.4			50
1.6			37
1.8			26
2.0			20
2.2			15.5
2.4			11.3
2.6			7.4
2.8			4.8
3.0			3.2
3.2			2.2

Table 16 shows the turbulence parameters as defined by MIL-A-8861A. This turbulence model was used for all flight segments, except for the low level terrain following flight, for which a separate gust plus maneuver spectrum was defined in Table 17. This spectrum was used in analysis of the low level resupply missions.

Maneuvers: - The maneuver spectra were obtained from Tables VII and VIII of MIL-A-8866A, for logistics, training and assault missions. For convenience of the analysis the data were reduced to equation form:

$$\Sigma N = N_{01}^{-\Delta g/g_1} + N_{02}^{-\Delta g/b_2}$$

The parameters of this equation for the various missions are presented in Table 18. In general experience, positive maneuvers significantly exceed negative maneuvers. For analysis purposes maneuver cycles were defined as follows:

- (i) A positive and a negative maneuver of like magnitude were combined to form a maneuver cycle. These are referred to as (+) maneuver cycles in TABLE 18.
- (ii) The excess of the positive maneuvers which could not be mated with like negative maneuvers are referred to as a (+) maneuver.

The above spectra were used for the basic and training missions. For the low level resupply missions and touch and go's the maneuver spectrum is included in the data of Table 17.

Internal Pressure: - The dominant source of internal load in the PABST structure is the internal pressure. For the PABST analysis, the pressurization envelope of the YC-15 was assumed to be applicable. Thus, the internal pressure was assumed to vary linearly from zero at sea level to 7.15 psi at 17,000 feet. Above 17,000 feet the pressure remains invariant at 7.15 psi.

Ground Air Ground Cycle. - This is the maximum stress excursion between the minimum ground stress and the maximum flight stress. For a typical PABST structural element, the stress experienced will be as shown schematically

TABLE 16  
PABST ATMOSPHERIC TURBULENCE PARAMETERS

Altitude Ft.	Mission Segment	P <sub>1</sub>	b1 * ft/sec.	P <sub>2</sub>	b2 * ft/sec.	Scale of Turbulence L, ft.
0-1,000	Climb, Cruise and Descent	1.00	2.50	.005	5.0	500
1,000-2,500	"	.42	2.93	.0033	5.75	1,750
2,500-5,000	"	.30	3.23	.0020	7.70	2,500
5,000-10,000	"	.15	3.20	.00095	8.25	2,500
10,000-20,000	"	.062	2.59	.00026	8.33	2,500
20,000-30,000	"	.025	2.11	.00011	7.92	2,500
30,000-40,000	"	.011	1.63	.000095	5.48	2,500

\*Based on Equivalent Airspeed V<sub>e</sub>, ft/sec.

TABLE 17  
LOW LEVEL PENETRATION GUST  
PLUS MANEUVER SPECTRUM

$\pm \Delta n_z, g's$	Cumulative Occurrences Per Flight Hour
.1	1,300
.2	420
.3	160
.4	52
.5	17
.6	4
.7	2.8
.8	.95

NOTE: This data supercedes the low level  
contour flight gust data of  
MIL-A-8861A

TABLE 18  
MANEUVER LOAD SPECTRA FOR  
AIRPLANE CG VERTICAL LOAD  
FACTORS

Spectrum Equation

$$\Sigma N = N_{01} e^{-\Delta g/b_1} + N_{02} e^{-\Delta g/b_2}$$

MISSION TYPE			N <sub>01</sub>	N <sub>02</sub>	b <sub>1</sub>	b <sub>2</sub>	$\Delta g$ Max
Basic Missions	Climb	±	2.7x10 <sup>5</sup>	2.5x10 <sup>2</sup>	.0492	.1646	
		+	9.0x10 <sup>4</sup>	50.0	.0869	.2817	
	Cruise	±	4.0x10 <sup>4</sup>	10 <sup>3</sup>	.0523	.0986	
		+	2.1x10 <sup>4</sup>	62.0	.0921	.2621	
	Descent	±	1.9x10 <sup>5</sup>	0	.0543	0	
		+	1.7x10 <sup>5</sup>	4.5x10 <sup>2</sup>	.0942	.2311	
Training Missions	Climb	±	1.6x10 <sup>5</sup>	0	.0598	0	
		+	5.2x10 <sup>5</sup>	2.7x10 <sup>3</sup>	.0835	.1820	
	Cruise	±	4.0x10 <sup>4</sup>	0	.0566	0	
		+	4.6x10 <sup>5</sup>	40	.0843	.2966	
	Descent	±	5.5x10 <sup>4</sup>	9.5x10 <sup>3</sup>	.0476	.0841	
		+	5.4x10 <sup>5</sup>	1.6x10 <sup>4</sup>	.0670	.1922	

Data for above equation was obtained from:

MIL-A-8866A Table VIII - Assault Spectrum

MIL-A-8866A Table VII - Transport Training Spectra

in Figure 62. During taxi and takeoff, the element experiences a variable stress due to runway roughness. After takeoff, the internal pressure build-up dominates the element stresses with small amplitude variations as a result of gust and maneuver inertia loads. During the flight phase, the inertia loads form a relatively small proportion of the total stress, generally less than 10% for the PABST airframe.

Utilization. - The basis for the PABST utilization was the YC-15 mission profiles and a desired service life of 30,000 flight hours. For convenience of the analysis, the YC-15 mission profiles were consolidated into three types of flights:

- (i) basic mission
- (ii) training mission
- (iii) low altitude resupply mission

Associated with each of the basic missions is one touch and go landing, and six touch and go landings with each of the training missions. The assumed PABST utilization is shown in Table 1. For the PABST analysis, the important parameter is the number of full pressure cycles, which is 16,360 and entirely due to the basic mission profiles. There are 2,648 partial pressurizations due to the training missions for a total of 19,008 pressurizations. The low altitude missions were assumed to be unpressurized because cruise altitude was 500 feet above the terrain.

To account for the variability of the payloads carried during normal operations, each of the missions was accomplished with two payload weights. In the case of the basic and training missions the payload weights selected were 20,250 and 54,250#. For the low level resupply missions, the payloads used were 27,000# and 62,000#. These were the design payloads for the STOL and CTOL operations. Table 1 shows the mission frequencies at each payload.

Mission Profiles. - The basic outline of the mission profiles are shown in Table 1. However, for analysis purposes, the missions have to be segmented and average values of flight parameters assigned to each segment. The segmented profiles with the flight parameters associated with each segment are included in Appendix B.

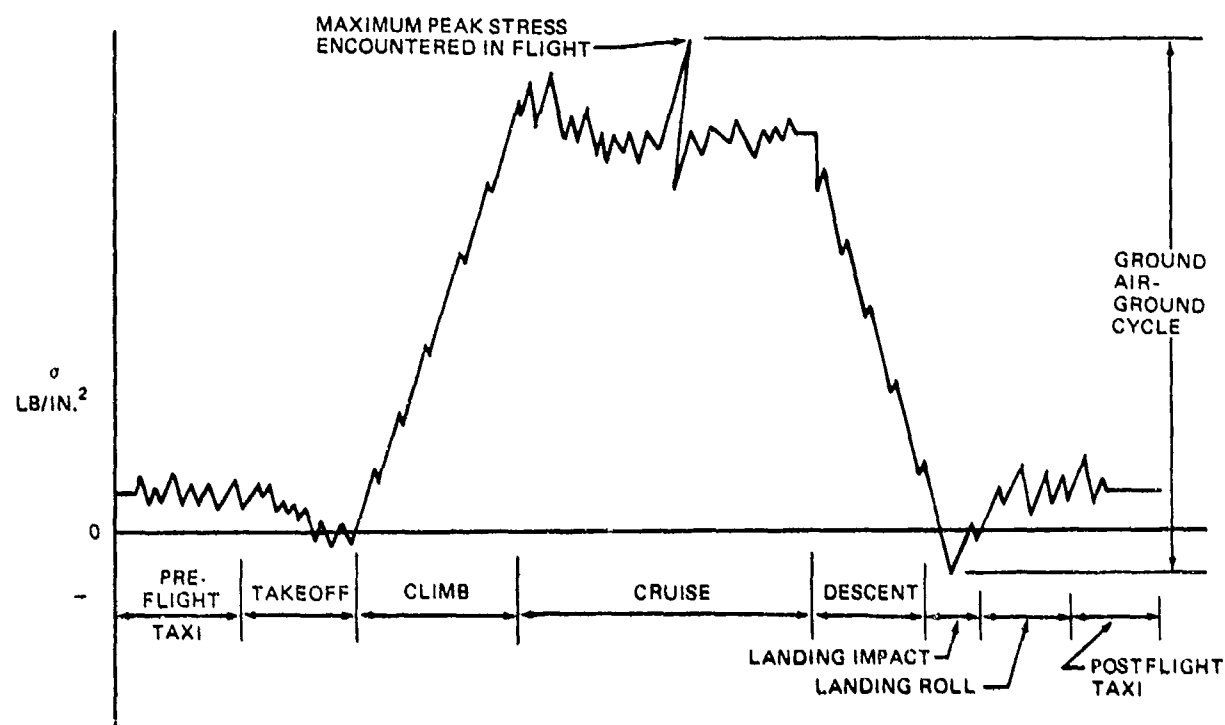


FIGURE 62. TYPICAL MISSION STRESS CYCLE

Payload Distributions. - The vast majority of the payloads to be carried by the AMST will be of the distributed kind, with attention being given to maintaining the airplane center of gravity within limits. These payload distributions are shown schematically in Figure 63. Vehicular payloads with large concentrated axle loads were also included in the external loads analysis. The required payloads were built up using the following vehicles:

- (i) Jeeps - 2465#
- (ii) 3/4 ton truck - 7,660#
- (iii) 5 ton truck - 27,125#
- (iv) 8 ton goer - 36,690#
- (v) 2-1/2 ton truck - 18,560#
- (vi) 15K forklift - 47,000#
- (vii) Howitzer - 62,000#
- (viii) armoured personnel carriers - 23,380#

The maximum axle load was 25,850# for the 15K forklift. The vehicular payloads did not result in any unusually high internal loads. In any event, the dominant sources of structural member loads is internal pressure. Thus, the inertia loads considered were based on the distributed payloads of Figure 63.

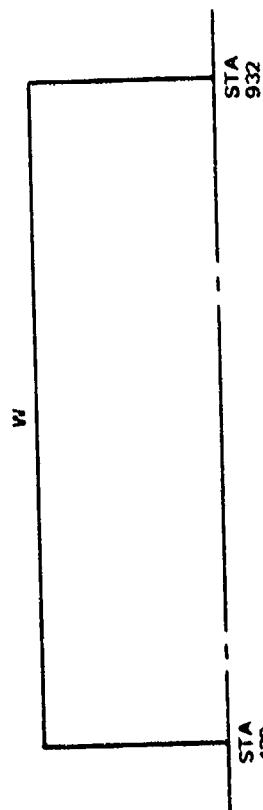
For the Phase Ib analysis, a complete range of conditions using the distributed and vehicular payloads were analyzed. A review of the internal loads resulting from these various payload distributions showed little variation in the internal structural member loads. Thus for this Phase II analysis, a much restricted range of conditions were analyzed. These conditions are listed in Table 19.

Analysis Check Points. - The criteria used in selecting the analysis check points was to aid in the design of the Full Scale Demonstration Component and to assure that it would be able to meet the fatigue and damage tolerance criteria. (Reference DESIGN CRITERIA). The points are shown graphically in Figure 64 for the cylindrical section, tapered section, close spaced longeron areas, wide spaced longeron areas, and compression areas under inertial loads.

The format internal loads solutions were utilized to obtain inertia and airload stresses for each of the check points. Table 20 lists the bar

(a) PAYLOADS F1 AND F2

PYLD NO.	PAYLOAD LB	W LB/IN.
F1	20,250	37.293
F2	27,000	49.724



(b) PAYLOADS F3 AND F4

PYLD NO.	PAYLOAD LB	W <sub>1</sub> LB/IN.	W <sub>2</sub> LB/IN.
F3	54,250	90.720	56.694
F4	62,000	103.680	64.790

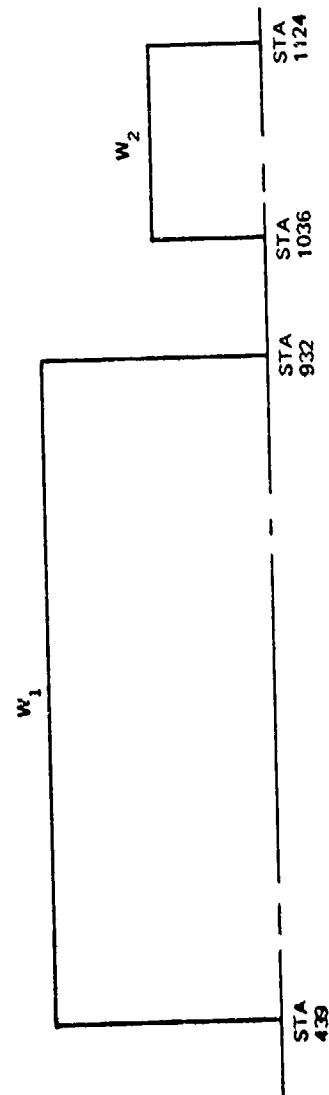


FIGURE 63. SCHEMATIC OF THE DISTRIBUTED AMST PAYLOADS EXTERNAL LOADS ANALYSIS FOR PABST

TABLE 19  
EXTERNAL LOAD CONDITIONS FOR DEVELOPMENT OF STRESS SPECTRA

FORMAT COND. NO.	EXTERNAL LOAD.COND. NO.	DESCRIPTION	PAYLOAD WEIGHT #	PAYLOAD NO.	INTERNAL PRESSURE P psi	VERTICAL LOAD FACTOR g's	PITCH. ACC. rads/sec <sup>2</sup>
1	-	1P only	-	-	7.15	-	-
2	15 FG	Basic STOL Cruise	20,250	F1	7.15	1.0	0
3	16 FG	Basic STOL Cruise	20,250	F1	7.15	1.77	0
4	19 FG	Basic CTOL Cruise	54,250	F3	7.15	1.0	0
5	20 FG	Basic CTOL Cruise	54,250	F3	7.15	.175	0
6	27 FG	Low Alt. STOL Cruise	27,000	F2	0	1.0	0
7	28 FG	Low Alt. STOL Cruise	27,000	F2	0	2.0	0
8	35 FG	Low Alt. CTOL Cruise	62,000	F4	0	1.0	0
9	36 FG	Low Alt. CTOL Cruise	62,000	F4	0	1.99	0
10	1 FG	Basic STOL Taxi	20,250	F1	0	1.0	0
11	3 FG	Basic CTOL Taxi	54,250	F3	0	1.0	0
12	11 FG	Low Alt. CTOL Taxi	62,000	F4	0	1.0	0
13	7 FG	Low Alt. STOL Taxi	27,000	F2	0	1.0	0
14	F525.119	2 Pt. Landing, S.B.	27,000	F2	0	Varies	Varies

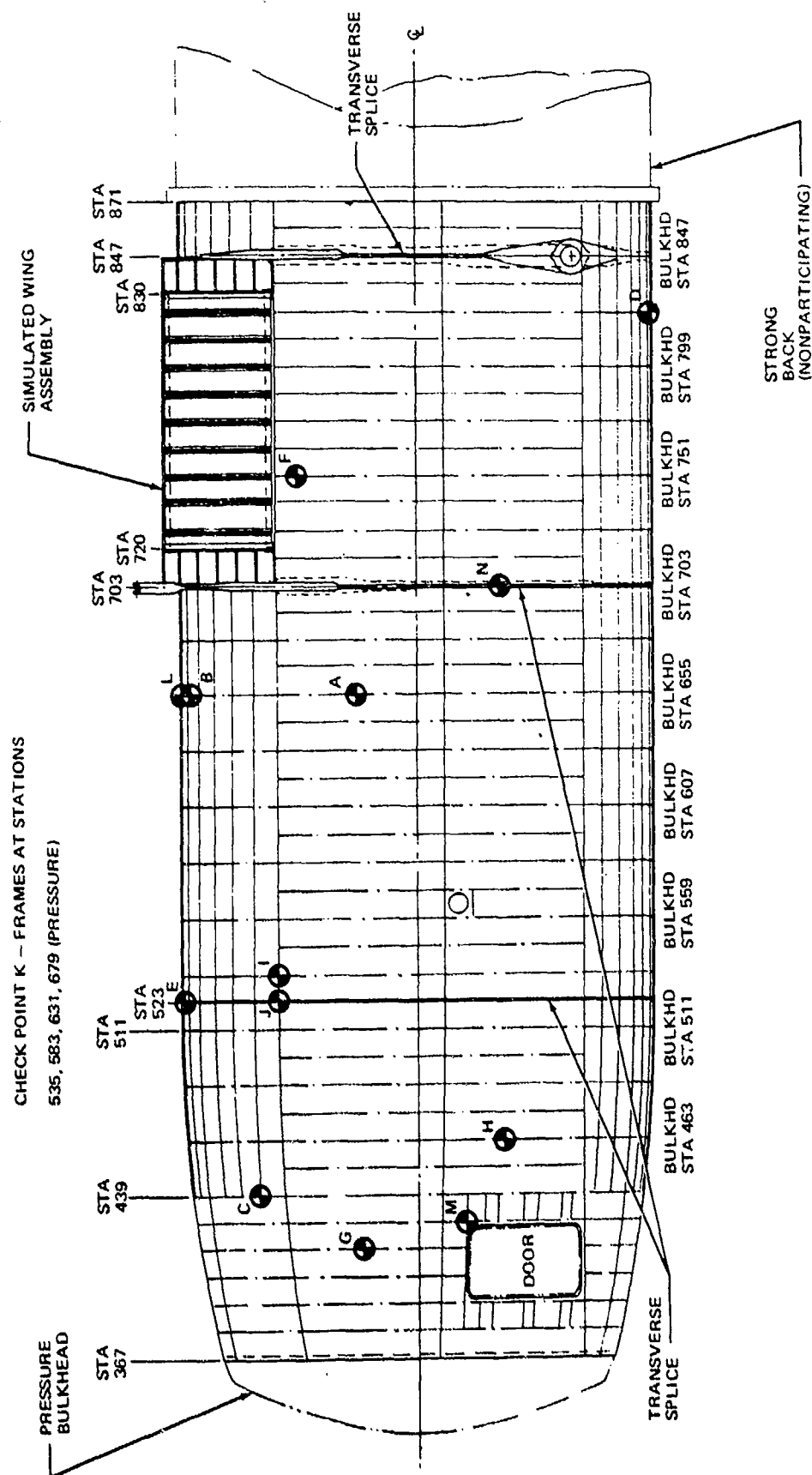


FIGURE 64. DAMAGE TOLERANCE ANALYSIS CHECK POINTS

TABLE 20  
LOCATIONS AND LONGITUDINAL STRESS OF THE ANALYSIS ELEMENTS

CHECK POINT				INTERNAL LOADS ANALYSIS	$\sigma_{xx}^{O.T.}$ - LB/SQ IN 20 LIFETIMES	TYPICAL STRESSES - LB/SQ IN.		
LTR	STA	LONG.	BAR NO.			$\sigma_{IP}$ PILLOWING	INERTIA + AIRLOAD	
							$\sigma_{1g}$	$d\sigma/dn$
A	655	8A		PHASE II PRELIM	15,500	13,632	227	295
B	655	2	578	PHASE II PRELIM		10,182	858	304
C	439	4	594	PHASE II PRELIM	14,053	14,053	57	49
D	823	16	782	PHASE II PRELIM	15368	15368	—	—
E	523	2		PHASE II PRELIM	15,000	14,324	519	343
	523	2	10	PHASE I(b)	16,700	14,314	910	1,185
F	751	8A	660	PHASE II PRELIM	10,000	8,990	410	234
			NODE 341	PHASE I(b)	11,100	10,356	51	-547
G	421	8A 8B AV	653 655	PHASE II PRELIM	11,100	11,093	7	-4
	421	8A 8B AV		PHASE I(b)	14,700	14,596	-342	185
H	465	9A	690	PHASE II PRELIM	13,500	13,745	-237	-223
			192 NODE 467	PHASE I(b)	13,320	14,269	-1,093	-112
J	523	8	642	PHASE II PRELIM	14,700	13,796	424	394
			65	PHASE I(b)	17,000	16,490	244	-227
L	655	1	565	PHASE II PRELIM	<10,000	7,700	1,140	340

numbers of the format model used in obtaining the inertia! and airload stresses for each of the check points. The internal pressure stresses were computed using the Douglas developed solution which accounts for skin bending at the frame and the effect of longitudinal stiffening.

Stress Spectra Generation. - The previous discussion covered the details of the variable load sources, turbulence spectra and the stress analysis. A modified version of the fatigue analysis computer program was used for the spectrum analysis. This program uses the data from load sources and for each segment of each mission profile constructs a  $\Delta n$  vs. frequency spectrum. The stress data,  $\sigma$  and  $d\sigma/dn$  are then used to convert the  $\sigma$  vs. frequency to  $(\sigma_{\max}, \sigma_{\min})$  vs. frequency spectrum. A spectrum (stress occurrences) for check point A based on Phase II preliminary internal loads is shown in Table 21. Ninety repetitions of the spectrum shown represents one lifetime.

The stress spectrum for check point A is presented in Table 21. The spectrum covers all the flights of the PABST utilization including the touch and go's. The maximum stress excursion (peak to peak) occurs in the ground air ground cycle. In Table 21 the first flight ground air ground cycle is referred to as FLGAG. It is formed by maximum stress experienced during flight including the excursions caused by gusts and maneuvers (G+M) and the minimum stress experienced during taxi. The variable stresses occurring during taxi on the ground and gusts and maneuvers in flight are included in Table 21. Little or no damage is anticipated from the taxi, gust and maneuver stress cycles. These were included in the spectrum because of their relatively high frequency. These stresses may become significant in flaw propagation as the flaw length gets large. It has been pointed out earlier that the stresses are dominated by the internal pressure loads. This can be seen in the flights where full pressurization is experienced. For instance during flight 1 full pressurization flight, a peak flight stress of  $14,273\#/in^2$  is experienced. During flight 11, touch and go flight where no pressurization is used, the peak stress is  $2,645\#/in^2$ . These low stress peaks will be completely blanked out by the high peaks of the full pressurization flights and result in a negligible influence on flaw growth. These low stresses are included in the spectrum due to their relatively high

frequency and in the interests of completeness.

Significant parameters of the longitudinal stress are included in Table 20. The one G and the incremental stress per G (inertia and airloads only) are included in the data, together with the one P pressure stress. The relative influence of inertia and pressure loads can therefore be assessed.

TABLE 21  
STRESS SPECTRUM FOR CHECK POINT A  
(90 REPETITIONS OF THE SPECTRUM REPRESENT ONE LIFETIME)

FLIGHT AND SEGMENT	MAX #/in <sup>2</sup>	MIN #/in <sup>2</sup>	NO. OF CYCLES
FLGAG	14,237	263	80
TAXI	788	380	2,160
TAXI	847	321	320
TAXI	905	263	80
G+M*	1,978	1,890	160
G+M	3,582	3,494	160
G+M	6,589	6,501	240
G+M	12,604	12,516	1,280
G+M	12,634	12,486	160
G+M	12,604	12,560	1,120
G+M	12,634	12,560	400
G+M	12,663	12,560	160
G+M	14,207	14,119	640
G+M	14,237	14,089	80
F2GAG	14,797	441	11
G+M	2,507	2,325	44
G+M	4,111	3,929	33
G+M	7,118	6,936	33
G+M	13,132	12,950	176
G+M	13,193	12,889	22
G+M	13,132	13,041	154
G+M	13,193	13,041	55

\*G+M = Gust + Maneuver

TABLE 21 (CONTINUED)  
STRESS SPECTRUM FOR CHECK POINT A

FLIGHT AND SEGMENT	MAX #/in <sup>2</sup>	MIN #/in <sup>2</sup>	NO. OF CYCLES
G+M	13,254	13,041	22
G+M	14,736	14,554	55
G+M	14,797	14,493	11
G+M	14,736	14,645	22
G+M	14,797	14,645	11
TAXI	1,322	636	297
TAXI	1,420	538	44
TAXI	1,517	441	11
F3GAG	14,237	263	80
TAXI	788	380	2,160
TAXI	847	321	320
TAXI	905	263	80
G+M	1,978	1,890	240
G+M	3,582	3,494	480
G+M	3,612	3,464	80
G+M	6,589	6,501	240
G+M	6,619	6,471	80
G+M	12,603	12,515	1,200
G+M	12,633	12,485	160
G+M	12,603	12,559	1,120
G+M	12,633	12,559	400
G+M	12,662	12,559	120

TABLE 21 (CONTINUED)  
STRESS SPECTRUM FOR CHECK POINT A

FLIGHT AND SEGMENT	MAX #/in <sup>2</sup>	MIN #/in <sup>2</sup>	NO. OF CYCLES
G+M	12,692	12,559	80
G+M	14,207	14,119	720
G+M	14,237	14,119	80
F4GAG	14,541	441	11
TAXI	1,322	636	297
TAXI	1,420	538	44
TAXI	1,517	441	11
G+M	2,272	2,150	33
G+M	3,876	3,754	33
G+M	6,883	6,761	44
G+M	12,897	12,775	132
G+M	12,937	12,735	22
G+M	12,897	12,836	88
G+M	12,937	12,836	33
G+M	12,977	12,836	11
G+M	14,501	14,379	66
G+M	14,541	14,339	11
F5GAG	12,692	263	14
TAXI	788	380	378
TAXI	847	321	56
TAXI	905	263	14
G+M	1,978	1,890	28

TABLE 21 (CONTINUED)  
STRESS SPECTRUM FOR CHECK POINT A

FLIGHT AND SEGMENT	MAX #/in <sup>2</sup>	MIN #/in <sup>2</sup>	NO. OF CYCLES
G+M	3,582	3,494	42
G+M	6,589	6,501	42
G+M	6,589	6,545	280
G+M	6,619	6,545	70
G+M	6,648	6,545	28
G+M	10,599	10,511	56
G+M	12,603	12,515	28
G+M	12,603	12,559	420
G+M	12,662	12,559	126
G+M	12,692	12,559	42
G+M	12,721	12,559	14
F6GAG	11,311	441	1
TAXI	1,322	636	27
TAXI	1,420	538	4
TAXI	1,517	441	1
G+M	2,507	2,325	3
G+M	4,111	3,929	3
G+M	7,118	6,936	7
G+M	7,179	6,875	1
G+M	11,128	11,037	23
G+M	11,189	11,037	6
G+M	11,250	11,037	2

TABLE 21 (CONTINUED)  
STRESS SPECTRUM FOR CHECK POINT A

FLIGHT AND SEGMENT	MAX #/in <sup>2</sup>	MIN #/in <sup>2</sup>	NO. OF CYCLES
G+M	11,311	11,037	1
F7GAG	8,683	263	14
TAXI	788	380	378
TAXI	847	321	56
TAXI	905	263	14
G+M	1,978	1,890	42
G+M	3,582	3,494	42
G+M	6,589	6,589	70
G+M	6,619	6,471	14
G+M	6,589	6,545	196
G+M	6,619	6,545	56
G+M	6,648	6,545	14
G+M	8,594	8,506	42
G+M	8,594	8,550	490
G+M	8,624	8,550	154
G+M	8,653	8,550	42
G+M	8,683	8,550	14
F8GAG	9,306	636	1
TAXI	1,322	636	4
G+M	2,507	2,325	3
G+M	4,111	3,929	3
G+M	7,118	6,936	5

TABLE 21 (CONTINUED)  
STRESS SPECTRUM FOR CHECK POINT A

FLIGHT AND SEGMENT	MAX #/in <sup>2</sup>	MIN #/in <sup>2</sup>	NO. OF CYCLES
G+M	7,179	6,875	1
G+M	7,118	7,027	17
G+M	7,179	7,027	4
G+M	7,240	7,027	1
G+M	9,123	8,941	2
G+M	9,123	9,032	30
G+M	9,184	9,032	9
G+M	9,245	9,032	3
G+M	9,306	9,032	1
F9GAG	2,645	263	80
TAXI	788	380	4,000
TAXI	847	321	720
TAXI	905	263	80
G+M	976	888	7,040
G+M	1,006	858	2,080
G+M	1,035	829	680
G+M	1,065	799	320
G+M	1,094	770	80
F10GAG	2,645	88	82
TAXI	788	380	61,008
TAXI	847	321	45,182
TAXI	905	263	16,400

TABLE 21 (CONTINUED)  
STRESS SPECTRUM FOR CHECK POINT A

FLIGHT AND SEGMENT	MAX #/in <sup>2</sup>	MIN #/in <sup>2</sup>	NO. OF CYCLES
TAXI	964	204	4,346
TAXI	1,022	146	738
TAXI	1,088	88	82
G+M	1,035	829	31,898
G+M	1,065	799	10,332
G+M	1,094	770	3,854
G+M	1,124	740	328
G+M	1,153	711	574
G+M	1,183	681	246
G+M	2,645	2,248	246
FLIGAG	2,645	343	5
TAXI	1,420	538	215
TAXI	1,517	441	35
TAXI	1,615	343	5
G+M	1,566	1,262	3,940
G+M	1,627	1,201	1,635
G+M	1,688	1,140	530
G+M	1,749	1,079	195
G+M	1,810	1,018	20
G+M	1,871	1,957	30
G+M	1,932	896	15
G+M	2,645	2,248	10

TABLE 21 (CONTINUED)  
STRESS SPECTRUM FOR CHECK POINT A

FLIGHT AND SEGMENT	MAX #/in <sup>2</sup>	MIN #/in <sup>2</sup>	NO. OF CYCLES
F12GAG	2,645	168	17
TAXI	973	369	2,346
TAXI	1,040	302	850
TAXI	1,174	168	34
G+M	1,344	1,022	3,672
G+M	1,390	976	1,190
G+M	1,435	931	442
G+M	1,481	885	34
G+M	1,527	839	68
G+M	1,573	793	34
G+M	2,645	1,984	17
F13GAG	2,645	593	17
TAXI	1,455	701	170
TAXI	1,563	593	17
G+M	2,109	1,557	8,840
G+M	2,219	1,447	3,672
G+M	2,329	1,337	1,190
G+M	2,440	1,226	442
G+M	2,550	1,116	34
G+M	2,660	1,006	68
G+M	2,771	895	34
G+M	2,645	2,248	34

## Damage Tolerance - Metallic Structure

This section includes the damage tolerance analysis methods, material property data, selected crack locations for analysis, and a summary of results for the Full Scale Demonstration Component (FSDC). In addition, the results of the damage tolerance analyses for four smaller test specimens are included. Information on the assembled bonded metallic structure is called "metal" in this section for convenience. Information applicable only to adhesives is presented separately in the section on the analysis of bonds.

A flow chart of the damage tolerance procedure for the metal structure is shown in Figure 65.

Requirements and Stresses. - The requirements are presented in the section on Fatigue and Damage Tolerance Criteria for Metallic Structure. The initial flaw sizes for slow crack growth structure are given in MIL-A-83444 (USAF).

The derivation of the stress spectra used for crack growth analysis and of the maximum one-time stresses used in foreign object damage analysis is discussed in the Spectra section. The limit principal stresses used in the residual strength analysis of the two bay crack cases were obtained from the internal loads presented in that section. Damage Tolerance analysis of the FSDC was performed for the Phase Ib, Phase 2 preliminary, and Phase 2 final loads.

The damage tolerance analyses were based on the Hart-Smith method of predicting the stress distribution in a pressurized stiffened cylinder, Figure 66. This method is more accurate than the classical solution since:

- (a) the distortion under load included in shell buckling theory is accounted for,
- (b) the deflected shape is defined by non-oscillatory exponential decay functions,
- (c) the correct frame stresses are obtained by using the junction stresses between the skin and frame determined by the skin bending moments, and

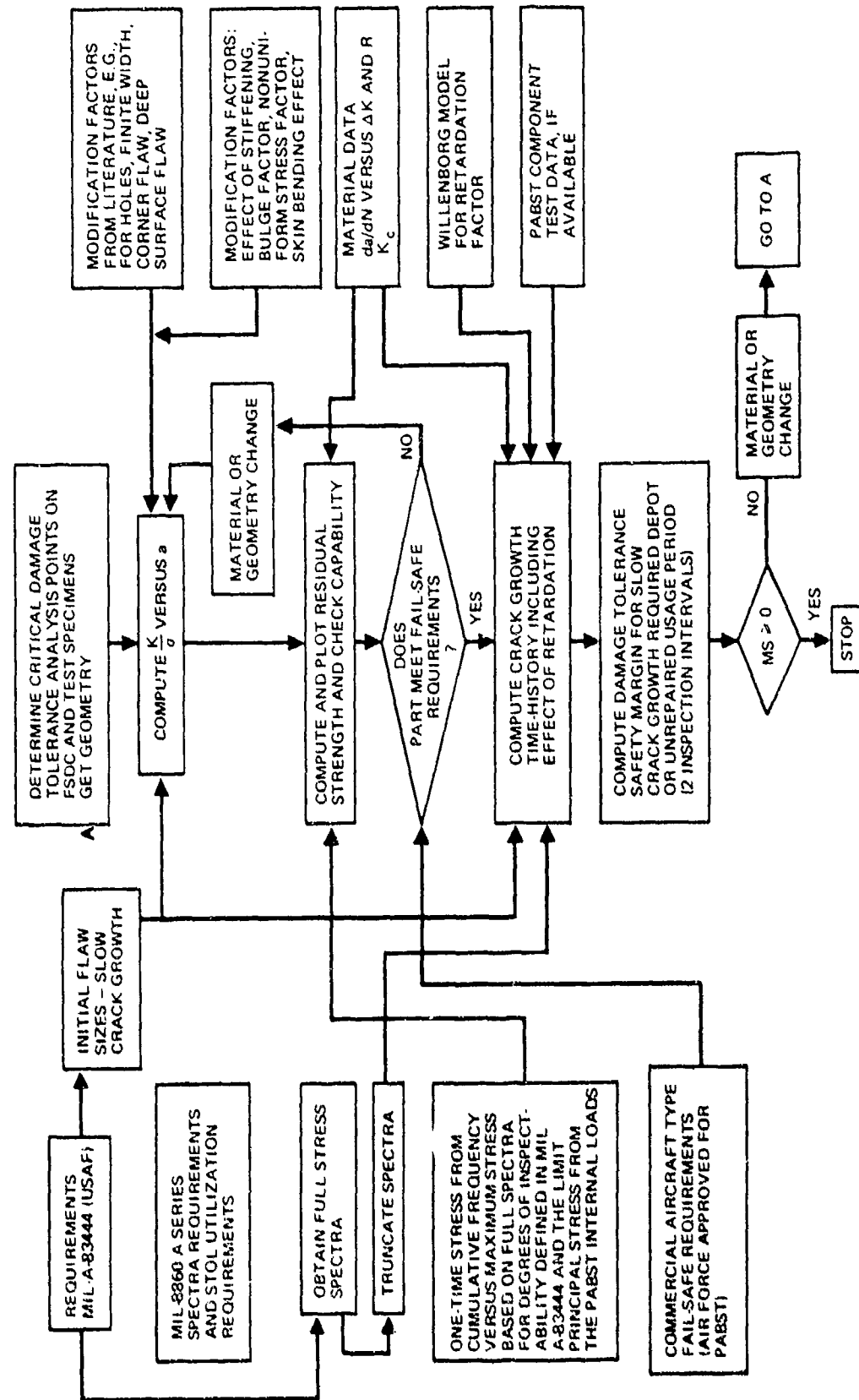


FIGURE 65. DAMAGE TOLERANCE ANALYSIS FLOW CHART FOR METAL STRUCTURE

- (d) the axial stiffener influence on the skin stresses is accounted for (through Poisson effects).

Damage Tolerance Analysis Methods (Metals). - The crack growth and residual strength analyses of the metallic structure were based on classical linear elastic fracture mechanics in which the model consists of a symmetric crack growing from a through-the-thickness flaw in an infinite sheet. A basic assumption made is that the local stress conditions at the crack tip are defined by the local stress intensity  $K$ , where:

$$K = \sigma \sqrt{\pi a}$$

$\sigma$  = gross area stress remote from the crack tip, psi

$a$  = half crack length, inches

The general equation for stiffened thin-walled structure of finite size is:

$$k = \sigma \sqrt{\pi a} \beta_1 \beta_2 \dots \beta_n$$

where the  $\beta_n$  terms are modification factors including but not limited to the following, as applicable:

$F (l/r)$  = Bowie correction for symmetric or asymmetric cracks at holes (Reference 2).

$\lambda_1$  = Finite width correction for eccentric cracks (Reference 2).

$\lambda_2$  = Finite width correction for single edge cracks (Reference 2).

$a_b$  = Liu back surface correction factor for corner flaws (Reference 3).

$M_k$  = Kobayashi factor for deep surface discontinuities (Reference 4).

$\gamma$  = Swift factor accounting for the effect of stiffening on a cracking sheet (Reference 5).

$B$  = Correction factor for the bulging of the cracking edge of a longitudinal skin crack in a pressurized cylinder (Reference 6).

$\xi$  = Effect of the non-uniform stress distribution in the pressurized uncracked stiffened cylinder on a longitudinal skin crack. See Figures 66 and 67.

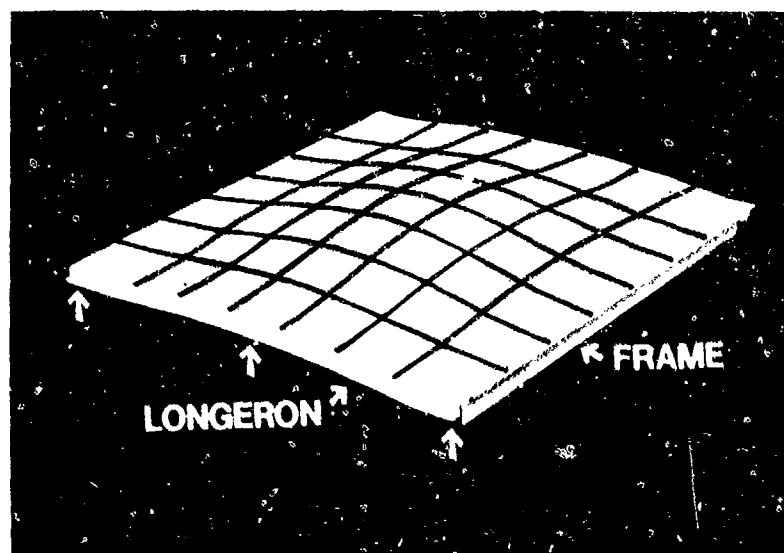
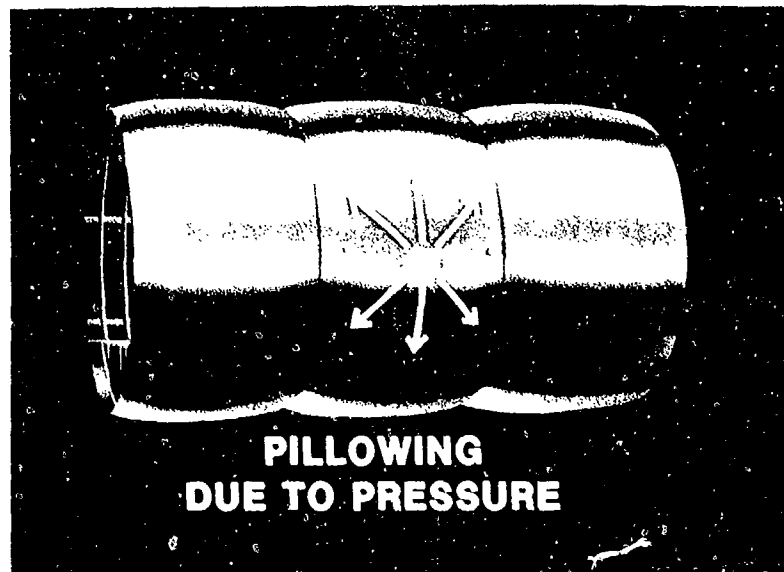
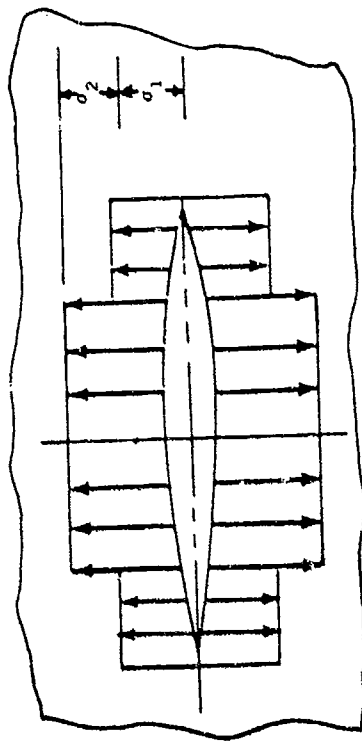
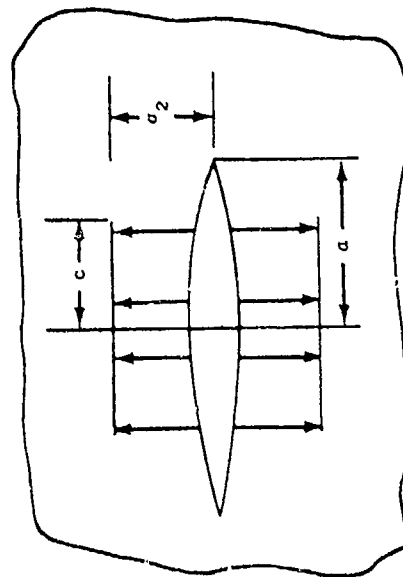


FIGURE 66. EFFECTS OF PRESSURE PILLOWING IN A STIFFENED CYLINDER

o NONUNIFORM STRESS DUE TO PRESSURIZATION

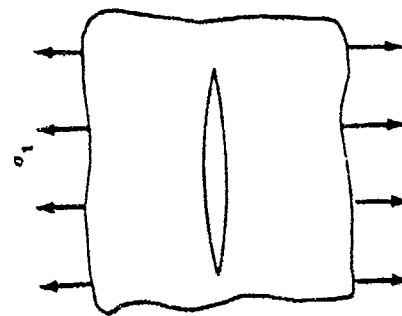


o GREEN'S FUNCTION APPROACH



+

o SUPERPOSITION



$$o \quad K = f(\sigma_1, a_2, a, c) = \sigma_1 \sqrt{\pi a}$$

FIGURE 67. NONUNIFORM STRESS DISTRIBUTION FACTOR,  $\xi$

F = Knock down factor for the effect of the skin bending stress, due to pillowing, on a circumferential crack near a frame in a pressurized shell. The analysis is based on the relationship between tension and bending presented in (Reference 7).

The crack growth time histories of the cracked structural members analyzed were calculated using a Douglas computer program that is an expanded version of the Air Force CRACKS program, and  $da/dN$  vs  $\Delta K$  material data. Residual strengths were calculated using critical stress intensity; i.e.,  $K_c$ , data. These material data are discussed in a subsequent subsection.

The method for estimating the margin on life for the slow crack growth analyses was based on the Forman equation for the  $da/dN$  vs  $\Delta K$  curve,

$$\frac{da}{dN} = \frac{C (\Delta K)^p}{(1-R) K_c - \Delta K}$$

where  $a$  = half crack length  
 $N$  = cycles  
 $R$  = Stress Ratio  
 $K_c$  = Critical stress intensity  
 $\Delta K$  = Difference in stress intensity  
 $p, C$  = Material constants

In region of the initial crack where the contribution to the total life-time is greatest,  $\Delta K$  is much less than  $K_c$ . For efficiently designed structure, the margin is low and the  $[(1-R)K_c - \Delta K]/C$  term can be assumed to be relatively constant in the applicable  $da/dN$  vs  $\Delta K$  region when the region is small enough to permit a linear approximation. A relationship between life and stress can then be obtained which is:

$$\sigma_1 = \sigma_2 \left[ \frac{N_2}{N_1} \right]^{1/p} \quad \text{or} \quad \sigma_{\text{allowable}} = \sigma_{\text{failure}} \left[ \frac{N_{\text{failure}}}{N_{\text{criteria}}} \right]^{-1/p}$$

$$\text{margin on life} = \left[ \frac{N_{\text{failure}}}{N_{\text{criteria}}} \right]^{-1/p} - 1$$

Material Data-Metals. - The FSDC structure was sized using preliminary  $da/dN$  vs  $\Delta K$  and  $K_c$  data obtained in Phase Ib. The preliminary margins on life and the residual strength margins of safety were later checked using final material property data obtained near the end of the final design phase, Phase II.

Preliminary Material Data: - The preliminary  $da/dN$  vs  $\Delta K$  curves from Phase Ib were taken from data available in the literature, primarily Battelle data, Reference 8. The average curves for 2024-T3 bare sheet and 7075-T6 clad sheet used for the sizing analysis of the FSDC skins and frames respectively are shown in Figures 68 and 69. It should be noted that, in Phase Ib, a decision was made that the curves for all aluminum alloys and R values would pass through  $10^{-8}$  at  $\Delta K = 2 \text{ ksi } \sqrt{\text{in}}$ . This decision was based on available NASA data for 2219 aluminum and had customer concurrence.

The preliminary values of  $K_c$  used for 2024-T3 bare sheet and 7075-T6 clad sheet were  $150 \text{ ksi } \sqrt{\text{in}}$  and  $60 \text{ ksi } \sqrt{\text{in}}$  respectively.

Final Material Data: - The final  $da/dN$  vs  $\Delta K$  curves were based on Douglas test data in the low  $\Delta K$  region with data from the literature, Reference 8 and 9, completing the upper part of the curves. The data for 2024-T3 bare sheet and for 7075-T6 clad sheet are shown in Figures 70 and 71 respectively. The changes in the low  $\Delta K$  region were sufficient to require the recheck of the margins on life since relatively small  $\Delta K$  displacements of the curves can lead to significant changes in  $da/dN$  and, therefore, in crack growth time history.

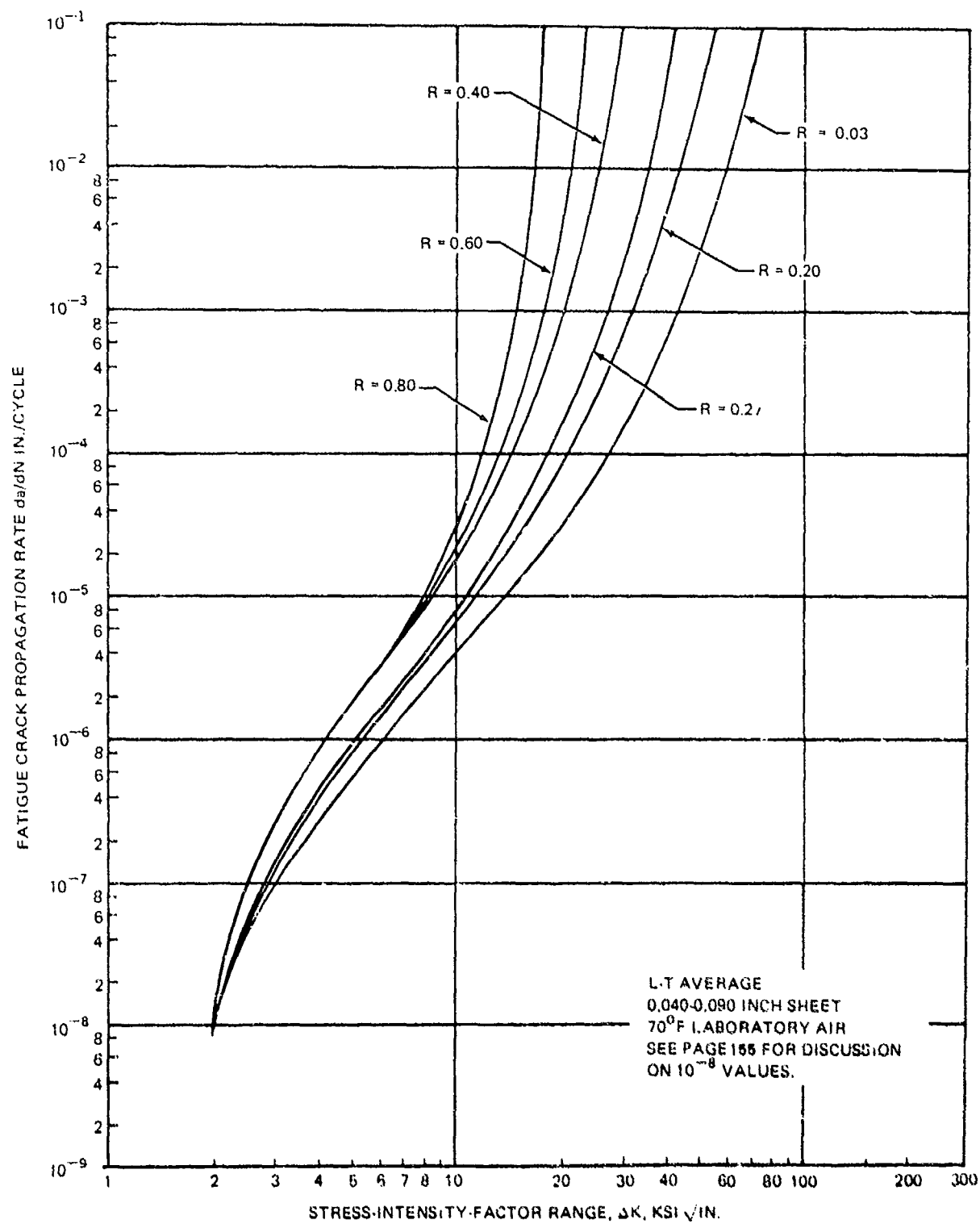


FIGURE 68. CURVES OF  $da/dN$  VERSUS  $\Delta K$  FOR 2024-T3 BARE SHEET - PRELIMINARY

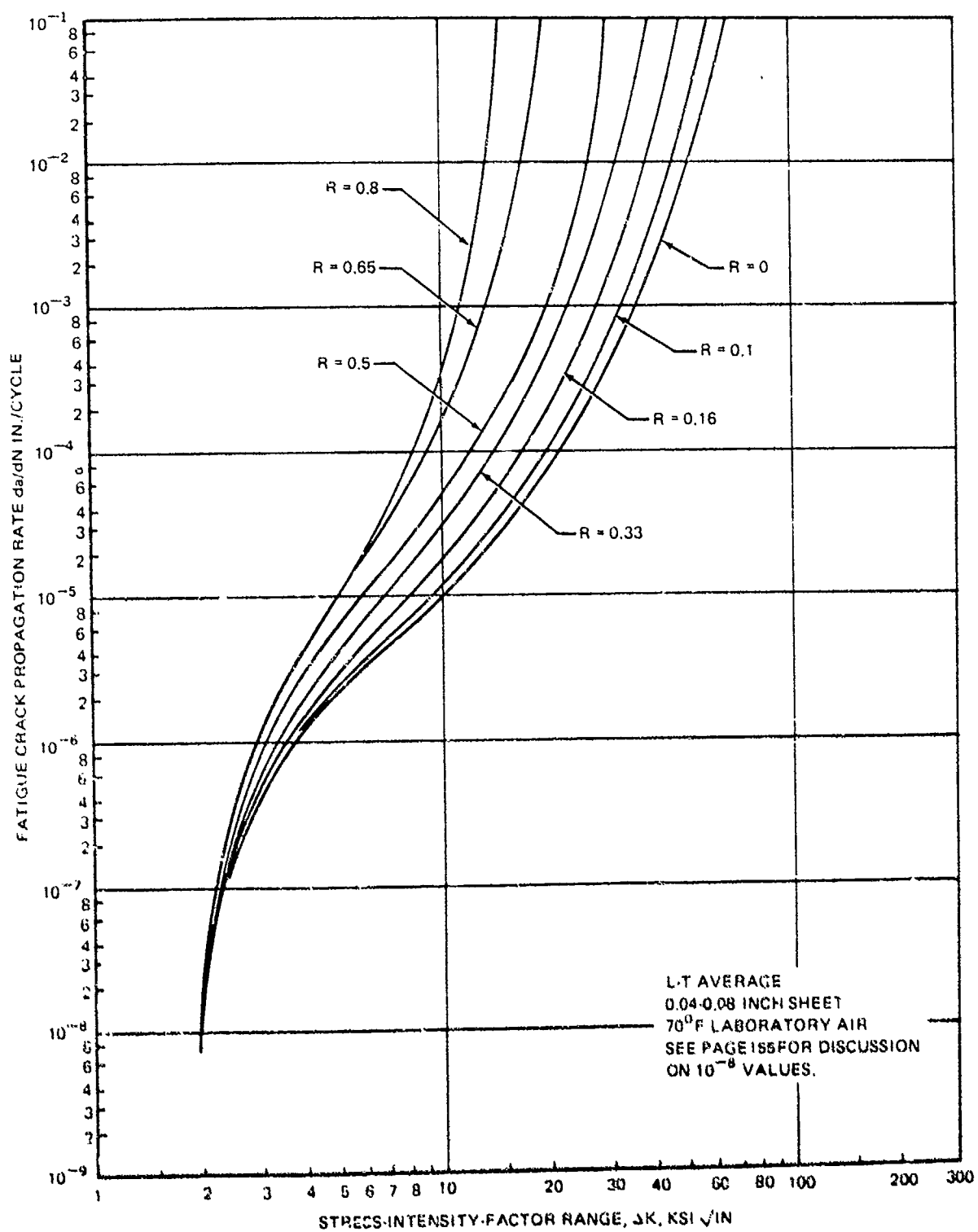


FIGURE 69. CURVES OF  $da/dN$  VERSUS  $\Delta K$  FOR 7075-T6 CLAD SHEET - PRELIMINARY

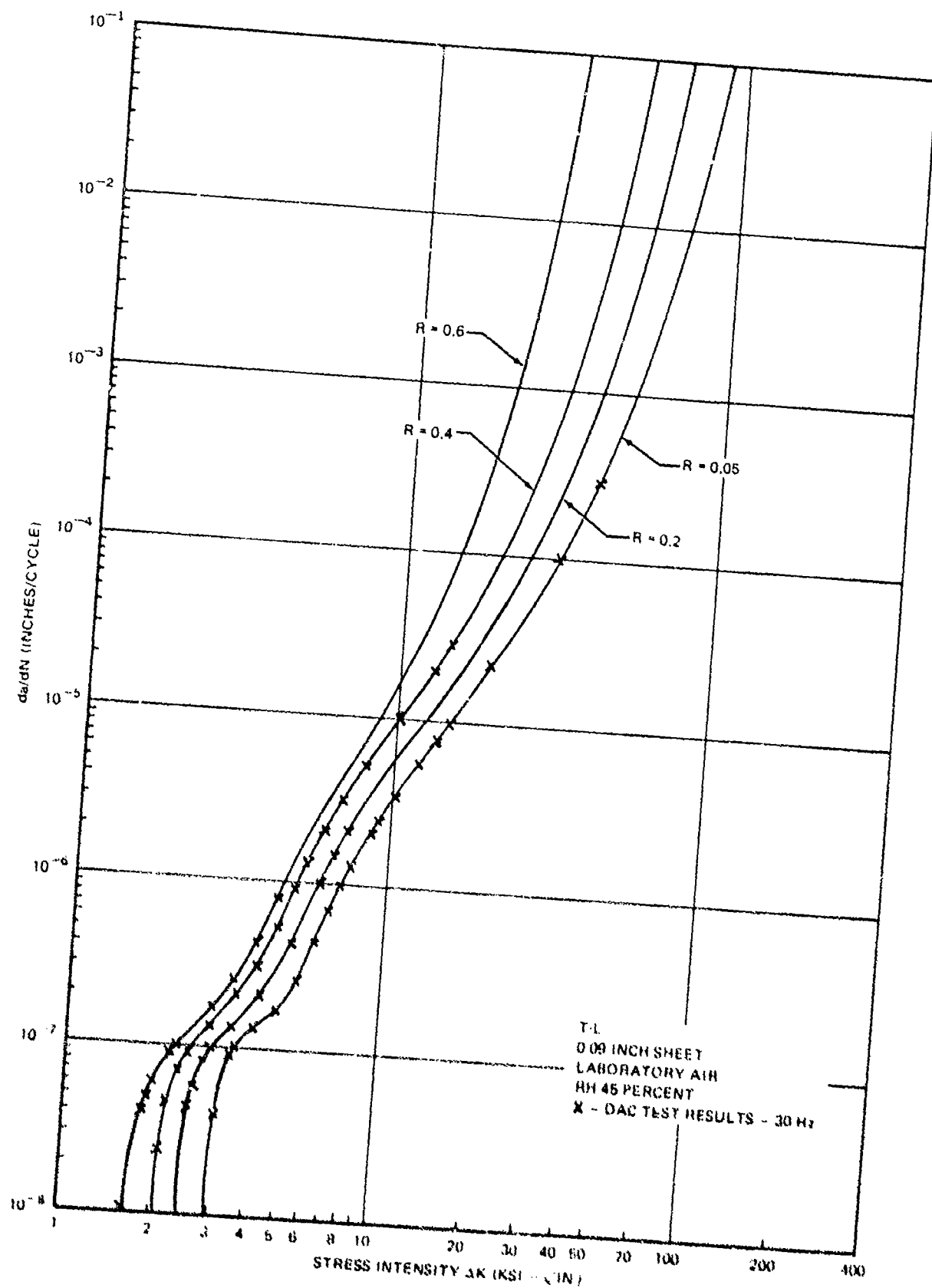


FIGURE 70. CURVES OF  $da/dN$  VERSUS  $\Delta K$  FOR 2024-T3 BARE SHEET - FINAL

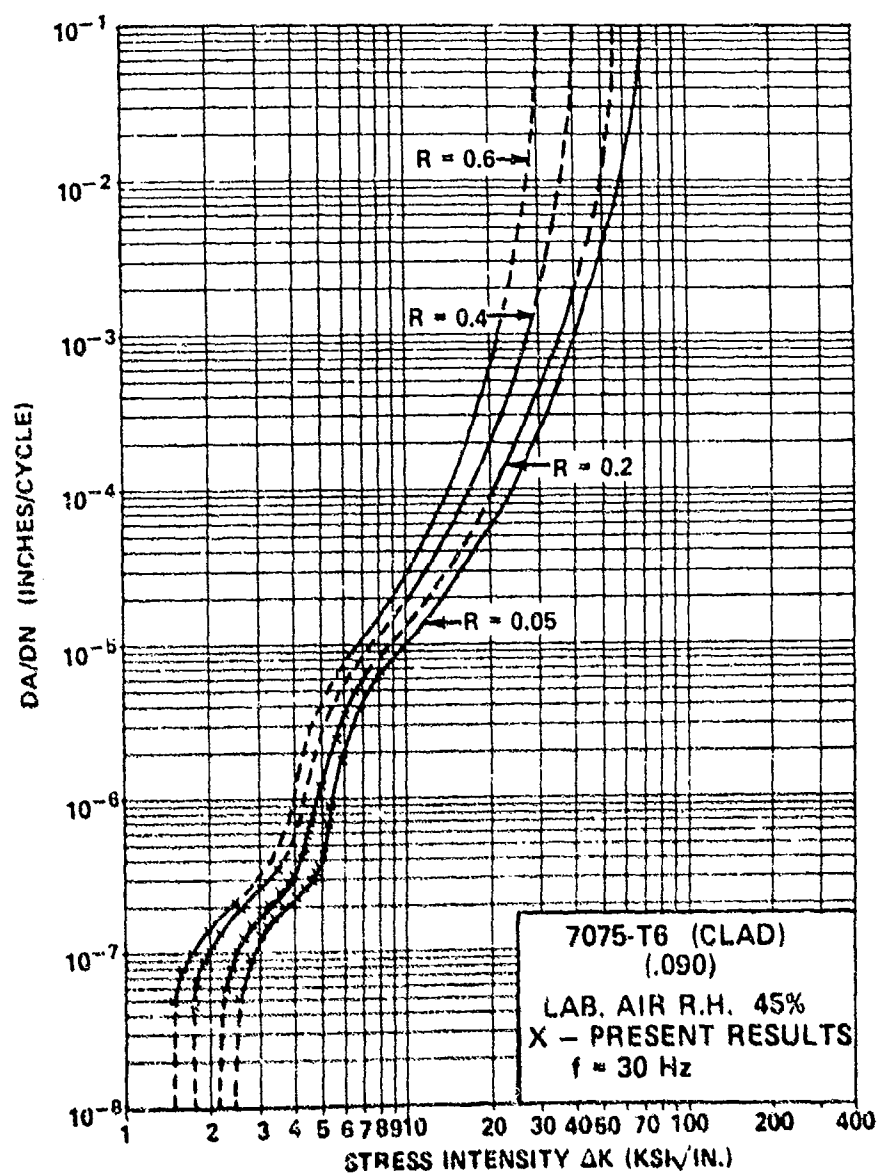


FIGURE 71. CURVES OF  $da/dN$  VERSUS  $\Delta K$  FOR 7075-T6 CLAD SHEET - FINAL

Retardation: - Four flat unstiffened center-cracked PABST panels were tested in Phase Ib to measure retardation in crack growth due to infrequent high loads under spectrum loading and to establish a retardation model for crack growth analysis. Attempts to correlate the data obtained with existing retardation models was not successful. A retardation factor of 0.8 and a Willenborg model based on previous Douglas experience was therefore used for PABST.

Location of Check Points. - The locations of the check points selected for damage tolerance analysis are shown in Figure 64. The points were chosen based on the MIL-A-83444 definition of "fracture critical structure." The phase Ib (preliminary design) fatigue stresses were searched to determine the parts with relatively high tension stresses and the parts were analyzed to ensure that they met damage tolerance requirements.

Results for Check Points E and H. - The results of the damage tolerance analysis for check points E and H are typical of FSDC circumferential and longitudinal skin cracks respectively. They are presented to show the crack growth and residual strength behavior of the skin. The analyses were based on the preliminary spectra and material properties. The skin, stiffening, and adhesive (or rivets) were considered to be elastic.

The analysis of check point E included the effect of: (a) the skin bending stress at the frame due to pressure, (b) the skin hoop stress due to pressure, and (c) stiffening; i.e., the longerons. The crack growth time history for the critical one bay circumferential skin crack is presented in Figure 72. The residual strength diagrams are shown in Figure 73.

In the upper diagram of Figure 73, the residual strength of the structure is shown for each half crack length. For example, entering the graph at a half crack length of 14 inches and reading vertically, the residual strength remaining in the cracked skin is 40 ksi. The remaining tensile (allowable) strength remaining in the central stiffener is 15 ksi with 50 ksi remaining in the outer stiffener. These stiffeners have, of course, absorbed the load being transferred out of the skin due to the cracking. Based on the fail safe design criteria on page 6, the cracked structure must be capable of carrying the

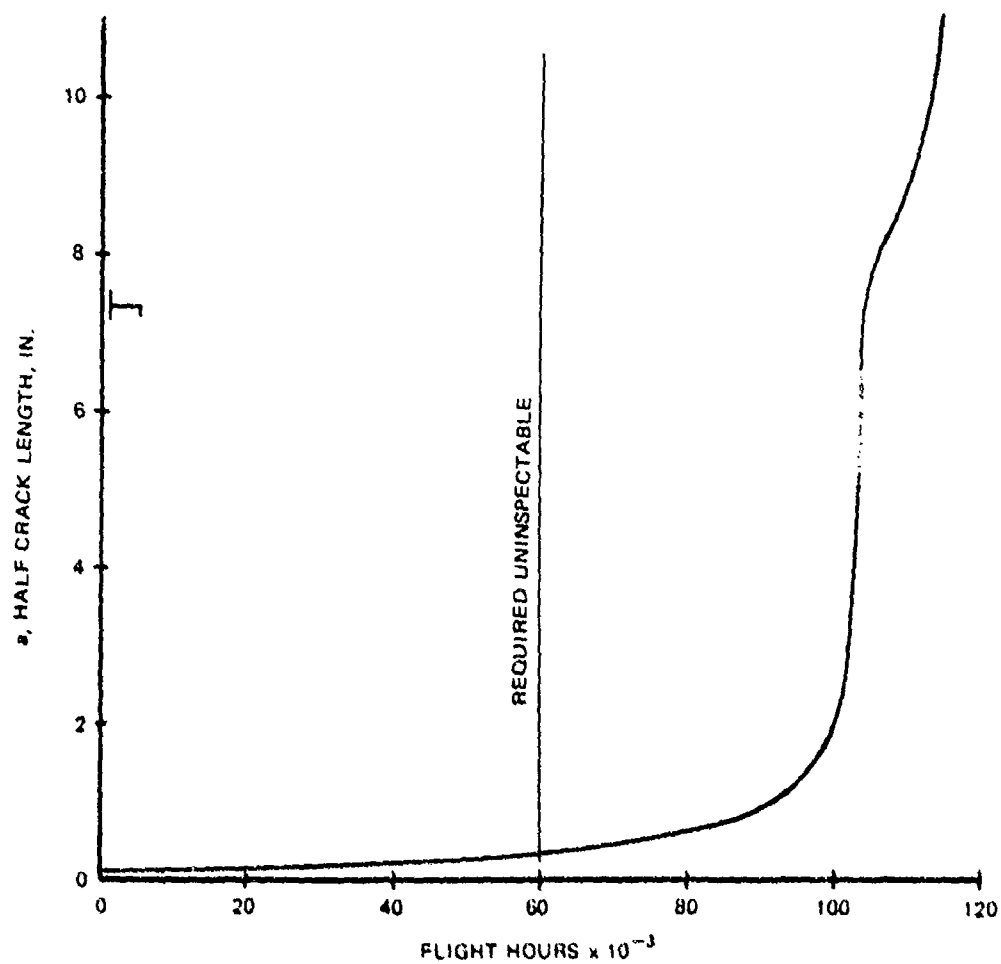


FIGURE 72. CRACK GROWTH TIME HISTORY FOR CIRCUMFERENTIAL SKIN CRACK AT CHECKPOINT E WITH PRELIMINARY LOADS

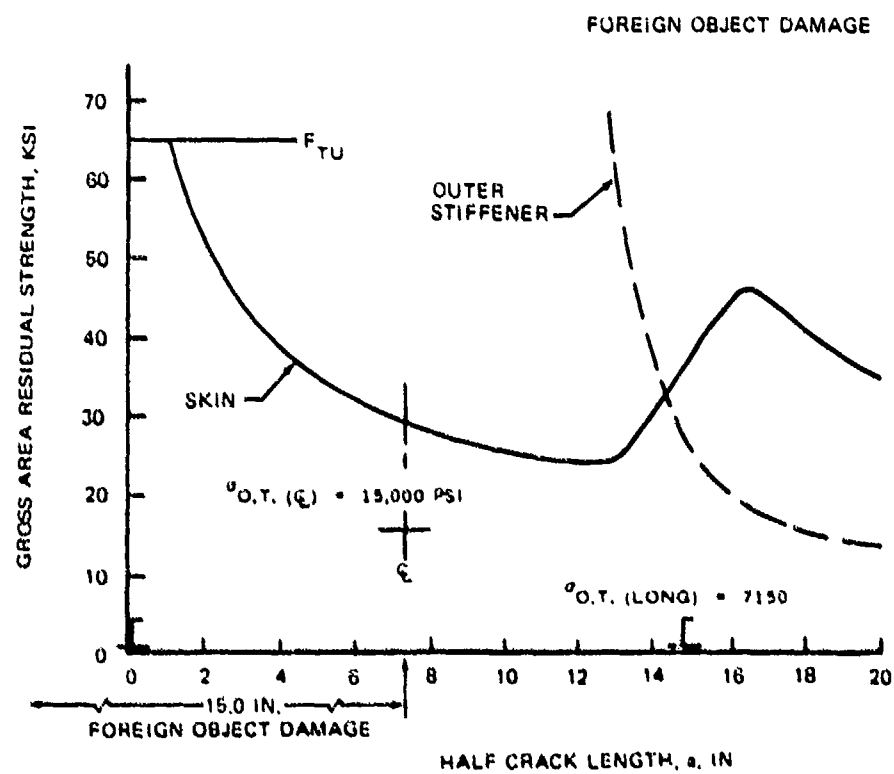
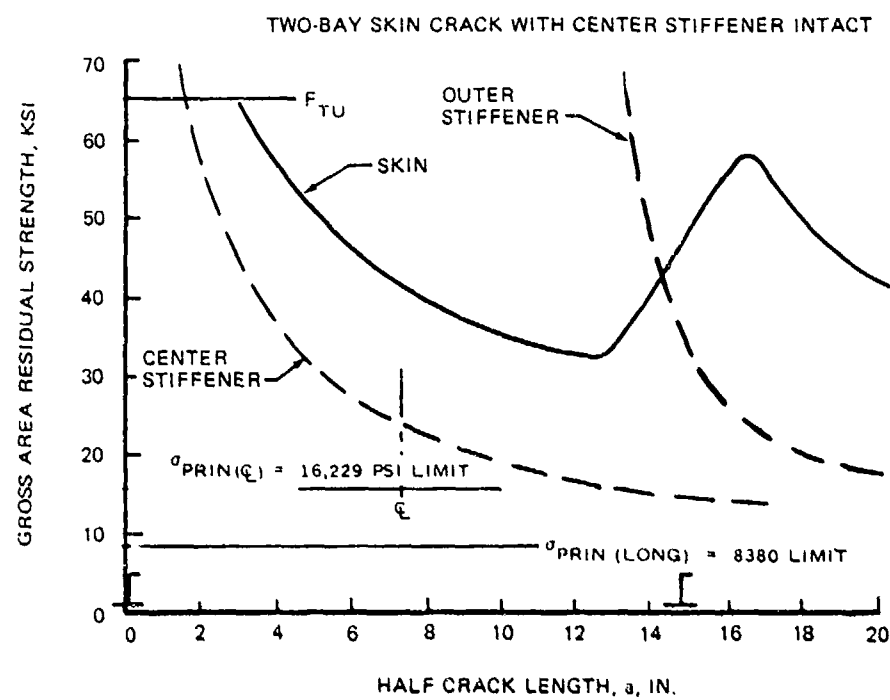


FIGURE 73. RESIDUAL STRENGTH FOR CHECKPOINT E WITH PRELIMINARY LOADS

maximum free-stream applied principal stress,  $\sigma_{PRIN.}$ . Because of pressure pillowing, this stress varies between stiffeners. The structure is adequate as long as the residual strength is greater than the applied stress.

The analysis of check point H included the effect of (a) the skin hoop stress due to pressure, (b) the non-uniform stress distribution on the longitudinal skin crack, (c) stiffening; i.e., the frame, and the (d) bulging of the crack edges due to pressure. The crack growth time history for the critical one bay longitudinal skin crack is presented in Figure 74. The residual strength diagrams are shown in Figure 75. The residual strength diagram is read in the same manner as described above. However, referring to the criteria on page 6, the structure for foreign object damage must be capable of carrying the maximum load occurring in 20 lifetimes or limit load, whichever is less. The critical applied stress for this check point is the one time stress,  $\sigma_{O.T.}$ . As in the previous case, this applied stress varies between the stiffeners because of pressure pillowing.

The fast fracture of the skin at a half crack length (a) of approximately two inches, shown in Figure 72 and 74, is typical for the FSDC crack growth time histories.

In the residual strength analysis, the limit principal stress was assumed to act perpendicular to the crack for the two bay skin crack with the center stiffener intact (at crack initiation) cases, Figures 73 and 75. A linear relation was assumed between the limit principal stresses at the centerline and at the longeron for the circumferential crack case since the correct distribution, a very difficult problem, has not been derived. For the longitudinal crack case, the limit principal stress was assumed to be constant between frames for the same reason. As expected residual strength was more critical in the wide spaced longeron region than in the close spaced region.

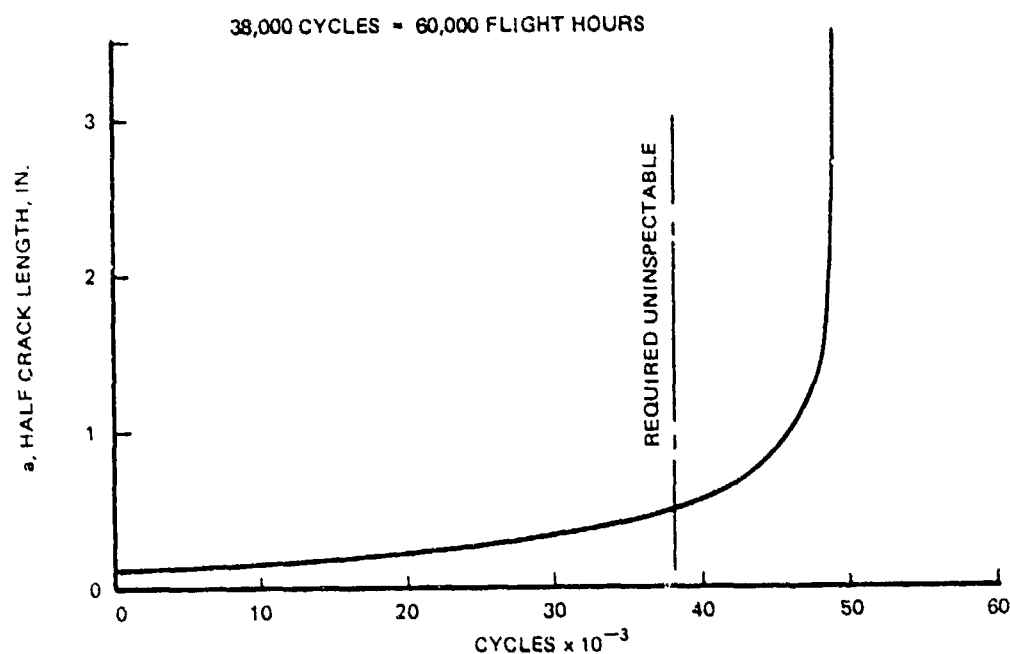


FIGURE 74. CRACK GROWTH TIME HISTORY FOR LONGITUDINAL CRACK AT CHECKPOINT H WITH PRELIMINARY LOADS

Results of Damage Tolerance Analysis. - Table 22 presents the results of the damage tolerance analyses of all of the check points, Figure 64. The analyses considered the skin, stiffening, and adhesive (or rivets) to be elastic. The structure shows positive margins for both Phase 1b and Phase 2 loads.

The Effect of a Multi-mass/Multi-Spring Model and of Plasticity. - As previously stated, the FSDC damage tolerance analysis summarized in Table 22 was based on elastic stiffening and adhesive (or rivets) and all stiffening modeled as a single mass. The single mass represented longerons well but needed to be checked for the frame/shear tee stiffening.

Comparing Mass/Spring Model Results for Frame/Shear Tee Stiffening: - An elastic/plastic analysis of the longitudinal skin crack at check point D, Figure 64, was made to compare the effect of the stiffening based on the one mass/one spring model used in the FSDC analysis with that of a three mass/three spring elastic/plastic IRAD model capability. The three mass/three spring model is shown in Figure 76. The plasticity capability was included

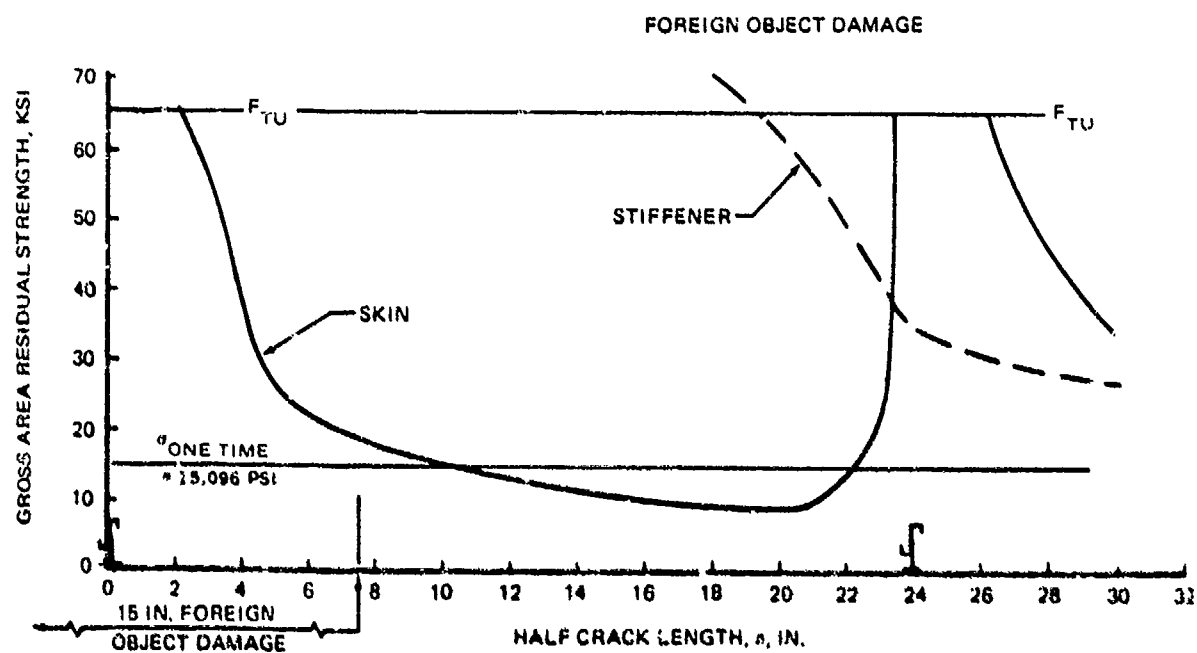
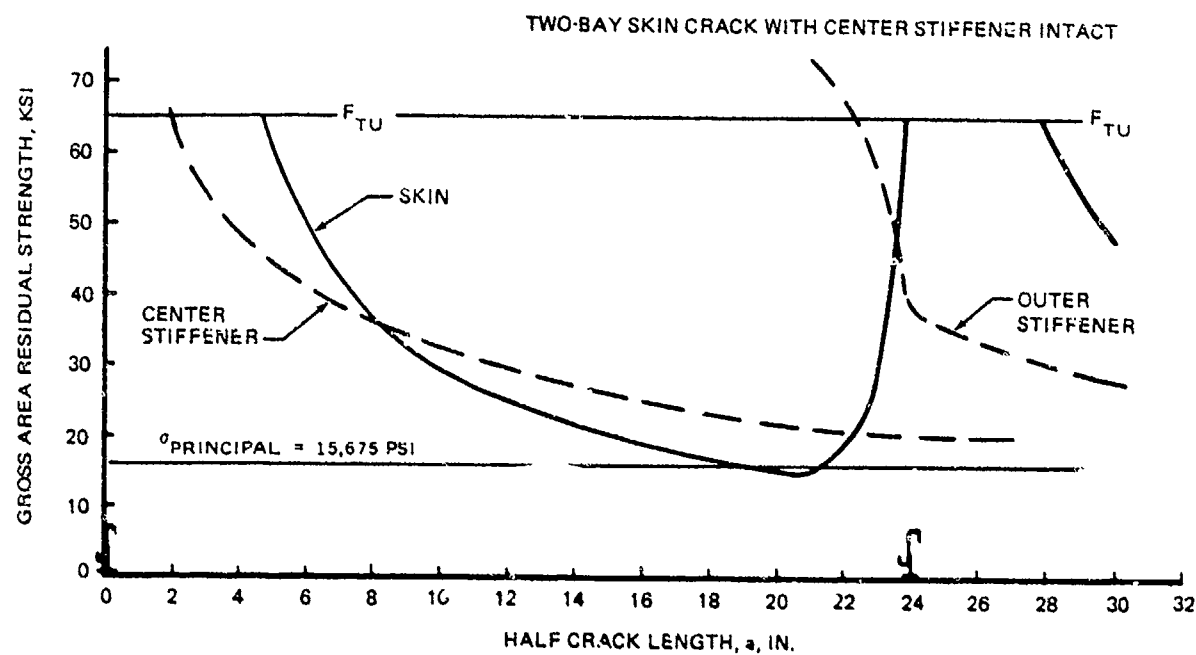


FIGURE 75. RESIDUAL STRENGTH FOR CHECKPOINT H WITH PRELIMINARY LOADS

TABLE 22.  
SUMMARY OF THE DAMAGE TOLERANCE ANALYSIS OF THE FSDC CHECKPOINTS

Critical Point	Location	Type of Crack	Crack Growth Criteria Met	Slow Crack Growth	Fail Safe
				Margin on Life	Two Bay Crack-Center Stiffener Intact
A	Sta 655 Long 8b	Circumferential Skin	M11-A-83444 Slow Crack Growth - Uninspectable	0.08 - $\phi$ 1B >0.20 - $\phi$ 2 Prel.	15" Foreign Object Damage-Center Stiffening Broken  $\phi$ 2 Prel. Criteria Met
B	Sta 655 Long 1 & 2	Circumferential Skin Longitudinal Skin		0.18 - $\phi$ 1B >0.20 - $\phi$ 2 Prel.  >0.20 - $\phi$ 2 Prel.	Criteria Met  Criteria Met
C	Sta 439 Long 4 & 8	Circumferential Skin		0.03 - $\phi$ 1B >0.20 - $\phi$ 2 Prel.	
D	Sta 823 Long 16	Longitudinal Skin		0.06 - $\phi$ 1B	
E	Sta 523 Long 1 & 2	Circumferential Skin		0.17 - $\phi$ 1B 0.21 - $\phi$ 2 Prel.	
F	Sta 751 Long 8A	Circumferential Skin	M11-A-83444 Slow Crack Growth - Uninspectable	>0.20 - $\phi$ 1B >0.20 - $\phi$ 2 Prel.	Criteria Met Criteria Met

TABLE 22 (CONTINUED)  
SUMMARY OF THE DAMAGE TOLERANCE ANALYSIS OF THE FSDC CHECKPOINTS

Critical Point	Location	Type of Crack	Crack Growth Criteria Met	Slow Crack Growth	Two Bay Crack-Center Stiffener Intact	Fail Safe
P	Sta 751 Long 8A	Longitudinal - Skin	MIL-A-83444 Slow Crack Growth - Uninspectable	Margin on Life > 0.20 - $\phi$ 1B > 0.20 - $\phi$ 2 Prel.	Criteria Met	15" Foreign Object Damage-Center Stiffening Broken Criteria Met
C	Sta 415 Long 8A-8B	Circumferential - Skin		> 0.20 - $\phi$ 1B		
C	Sta 415 Long 8A-8B	Longitudinal - Skin		> 0.20 - $\phi$ 1B		
H	Sta 463 Long 9A	Circumferential - Skin		> 0.20 - $\phi$ 1B > 0.20 - $\phi$ 2 Prel		
H	Sta 463 Long 9A	Longitudinal - Skin		0.09 - $\phi$ 1B and $\phi$ 2 Prel.	Criteria Met	Criteria Met
I	Sta 535 Long 9A	Longitudinal - Longitudinal Splice	MIL-A-83444 Slow Crack Growth Uninspectable	0.07 - $\phi$ 1B 0.02 - $\phi$ 2 Prel.	N.A.	N.A.
J	Sta 523 Long 8	Circumferential - Circumferential Splice	MIL-A-83444 Depot 3.1.2a MIL-A-83444 Depot 3.1.2b	0.20 - $\phi$ 1B 0.12 - $\phi$ 2 Prel.	N.A.	N.A.

TABLE 22 (CONTINUED)  
SUMMARY OF THE DAMAGE TOLERANCE ANALYSIS OF THE FSDC CHECKPOINTS

Critical Point	Location	Type of Crack	Crack Growth Criteria Met	Slow Crack Growth	Fail Safe	
				Margin on Life	Two Bay Crack-Center Stiffener Intact	15" Foreign Object Damage-Center Stiffening Broken
K	Stations 535, 583, 631, 679	Transverse - Frame (Pressure)	Mil-A-83444 Slow Crack Growth Uninspectable	> 0.20 - $\phi$ 2 Prel.	N.A.	N.A.
L	Sta 655 Long 1	Transverse - Longeron		0.22 - $\phi$ 2 Prel.		
M	Sta Long	Skin at Door Corner		0.88 - $\phi$ 2 Prel.		
N	Sta 703 Long 9A	Circumferential - Bonded Skin Splice		OK by Comparison to Check Point A		

to check the stress state of the stiffening and fastening materials.

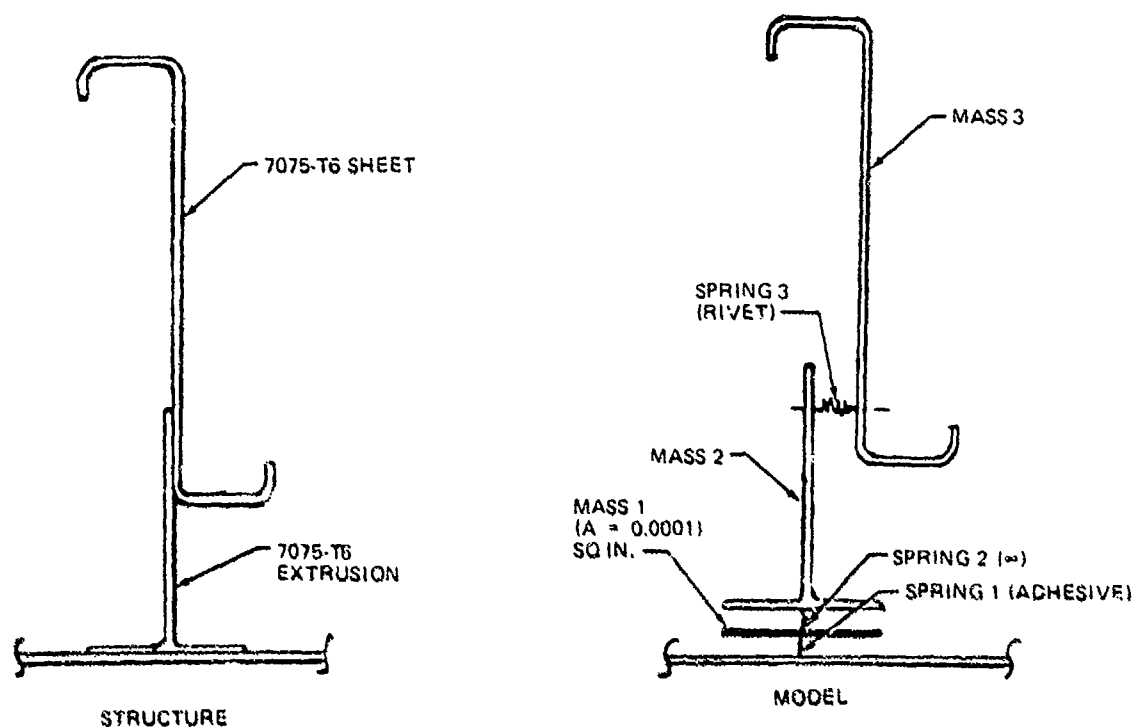


FIGURE 76. THREE-MASS/THREE-SPRING MODEL FOR CHECK POINT D

The elastic-plastic or load-deflection models for the shear tee, frame, adhesive, and rivet materials are shown in Figures 77, 78, 79 and 80 respectively. The solution, in the form of the modification factor  $\gamma$  versus the

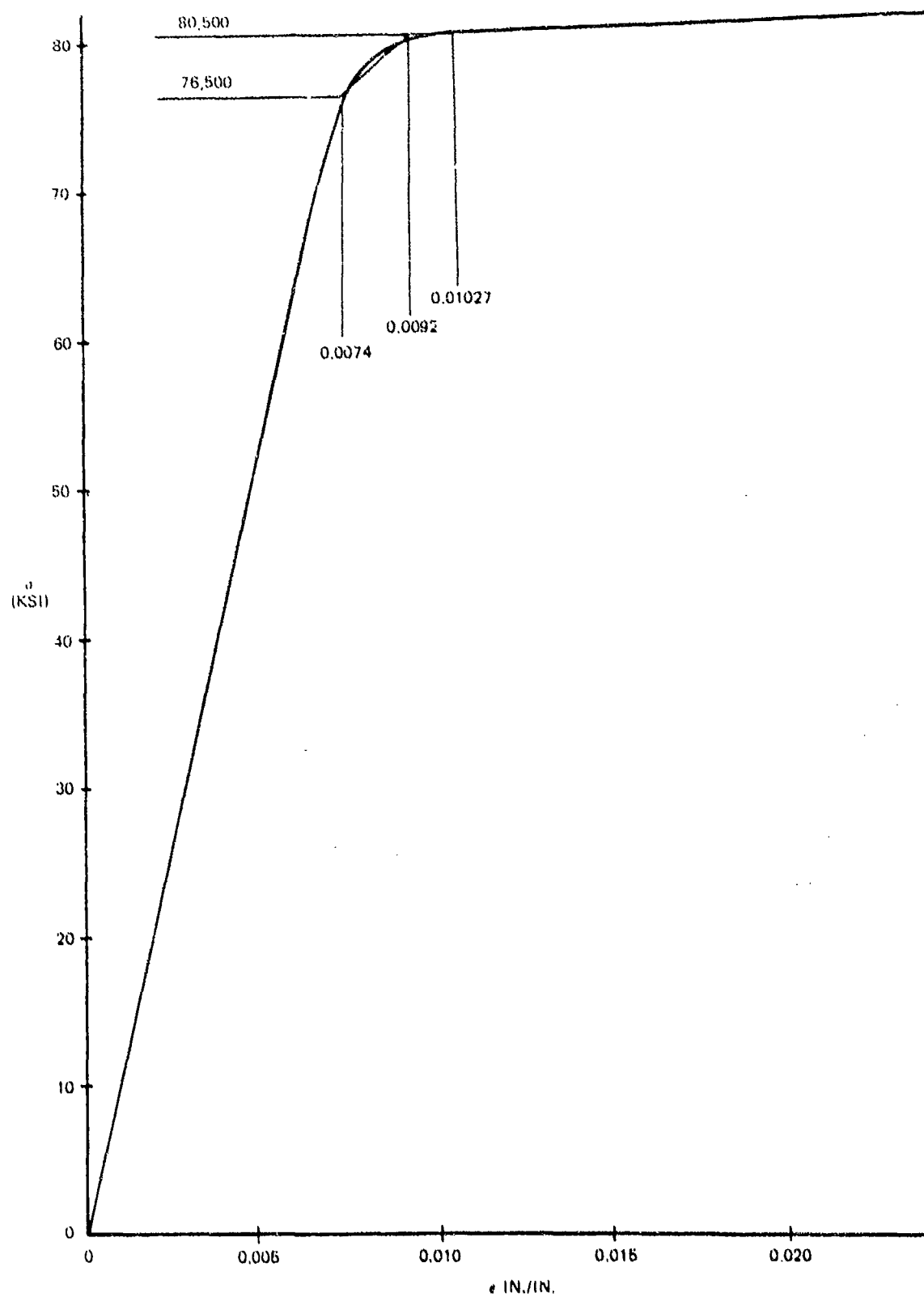


FIGURE 77. 7075-T6 EXTRUSION ELASTIC-PLASTIC MODEL - CHECKPOINT D

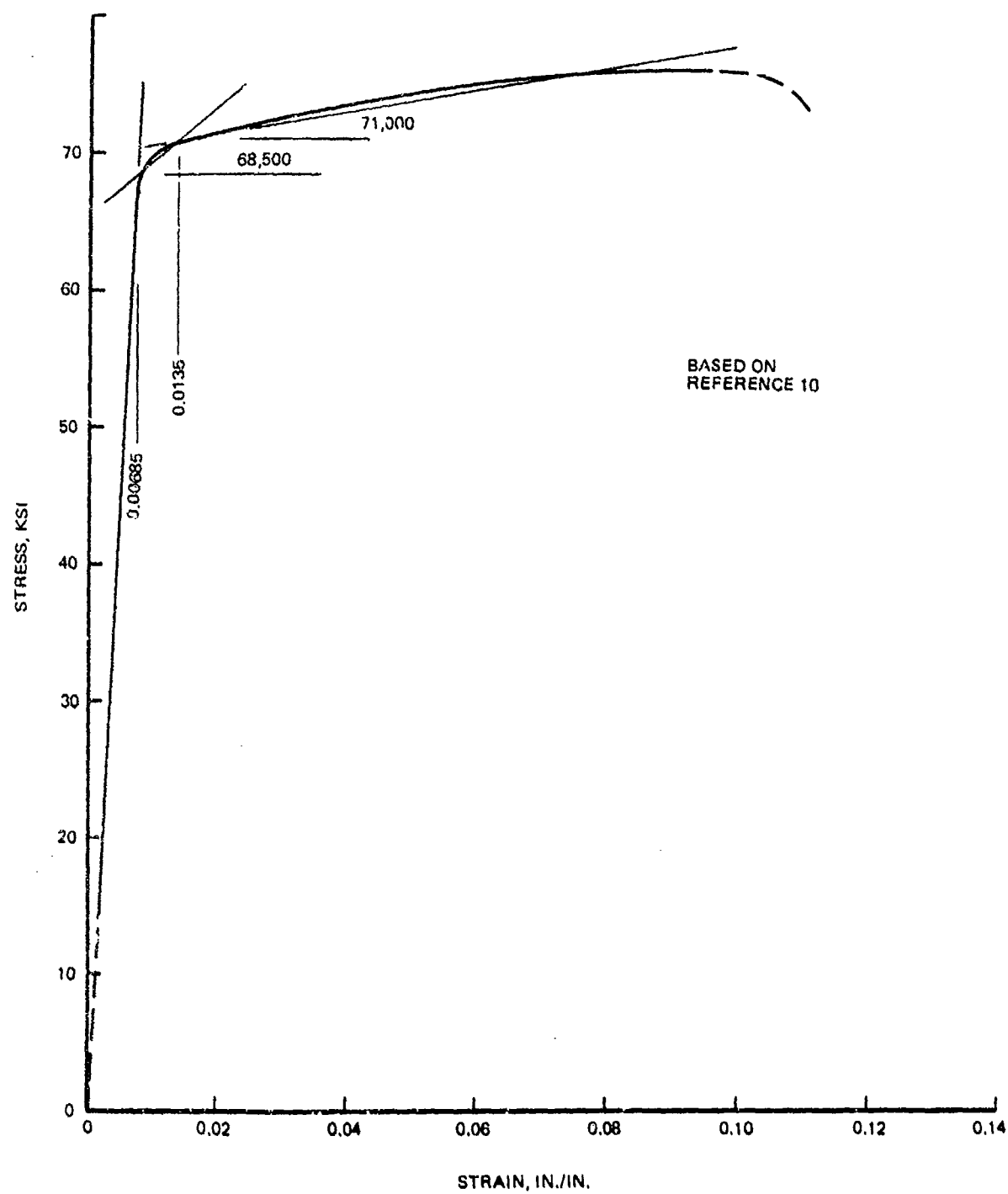


FIGURE 78. 7075-T6 CLAD SHEET ELASTIC-PLASTIC MODEL - CHECKPOINT D

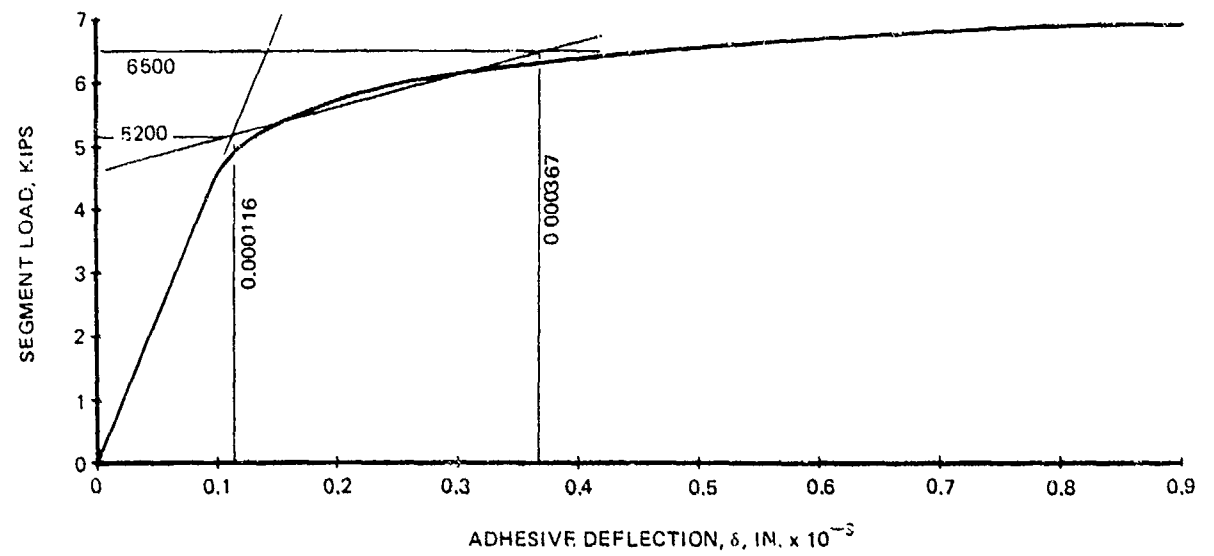


FIGURE 79. FM-73 ADHESIVE LOAD - DEFLECTION MODEL - CHECK POINT D

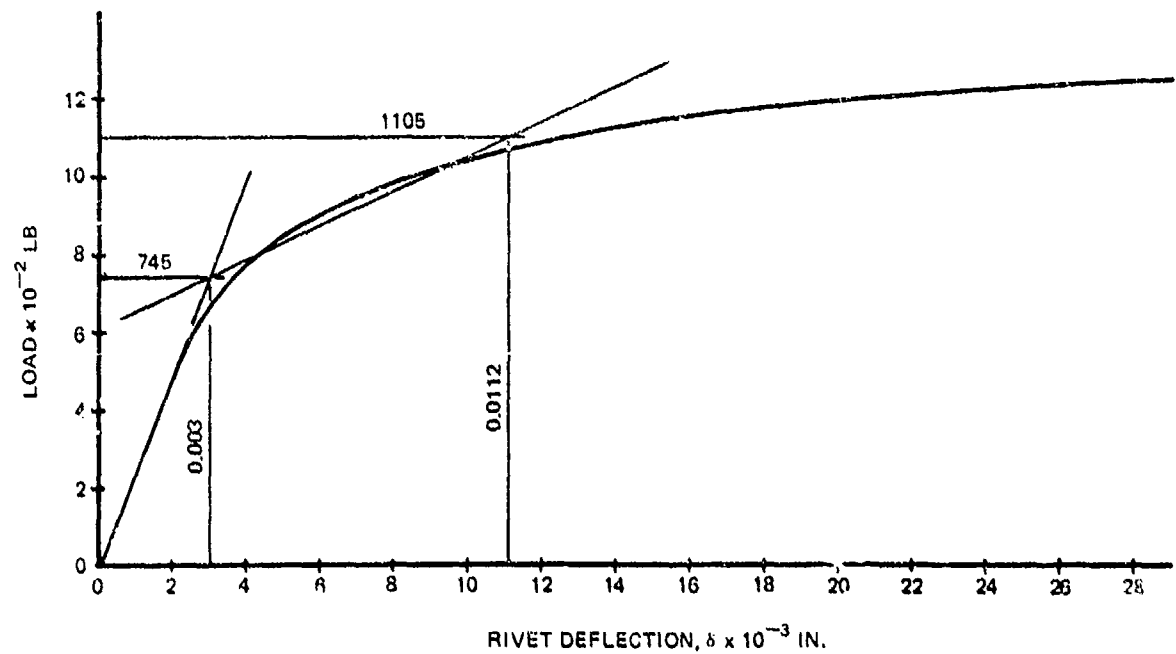


FIGURE 80. RIVET LOAD - DEFLECTION MODEL - CHECK POINT D

half crack length, is shown in Figure 81. For the maximum skin stress of 15368 psi, the frame outer cap and adhesive segment stresses were both elastic. The agreement between the one mass-one spring model and the more accurate three mass-three spring model, as shown in the Figure, was reasonably close and the one mass-one spring model conservative. An updated analysis of check points with longitudinal skin cracks was, therefore, not required.

Comparing Mass/Spring Model Results for the Wide Spaced Longeron Region. - An elastic/plastic analysis of the circumferential skin crack at Check Point A, Figure 64, was made to determine the stress state of the tear strap and of the adhesive. Check Point A is one of the most critical locations for residual strength.

The three mass/three spring elastic/plastic model was used. The 7475-T761 tear strap was divided into three masses and reconnected with two infinite springs. The results from the multi-mass elastic analysis were compared with the one mass/one spring elastic solution used in the FSDC analysis as a check on the two solutions.

The elastic-plastic model for the tear strap is shown in Figure 82 and the adhesive load-deflection model in Figure 83. The results of the analysis are shown in Figure 84. The solution for the maximum stress of 24899 psi (for phase Ib loads) is plastic. The shift in the  $\gamma$  versus half crack length curve to the final plastic values is shown by the targets marked with a "p." The change is significant and shows the importance of determining the true stress state of the stiffening.

Analysis - Test Correlation for a Transverse Riveted Splice Specimen. - A transverse riveted splice specimen, Figure 85 was tested under constant amplitude cyclic loading. The maximum stress was 10972 psi and the minimum stress was 1046 psi. The panel failed at 166,300 cycles from cracks which initiated voluntarily at the rivet holes. Hole #7 experienced the greatest crack growth and the hole was analyzed.

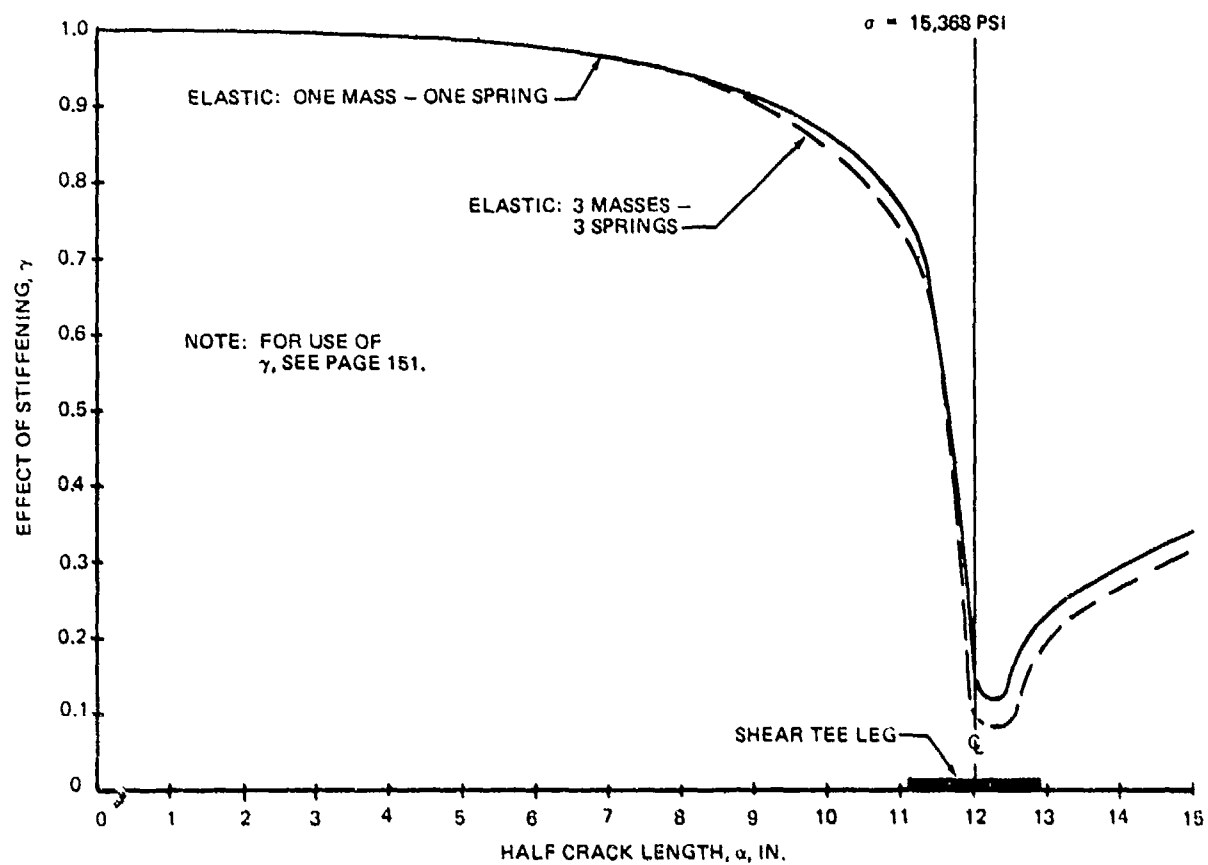


FIGURE 81. EFFECT OF CONSIDERING A MULTIMASS/MULTISPRING MODEL AT CHECK POINT D

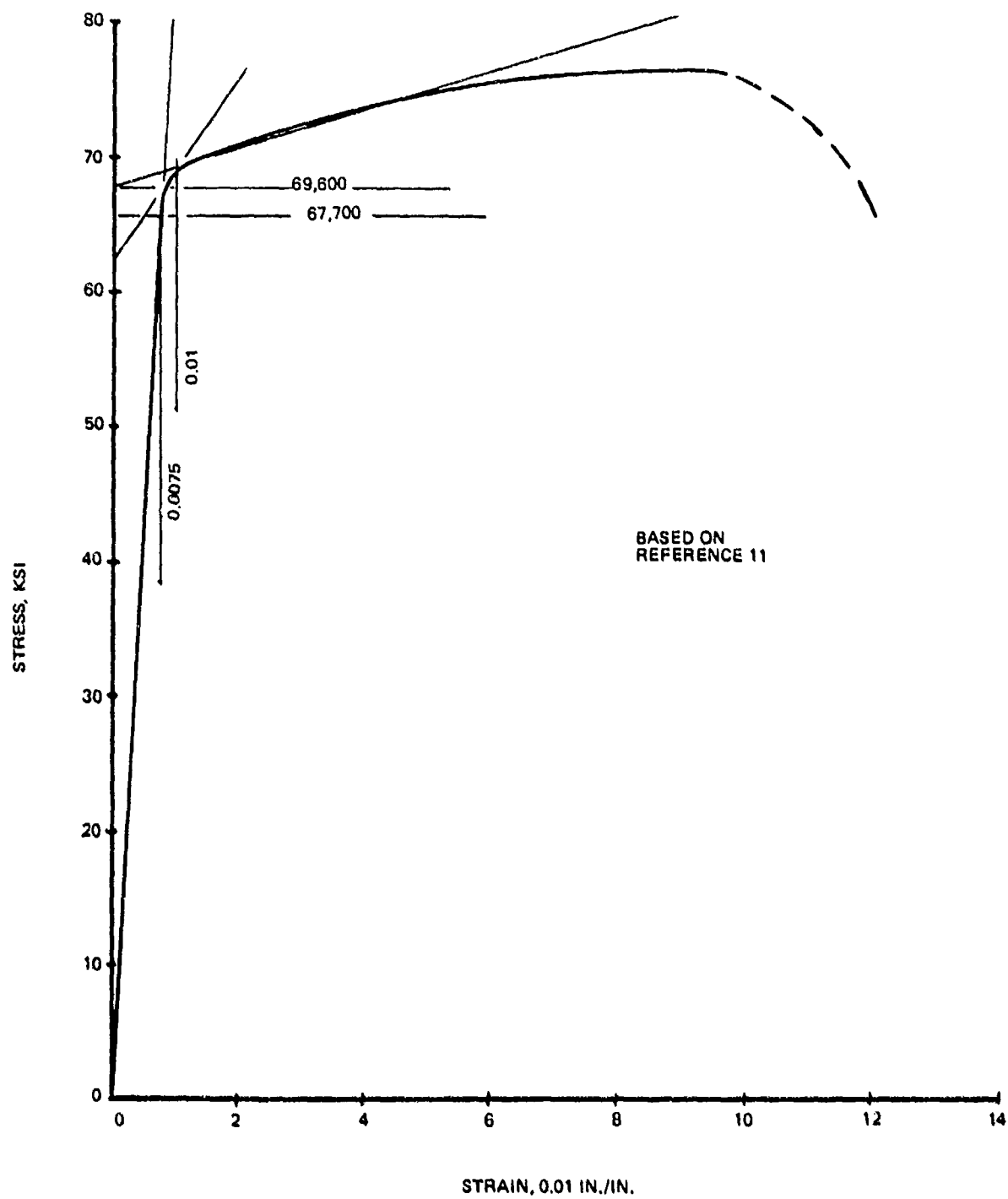


FIGURE 82. 7475-T761 SHEET ELASTIC - PLASTIC MODEL - CHECK POINT A

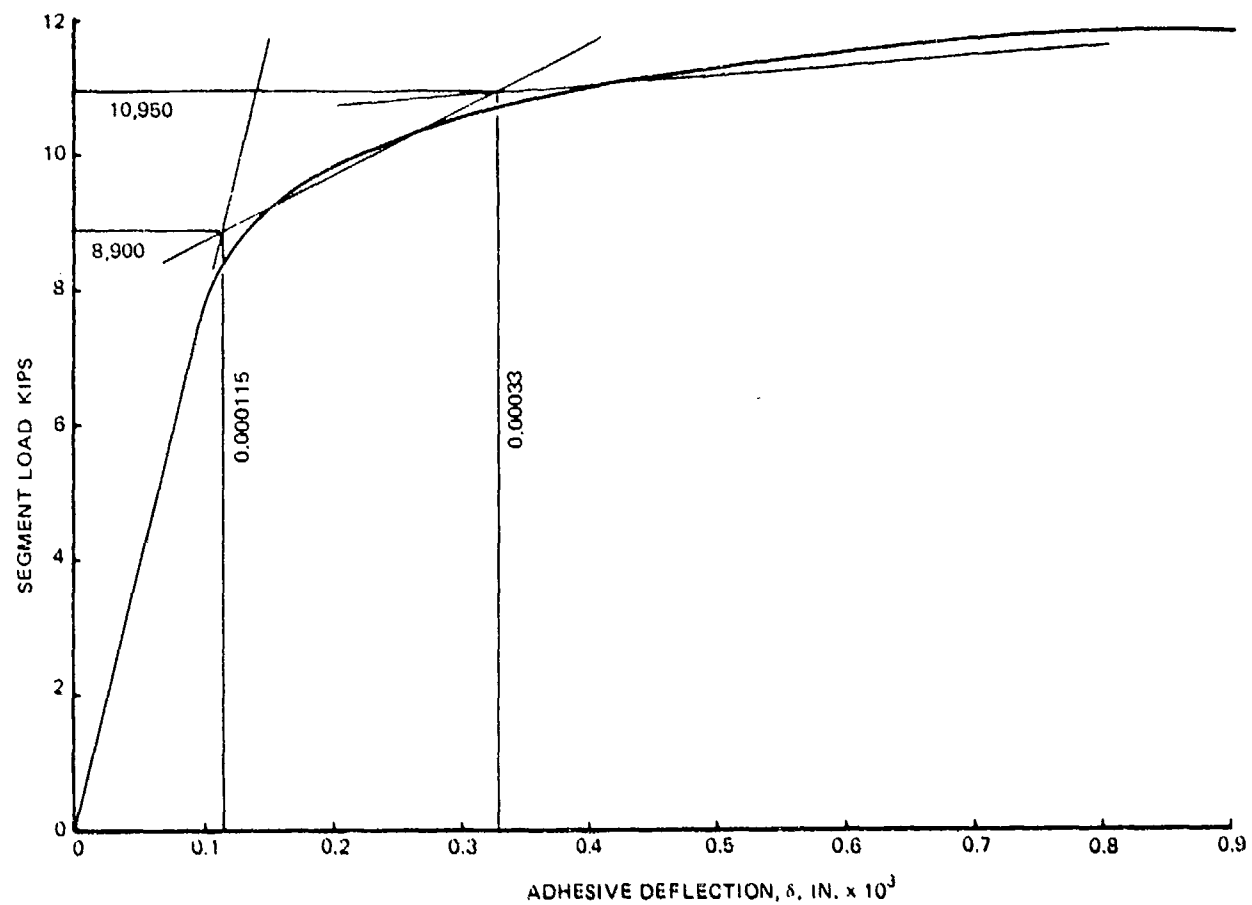


FIGURE 83. FM-73 ADHESIVE LOAD-DEFLECTION MODEL - CHECK POINT A

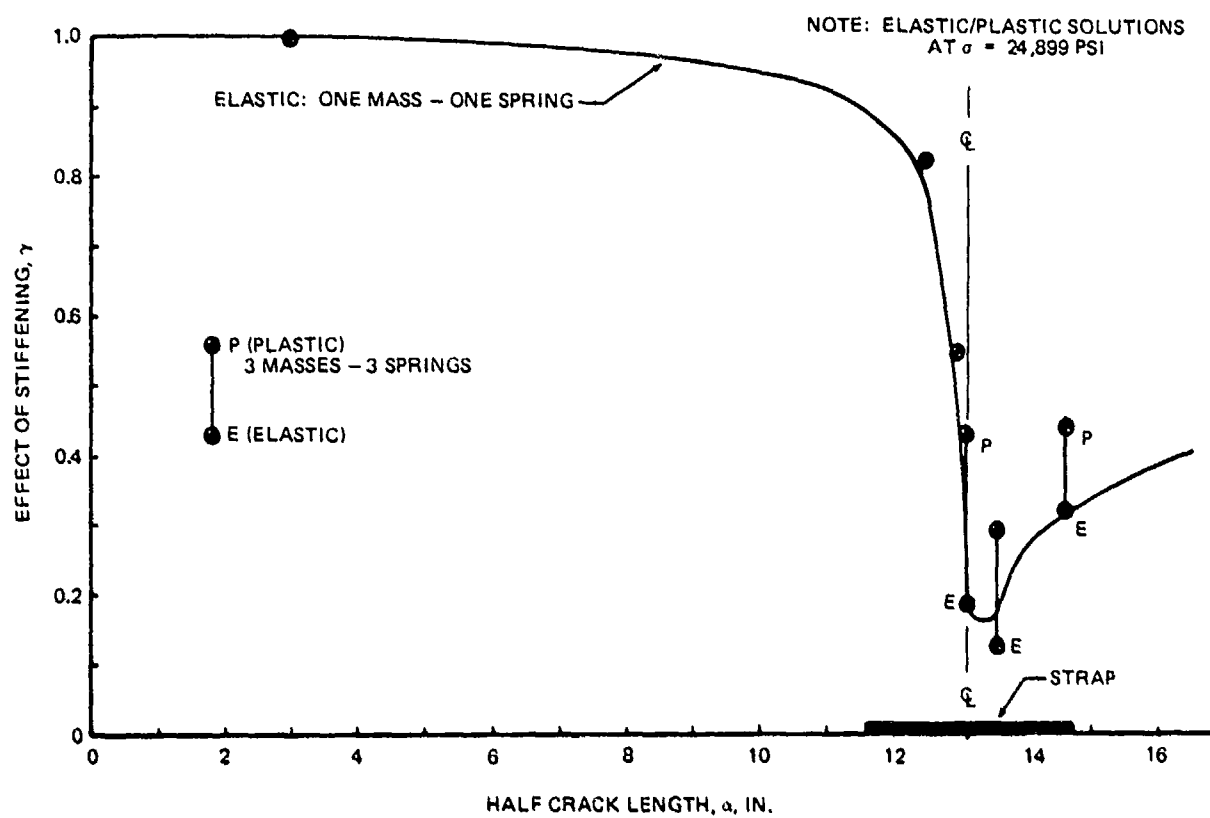


FIGURE 84. EFFECT OF CONSIDERING PLASTICITY AND A MULTIMASS/MULTISPRING MODEL AT CHECK POINT A

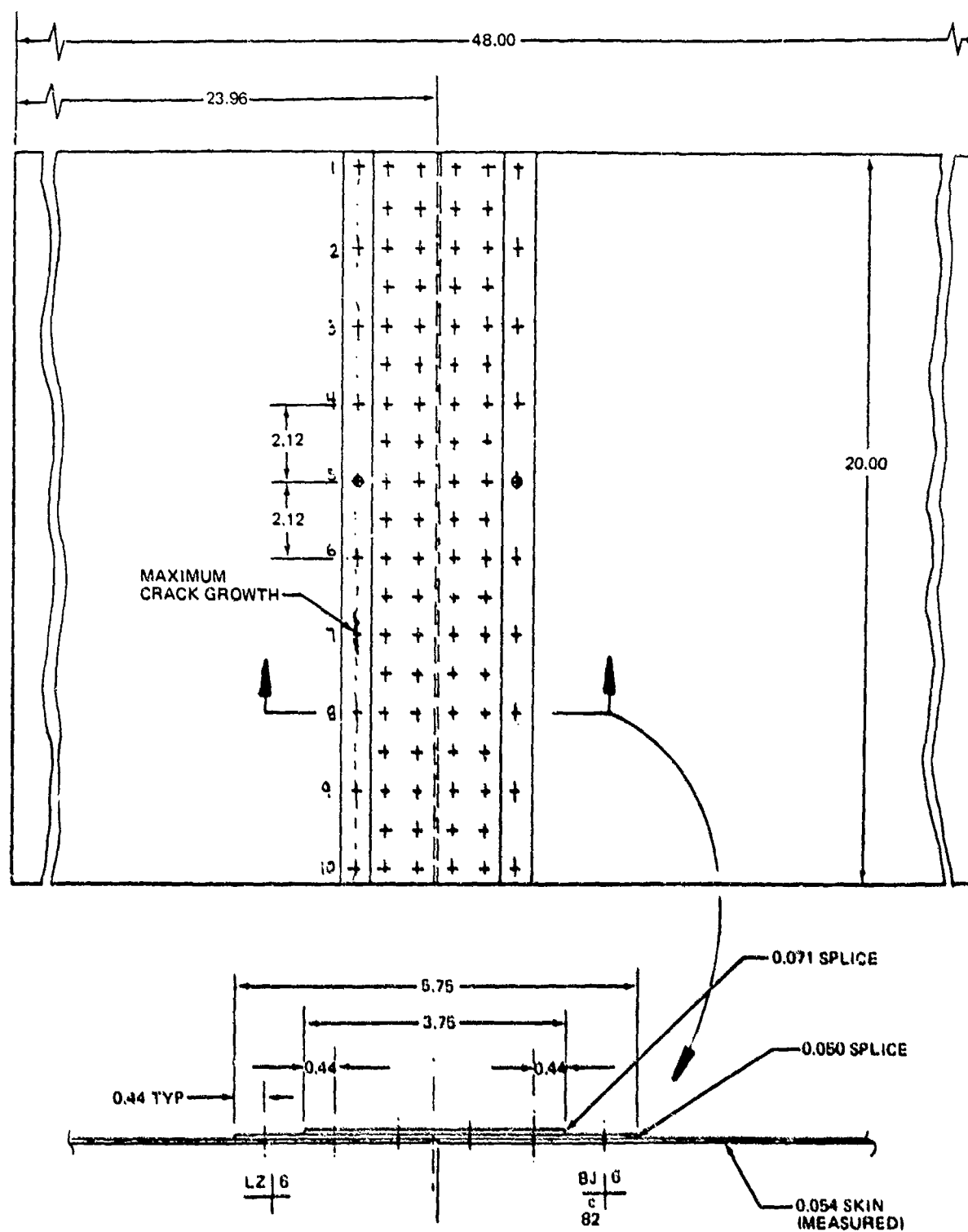


FIGURE 85. TRANSVERSE RIVETED SPLICE SPECIMEN

The analysis was based on: (a) the preliminary  $da/dN$  vs  $\Delta K$  data of Figure 66, (b) the Bowie correction for a hole (reference 2), and (c) the effect of fastener bearing in the hole. The best correlation was obtained for a 25% load transfer in the rivet. This value along with preliminary material data was then used to analyze the riveted splices of the FSDC, Figure 86.

It should be noted that use of a collinear correction in the analysis degraded the results. The diameter of the next rivet was so small that the correction factor for adjacent holes had no effect on the solution.

Shear Interaction Test Specimen. - A curved stiffened panel specimen will be tested under cyclic tension, compression, shear, and pressure. The environment will be room temperature and laboratory air.

The geometry represents the wide spaced region on the PABST fuselage sidewall. The radius was 108 inches.

The specimen was analyzed for four damage tolerance flaws and for one foreign object damage case. The locations of the assumed damage are shown in Figures 87 and 88.

The load spectra is presented in Figure 89.

The assumed initial flaws were 0.25 inch through flaws. Flaws #1, 2 and 4 were assumed to be close to the light frame, the heavy frame, and the longeron respectively. Crack #3 was a midbay crack.

The analysis included the effects of: Pressure pillow, finite width, effect of stiffening, bulging and non-uniform stress distribution.

The critical crack was crack #4. The crack growth time history is shown in Figure 90. The residual strength diagram for crack #5 is presented in Figure 91.

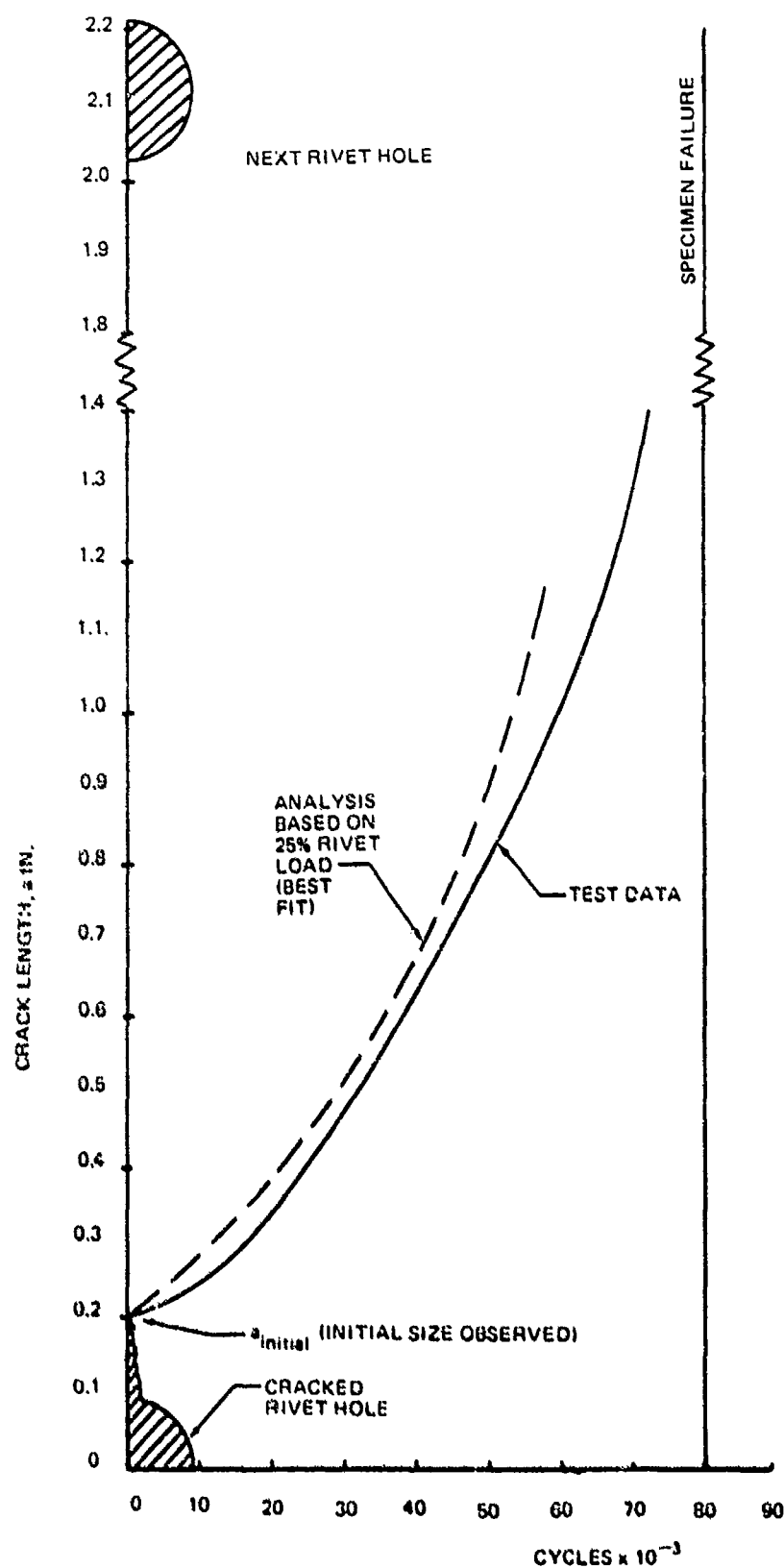


FIGURE 86. ANALYSIS-TEST CORRELATION FOR THE TRANSVERSE RIVETED SPLICE SPECIMEN

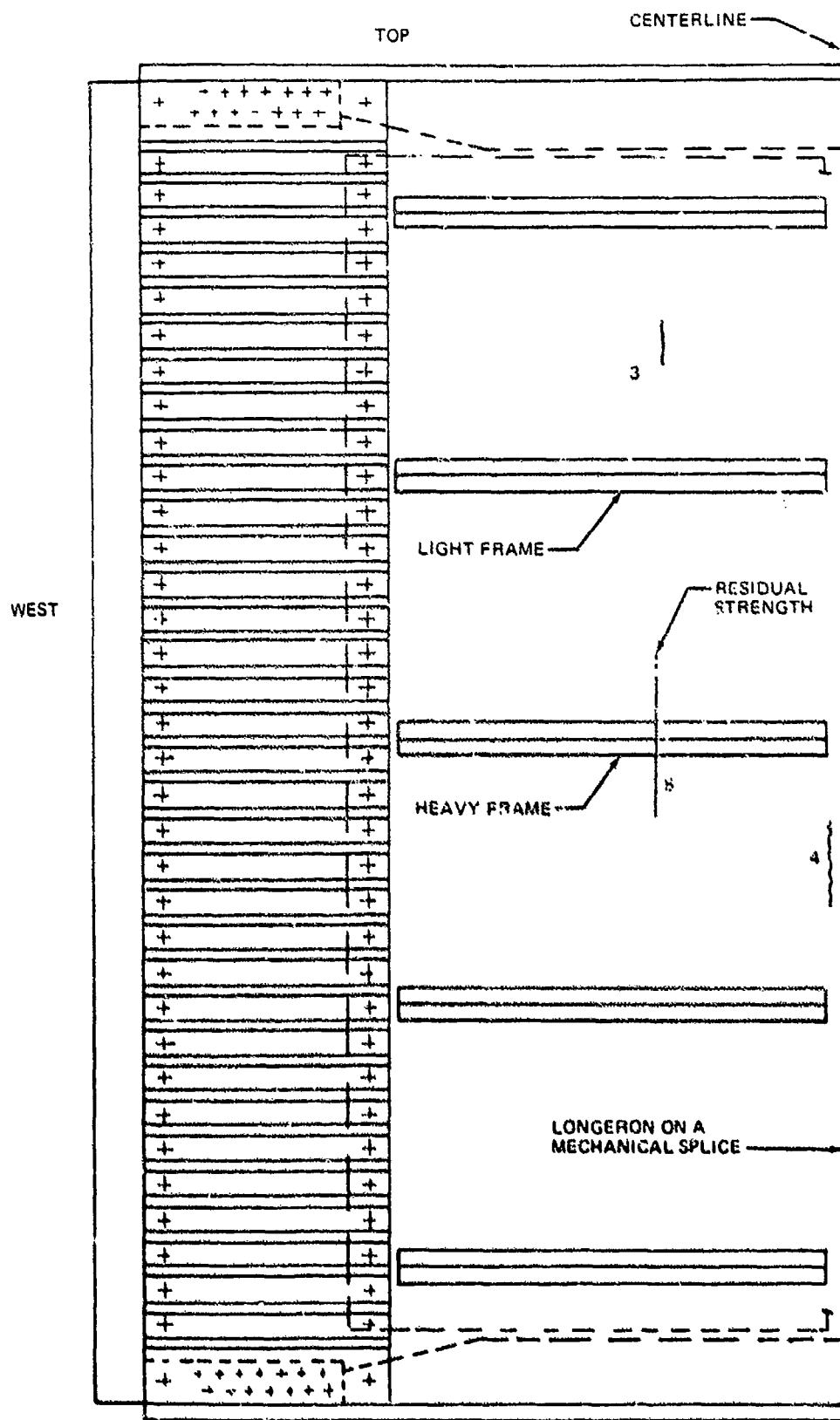


FIGURE 87. CRACK LOCATIONS ON LEFT SIDE OF SHEAR PANEL

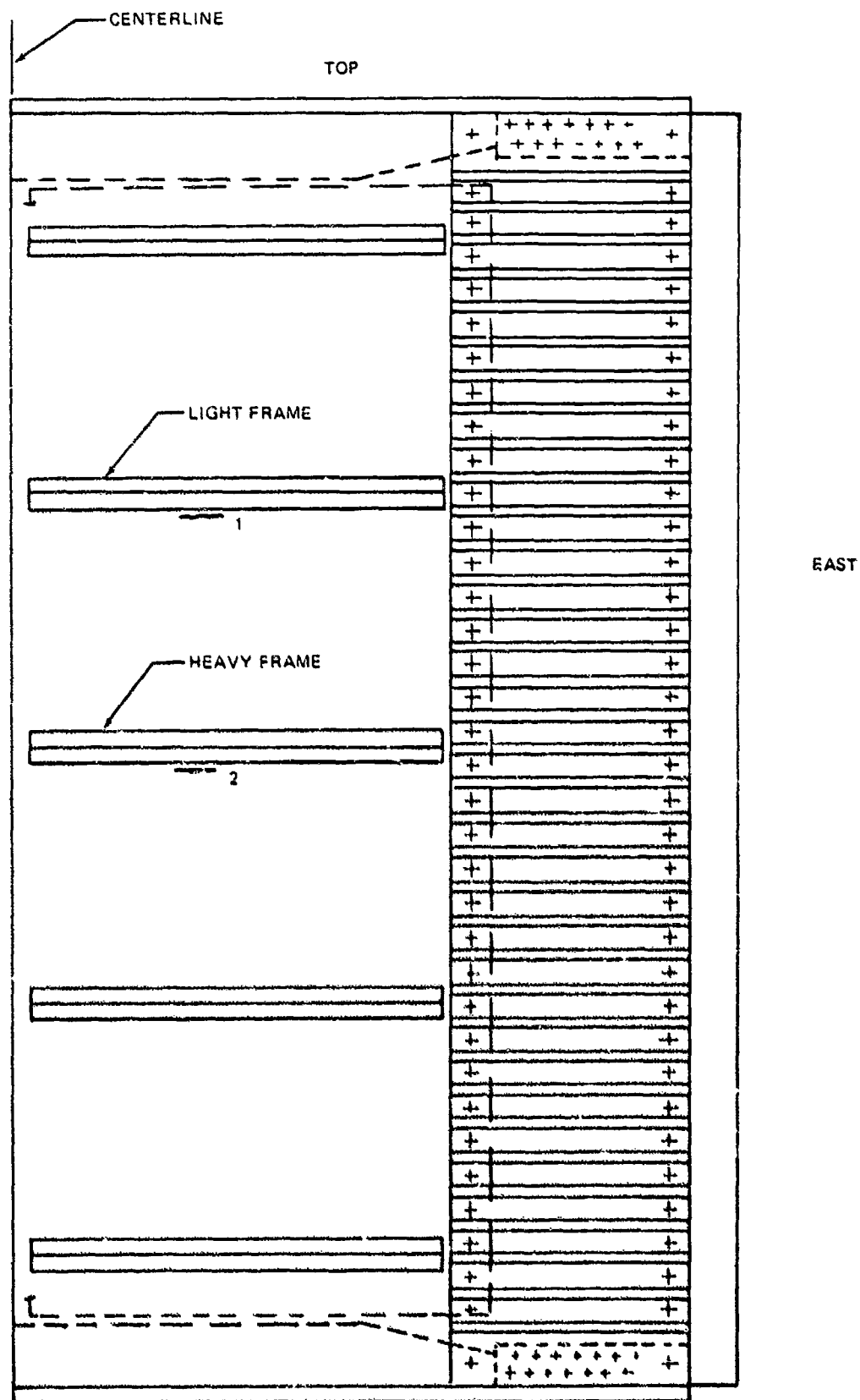
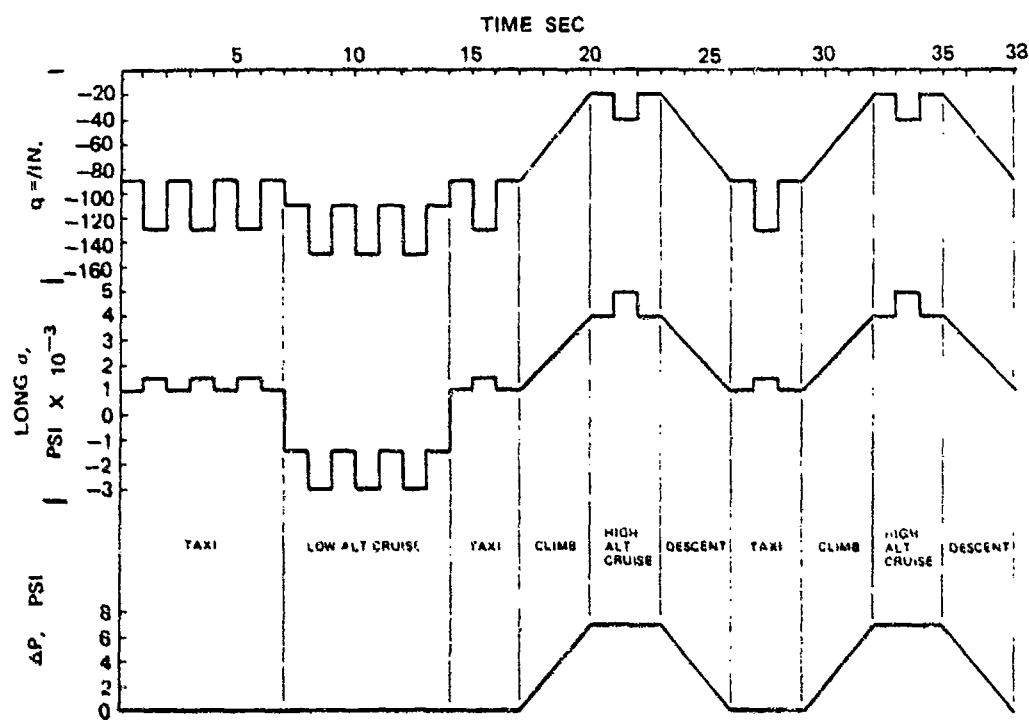


FIGURE 88. CRACK LOCATIONS ON RIGHT SIDE OF SHEAR PANEL



SPECTRUM REPEATED 9500 TIMES = 1 LIFETIME

FIGURE 89. SHEAR INTERACTION TEST SPECIMEN SPECTRA

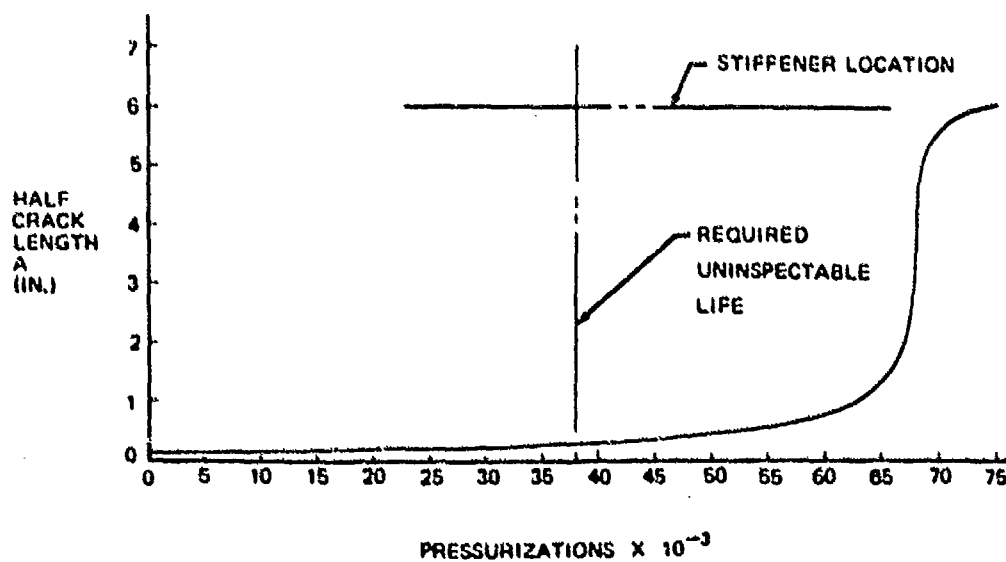


FIGURE 90. CRACK GROWTH TIME HISTORY OF SHEAR INTERACTION PANEL CRACK NO. 4

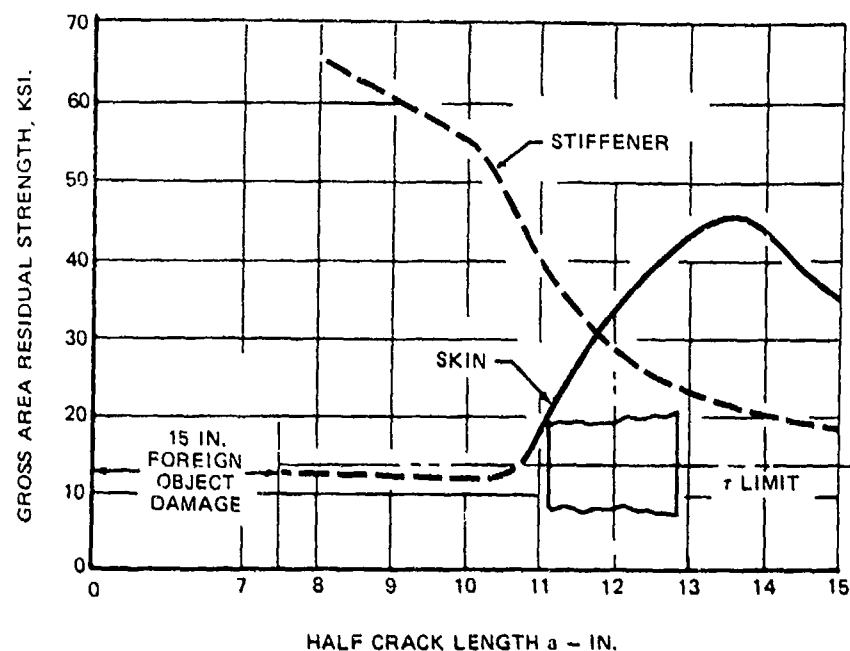


FIGURE 91. RESIDUAL STRENGTH DIAGRAM FOR SHEAR INTERACTION PANEL CRACK NO. 5

Curved Test Panel With Door. - A curved stiffened specimen with a door will be tested under cyclic 7.15 psi pressure loading. The environment will be room temperature and laboratory air.

The geometry represents the forward section of the PABST fuselage. The test panel is shown in Figure 92. The radius above Longerons 1 and below Longerons 2 is 82 inches. Between the longerons, the radius is 136 inches.

The specimen was analyzed for six damage tolerance flaws and two foreign object damage cases. The locations of the assumed damage are shown in Figure 92. The analysis included the same effects as for the shear interaction test specimen.

The critical skin cracks were circumferential crack #4 and longitudinal crack #5. The crack growth time histories as shown in Figure 93 and 94 respectively.

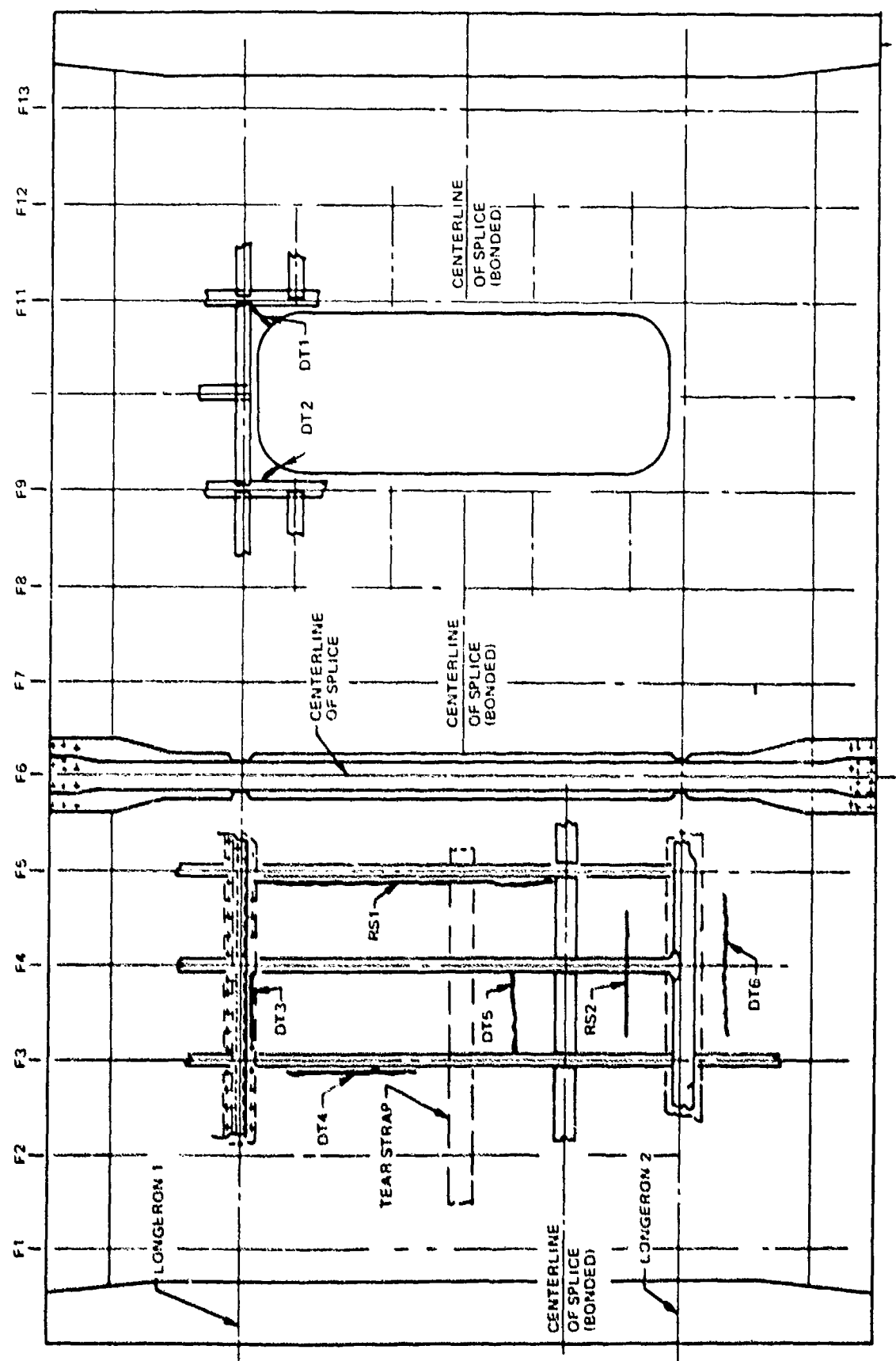


FIGURE 92 CRACK LOCATIONS ON CURVED TEST PANEL WITH DOOR

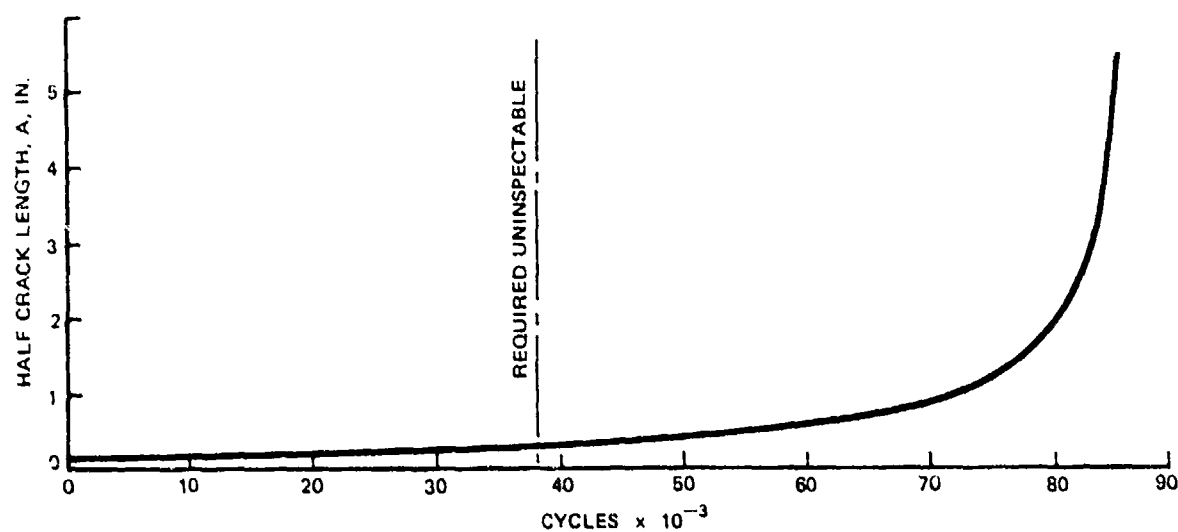


FIGURE 93. CRACK GROWTH TIME HISTORY OF CURVED PANEL CRACK NO. 4

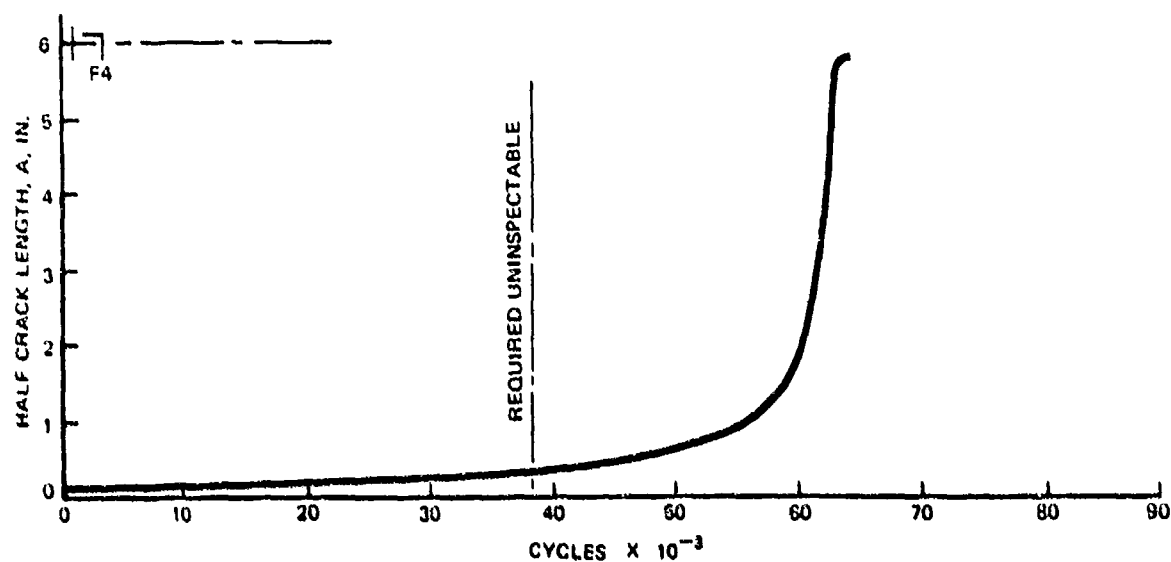


FIGURE 94. CRACK GROWTH TIME HISTORY OF CURVED PANEL CRACK NO. 5

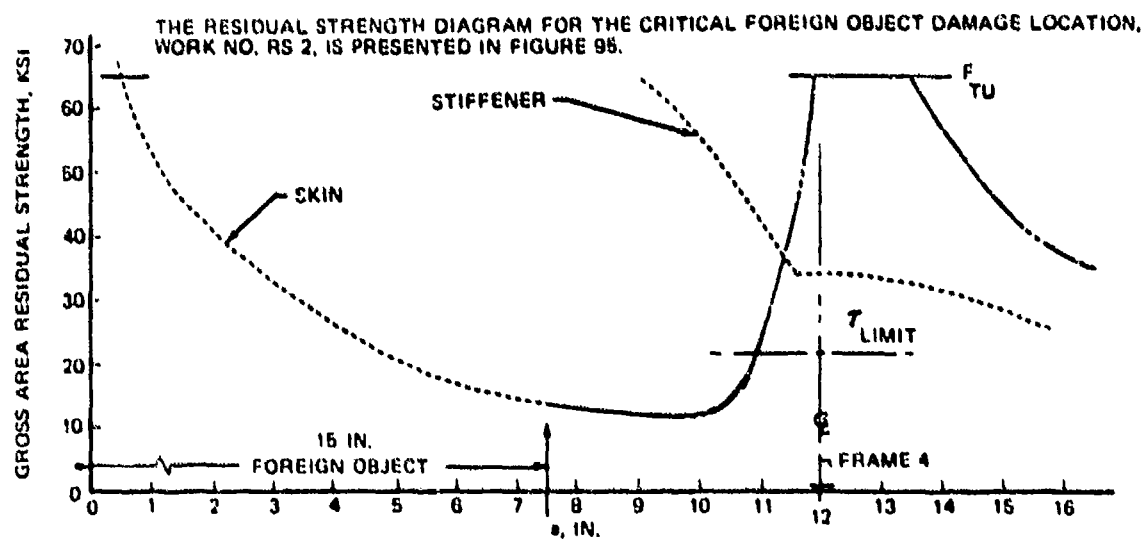


FIGURE 95. RESIDUAL STRENGTH DIAGRAM FOR CURVED PANEL CRACK RS 2

## Adhesive Bonded Joint Analysis

The ultimate mode analysis methods for adhesive bonded joints are described in Reference 1. The analysis of adhesive-bonded-double-strap longitudinal splices is presented on pages 135-139 of that Reference and on pages 141-143 for single-strap (flush) bonded circumferential splices. No pure bonded single-lap splices were used.

This section describes the effect of damage tolerance requirements on adhesive bonded joints. A thorough analysis of potential bond failures associated with damage to metal elements in bonded structure is reported in Reference 12. The conclusions for bonded joints are that:

- (1) The analysis of the residual strength of damaged bonded structure must be non-linear, accounting for adhesive plasticity, stiffener yielding, and the change in load paths as a disbond progresses. Therefore, closed form solutions are more appropriate than finite-element ones.
- (2) Most high loads in adhesive bonds result from fail safe damage to metal structure rather than from high load transfer in the intact structure. The reason is that fail safe damage does not necessarily occur in the smoothly tapered region associated with known high load areas.
- (3) Consideration of damage tolerance of bonded structure drives the configuration towards one of many small stiffeners, each with a high ratio of bond width to cross-sectional area and spaced closer together than is customary for riveted designs. The reason for this is that bonds are stiffer than fasteners so the stiffeners can become disbonded.
- (4) Subject to satisfaction of condition (3), the secondary bond failure associated with a primary metal failure is not usually instantaneously catastrophic. In most cases, a finite disbond occurs and is self arresting, requiring a greater load to propagate the disbond. This phenomenon has been observed in tests.

(5) If the geometry of (3) is violated, the failure mode will usually consist of the stiffeners unzipping from end to end and falling off intact or breaking at some remote location. The skin crack will not be arrested. The analytical prediction of this failure mode was verified by tests.

It should be noted that the non-linear analysis methods developed for bonded single-lap joints were used to improve the longitudinal single-lap mechanical skin splices. The key parameter as shown in the analysis is the  $l/t$  ratio. A high ratio results in a smooth deflection at the joint which minimizes the bending due to load path eccentricity. This is shown in Figure 71 of Reference 1. The  $l/t$  ratio of 80 selected for the FSDC represents about a 33% stress concentration beyond the nominal operating stress. A ratio of 20 would have resulted in the bending stress alone being equal to the total FSDC stress.

A significant observation in regard to bonded joints in fuselage structure is that, for the metal gages used in the FSDC, the metal element usually becomes critical before the bond. This conclusion applies to pure structure, in which the yielding of the metal precedes any bond failure. It also holds at discontinuities in the metal elements, such as the frame cutout at stiffener intersections, at which the initial problem is usually a fatigue crack induced in the continuous member over a discontinuity. With a little attention to the detailing to avoid peel-stress problems, the load levels associated with bonded fuselage structure are not usually beyond what adhesive bonds can withstand.

## TRADE STUDIES

This section contains trade studies which were used to determine the merits of various combinations of structural arrangements, the impact on NDI methods, and manufacturing and joining methods as they affect the selected and approved structural design concepts. The following trade studies are included in this section.

- Stiffener flange shape Trade Study
- Damage Tolerance Parametric Studies

## Stiffener Flange Shape Study

Summary. - Two cross sections for the flange which is adhesively bonded to the skin and/or doubler were evaluated. One cross section had a uniform taper and the other had a constant thickness with a chamfer. The latter design was selected for the FSDC for the following reasons: 1) more effective in stopping skin cracks, 2) easier to inspect with NDI, and 3) lower cost.

Purpose. - This trade study was conducted to determine the most efficient cross sectional shape for the longeron and shear tee flange which is bonded to the skin or doubler with respect to structural efficiency, inspectability, and cost. The shapes which were evaluated are shown in Table 23. they are the uniformly tapered flange and the constant thickness flange with chamfer.

Shape Selection. - The uniform taper was evaluated first since the uniformly decreasing thickness appeared to provide a greater flexibility. This flexibility was desirable for minimizing bondline tensile stresses along the stiffener edge. However, the constant thickness flange with chamfer proved to have greater advantages than the uniformly tapered flange. The constant thickness flange is much easier to check with NDI equipment for evaluating the condition of the bondline. In addition, it is much easier to install mechanical fasteners with this type of flange arrangement. An example is the attaching of the internal longeron on the circumferential butt splice at station 523.

The constant thickness flange with the relatively thick edge is more effective in slowing crack growth than the thinner uniformly tapered edge. A skin crack growing toward a bonded stiffener is retarded better by a rapid cross-sectional buildup in the stiffener area. This effectively holds the crack tip shut and retards the growth under the stiffener. In the case of a small area stiffener the crack tip is retarded very little. Stiffeners with long thin bonded flanges have been found to generate a sympathetic crack (in the stiffener) directly above the skin crack even before the skin crack has emerged from the other side of the stiffener.

Since a thin edge on the stiffener is needed to provide peel stress relief, a compromise was made. A narrow tapered strip; i.e., chamfer at the flange edge was adopted.

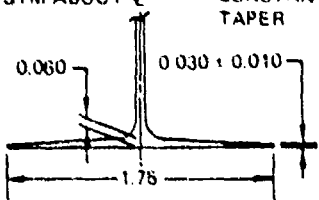
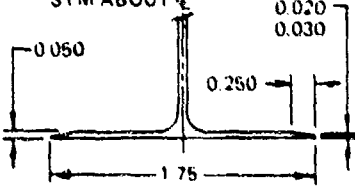
The constant thickness flange adopted for the frame shear tee and longeron greatly simplifies the design of the stretch forming die. The tapered flange design would also necessitate a more complex machining operation on the stretch forming die.

Test Panels. - A test panel was fabricated with test voids in the adhesive by bonding a .050 inch thick .15 inch and .25 inch wide chamfered aluminum doubler as shown in Figure 97. These voids simulated possible faying edge bond defects of three different widths (.125 inch, .250 inch and .375 inch). The panel was evaluated using the Fokker and NDT-210 Bondtesters to determine if the design could be inspected by sonic methods. All three sizes of built-in defects could be detected in the .25 chamfer side by both instruments. The .15 chamfer side defects could not be detected using the NDT-210 Bondtester and the test using the Fokker instrument was determined to be impractical.

It was noted that the adhesive fillet at the faying edge of the test specimen chamfers had been removed in machining and this absence of fillet contributed to the success of the .25 chamfer test. In a production scheme, the adhesive flash at the faying edge of the chamfer would have to be controlled to permit the sonic testing of the chamfer area.

Two additional test panels were fabricated to simulate a "heavy" longeron (Figure 97) and an area with several thick doublers such as the door region as shown in Figure 98. All panels were successfully fabricated and inspected through the chamfered edge.

**TABLE 23**  
**SUMMARY OF TAPERED FLANGE VERSUS CONSTANT  $t$  WITH EDGE CHAMFER**

CONFIGURATION	ADVANTAGES	DISADVANTAGES
<p>SYM ABOUT <math>\bar{Q}</math>      CONSTANT TAPER</p> 	<ul style="list-style-type: none"> <li>◦ LESS WEIGHT</li> </ul>	<ul style="list-style-type: none"> <li>◦ DIFFICULT AND COSTLY TO MATCH TAPERS FOR SPLICES</li> <li>◦ DIFFICULT TO NDI</li> <li>◦ LESS EFFECTIVE IN STOPPING SKIN CRACKS</li> <li>◦ COSTLIER TOOLING FOR STRETCH FORMING</li> </ul>
<p>CONSTANT <math>t</math> WITH CHAMFER SYM ABOUT <math>\bar{Q}</math></p> 	<ul style="list-style-type: none"> <li>◦ EASIER TO SPLICE</li> <li>◦ RELATIVELY EASY TO NDI</li> <li>◦ MORE EFFECTIVE IN STOPPING SKIN CRACKS</li> <li>◦ LOWER TOOLING COST FOR STRETCH FORMING</li> </ul>	<ul style="list-style-type: none"> <li>◦ SLIGHTLY HEAVIER</li> </ul>

NOTE: DIMENSIONS SHOWN ARE TYPICAL

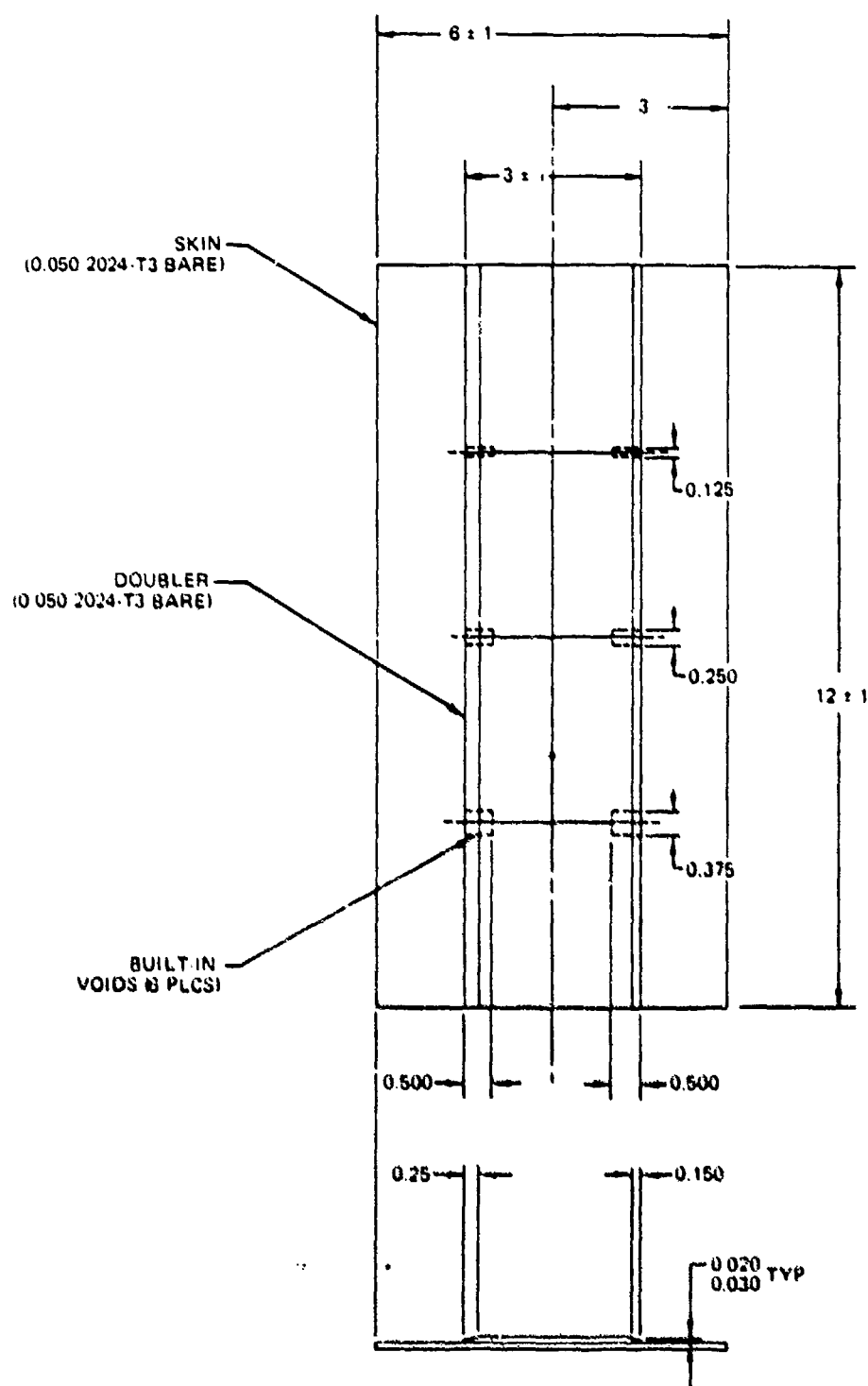


FIGURE 96. TYPICAL EXTRUSION (SIMULATED) ON SKIN PANEL

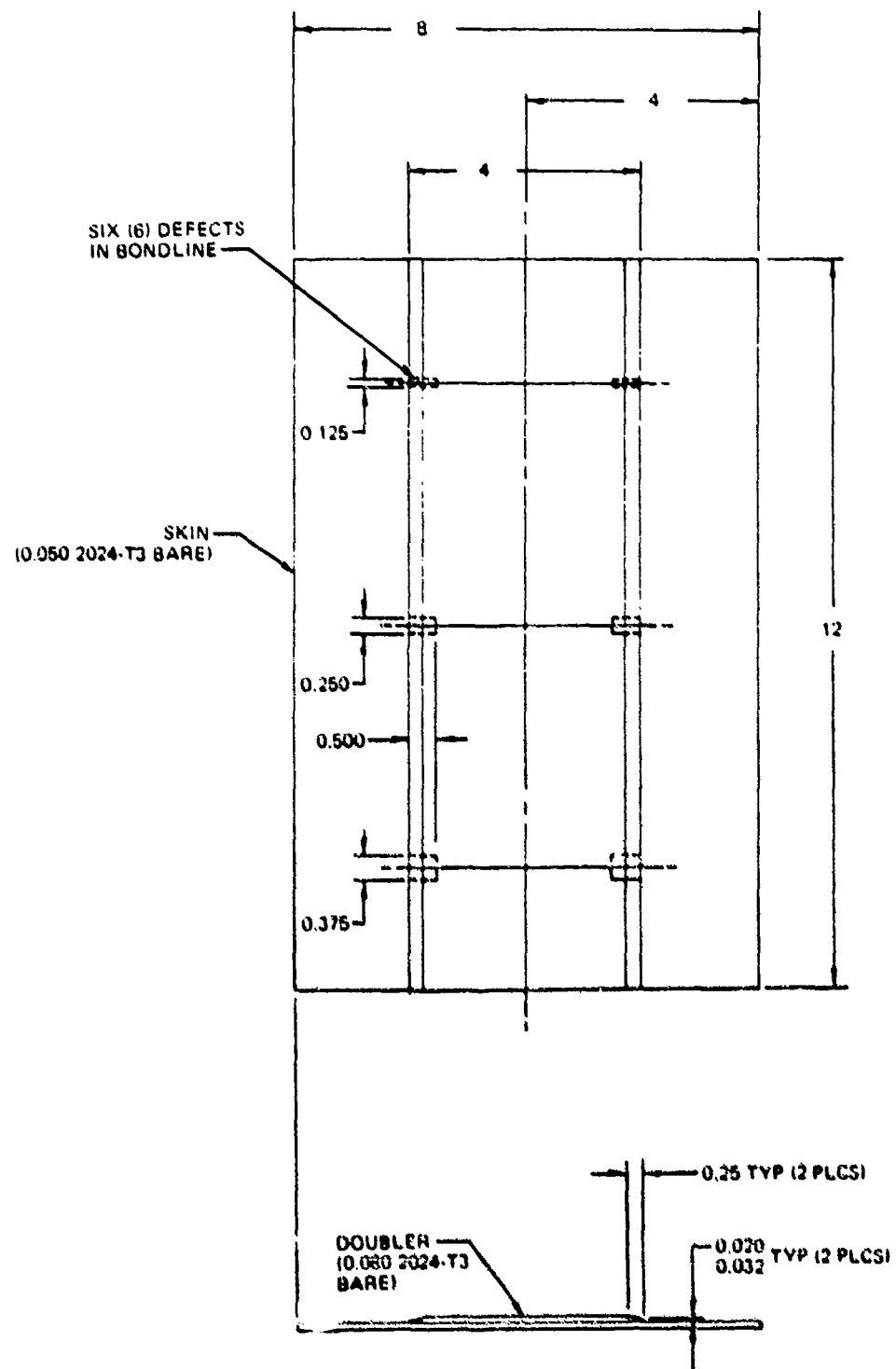


FIGURE 97. TYPICAL "HEAVY" EXTRUSION (SIMULATED) ON SKIN PANEL

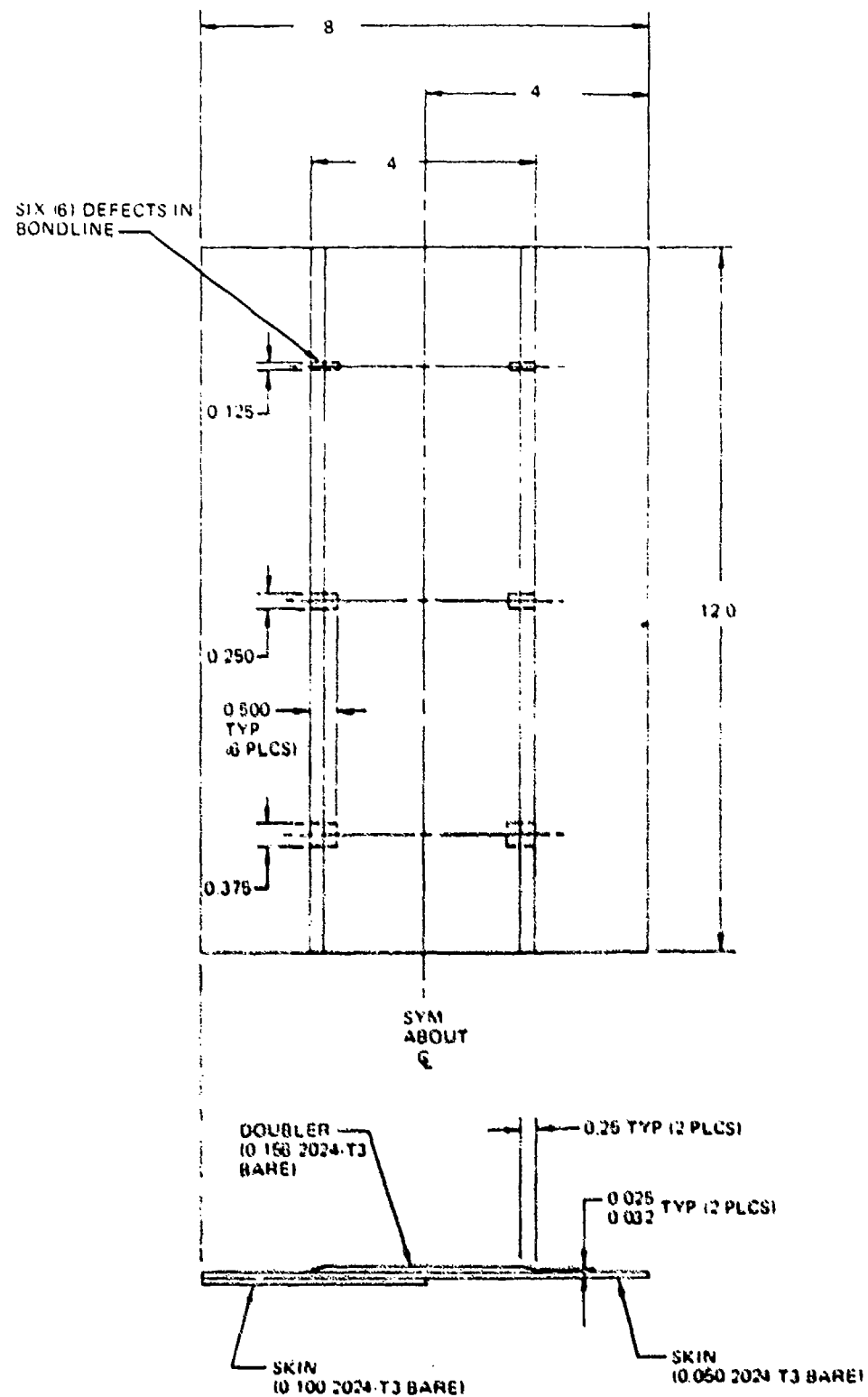


FIGURE 98. SIMULATED EXTRUSION WITH SKIN AND DOUBLER

## Damage Tolerance Parametric Studies

Five studies were performed during the design of the FSDC (Full Scale Demonstration Component). Three studies investigated the sensitivity of life prediction to variations in basic damage tolerance input data as follows:

- Study #1 - Effect of Variations in Aircraft Usage (Stress Spectra),
- Study #2 - Effect of Variations in Metallic Material Property Data ( $da/dN$  vs  $\Delta K$ ), and
- Study #3 - Effect of Variations in Initial Flaw Size.

The other two studies determined the effect of variations in geometry on crack growth and on residual strength:

- Study #4 - Effect of Variations in Skin Thickness and in Longerons Area and Spacing, and
- Study #5 - Effect of Variations in Crack Stopper Area and Spacing in the Wide Spaced Longerons Region.

The location of these studies on the FSDC structure is shown in Figure 99. The design criteria and analysis methods described in the criteria and Damage Tolerance Sections were used including the slow crack growth criteria of the MIL-A-83444 (USAF) specification.

The spectra and the limit stresses used in the crack growth and residual strength analysis were based on airplane loads for the preliminary design phase, Reference 1, pages 67 through 79. The internal loads were obtained by the FORMAT finite element analysis method, as described in the Internal Loads Section. The stress spectra values for studies #2 and #4 and for studies #1, #3 and #5 are shown in Tables A1 and A2 of the Appendix respectively. The effect of skin pillowing between stiffening members due to pressure was included.

The geometry associated with the studies is presented in Table 24. The design of the structural members is shown in the Design Section.

The material data ( $da/dN$  vs  $\Delta K$ ) for 2024-T3 bare sheet used for studies #1, #3, #4, and #5 are shown in Figure 68. The material data for study #2

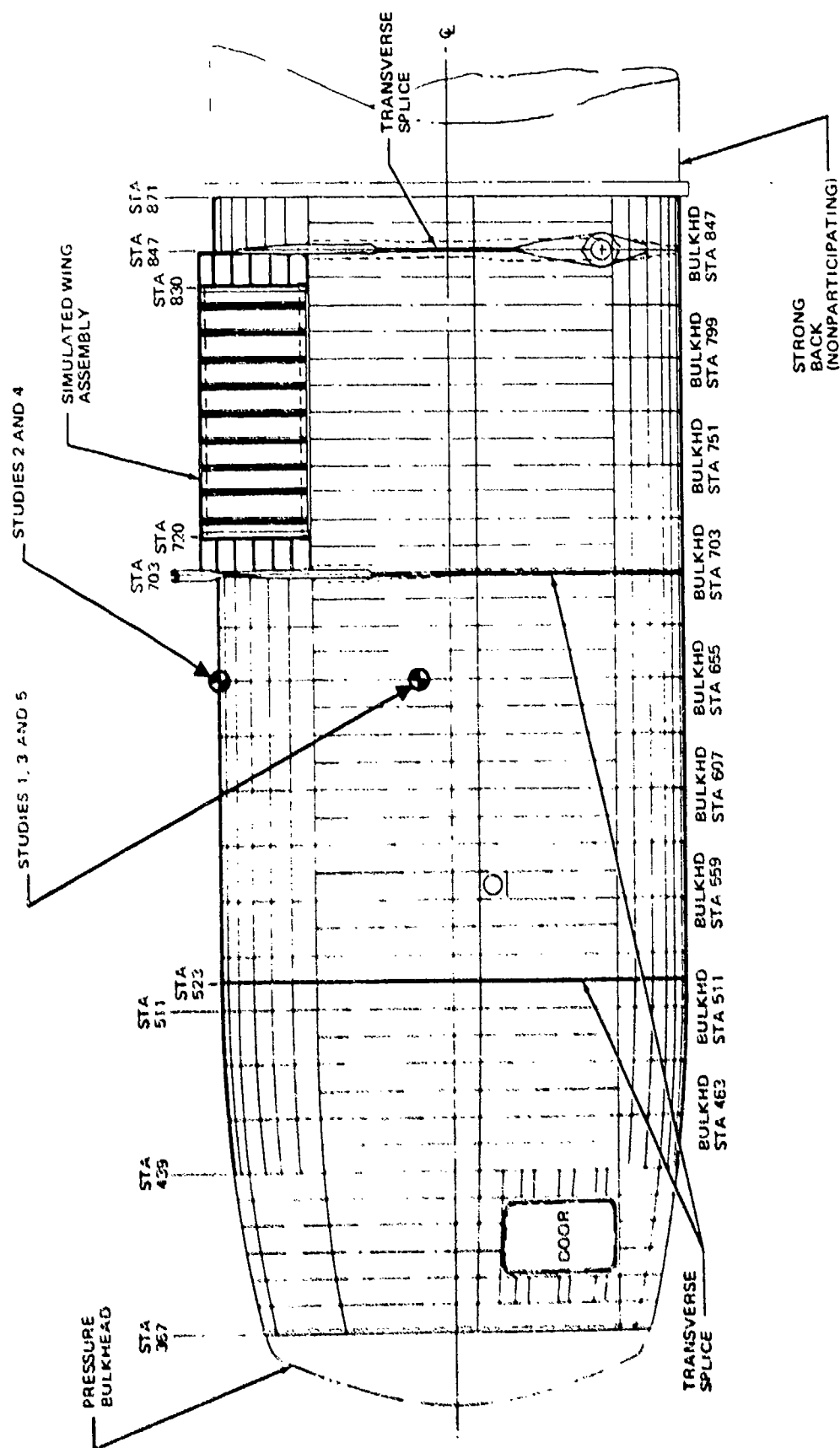


FIGURE 99 DAMAGE TOLERANCE STUDY LOCATIONS

TABLE 24  
STRUCTURAL GEOMETRY FOR STUDIES

STUDY NO.	LOCATION ON STRUCTURE	SKIN THICKNESS	LONGERON OR STRAP AREA	LONGERON OR STRAP SPACING	FRAME AREA	FRAME SPACING
	FIGURE	INCHES	INCHES <sup>2</sup>	INCHES	INCHES <sup>2</sup>	INCHES
1	STATION 655, WIDE SPACED LONGERON REGION, AT SIDE OF FUSELAGE	0.05	0.213 (STRAP)	26.3	0.49	24.0
3			0.488 (LONGERON)	82.0		
5			VARIABLE	VARIABLE		
2	STATION 655, CLOSE SPACED LONGERON REGION, AT TOP OF FUSELAGE	0.05	0.219 (LONGERON)	14.7	0.515	24.0
4		VARIABLE	VARIABLE	VARIABLE		

is described in the subsection for that study. The Willenborg model with an 0.8 factor was used to account for retardation in all five studies.

All of the cracks analyzed were one bay circumferential skin cracks. The principal stresses used in residual strength analyses were assumed to act in a direction normal to the crack.

It can be seen from the study results presented in the following subsections that small changes in basic input data can make large differences in the life of the metallic structure.

Study #1. Effect of Variations in Aircraft Usage (Stress Spectra). - A sensitivity study was conducted to determine the effect of variations in

aircraft usage on life by comparing the associated changes in crack growth time history. The usage affects the stress spectra.

The structure, materials, criteria and methods of analysis are described on pages 190 to 192. The five aircraft utilizations used are presented in Table 25.

The basic spectra, utilization #1, is shown in Appendix Table A2. The variations from the basic spectra utilization were:

- Utilization 2: 3000 hours removed from the low level mission and added to the basic mission. See Appendix Table A3 for the spectra,
- Utilization 3: 3000 hours removed from the basic mission and added to the low level mission. See Appendix Table A4 for the spectra,
- Utilization 4: Doubled the training effort and removed all of it (1281 hours) from the basic mission. See Appendix Table A5 for the spectra, and
- Utilization 5: Doubled the training effort and removed all of it (1281 hours) from the low level resupply mission. See Appendix Table A6 for the spectra.

The changes in the crack growth time history for a one bay crack for all five spectra are shown in Figure 100. The maximum variation ranges from 88% of the basic life for Utilization 2 to 116% for Utilization 3.

Study #2. Effect of Variations in Metallic Material Data  $da/dN$  vs  $\Delta K$ . - The effect of varying  $da/dN$  vs  $\Delta K$  on life was studied using the stiffened skin geometry of the close spaced longeron region, see Figure 99 and Table 24. The average material property curves of 7475-T761 bare sheet, Figure 101, were used as the basis of the parametric study. The 7475-T761 alloy was a candidate material studied in the PABST preliminary design phase for the skin. The qualitative results for crack growth time history would also apply to other aluminum alloys used for fuselage skins.

TABLE 25  
UTILIZATIONS FOR THE SENSITIVITY STUDIES

FLIGHT DESCRIPTION	HOURS PER FLIGHT	UTILIZATION #1		UTILIZATION #2		UTILIZATION #3		UTILIZATION #4		UTILIZATION #5	
		FLIGHTS/ LIFETIME	HOURS/ LIFETIME	FLIGHTS/ LIFETIME	HOURS/ LIFETIME	FLIGHTS/ LIFETIME	HOURS/ LIFETIME	FLIGHTS/ LIFETIME	HOURS/ LIFETIME	FLIGHTS/ LIFETIME	HOURS/ LIFETIME
		This is the Basic Utilization		3,000 hrs from Low Level & Put into Basic Missions		3,000 Hrs from Basic Missions & put into Low Level Missions		Training Effort Doubled at the Expense of Basic		Training Effort Doubled at Expense of Low Level Flights	
Basic Outbound 20,250# Payload	1.283	7,236	9,290	8,270	10,610	6,210	7,967	6,800	8,724	7,236	9,290
Basic Outbound 54,250# Payload	1.001	947	947	1,080	1,081	810	811	890	891	947	948
Basic Return 20,250# Payload	1.382	7,236	10,000	8,270	11,429	6,210	8,582	6,800	9,398	7,236	10,000
Basic Return 54,250# Payload	1.012	947	947	1,080	1,081	810	811	890	891	947	958
Training Outbound 20,250# Payload	.50	1,234	617	1,234	617	1,234	617	2,468	1,234	2,468	1,234
Training Outbound 54,250# Payload	.436	90	39	90	39	90	39	180	78	180	78
Training Return 54,250# Payload	.50	90	45	90	45	90	45	180	90	180	90
Training Return 20,250# Payload	.47	1,234	580	1,234	580	1,234	580	2,468	1,160	2,468	1,160
Touch & Go with Basic Mission	.1	7,236	724	8,270	827	8,270	827	320	32	---	---
Touch & Go's with Training Missions	.1	7,404	740	7,404	740	7,404	740	14,808	1,481	14,808	1,481
Touch & Go's with Training Missions	.1	540	54	540	54	540	54	1,080	108	1,080	108
Low Level Resupply 27,000# Payload	2.0	1,500	3,000	750	1,500	2,250	4,500	1,500	3,000	1,180	2,360
Low Level Resupply 62,000# Payload	2.0	1,500	3,000	750	1,500	2,250	4,500	1,500	3,000	1,180	2,360
TOTALS			29,983		30,103		30,073		30,087		30,067

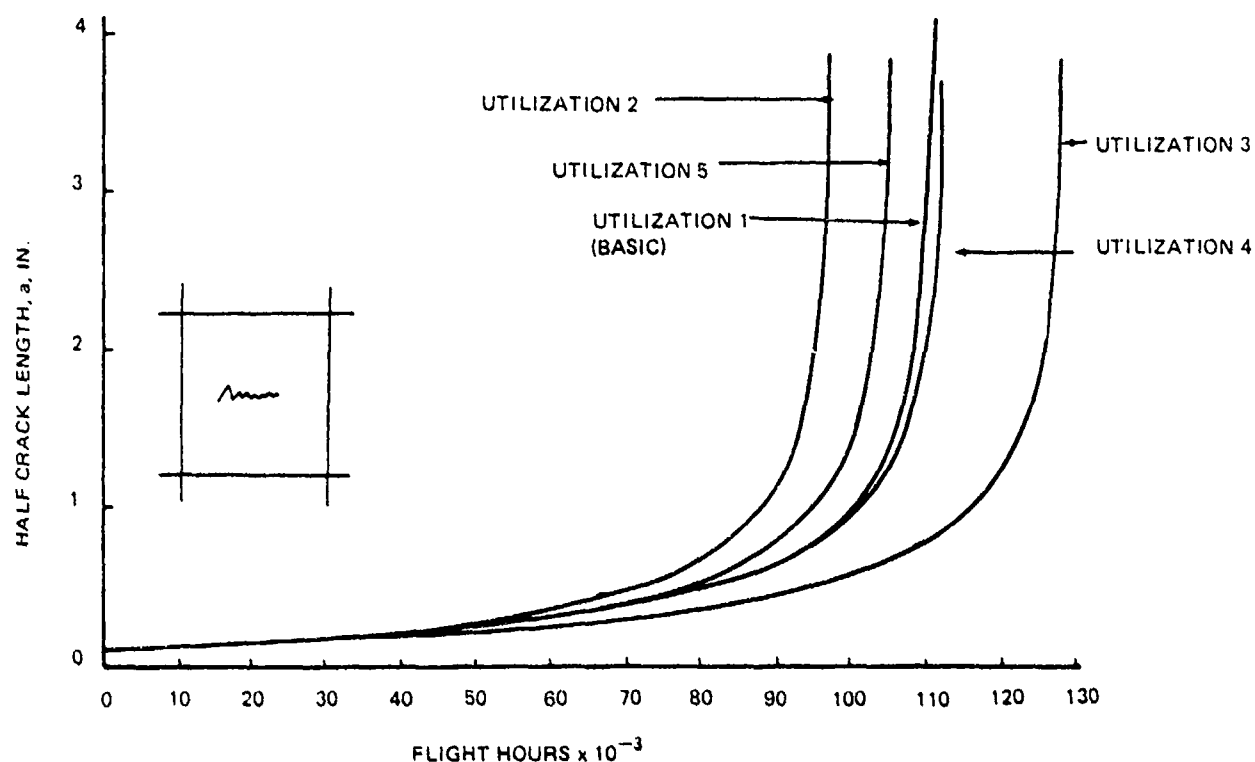


FIGURE 100. THE EFFECT OF VARIATION IN AIRCRAFT USAGE ON LIFE PREDICTION

The variations in the material property curves from the initial values selected for the study, Figure 101, were to shift:

- ° the lower end of the curves to  $\Delta K=3$ . at  $da/dn=10^{-8}$ , Figure 102
- ° the lower end of the curves to  $\Delta K=1.35$  at  $da/dn=10^{-8}$ , Figure 103
- ° the entire set of curves laterally such that  $\Delta K=3$ . at  $da/dn=10^{-8}$ , Figure 104; i.e., reducing crack growth rate, and
- ° the entire set of curves laterally such that  $\Delta K=1.35$  at  $da/dn=10^{-8}$ , Figure 105; i.e., increasing crack growth rate.

The effect was studied for both circumferential and longitudinal skin cracks using the longitudinal spectra of Appendix Table A1 and the hoop spectra generated by pressure only respectively. Skin pillowing effects due to pressure were included.

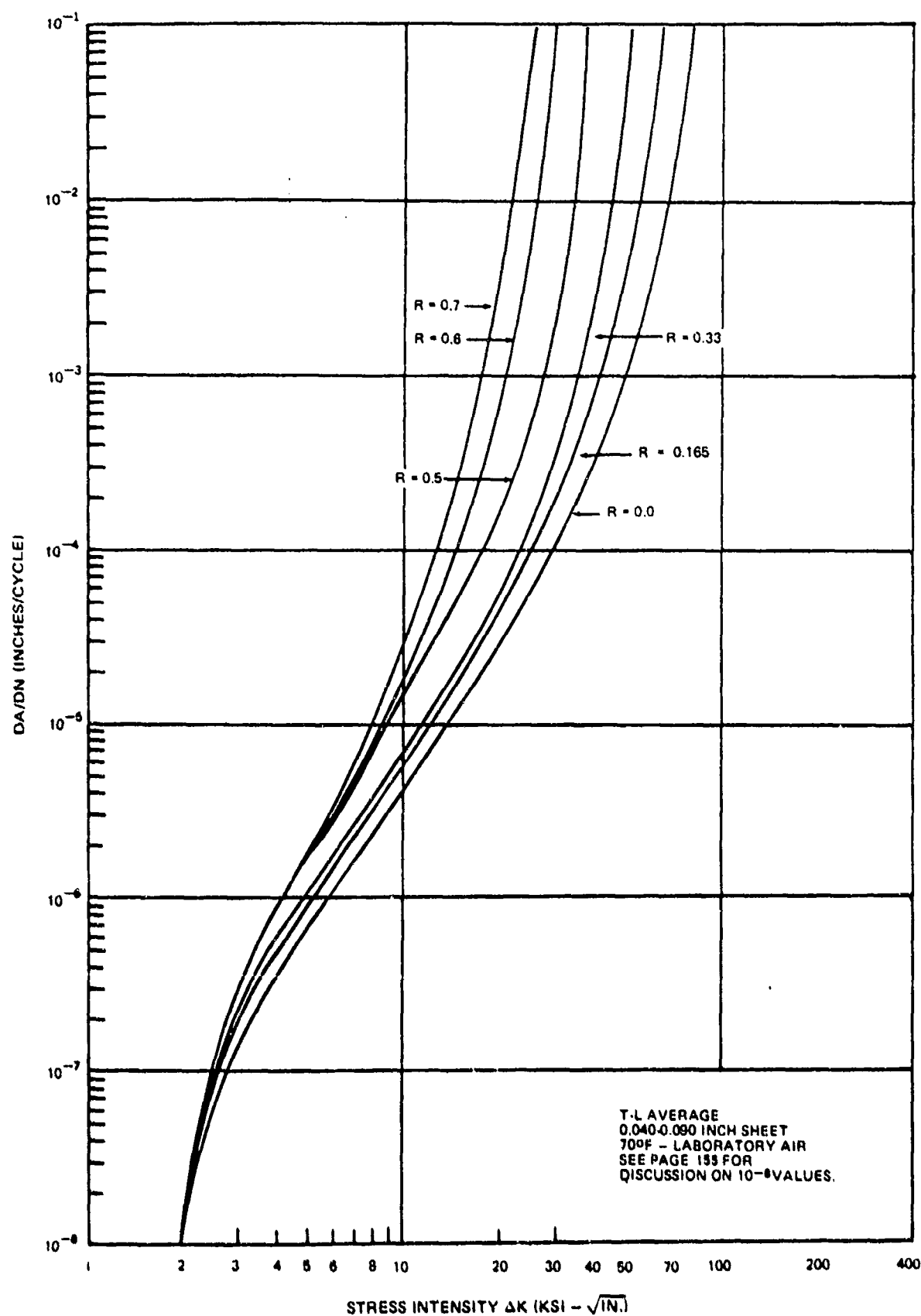


FIGURE 101. PRELIMINARY CURVES OF  $da/dN$  VERSUS  $\Delta K$  FOR 7475-T761 BARE SHEET - BASELINE

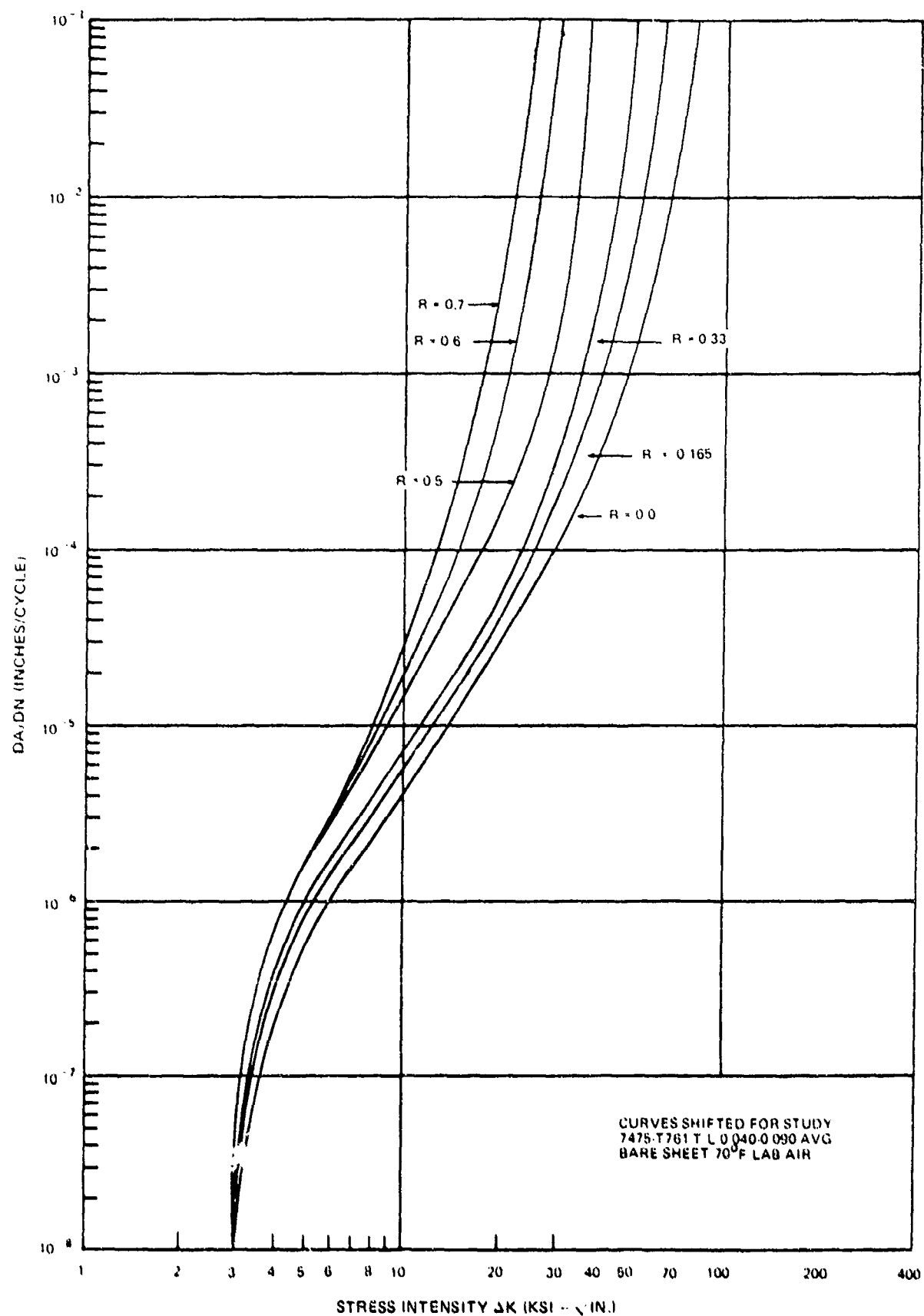


FIGURE 102. LOWER END OF CURVES SHIFTED TO  $\Delta K = 3.0$  AT  $da/dN = 10^{-8}$

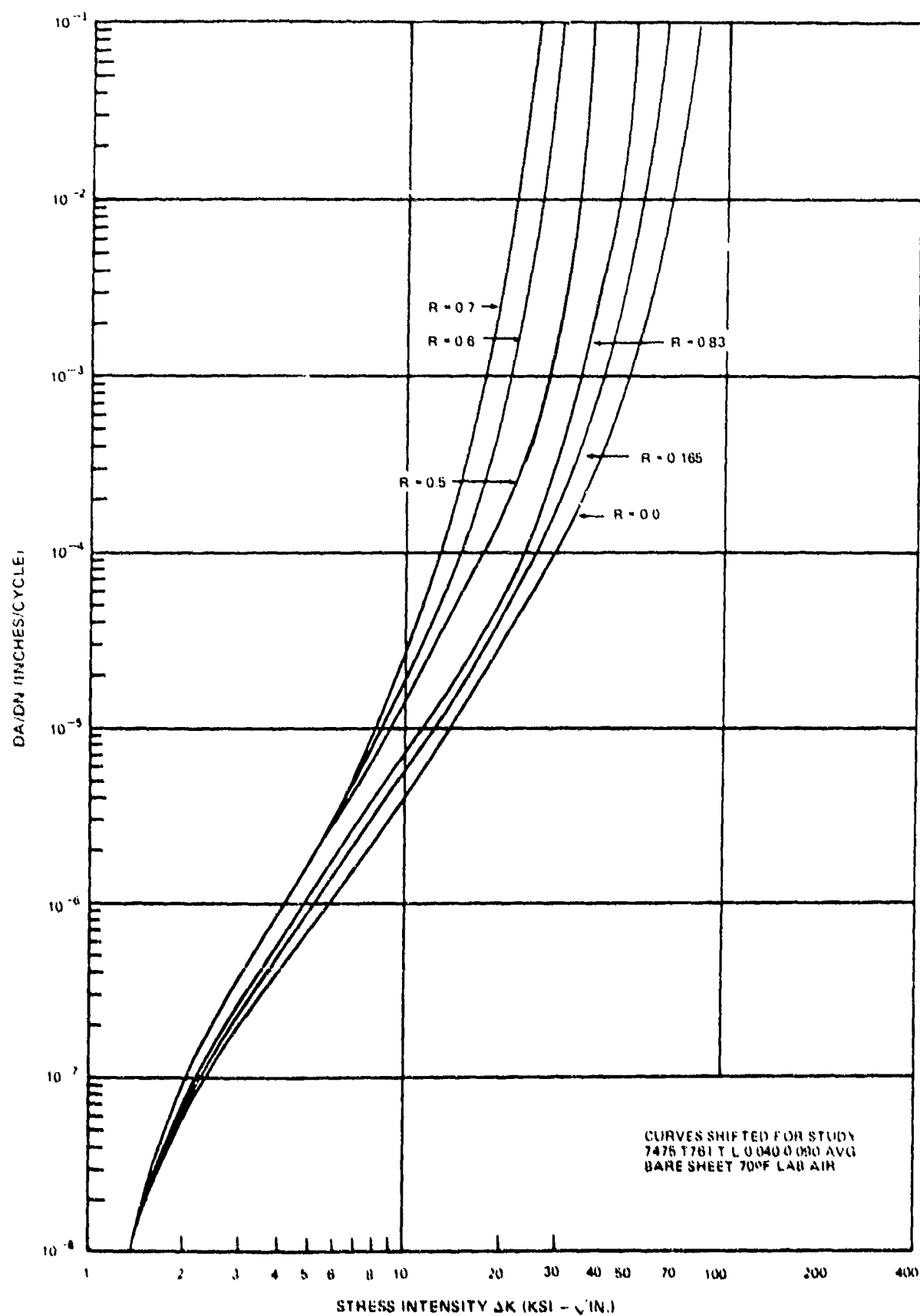


FIGURE 103. LOWER END OF CURVES SHIFTED TO  $\Delta K = 1.35$  AT  $da/dN = 10^{-8}$

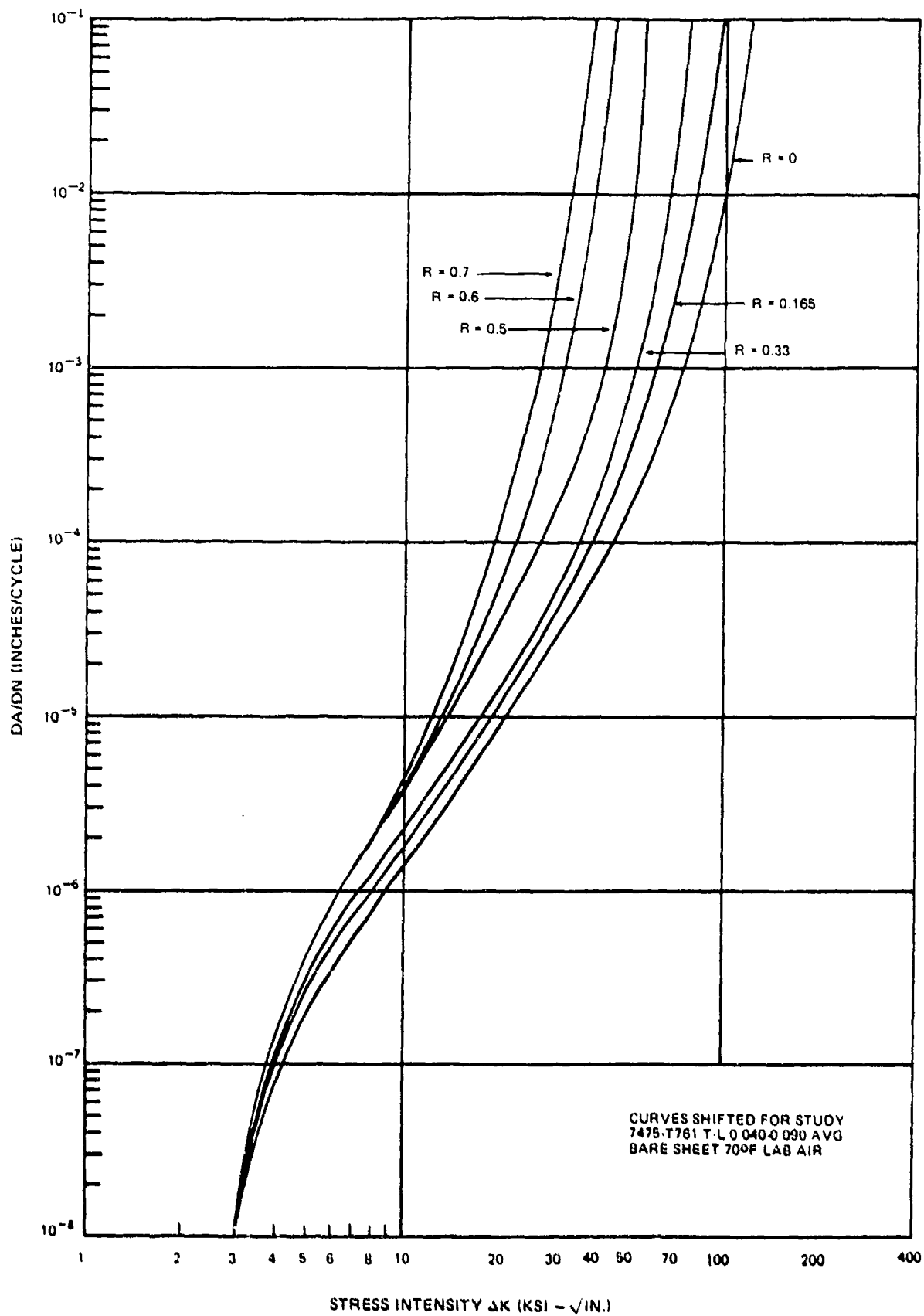


FIGURE 104. ENTIRE CURVE SHIFTED Laterally SUCH THAT  $\Delta K = 3.0$  AT  $da/dN = 10^{-8}$

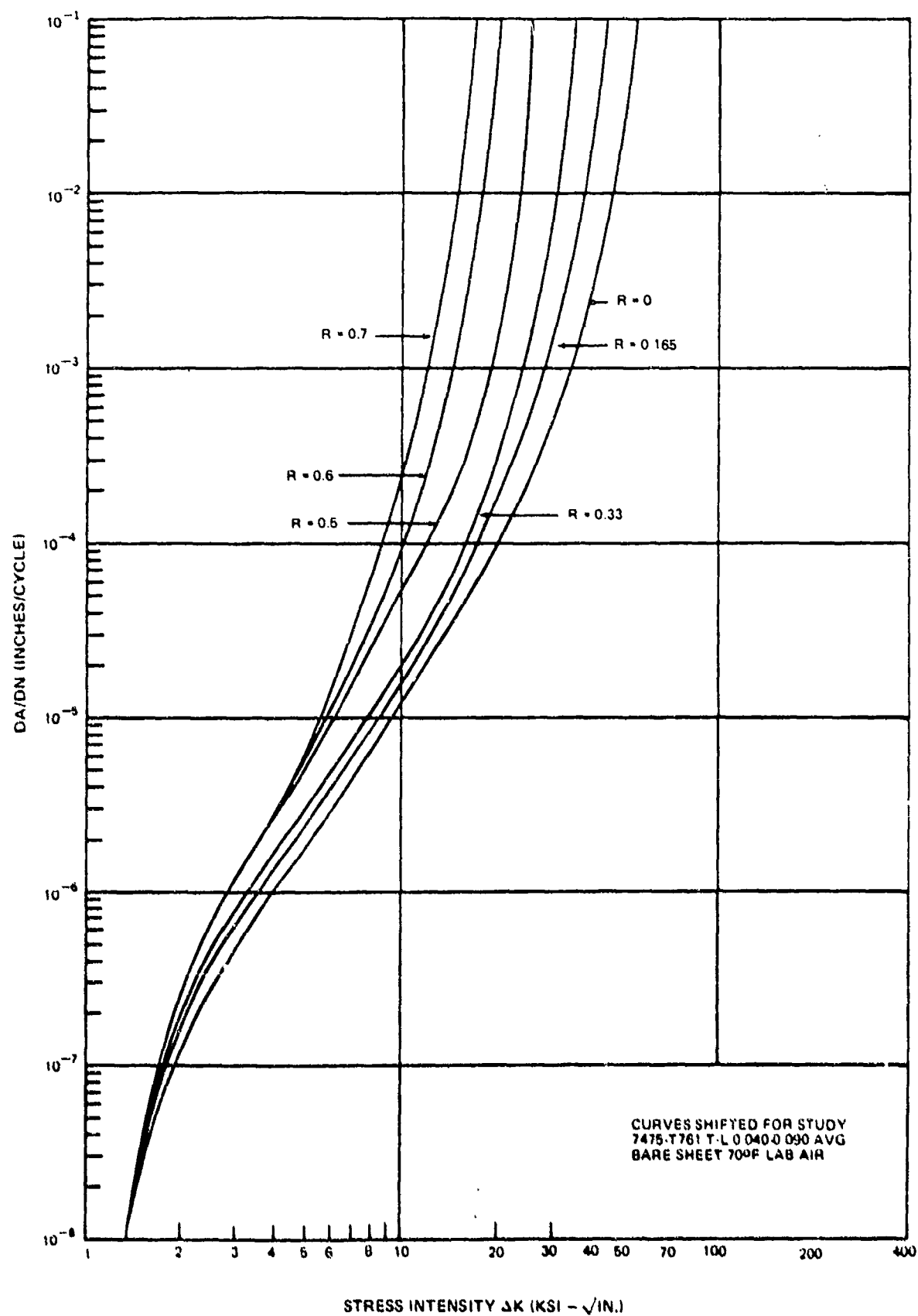


FIGURE 105. ENTIRE CURVE SHIFTED Laterally SUCH THAT  $\Delta K = 1.35$  AT  $da/dN = 10^{-8}$

The results are shown in Figure 106 and 107. It can be seen that relatively small changes in  $\Delta K$  cause large changes in life. For the longitudinal crack, the life remains the same for three of the perturbed curves because the applied  $\Delta K$  values occurred beyond the perturbed region of the shifted material property curves.

The importance of obtaining accurate  $da/dN$  vs  $\Delta K$  data for the damage tolerance analysis of metallic structure cannot be emphasized too strongly.

Study #3 Effect of Variations in Initial Crack Size. - Three through-crack sizes were used to determine the effect of initial crack size variation on life. The total initial crack lengths (2A) were:

- ° 0.10", corresponding to the fail safe criteria of MIL-A-83444.
- ° 0.25", corresponding to the slow crack growth criteria of MIL-A-83444, and
- ° 0.50", an arbitrary value.

The geometry of the wide spaced longeron region, Figure 99 and Table 25 was used with a circumferential one bay skin crack. The material properties, spectra, criteria, and methods used are described on pages 190 through 192.

The results are shown in Figure 108. The life increased 204% with the 50% decrease in total crack length from = 0.50" to 0.25." The life increased 446% for a decrease in initial total crack width from 0.50" to 0.10."

These life ratios apply only to the specific geometry, spectra, material properties and retardation model used. However, the trend will hold for other structural examples.

Study #4 Effect of Variation in Skin Thickness and in Longeron Area and Spacing. - The effect of varying geometry on life and on residual strength was studied using the combinations of skin thickness, (t), longeron area (a), and spacing (S) shown in Table 26.

The spectra, material data, criteria, analysis methods and the location

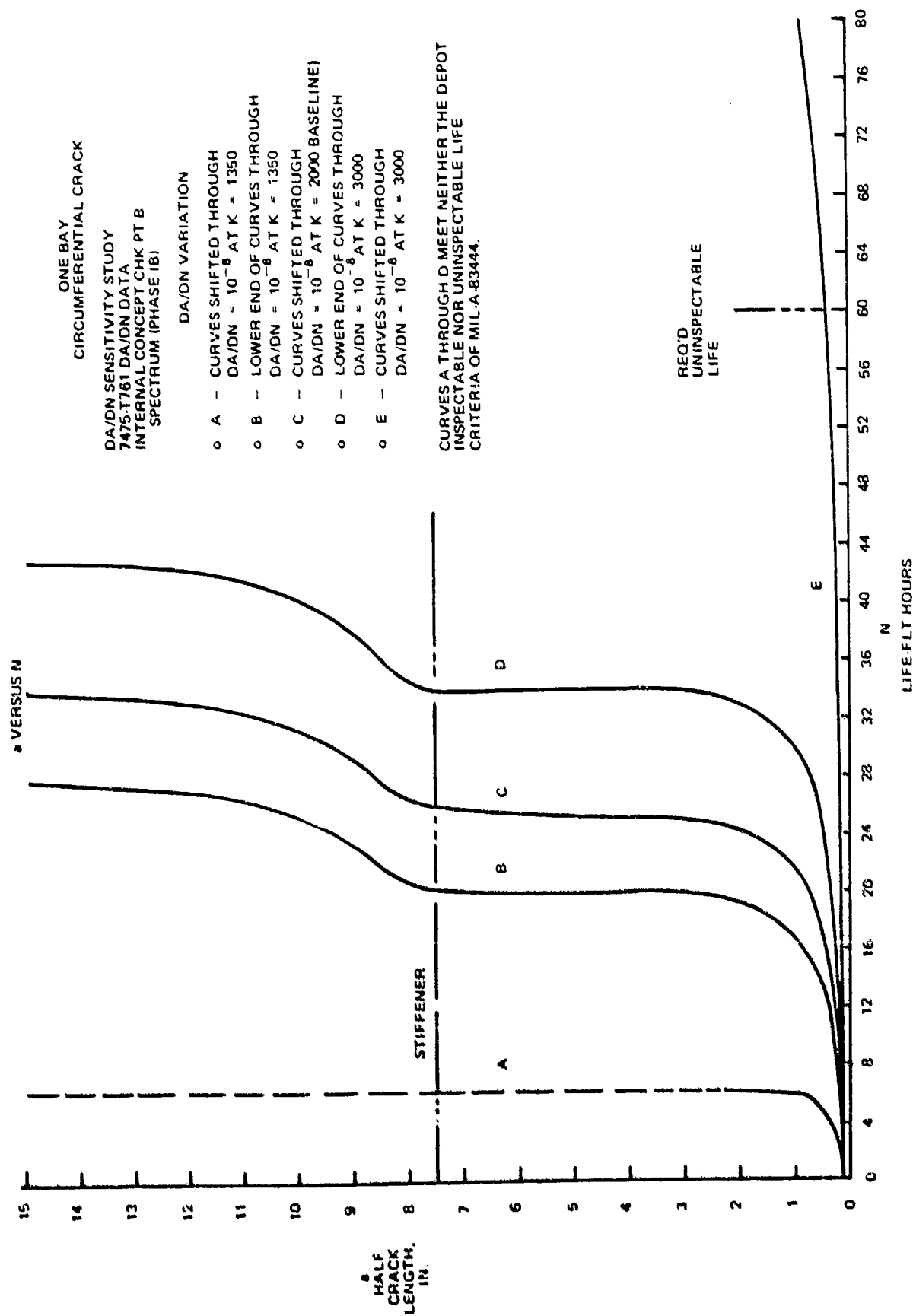


FIGURE 106 EFFECT OF VARYING MATERIAL PROPERTIES ON A CIRCUMFERENTIAL CRACK

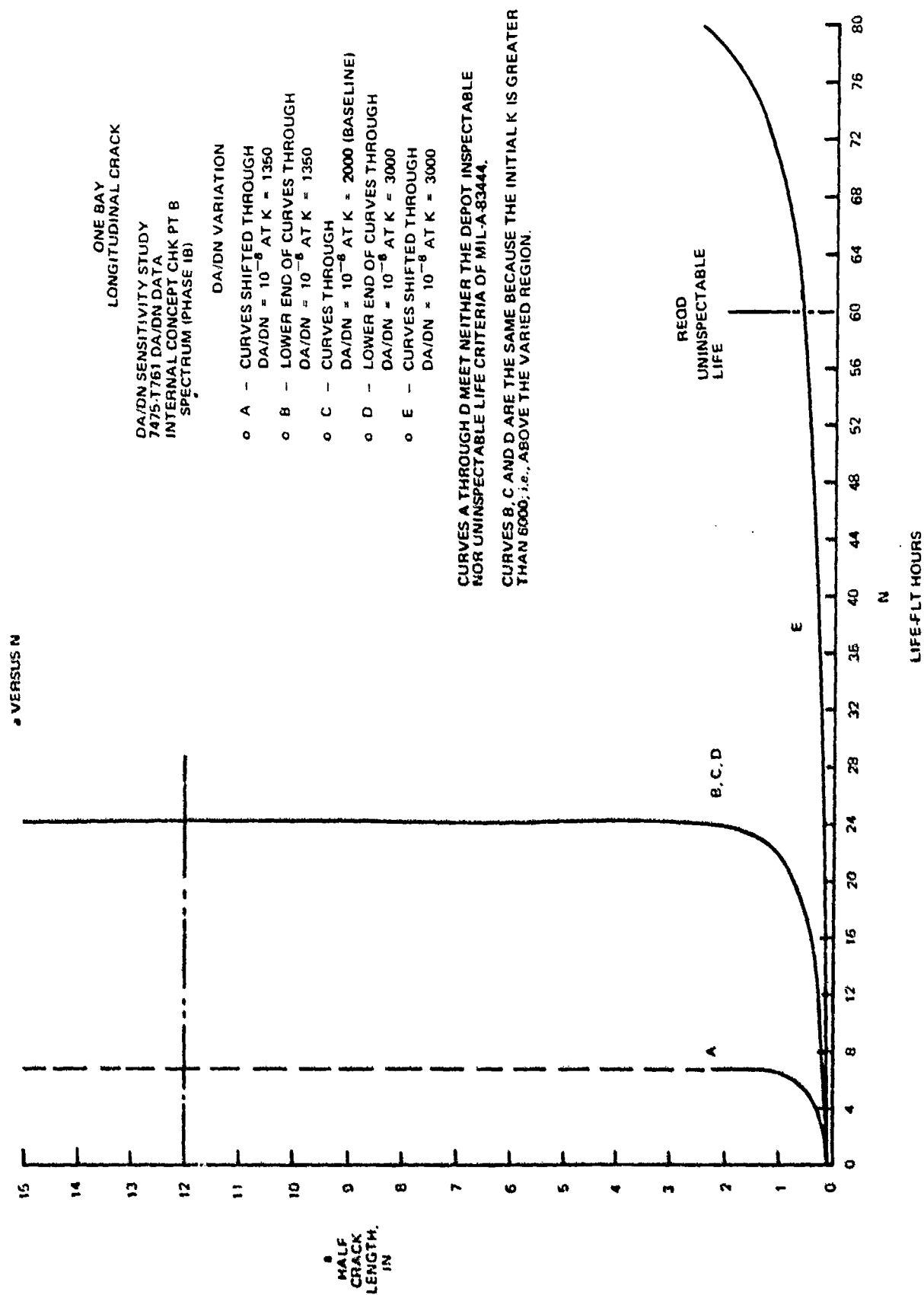


FIGURE 107. EFFECT OF VARYING MATERIAL PROPERTIES ON A LONGITUDINAL CRACK

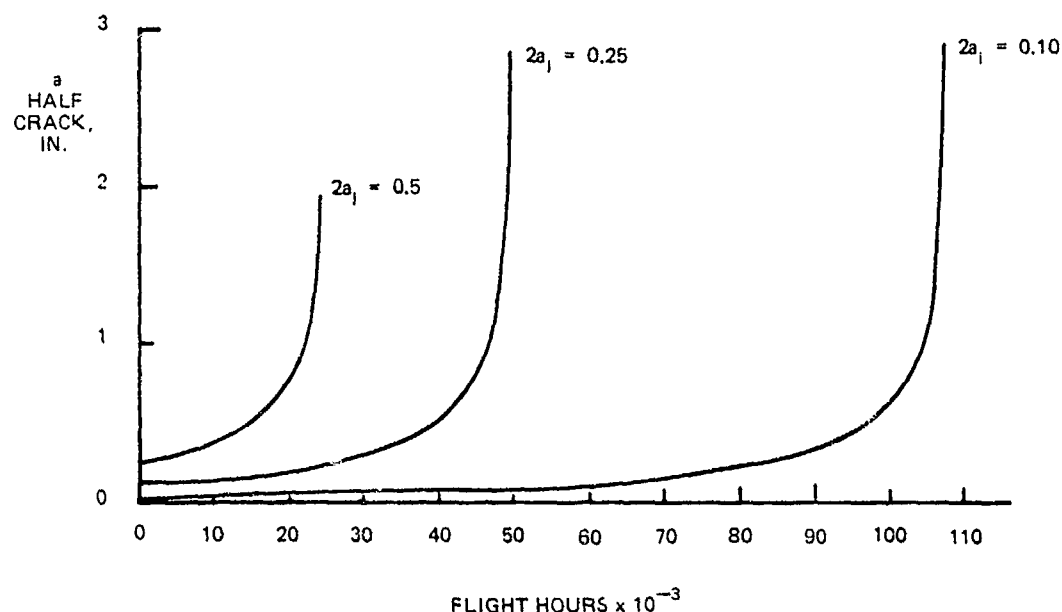


FIGURE 108. EFFECT OF INITIAL FLAW SIZE VARIATION ON LIFE

of the circumferential skin crack on the structure are described on pages 197 to 199.

Each combination of geometry was analyzed for: (a) crack growth time history, (b) residual strength of a two bay crack with center stiffener intact, and (c) 15 inch foreign object damage. An example solution is shown in Figures 109 and 110 for the case of  $A = 0.237$ ,  $S = 16.16$ , and  $t = 0.040$ . It can be seen that this geometry does not meet the crack growth or the residual strength criteria.

The results of the study are shown in Figure 111 for crack growth time history. Residual strength was less critical. The combinations of geometry were qualified to the slow crack growth uninspectable criteria of two lifetimes; i.e., 60,000 flight hours. As can be seen, the life criteria was not met for some of the geometries having a skin thickness less than 0.050". Life is increased by increasing  $t$  and  $A$  and by decreasing  $S$ . These trends apply to all structure but the numerical values shown apply only to the geometry, spectra, initial flaw sizes, and material properties used for this particular study.

TABLE 26

## SKIN THICKNESS, LONGERON AREA AND SPACING VARIATIONS STUDIED

SKIN THICKNESS	LONGERON AREA	LONGERON SPACING	SMEARED THICKNESS $t$	INITIAL GAG STRESS $\sigma$ INITIAL SPECTRA
0.040	0.237	11.90	0.0599	20,123
0.040	0.281	11.90	0.0636	18,952
0.040	0.313	11.90	0.0663	18,179
0.040	0.237	14.13	0.0568	21,221
0.040	0.281	14.13	0.0599	20,123
0.040	0.313	14.13	0.0622	19,379
0.040	0.237	16.16	0.0547	22,036
0.040	0.281	16.16	0.0574	21,000
0.040	0.313	16.16	0.0594	20,291
0.05	0.237	11.9	0.0699	17,194
0.05	0.281	11.9	0.0736	16,355
0.05	0.313	11.9	0.0763	15,737
0.071	0.237	11.90	0.0909	13,260
0.071	0.281	11.90	0.0946	12,741
0.071	0.313	11.90	0.0973	12,388
0.071	0.237	14.13	0.0876	13,728
0.071	0.281	14.13	0.0909	13,260
0.071	0.313	14.13	0.0932	12,933
0.071	0.237	16.16	0.0857	14,064
0.071	0.281	16.16	0.0884	13,635
0.071	0.313	16.16	0.0904	13,334
0.1	0.237	16.16	0.1147	10,509

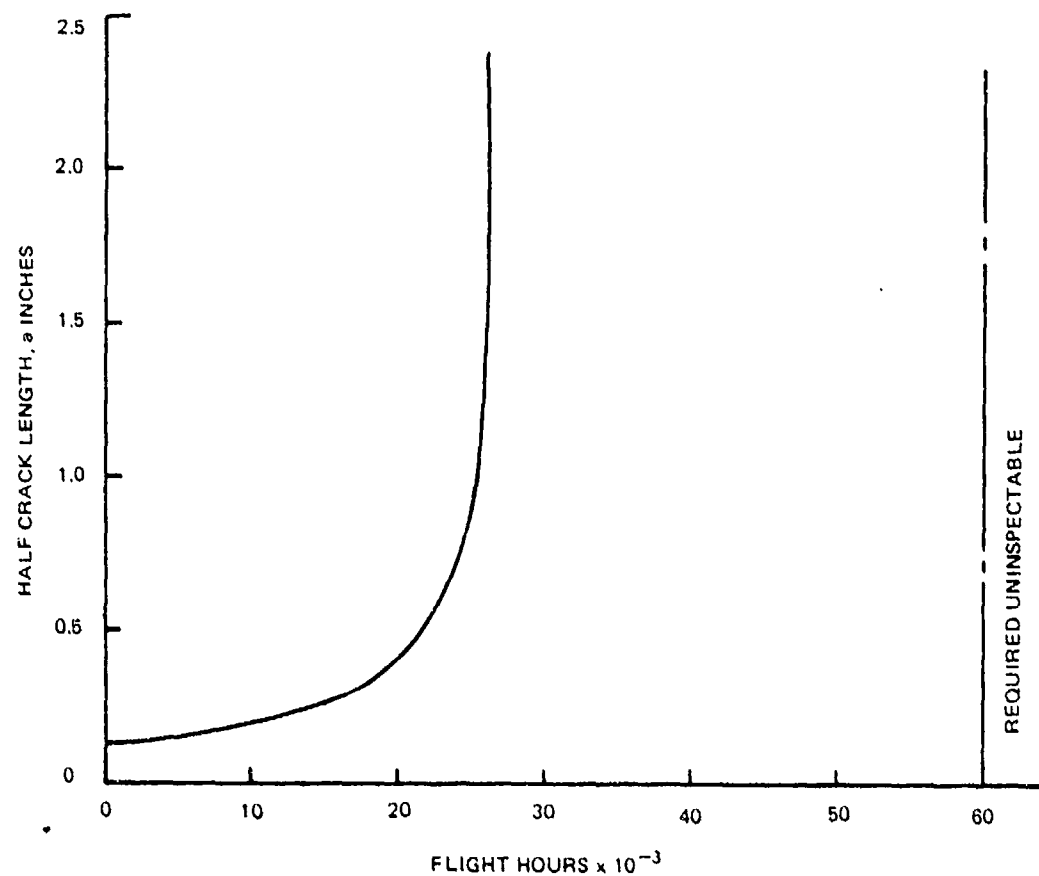


FIGURE 109. CRACK GROWTH TIME HISTORY FOR  $A = 0.237$ ,  $t = 0.04$ , SPACING = 16.16

Figure 112 shows a plot of spectra initial stress value versus life for all of the geometry combinations analyzed. The results fall on a single curve; i.e., the life is a function of initial stress which in turn is a function of smeared thickness,  $\bar{t}$ . Future sensitivity studies can be simplified by analyzing only enough geometries to describe the curve provided that cases are chosen which fall on both sides of the required life. Attempts were made in this study to predict the initial stress, and therefore the geometry, that would just meet the required life. Data on one side of the criteria value and the Forman equation for  $da/dN$  vs  $\Delta K$  were used without success. The accurate method is to read the required value from the curve and then perform a damage tolerance analysis of the corresponding geometry to verify the life and residual strength.

$A_{LONG} = 0.237$ , SPACING = 16.16-IN., SKIN THICKNESS = 0.040

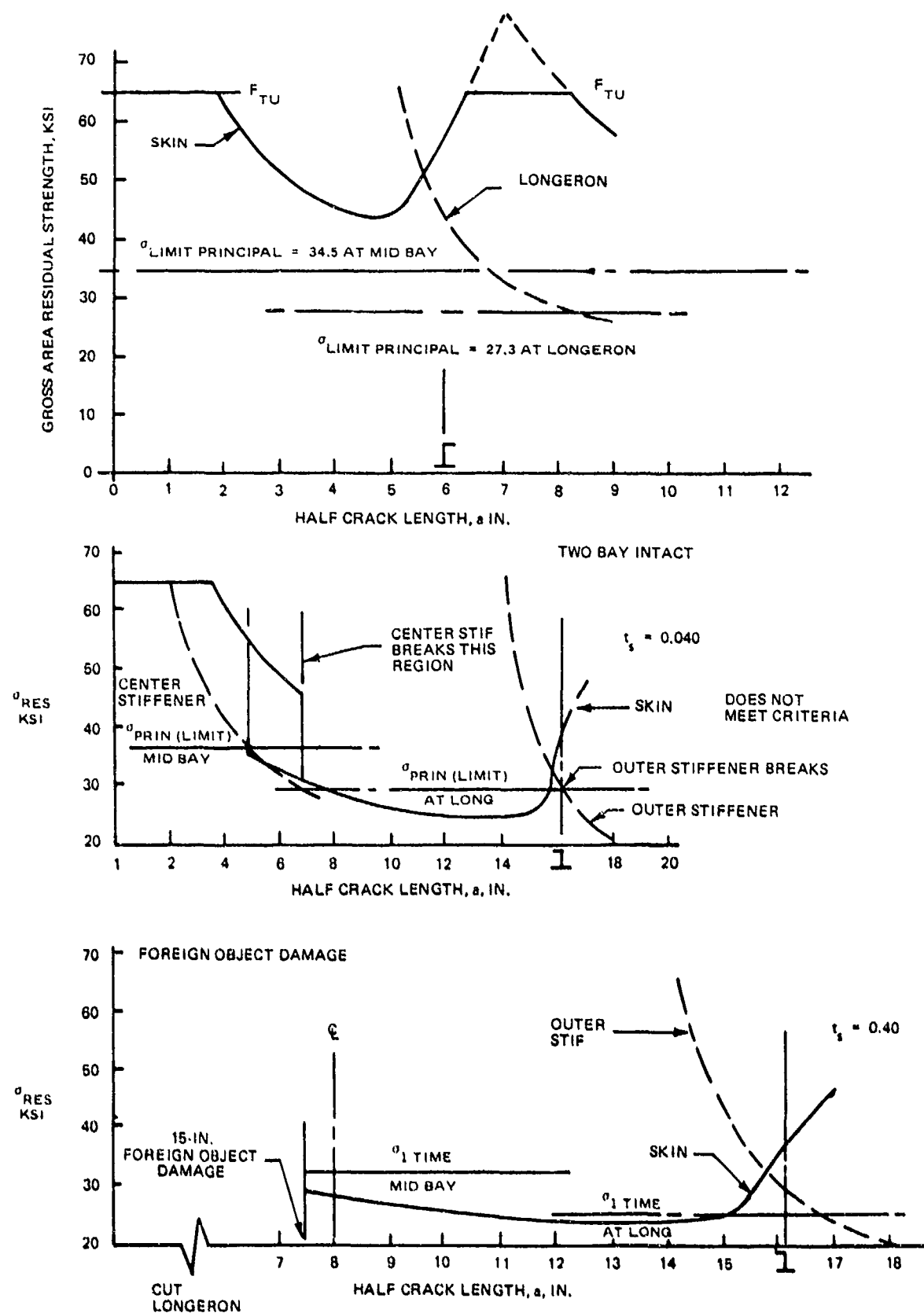
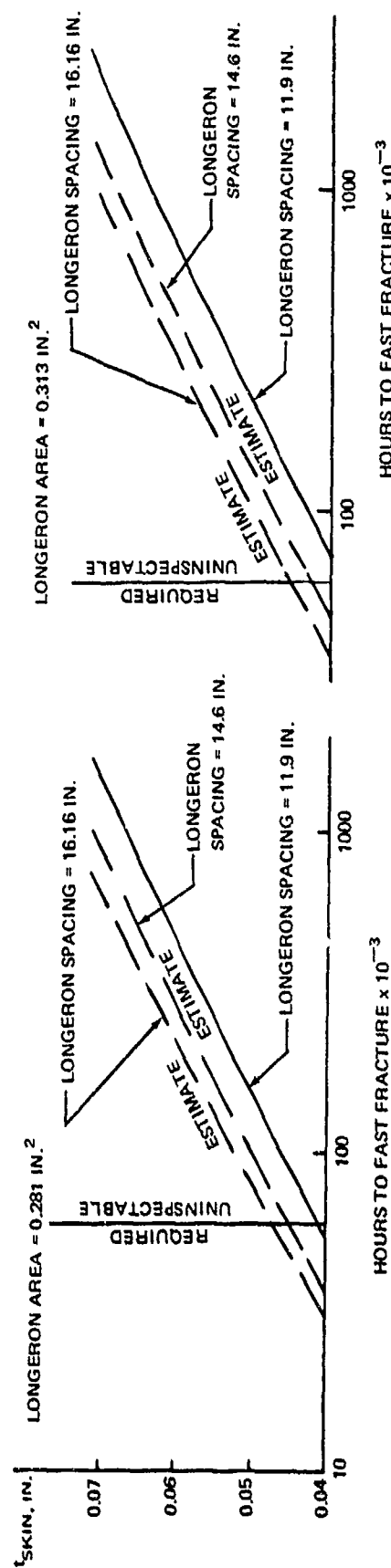


FIGURE 110. RESIDUAL STRENGTH FOR  $A = 0.237$ ,  $t = 0.04$ , SPACING = 16.16



SPECTRUM LOAD - PABST CHECK POINT B - CIRCUMFERENTIAL ONE-BAY CRACK  
LONGERON AREA = 0.237 IN.<sup>2</sup>

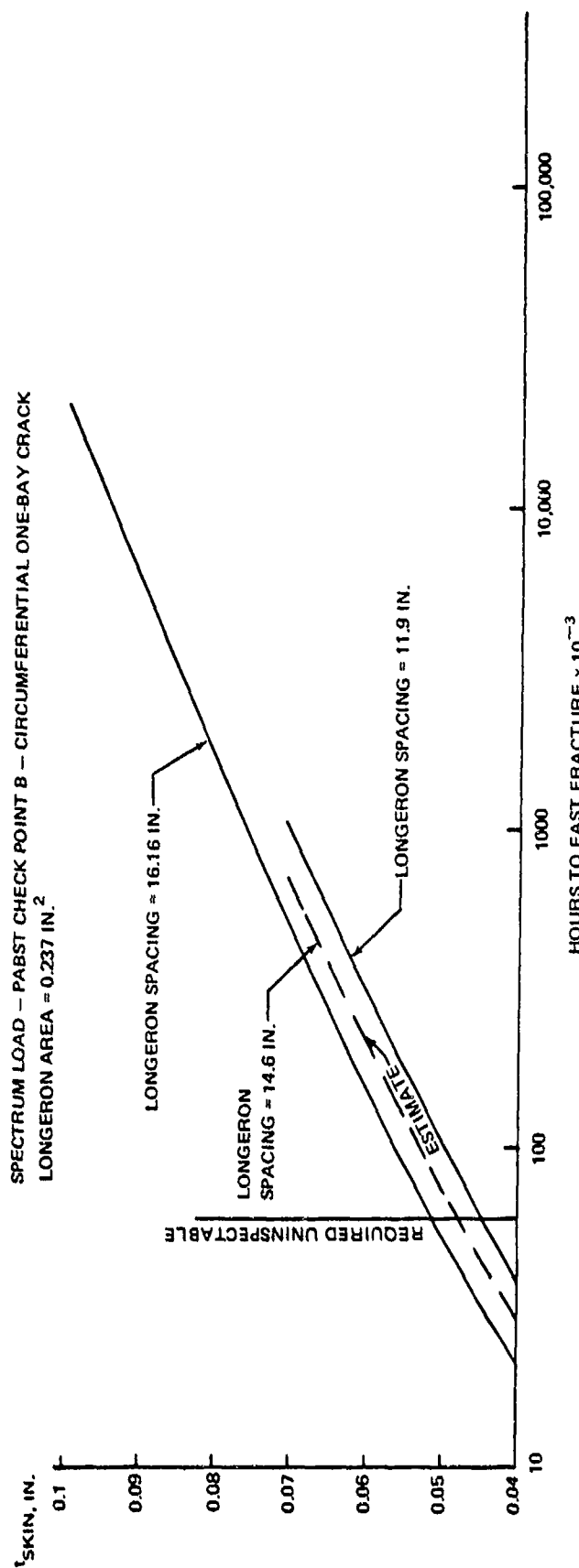


FIGURE 111. SUMMARY OF SENSITIVITY OF LIFE TO GEOMETRY VARIATION

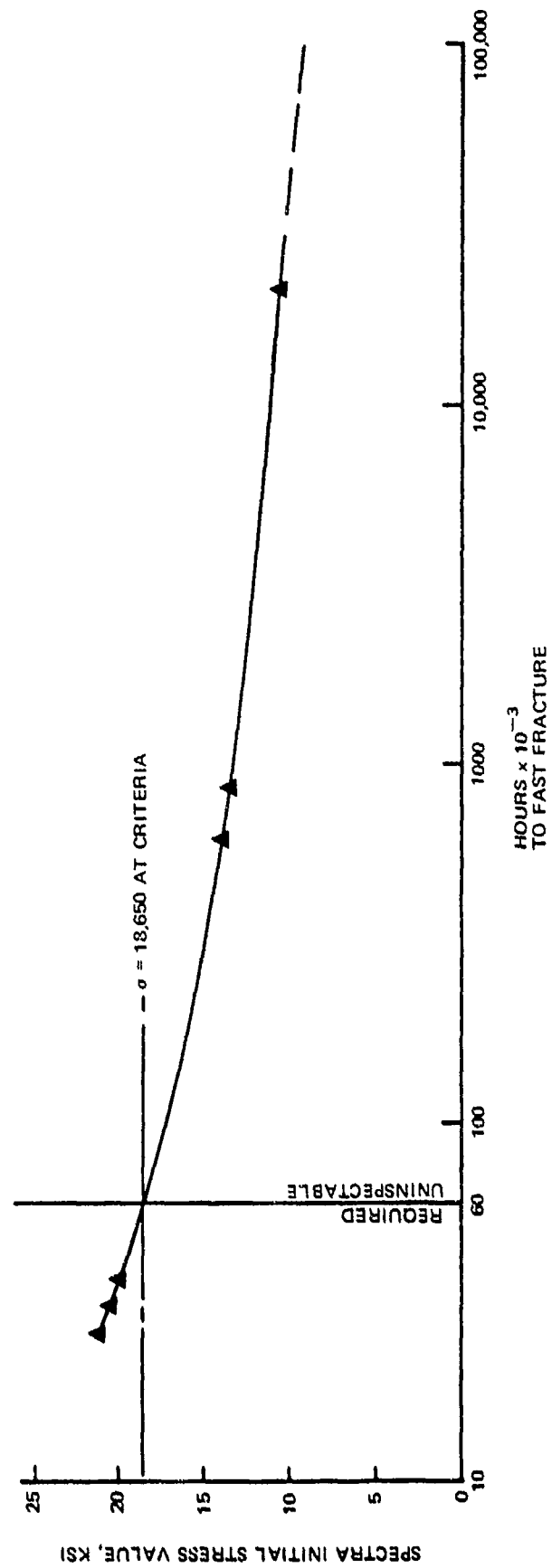


FIGURE 112. SPECTRA INITIAL STRESS VALUE VERSUS LIFE

Study #5 Effect of Variations in Crack Stopper Area and Spacing in the Wide Spaced Longeron Region. - The effect on life and residual strength of using 7475-T761 bare-sheet tear straps in the wide spaced longeron region, Figure 99 was studied by varying the strap area and spacing; i.e., increasing the number of straps considered from two to five. The geometries studied are summarized in Table 27. It can be seen that most straps were 3" x 0.071".

The criteria, analysis methods, spectra, and materials data are presented on pages 190 through 192. The tear straps were considered to have no effect on skin deflection; i.e., pillowing due to pressure, or on the skin shear stress. However, the strap areas were included in the principal ( $\sigma_{\text{prin.}}$ ) and one time ( $\sigma_{\text{O.T.}}$ ) stress calculations required by the design criteria. The first longeron below the fuselage centerline, Figure 99, was considered to be the center stiffener for residual strength and for foreign object damage analysis.

Figure 113 shows that at least two straps (26.3 inch spacing) are required for 0.213 square inch straps to meet the criteria for slow crack growth. The stress level in the skin decreases thus increasing the life as the number of straps increases.

The results of the residual strength analyses for the geometries studied are shown in Figures 114 through 120. The comparisons with the residual strength criteria are summarized in Table 27. The greatest residual strength improvement occurs from decreasing the spacing as can be seen from the results for one, two, three, four and five 0.213 area straps. The effect of an increase in strap area on residual strength is shown in Figures 118 and 119 for five straps and in Figure 120 for two straps. Increasing the strap area produced less improvement in residual strength than was achieved by decreasing the spacing. This was especially true for the case of two straps, Figure 120, where almost doubling the strap area produced an almost insignificant effect on the residual strength capability.

TABLE 27  
TEAR STRAP GEOMETRIES AND RESIDUAL STRENGTH RESULTS

NUMBER OF STRAPS	STRAP DIMENSIONS INCHES	STRAP AREA INCHES <sup>2</sup>	STRAP SPACING INCHES	DOES RESIDUAL STRENGTH MEET CRITERIA?		FIGURE NUMBER
				TWO BAY SKIN CRACK WITH CENTER STIFFENER INTACT	FOREIGN OBJECT DAMAGE - 15" SKIN CRACK WITH CENTER STIFFENER CUT	
1	3x0.071	0.213	39.4	NO	MARGINAL	114
2	↑	↑	26.3	NO	YES	115
3	↓	↓	19.7	MARGINAL	YES	116
4	↓	↓	15.76	YES	YES	117
5	3x0.071	0.213	13.16	YES	YES	118
5	2x0.071	0.142	13.16	YES	YES	119
2	3x0.080	0.240	26.3	NO	--	119
2	3x0.090	0.270	26.3	MARGINAL	--	119

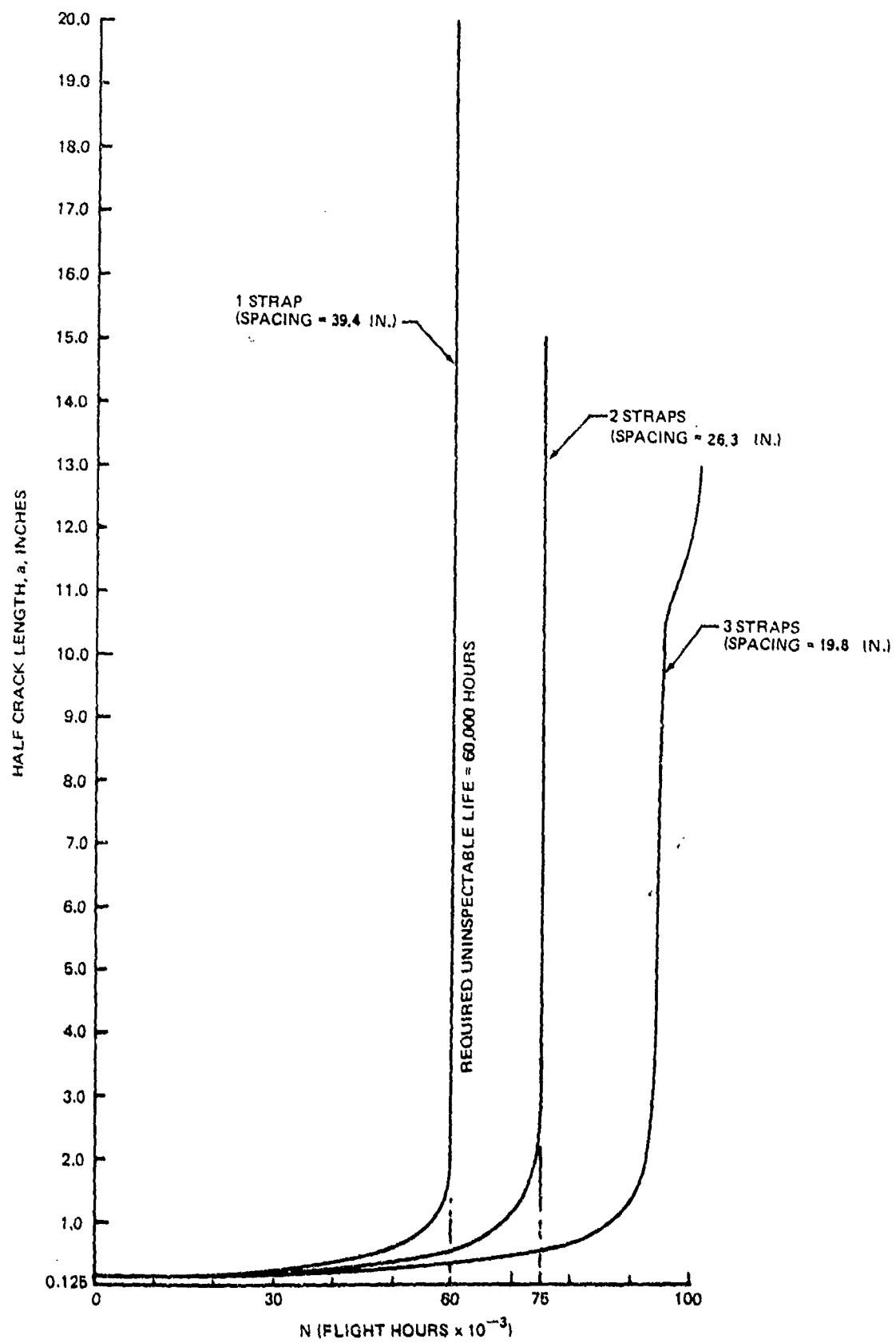


FIGURE 113. EFFECT ON LIFE OF VARYING TEAR STRAP SPACING FOR A 0.213-SQ-IN. STRAP

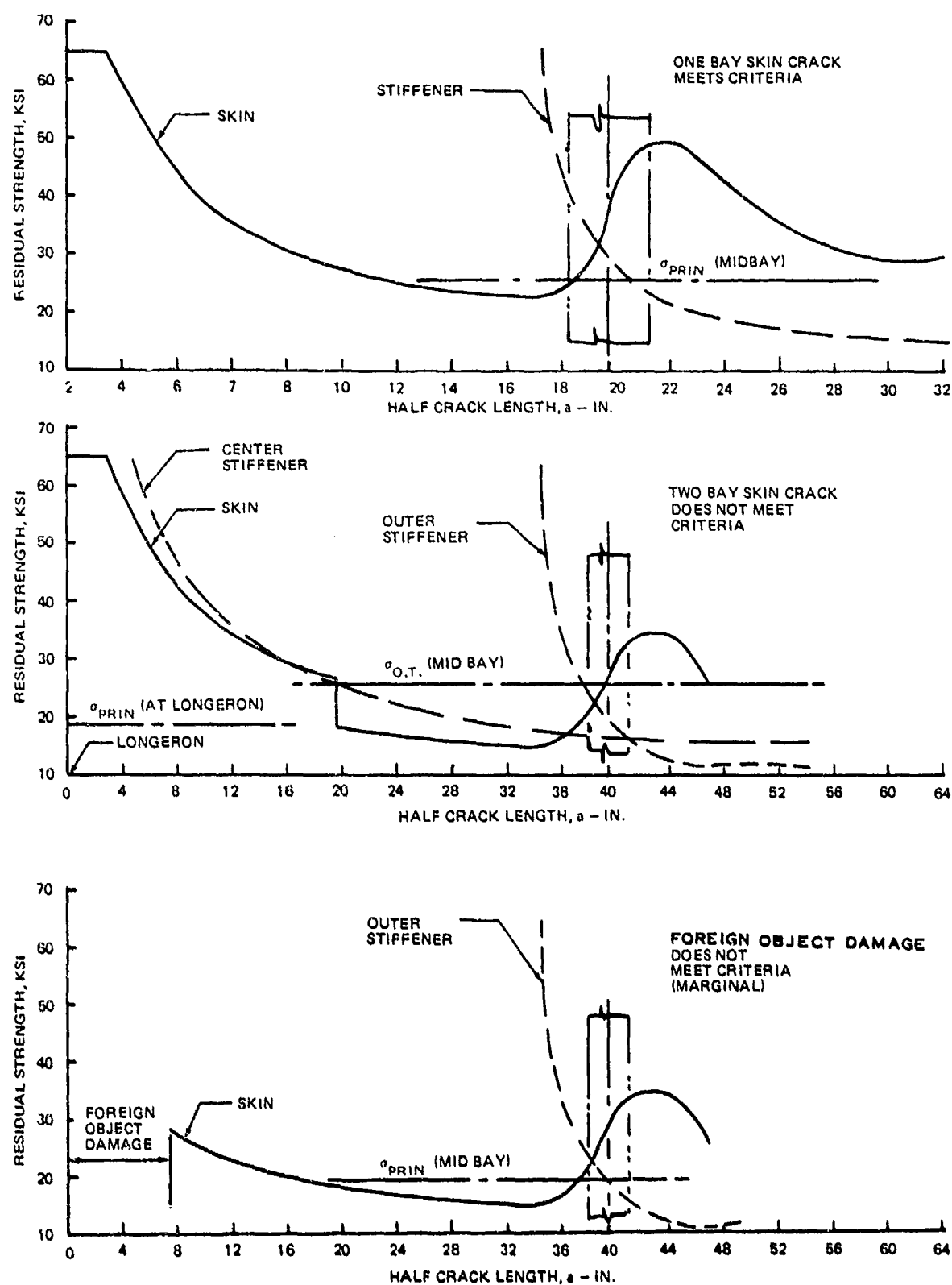


FIGURE 114. RESIDUAL STRENGTH FOR ONE STRAP WITH AREA = 0.213 SQ IN. AND 39.4 IN. SPACING

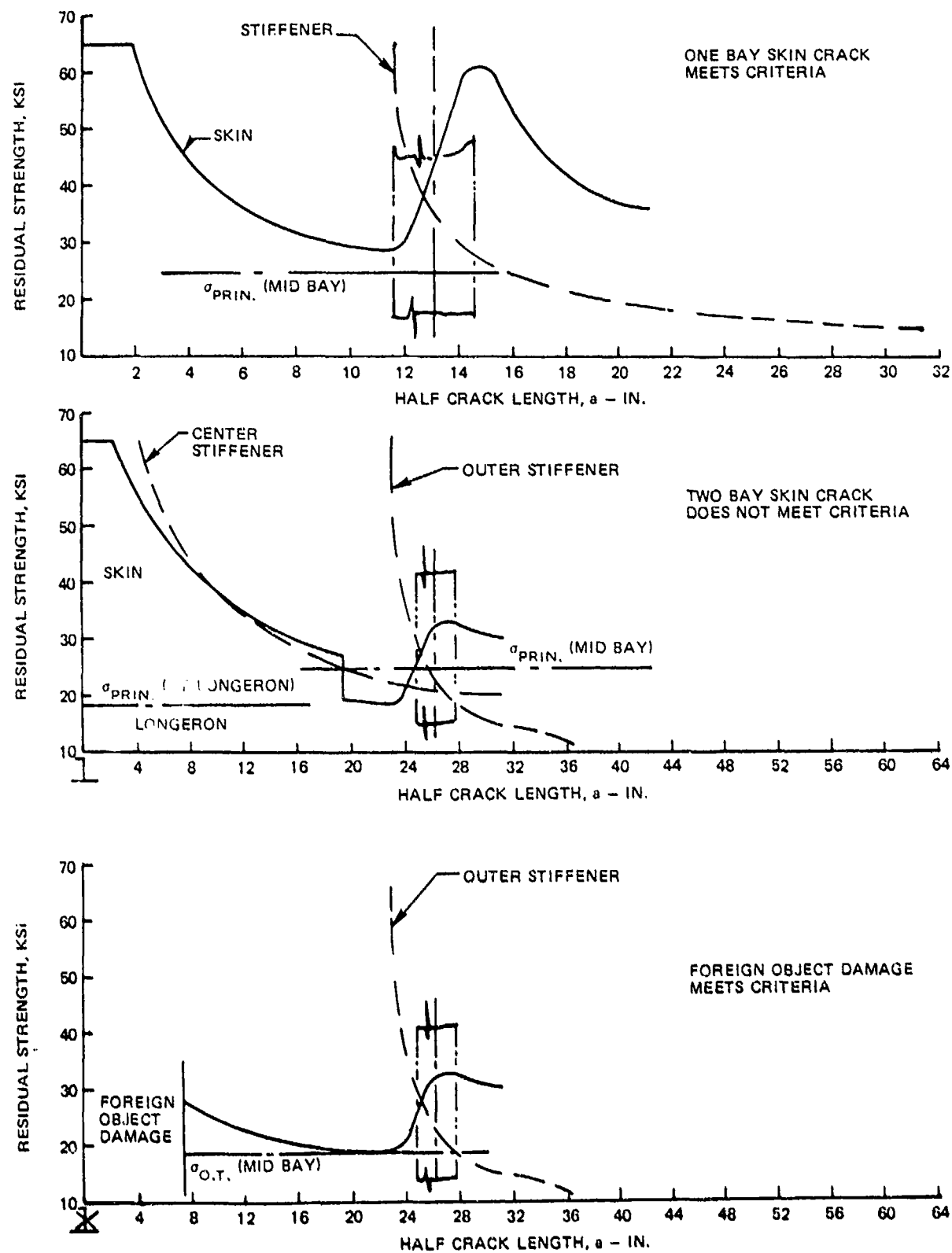


FIGURE 115. RESIDUAL STRENGTH FOR TWO STRAPS WITH AREA = 0.213 SQ IN. AND 26.3 IN. SPACING

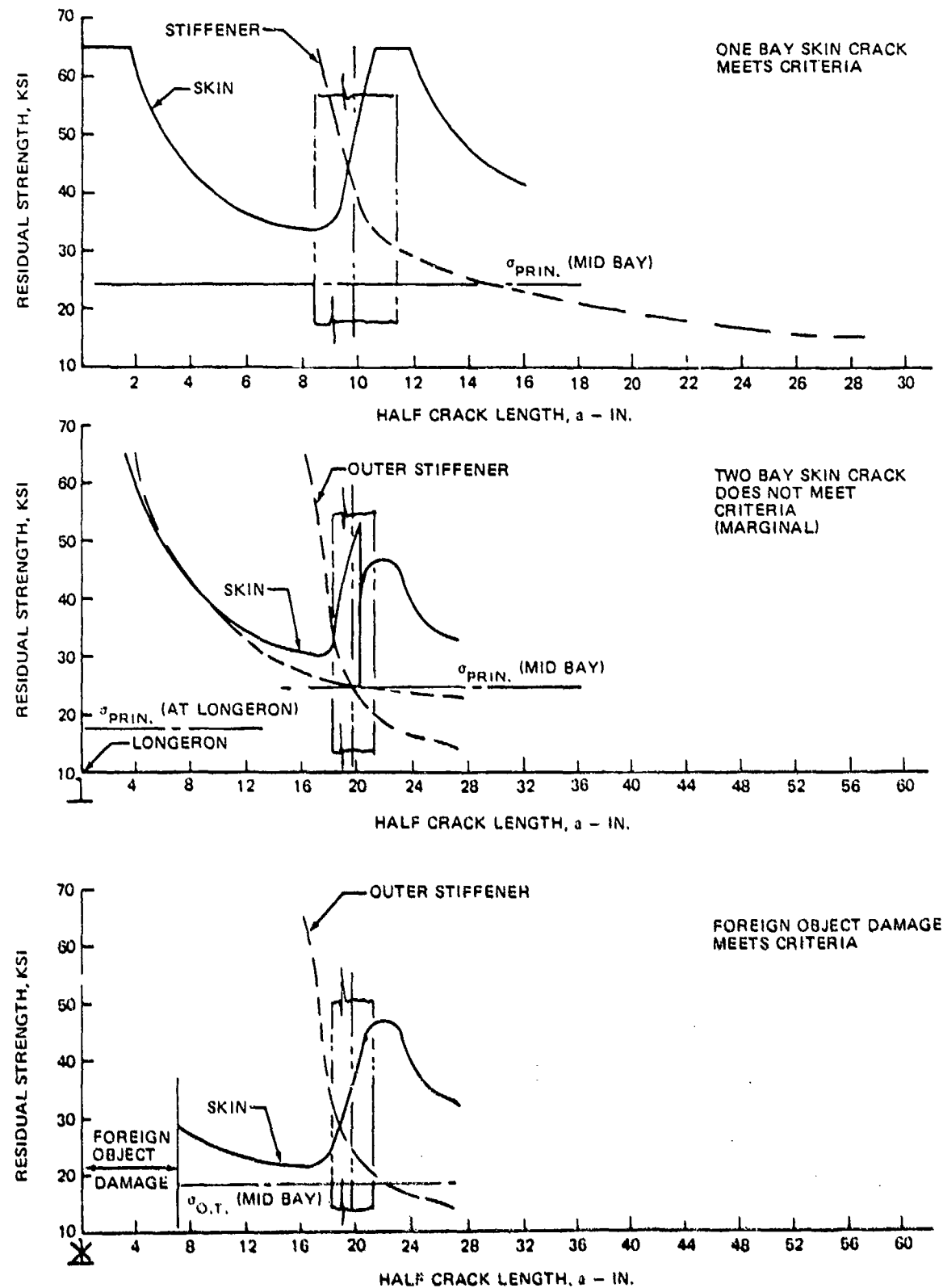


FIGURE 116. RESIDUAL STRENGTH FOR THREE STRAPS WITH AREA = 0.213 SQ IN. AND 19.7 IN. SPACING

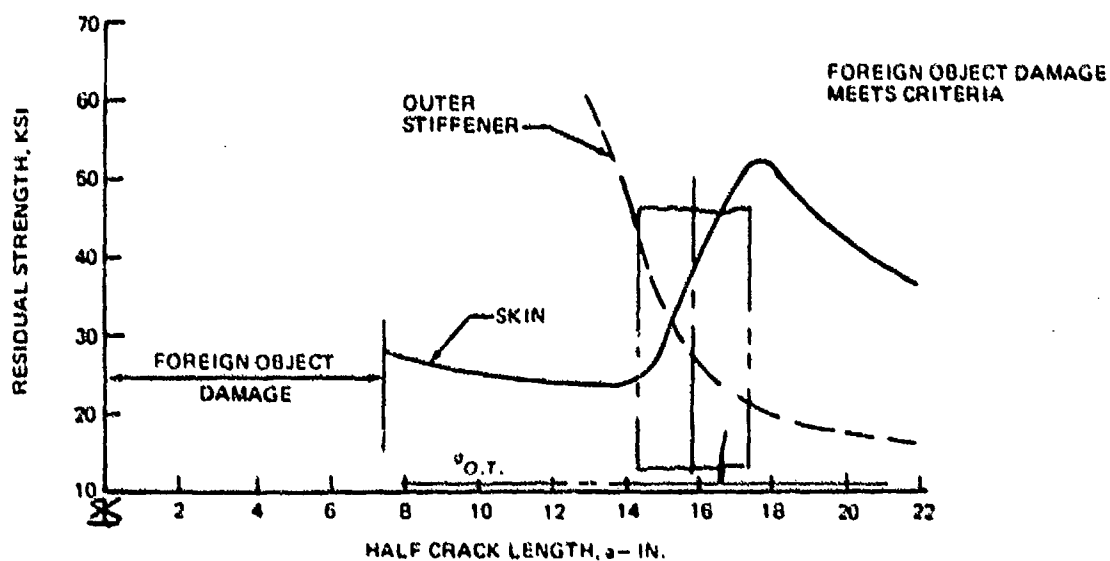
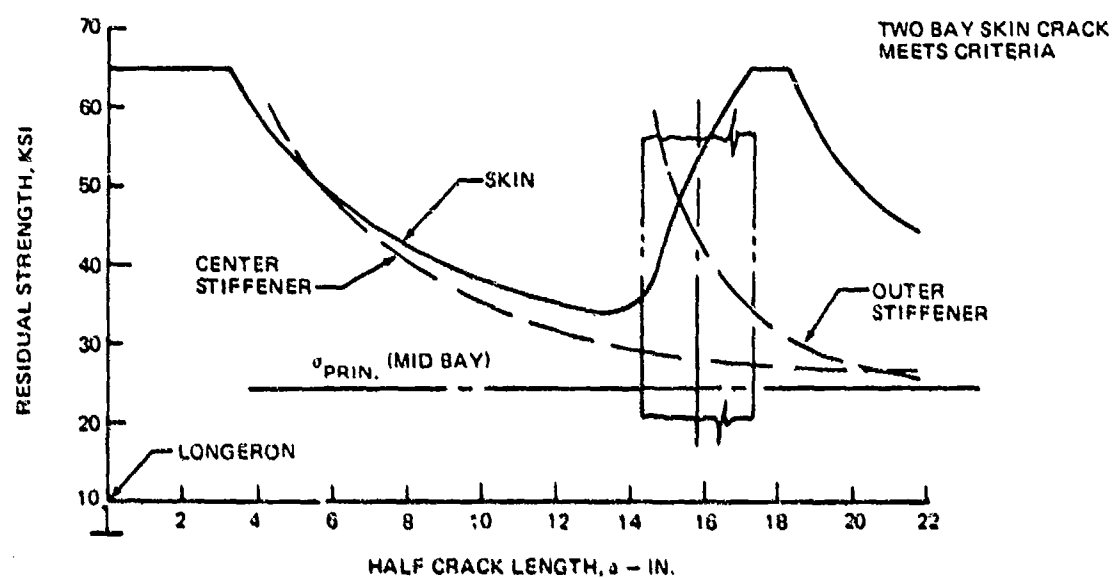
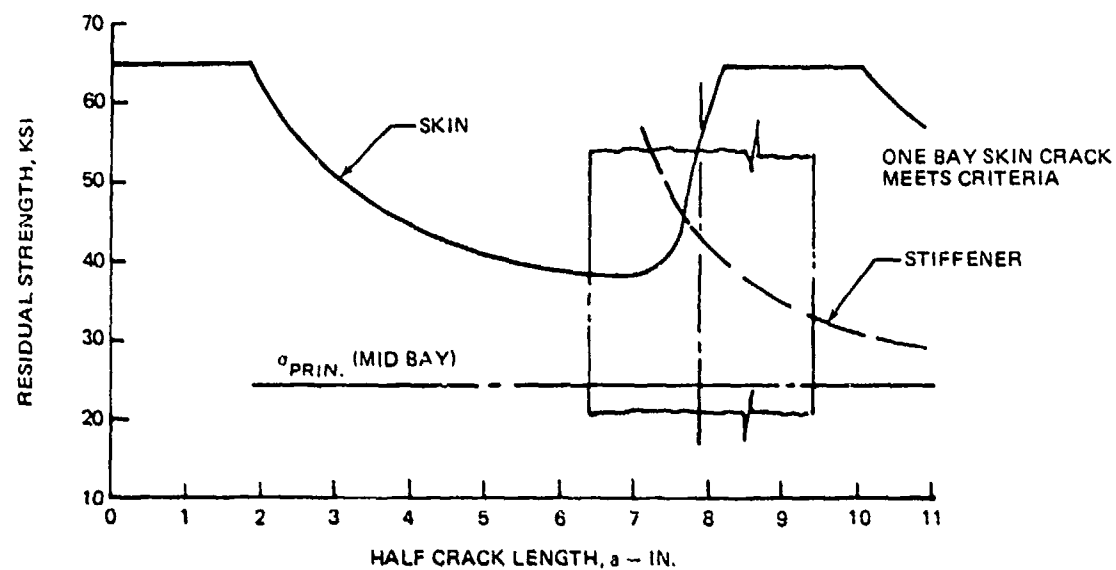


FIGURE 117. RESIDUAL STRENGTH FOR FOUR STRAPS WITH AREA = 0.213 SQ IN. AND 15.76 IN. SPACING

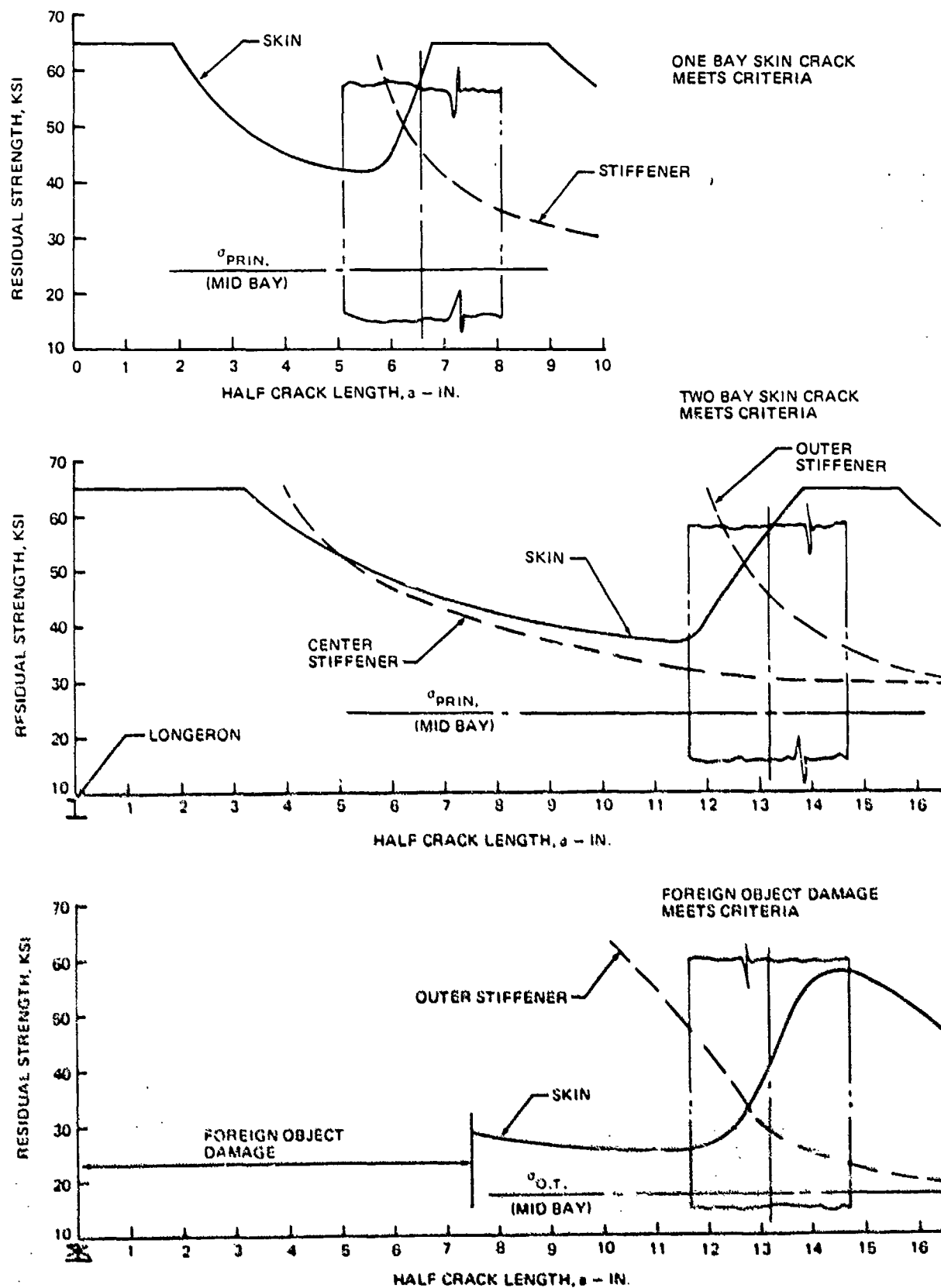


FIGURE 118. RESIDUAL STRENGTH FOR FIVE STRAPS WITH AREA = 0.213 SQ IN. AND 13.16 IN. SPACING.

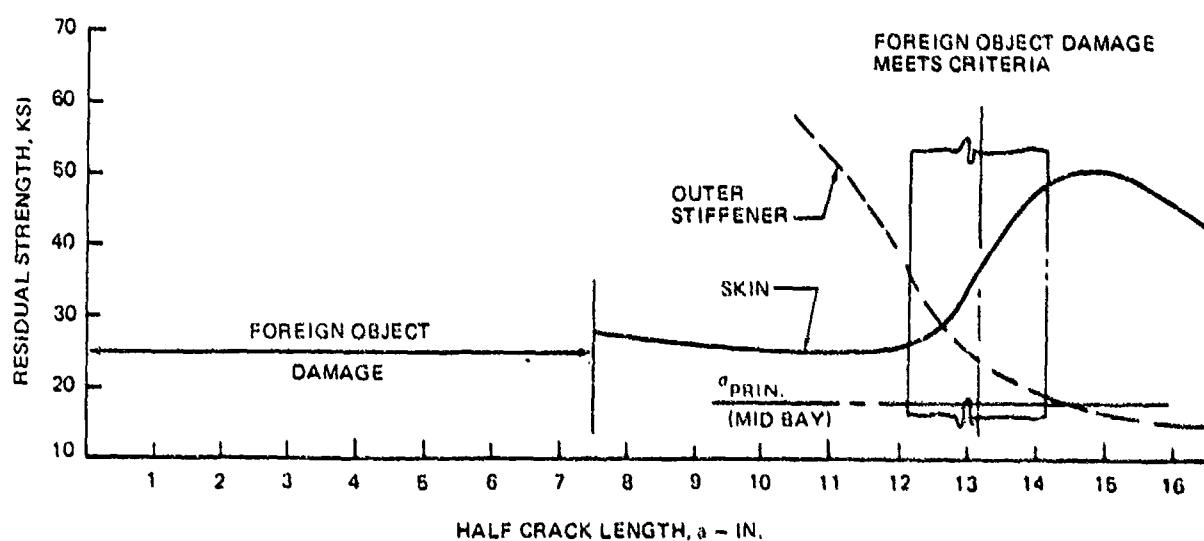
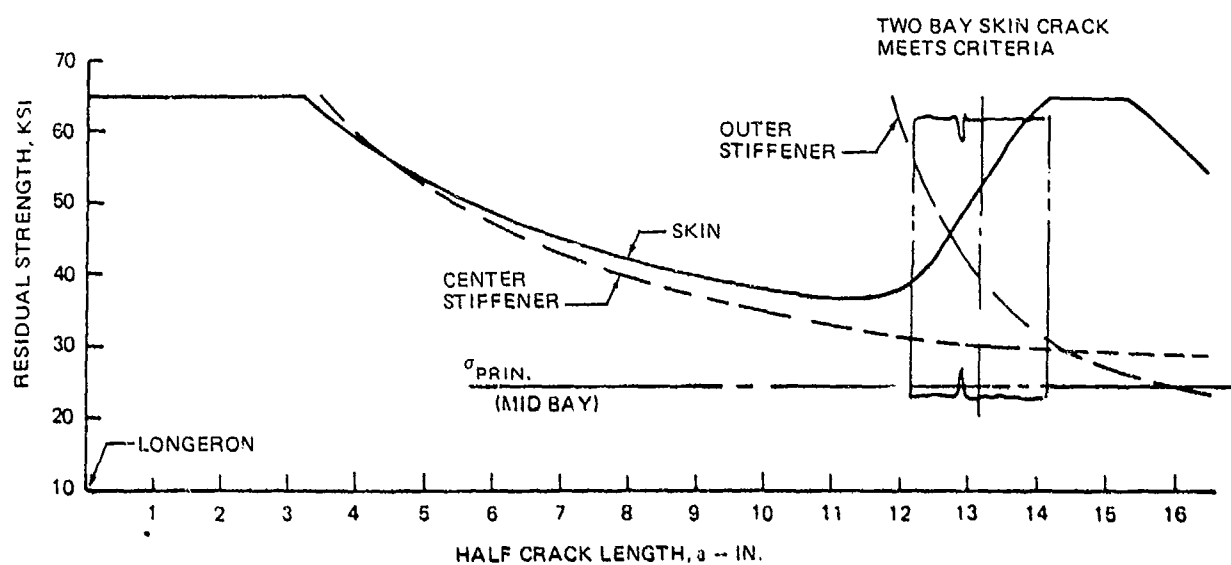
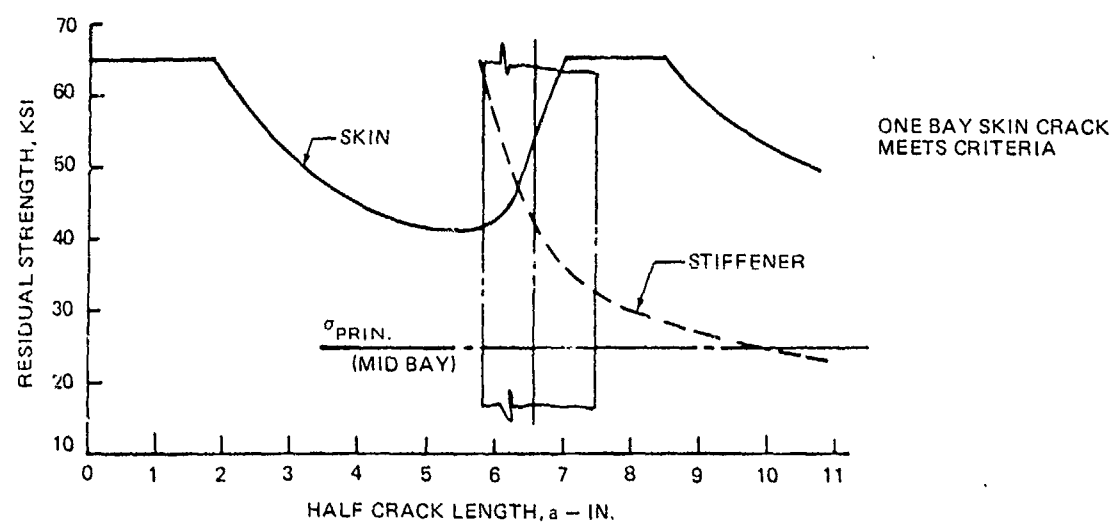


FIGURE 119. RESIDUAL STRENGTH FOR FIVE STRAPS WITH AREA = 0.142 SQ IN. AND 13.16-IN. SPACING

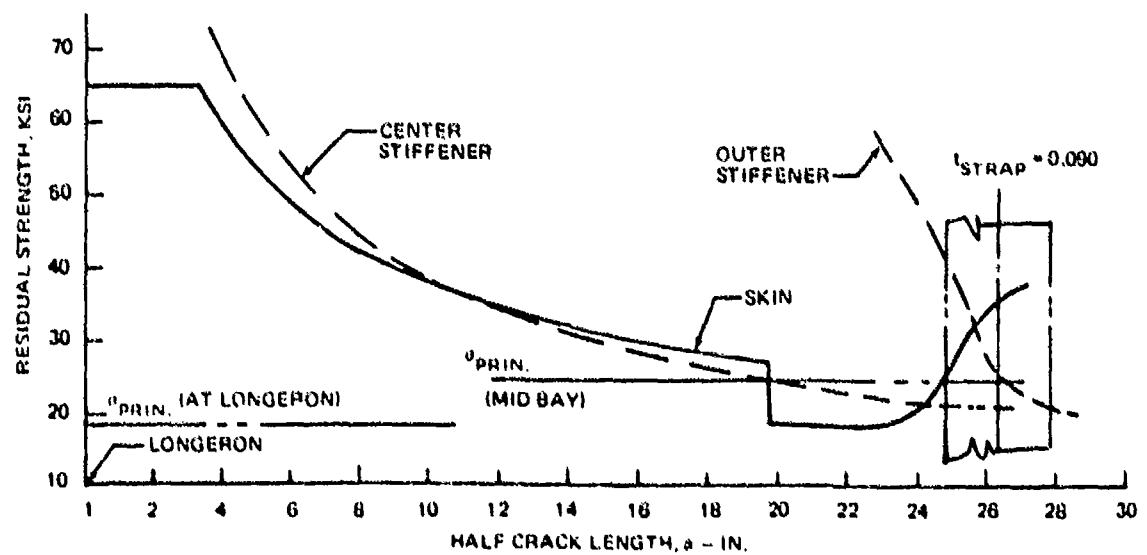
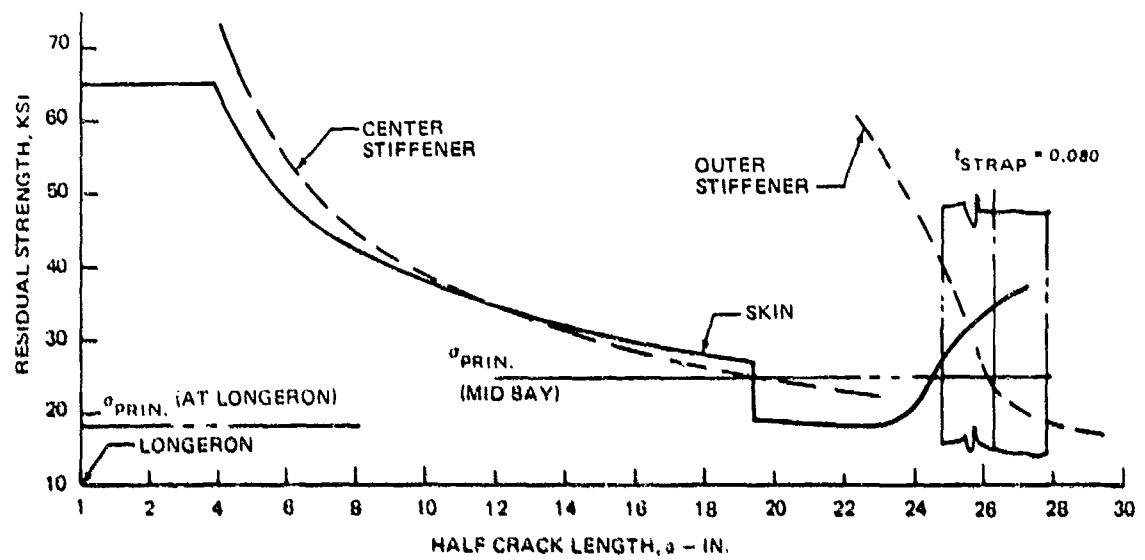
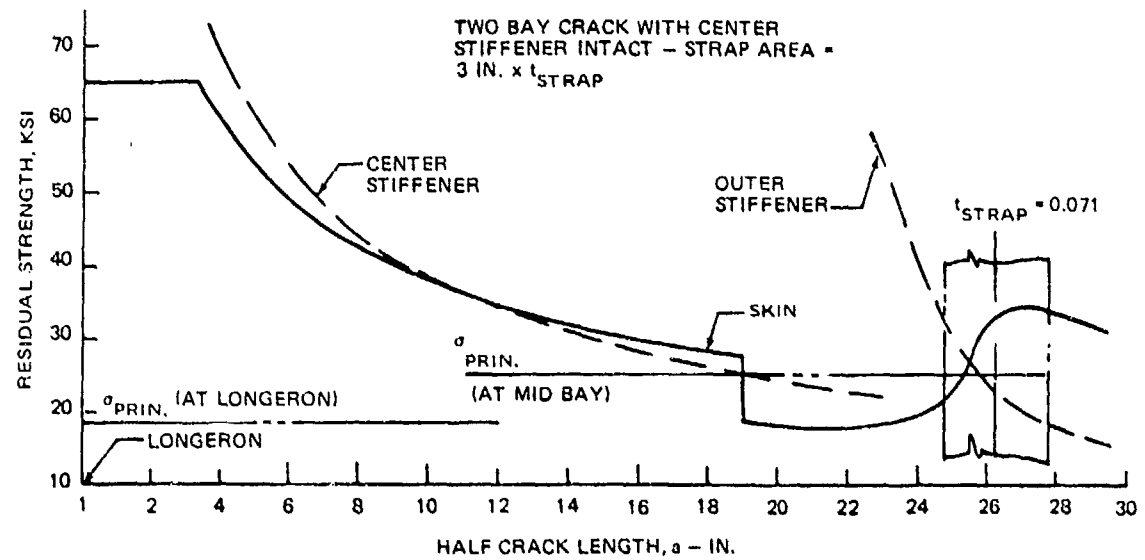


FIGURE 120. EFFECT OF STRAP AREA VARIATION ON RESIDUAL STRENGTH FOR TWO STRAPS

## SUMMARY

The Full Scale Demonstration Component is composed of a 42 foot long bonded fuselage simulating the forward section of the C-15, a domed pressure bulkhead and a strong back test support. This component combines and demonstrates the concepts of close spaced internal longerons, wide spaced internal longerons, and close spaced external longerons in the double contoured non-constant section nose as well as the circular constant section. Wing to fuselage interaction is also demonstrated by a simulated wing assembly.

The component is designed, based on the external loads applied at the nose pressure bulkhead, floor structure, and wing front spars, in addition to the internal pressurization loads. External loads were generated based on the C-15 design speeds, gross weights, cargo loading capability and payloads. Internal loads were generated using finite elements analysis techniques, and the margins of safety calculated using static test results.

The design criteria was based on: (1) the C-15 design weight and basic parameters applicable to PABST, (2) the applicable portions of the MIL-A-008860A series and MIL-A-83444 (USAF) specifications and of MIL-STD-1530 (USAF).

The FSDC was analyzed for damage tolerance requirements using the geometry at 14 critical points on the fuselage, which were selected on the basis of the phase 1b and preliminary phase 2 internal loads. Preliminary material property data were used. The critical points were checked for slow crack growth for phase 1b and preliminary phase 2 stress spectra. Retardation was included. In addition, the structure was checked for two fail safe conditions: (1) a two bay crack with central stiffener intact and (2) 15 inch foreign object damage with the center stiffener broken. Sensitivity studies were performed to study the effect on life prediction of variations in: (1) aircraft usage, (2) material property data, (3) initial flaw size, and (4) geometry in both the close spaced and wide spaced longeron regions.

The variable stress spectra were based on the atmospheric turbulence requirements of MIL-A-8861 specification and the flight maneuver, ground taxi and landing impact data of MIL-A-8867 specification. A separate gust plus maneuver turbulence spectrum was used for the low level, terrain following segments of the flight profiles.

The flight profile distribution was based on the projected C-15 utilization. This utilization requires a total 19,014 pressurizations per lifetime of each aircraft. Pressure loads form a very large proportion of the total stress and must be properly assessed. A stress spectrum for use in the damage tolerance analysis was derived for each of the 14 critical check points.

The analyses performed for adhesive-bonded joints include the elastic-plastic analysis of double-lap longitudinal splices, the geometrically non-linear analysis of single-lap bonded joints used to set the  $l/t$  ratio for the longitudinal mechanical splices, the pillowing of the pressurized skin restrained by the stiffeners from which it tries to peel off, and the geometrically non-linear single-strap (flush) circumferential splices. Some work was accomplished also for one-dimensional and two-dimensional defects. In addition to the analyses above for intact structure, a series of analysis methods was prepared to assess the residual strength of the adhesive bonds at discontinuities or cracks in the metal structure.

## CONCLUSIONS

During Phase II, the Full Scale Demonstration Component, a bonded large forward fuselage section of a STOL type aircraft, was designed. It will be fabricated in Phase III and tested in Phase IV. The design, analysis and component testing accomplished to date have indicated that there are no large pitfalls or surprises that would preclude the use of bonding for primary fuselage structure.

In addition, in Phase II a series of tests were conducted to determine the preconditioning, test environment, load rates and cycle that simulate "real life" conditions for bonded structure. These tests include wedge crack, lap shear, peel, thick adherend, double cantilever, neat adhesive and RAAB specimens. The data was used to verify the use of bonding for aircraft structure.

Three large component test specimens were designed during this phase. A bonded stiffened shear-compression panel was fabricated and a fatigue test in a room temperature - laboratory air environment started. An identical panel will be tested in a real environment in Phase III. In addition, a pressurized shell with a door representing a nose section will be fatigue tested in Phase III.

The Phase II, III, and IV test data will be reported in subsequent reports.

## APPENDIX A

The stress spectra for the damage tolerance parametric studies discussed in the Trade Studies Section are presented in this Appendix. Table A1 and A2 list the stress spectra for studies #2 and #4 and for studies #1, #3, and #5 respectively. The spectra variations used in study #1 are presented in Tables A3 through A6.

TABLE A1  
STRESS SPECTRA FOR STUDIES NO. 2 AND NO. 4

ONE SPECTRA REPRESENTS 1000 HOURS

	LOAD BLOCK	NUMBER OF CYCLES PER LOAD CYCLE	NUMBER OF CYCLES AT END OF BLOCK	SIGMA MAX	SIGMA MIN
GAG	1	241.	241.	18759.00	-2217.00
FLT	2	478.	719.	4500.00	3150.00
FLT	3	639.	1358.	6500.00	5850.00
FLT	4	5417.	6775.	9500.00	8550.00
FLT	5	440.	7215.	10500.00	9450.00
FLT	6	3545.	10760.	15500.00	13950.00
FLT	7	859.	11619.	16500.00	14850.00
FLT	8	3435.	15054.	19500.00	17550.00
GAG	9	32.	15086.	19912.00	-2313.00
FLT	10	6.	15092.	4500.00	3150.00
FLT	11	110.	15202.	5500.00	3850.00
FLT	12	14.	15216.	6500.00	4550.00
FLT	13	91.	15307.	7500.00	6750.00
FLT	14	11.	15318.	8500.00	5950.00
FLT	15	961.	16279.	10500.00	9450.00
FLT	16	276.	16555.	11500.00	10350.00
FLT	17	24.	16579.	12500.00	11250.00
FLT	18	3.	16582.	13500.00	9450.00
FLT	19	91.	16673.	17500.00	15750.00
FLT	20	240.	16913.	20500.00	18450.00
FLT	21	56.	16969.	21500.00	19350.00
FLT	22	5.	16974.	22500.00	20250.00
GAG	23	241.	17215.	18758.00	-2217.00
FLT	24	108.	17323.	3500.00	2450.00
FLT	25	808.	18131.	4500.00	3150.00
FLT	26	21.	18152.	550.00	2750.00
FLT	27	1681.	19833.	6500.00	5850.00
FLT	28	6.	19839.	7500.00	3750.00
FLT	29	5871.	25710.	9500.00	8550.00
FLT	30	487.	26197.	10500.00	9450.00
FLT	31	19.	26216.	11500.00	8050.00
FLT	32	1.	26217.	12500.00	8750.00
FLT	33	3262.	29479.	15500.00	13950.00
FLT	34	817.	30296.	16500.00	14850.00
FLT	35	17.	30313.	17500.00	15750.00
FLT	36	3946.	34259.	19500.00	17550.00
FLT	37	62.	34321.	20500.00	18450.00
FLT	38	8.	34329.	21500.00	19350.00
GAG	39	32.	34361.	19912.00	-2312.00
FLT	40	10.	34371.	4500.00	3150.00
FLT	41	97.	34458.	5500.00	3850.00
FLT	42	12.	34470.	6500.00	4550.00
FLT	43	88.	34558.	7500.00	6750.00
FLT	44	11.	34569.	8500.00	5950.00
FLT	45	661.	35230.	10500.00	9450.00
FLT	46	172.	35402.	11500.00	10350.00
FLT	47	13.	35415.	12500.00	11250.00
FLT	48	1.	35416.	13500.00	9450.00
FLT	49	79.	35495.	17500.00	15750.00
FLT	50	265.	35760.	20500.00	18450.00
FLT	51	57.	35817.	21500.00	19350.00
FLT	52	4.	35821.	22500.00	20250.00
GAG	53	41.	35862.	15325.00	-2217.00
FLT	54	7.	35869.	3500.00	2450.00
FLT	55	100.	35969.	4500.00	3150.00
FLT	56	2.	35971.	5500.00	2750.00
FLT	57	121.	36092.	6500.00	5850.00
FLT	58	1283.	37375.	9500.00	8550.00
FLT	59	93.	37468.	10500.00	9450.00
FLT	60	5.	37473.	11500.00	8050.00

TABLE A1 (CONTINUED)  
STRESS SPECTRA FOR STUDIES NO. 2 AND NO. 4

	LOAD BLOCK	NUMBER OF CYCLES PER LOAD CYCLE	NUMBER OF CYCLES AT END OF BLOCK	SIGMA MAX	SIGMA MIN
FLT	61	38.	37511.	13500.00	12150.00
FLT	62	4.	37515.	14500.00	13050.00
FLT	63	1333.	38849.	15500.00	13950.00
FLT	64	546.	39394.	16500.00	14850.00
FLT	65	15.	39409.	17500.00	15750.00
GAG	66	3.	39412.	16479.00	-2313.00
FLT	67	46.	39458.	5500.00	4950.00
FLT	68	12.	39470.	6500.00	5850.00
FLT	69	9.	39479.	7500.00	6750.00
FLT	70	1.	39480.	8500.00	7650.00
FLT	71	49.	39529.	10500.00	9450.00
FLT	72	15.	39544.	11500.00	10350.00
FLT	73	1.	39545.	12500.00	11250.00
FLT	74	3.	39548.	15500.00	13950.00
FLT	75	87.	39635.	17500.00	15750.00
FLT	76	8.	39643.	18500.00	16650.00
FLT	77	1.	39644.	19500.00	17550.00
GAG	78	41.	39685.	11551.00	-2217.00
FLT	79	148.	39833.	500.00	450.00
FLT	80	1002.	40835.	3500.00	3150.00
FLT	81	154.	40989.	8500.00	7650.00
FLT	82	4.	40993.	9500.00	6650.00
FLT	83	2149.	43142.	12500.00	11250.00
FLT	84	54.	43196.	13500.00	12150.00
FLT	85	5.	43201.	14500.00	13050.00
GAG	86	3.	43204.	12226.00	-2313.00
FLT	87	1.	43205.	4500.00	3150.00
FLT	88	43.	43248.	5500.00	4950.00
FLT	89	11.	43259.	6500.00	5850.00
FLT	90	31.	43290.	7500.00	6750.00
FLT	91	9.	43299.	8500.00	7650.00
FLT	92	1.	43300.	9500.00	6650.00
FLT	93	10.	43310.	10500.00	9450.00
FLT	94	1.	43311.	11500.00	8050.00
FLT	95	96.	43407.	12500.00	11250.00
FLT	96	37.	43444.	13500.00	12150.00
FLT	97	3.	43447.	14500.00	13050.00
GAG	98	241.	43688.	2500.00	-2217.00
FLT	99	30102.	73790.	3500.00	2450.00
FLT	100	1187.	74977.	4500.00	1350.00
GAG	101	41.	75018.	2500.00	-2217.00
FLT	102	184804.	259822.	3500.00	2450.00
FLT	103	7286.	267108.	4500.00	1350.00
GAG	104	3.	267111.	-2432.00	-2313.00
GAG	105	50.	267161.	1764.00	-2397.00
FLT	106	88000.	355161.	2500.00	750.00
FLT	107	26000.	381161.	3500.00	350.00
GAG	108	50.	381211.	3404.00	-3150.00
FLT	109	114057.	495268.	4500.00	3150.00
GLT	110	14307.	509575.	5500.00	1650.00
FLT	111	1301.	510876.	6500.00	650.00

TABLE A2  
STRESS SPECTRA FOR STUDIES NO. 1, NO. 3, AND NO. 5

ONE SPECTRA REPRESENTS 333.3 HOURS

	LOAD BLOCK	NUMBER OF CYCLES PER LOAD CYCLE	NUMBER OF CYCLES AT END OF BLOCK	SIGMA MAX	SIGMA MIN
F1GAG	1	80.	80.	14237.00	263.00
G+M	2	1280.	1360.	12604.00	12516.00
G+M	3	160.	1520.	12634.00	12486.00
G+M	4	1120.	2640.	12604.00	12560.00
G+M	5	400.	3040.	12634.00	12560.00
G+M	6	160.	3200.	12663.00	12560.00
G+M	7	640.	3840.	14207.00	14119.00
G+M	8	80.	3920.	14237.00	14089.00
F2GAG	9	11.	3931.	14797.00	441.00
G+M	10	176.	4107.	13132.00	12550.00
G+M	11	22.	4129.	13193.00	12489.00
G+M	12	154.	4281.	13132.00	13041.00
G+M	13	55.	4338.	13193.00	13041.00
G+M	14	22.	4360.	13254.00	13041.00
G+M	15	55.	4415.	14736.00	14554.00
G+M	16	11.	4426.	14797.00	14493.00
G+M	17	22.	4448.	14736.00	14645.00
G+M	18	11.	4459.	14797.00	14645.00
F3GAG	19	80.	4539.	14237.00	263.00
G+M	20	1200.	5739.	12603.00	12515.00
G+M	21	160.	5899.	12603.00	12485.00
G+M	22	1120.	7019.	12603.00	12559.00
G+M	23	400.	7419.	12633.00	12559.00
G+M	24	120.	7539.	12662.00	12559.00
G+M	25	80.	7619.	12692.00	12559.00
G+M	26	720.	8339.	14207.00	14119.00
G+M	27	80.	8419.	14237.00	14119.00
F4GAG	28	11.	8430.	14541.00	441.00
G+M	29	132.	8562.	12897.00	12775.00
G+M	30	22.	8584.	12937.00	12735.00
G+M	31	98.	8672.	12897.00	12836.00
G+M	32	33.	8705.	12937.00	12836.00
G+M	33	11.	8716.	12977.00	12836.00
G+M	34	66.	8782.	14501.00	14379.00
G+M	35	11.	8793.	14541.00	14339.00
F5GAG	36	14.	8807.	12662.00	263.00
G+M	37	56.	8863.	10559.00	10511.00
G+M	38	28.	8891.	12603.00	12515.00
G+M	39	420.	9311.	12603.00	12559.00
G+M	40	126.	9437.	12662.00	12559.00
G+M	41	42.	9479.	12692.00	12559.00
G+M	42	14.	9493.	12721.00	12559.00
F6GAG	43	11.	9494.	11311.00	441.00
G+M	44	23.	9517.	11128.00	11037.00
G+M	45	6.	9523.	11189.00	11037.00
G+M	46	2.	9525.	11250.00	11037.00
G+M	47	1.	9526.	11311.00	11037.00
F7GAG	48	14.	9540.	8683.00	263.00
G+M	49	70.	9610.	6589.00	6501.00
G+M	50	14.	9624.	6619.00	6471.00
G+M	51	196.	9820.	6589.00	6545.00
G+M	52	56.	9876.	6619.00	6545.00
G+M	53	14.	9890.	6648.00	6545.00
G+M	54	42.	9932.	8554.00	8506.00
G+M	55	490.	10422.	8594.00	8550.00
G+M	56	154.	10576.	8624.00	8550.00
G+M	57	42.	10618.	8653.00	8550.00
G+M	58	14.	10632.	8683.00	8550.00

TABLE A2 (CONTINUED)  
STRESS SPECTRA FOR STUDIES NO. 1, 3 AND NO. 5

	LOAD BLOCK	NUMBER OF CYCLES PER LOAD CYCLE	NUMBER OF CYCLES AT END OF BLOCK	SIGMA MAX	SIGMA MIN
F8GAG	59	1.	10633.	9306.00	536.00
F8G+M	60	5.	10638.	7118.00	6936.00
G+M	61	1.	10639.	7179.00	6875.00
G+M	62	17.	10656.	7110.00	7027.00
G+M	63	4.	10660.	7179.00	7027.00
G+M	64	1.	10661.	7240.00	7027.00
G+M	65	2.	10663.	9123.00	8941.00
G+M	66	30.	10693.	9123.00	9032.00
G+M	67	9.	10702.	9184.00	9032.00
G+M	68	3.	10705.	9245.00	9032.00
G+M	69	1.	10706.	9306.00	9032.00
F9GAG	70	80.	10786.	2645.00	263.00
F0GAG	71	82.	10868.	2645.00	88.00
F1GAG	72	5.	10873.	2645.00	343.00
F2GAG	73	17.	10890.	2645.00	168.00
F3GAG	74	17.	10907.	2645.00	593.00

TABLE A3

## STRESS SPECTRA WITH UTILIZATION 2 FOR STUDY NO. 1

ONE SPECTRA REPRESENTS 333.3 HOURS

	LOAD BLOCK	NUMBER OF CYCLES PER LOAD CYCLE	NUMBER OF CYCLES AT END OF BLOCK	SIGMA MAX	SIGMA MIN
F1GAG	1	91.	91.	14237.00	263.00
TAX-I	2	2469.	2560.	788.00	380.00
TAX-I	3	366.	2926.	847.00	321.00
TAX-I	4	91.	3017.	905.00	263.00
G+M	5	183.	3200.	1978.00	1890.00
G+M	6	183.	3383.	3582.00	3494.00
G+M	7	274.	3657.	5589.00	6501.00
G+M	8	1463.	5120.	12604.00	12516.00
G+M	9	183.	5303.	12634.00	12486.00
G+M	10	1280.	6583.	12604.00	12560.00
G+M	11	457.	7040.	12634.00	12560.00
G+M	12	183.	7223.	12663.00	12560.00
G+M	13	731.	7954.	14237.00	14119.00
G+M	14	91.	8045.	14237.00	14089.00
F2GAG	15	13.	8058.	14757.00	441.00
G+M	16	50.	8108.	2507.00	2325.00
G+M	17	38.	8146.	4111.00	3929.00
G+M	18	38.	8184.	7113.00	6936.00
G+M	19	201.	8285.	13132.00	12950.00
G+M	20	25.	8410.	13153.00	12899.00
G+M	21	176.	8536.	13132.00	13041.00
G+M	22	63.	8649.	13153.00	13041.00
G+M	23	25.	8674.	13254.00	13041.00
G+M	24	63.	8737.	14736.00	14554.00
G+M	25	13.	8750.	14757.00	14453.00
G+M	26	25.	8775.	14736.00	14645.00
G+M	27	13.	8783.	14757.00	14645.00
TAX-I	28	339.	9127.	1322.00	636.00
TAX-I	29	50.	9177.	1423.00	538.00
TAX-I	30	13.	9190.	1517.00	441.00
F3GAG	31	91.	9281.	14237.00	263.00
TAX-I	32	2469.	11750.	788.00	380.00
TAX-I	33	366.	12116.	847.00	321.00
TAX-I	34	91.	12207.	905.00	263.00
G+M	35	274.	12481.	1978.00	1890.00
G+M	36	549.	13030.	3582.00	3494.00
G+M	37	91.	13121.	3612.00	3464.00
G+M	38	274.	13305.	6589.00	6501.00
G+M	39	91.	13486.	6619.00	6471.00
G+M	40	1371.	14657.	12603.00	12515.00
G+M	41	183.	15040.	12633.00	12485.00
G+M	42	1280.	16320.	12603.00	12559.00
G+M	43	457.	16777.	12633.00	12559.00
G+M	44	137.	16914.	12662.00	12559.00
G+M	45	91.	17005.	12692.00	12559.00
G+M	46	823.	17828.	14207.00	14119.00
G+M	47	91.	17919.	14237.00	14119.00
F4GAG	48	13.	17932.	14541.00	441.00
TAX-I	49	339.	18271.	1322.00	636.00
TAX-I	50	50.	18321.	1423.00	538.00
TAX-I	51	13.	18334.	1517.00	441.00
G+M	52	38.	18372.	2272.00	2150.00
G+M	53	38.	18410.	3876.00	3754.00
G+M	54	50.	18460.	6843.00	6761.00
G+M	55	151.	18611.	12847.00	12775.00
G+M	56	25.	18636.	12937.00	12735.00
G+M	57	100.	18736.	12897.00	12836.00
G+M	58	38.	18774.	12937.00	12836.00
G+M	59	13.	18787.	12977.00	12836.00
G+M	60	75.	18862.	14501.00	14179.00
G+M	61	13.	18875.	14541.00	14339.00
F5GAG	62	14.	18889.	12692.00	263.00
TAX-I	63	378.	19267.	788.00	380.00
TAX-I	64	56.	19323.	847.00	321.00
TAX-I	65	14.	19337.	905.00	263.00

TABLE A3 (CONTINUED)

## STRESS SPECTRA WITH UTILIZATION 2 FOR STUDY NO. 1

	LOAD BLOCK	NUMBER OF CYCLES PER LOAD CYCLE	NUMBER OF CYCLES AT END OF BLOCK	SIGMA MAX	SIGMA MIN
G+M	66	28.	15365.	1578.00	1390.00
G+M	67	42.	19407.	3582.00	3494.00
G+M	68	42.	19449.	6589.00	6501.00
G+M	69	280.	19729.	6589.00	6545.00
G+M	70	70.	19759.	6619.00	6545.00
G+M	71	28.	19827.	6648.00	6545.00
G+M	72	56.	19883.	10559.00	10511.00
G+M	73	28.	19911.	12603.00	12515.00
G+M	74	420.	20331.	12603.00	12559.00
G+M	75	126.	20457.	12662.00	12559.00
G+M	76	42.	20499.	12692.00	12559.00
G+M	77	14.	20513.	12721.00	12559.00
F6GAG	78	1.	20514.	11311.00	441.00
TAXI	79	27.	20541.	1322.00	635.00
TAXI	80	4.	20545.	1420.00	538.00
TAXI	81	1.	20546.	1517.00	441.00
G+M	82	3.	20549.	2507.00	2325.00
G+M	83	3.	20552.	4111.00	3929.00
G+M	84	7.	20559.	7118.00	6936.00
G+M	85	1.	20560.	7179.00	6875.00
G+M	86	23.	20583.	11129.00	11037.00
G+M	87	6.	20589.	11189.00	11037.00
G+M	88	2.	20591.	11250.00	11037.00
G+M	89	1.	20592.	11311.00	11037.00
F7GAG	90	14.	20606.	2683.00	263.00
TAXI	91	378.	20984.	788.00	380.00
TAXI	92	56.	21040.	847.00	321.00
TAXI	93	14.	21054.	905.00	263.00
G+M	94	42.	21096.	1578.00	1890.00
G+M	95	42.	21138.	3582.00	3494.00
G+M	96	14.	21152.	6619.00	6471.00
G+M	97	196.	21348.	6591.00	6545.00
G+M	98	56.	21404.	6619.00	6545.00
G+M	99	14.	21418.	6648.00	6545.00
G+M	100	42.	21460.	8594.00	8506.00
G+M	101	490.	21950.	8554.00	8550.00
G+M	102	154.	22104.	8624.00	8550.00
G+M	103	42.	22146.	8653.00	8550.00
G+M	104	14.	22160.	8693.00	8550.00
F8GAG	105	1.	22161.	9306.00	836.00
TAXI	106	4.	22165.	1322.00	636.00
G+M	107	3.	22168.	2507.00	2325.00
G+M	108	3.	22171.	4111.00	3929.00
G+M	109	5.	22176.	7118.00	6936.00
G+M	110	1.	22177.	7179.00	6875.00
G+M	111	17.	22194.	7118.00	7027.00
G+M	112	4.	22198.	7179.00	7027.00
G+M	113	1.	22199.	7240.00	7027.00
G+M	114	2.	22201.	9123.00	8941.00
G+M	115	30.	22231.	9123.00	9032.00
G+M	116	9.	22240.	9184.00	9032.00
G+M	117	3.	22243.	9245.00	9032.00
G+M	118	1.	22244.	9306.00	9032.00
F9GAG	119	91.	22535.	2645.00	263.00
TAXI	120	4572.	26907.	718.00	380.00
TAXI	121	823.	27730.	847.00	321.00
TAXI	122	91.	27821.	905.00	263.00
G+M	123	8046.	35867.	976.00	888.00
G+M	124	2377.	38244.	1006.00	858.00
G+M	125	777.	39071.	1035.00	829.00
G+M	126	366.	39387.	1045.00	799.00
G+M	127	91.	39478.	1094.00	770.00
F0GAG	128	82.	39560.	2645.00	89.00

TABLE A3 (CONTINUED)

## STRESS SPECTRA WITH UTILIZATION 2 FOR STUDY NO. 1

	LOAD BLOCK	NUMBER OF CYCLES PER LOAD CYCLE	NUMBER OF CYCLES AT END OF BLOCK	SIGMA MAX	SIGMA MIN
TAXI	129	61008.	100568.	788.00	380.00
TAXI	130	45182.	145750.	847.00	321.00
TAXI	131	16400.	162150.	905.00	263.00
TAXI	132	4346.	166496.	964.00	204.00
TAXI	133	738.	167234.	1022.00	146.00
TAXI	134	82.	167316.	1094.00	88.00
G+M	135	259776.	427092.	576.00	888.00
G+M	135	76752.	503844.	1006.00	858.00
G+M	137	31694.	535742.	1035.00	829.00
G+M	138	10332.	546074.	1065.00	799.00
G+M	139	3854.	549928.	1094.00	770.00
G+M	140	328.	550256.	1124.00	740.00
G+M	141	574.	550830.	1151.00	711.00
G+M	142	246.	551076.	1183.00	681.00
G+M	143	246.	551322.	1245.00	2243.00
FIGAG	144	5.	551327.	2645.00	343.00
TAXI	145	1250.	552577.	1322.00	636.00
TAXI	146	215.	552792.	1420.00	538.00
TAXI	147	35.	552927.	1517.00	441.00
TAXI	148	5.	552932.	1615.00	343.00
G+M	149	13370.	566162.	1505.00	1323.00
G+M	150	3940.	570102.	1566.00	1262.00
G+M	151	1635.	571737.	1627.00	1201.00
G+M	152	530.	572267.	1688.00	1140.00
G+M	153	195.	572462.	1749.00	1079.00
G+M	154	20.	572482.	1810.00	1018.00
G+M	155	30.	572512.	1871.00	957.00
G+M	156	15.	572527.	1932.00	896.00
G+M	157	10.	572537.	2645.00	2248.00
F2GAG	158	9.	572546.	2645.00	168.00
TAXI	159	1615.	574161.	906.00	436.00
TAXI	160	1173.	575334.	973.00	369.00
TAXI	161	425.	575759.	1040.00	302.00
TAXI	162	17.	575776.	1174.00	168.00
G+M	163	14960.	590736.	1252.00	1141.00
G+M	164	4420.	595156.	1294.00	1068.00
G+M	165	1836.	596992.	1344.00	1022.00
G+M	166	595.	597587.	1390.00	976.00
G+M	167	221.	597808.	1435.00	931.00
G+M	168	17.	597825.	1491.00	885.00
G+M	169	34.	597859.	1527.00	839.00
G+M	170	17.	597876.	1573.00	793.00
G+M	171	9.	597885.	2645.00	1984.00
F3GAG	172	9.	597894.	2645.00	591.00
TAXI	173	85.	597979.	1455.00	701.00
TAXI	174	9.	597989.	1561.00	593.00
G+M	175	14969.	612457.	1594.00	1668.00
G+M	176	4420.	617377.	2111.00	1557.00
G+M	177	1836.	619213.	2219.00	1447.00
G+M	178	595.	619808.	2327.00	1337.00
G+M	179	221.	620029.	2440.00	1226.00
G+M	180	17.	620045.	2550.00	1116.00
G+M	181	34.	620080.	2661.00	1006.00
G+M	182	17.	620097.	2771.00	865.00
G+M	183	17.	620114.	2645.00	2248.00

TABLE A4

## STRESS SPECTRA WITH UTILIZATION 3 FOR STUDY NO. 1

ONE SPECTRA REPRESENTS 333.3 HOURS

	LOAD BLOCK	NUMBER OF CYCLES PER LOAD CYCLE	NUMBER OF CYCLES AT END OF BLOCK	SIGMA MAX	SIGMA MIN
F1GAG	1	69.	69.	14237.00	263.00
TAXI	2	1854.	1923.	789.00	380.00
TAXI	3	275.	2198.	847.00	321.00
TAXI	4	69.	2267.	905.00	263.00
G+M	5	137.	2404.	1970.00	1890.00
G+M	6	137.	2541.	3582.00	3494.00
G+M	7	206.	2747.	6599.00	6501.00
G+M	8	1000.	3846.	12604.00	12516.00
G+M	9	137.	3983.	12634.00	12486.00
G+M	10	961.	4044.	12604.00	12560.00
G+M	11	343.	5287.	12634.00	12560.00
G+M	12	137.	5424.	12663.00	12560.00
G+M	13	549.	5973.	14207.00	14119.00
G+M	14	69.	6042.	14237.00	14089.00
F2GAG	15	0.	6051.	14797.00	441.00
G+M	16	38.	6089.	2507.00	2325.00
G+M	17	28.	6117.	4111.00	3529.00
G+M	18	28.	6145.	7118.00	6936.00
G+M	19	151.	6296.	13132.00	12950.00
G+M	20	19.	6315.	13193.00	12889.00
G+M	21	132.	6447.	13132.00	13041.00
G+M	22	47.	6494.	13153.00	13041.00
G+M	23	19.	6513.	13254.00	13041.00
G+M	24	47.	6560.	14736.00	14554.00
G+M	25	9.	6569.	14757.00	14493.00
G+M	26	19.	6599.	14736.00	14645.00
G+M	27	0.	6597.	14797.00	14645.00
TAXI	28	254.	6851.	1322.00	636.00
TAXI	29	38.	6889.	1420.00	538.00
TAXI	30	0.	6898.	1517.00	441.00
F3GAG	31	69.	6967.	14237.00	263.00
TAXI	32	1854.	8821.	789.00	380.00
TAXI	33	275.	9096.	847.00	321.00
TAXI	34	69.	9165.	905.00	263.00
G+M	35	206.	9371.	1970.00	1890.00
G+M	36	412.	9783.	3582.00	3494.00
G+M	37	69.	9852.	3612.00	3466.00
G+M	38	206.	10058.	6599.00	6501.00
G+M	39	69.	10127.	6619.00	6471.00
G+M	40	1030.	11157.	12603.00	12516.00
G+M	41	137.	11294.	12633.00	12485.00
G+M	42	961.	12255.	12603.00	12559.00
G+M	43	343.	12598.	12633.00	12559.00
G+M	44	103.	12701.	12662.00	12559.00
G+M	45	69.	12770.	12652.00	12559.00
G+M	46	618.	13382.	14207.00	14119.00
G+M	47	69.	13457.	14237.00	14119.00
F4GAG	48	0.	13466.	14541.00	441.00
TAXI	49	259.	13725.	1322.00	636.00
TAXI	50	38.	13763.	1420.00	538.00
TAXI	51	0.	13772.	1517.00	441.00
G+M	52	28.	13800.	2272.00	2150.00
G+M	53	28.	13828.	3174.00	2754.00
G+M	54	38.	13861.	6393.00	6761.00
G+M	55	113.	13979.	12957.00	12775.00
G+M	56	19.	13998.	12937.00	12735.00
G+M	57	75.	14073.	12897.00	12436.00
G+M	58	28.	14101.	12937.00	12836.00
G+M	59	0.	14110.	12977.00	12836.00
G+M	60	56.	14166.	14501.00	14379.00
G+M	61	9.	14175.	14541.00	14379.00
F5GAG	62	14.	14189.	12652.00	263.00

TABLE A4 (CONTINUED)

## STRESS SPECTRA WITH UTILIZATION 3 FOR STUDY NO. 1

	LOAD BLOCK	NUMBER OF CYCLES PER LOAD CYCLE	NUMBER OF CYCLES AT END OF BLOCK	SIGMA MAX	SIGMA MIN
TAXI	63	378.	14567.	783.00	380.00
TAXI	64	56.	14623.	847.00	321.00
TAXI	65	14.	14637.	905.00	263.00
G+M	66	28.	14665.	1978.00	1890.00
G+M	67	42.	14707.	3582.00	3494.00
G+M	68	42.	14749.	6589.00	6501.00
G+M	69	280.	15029.	6589.00	6545.00
G+M	70	70.	15069.	6619.00	6545.00
G+M	71	28.	15127.	6648.00	6545.00
G+M	72	56.	15183.	10559.00	10511.00
G+M	73	28.	15211.	12603.00	12519.00
G+M	74	420.	15631.	12603.00	12559.00
G+M	75	126.	15757.	12662.00	12559.00
G+M	76	42.	15799.	12652.00	12539.00
G+M	77	19.	15818.	12721.00	12559.00
F6GAG	78	1.	15819.	11311.00	441.00
TAXI	79	27.	15846.	1322.00	636.00
TAXI	80	4.	15850.	1420.00	533.00
TAXI	81	1.	15851.	1517.00	441.00
G+M	82	3.	15854.	2507.00	2325.00
G+M	83	3.	15857.	4111.00	3929.00
G+M	84	7.	15864.	7113.00	6936.00
G+M	85	1.	15865.	7179.00	6875.00
G+M	86	23.	15888.	11128.00	11037.00
G+M	87	6.	15894.	11189.00	11037.00
G+M	88	2.	15896.	11250.00	11037.00
G+M	89	1.	15897.	11311.00	11037.00
F7GAG	90	14.	15911.	8683.00	263.00
TAXI	91	378.	16289.	788.00	380.00
TAXI	92	56.	16345.	847.00	321.00
TAXI	93	14.	16359.	905.00	263.00
G+M	94	42.	16401.	1978.00	1890.00
G+M	95	42.	16443.	3582.00	3494.00
G+M	96	14.	16457.	6619.00	6471.00
G+M	97	196.	16653.	6599.00	6545.00
G+M	98	56.	16709.	6619.00	6545.00
G+M	99	14.	16723.	6643.00	6545.00
G+M	100	42.	16765.	8554.00	8506.00
G+M	101	490.	17255.	8594.00	8550.00
G+M	102	154.	17409.	8624.00	8550.00
G+M	103	42.	17451.	8653.00	8550.00
G+M	104	14.	17465.	8683.00	8550.00
F8GAG	105	1.	17466.	9306.00	636.00
TAXI	106	4.	17470.	1322.00	636.00
G+M	107	3.	17473.	2507.00	2325.00
G+M	108	3.	17476.	4111.00	3929.00
G+M	109	5.	17481.	7118.00	6936.00
G+M	110	1.	17482.	7179.00	6875.00
G+M	111	17.	17499.	7119.00	7027.00
G+M	112	4.	17503.	7179.00	7027.00
G+M	113	1.	17504.	7240.00	7027.00
G+M	114	2.	17506.	9123.00	8941.00
G+M	115	30.	17536.	9123.00	9032.00
G+M	116	9.	17545.	9184.00	9032.00
G+M	117	3.	17548.	9245.00	9032.00
G+M	118	1.	17549.	9306.00	9032.00
F9GAG	119	91.	17640.	2645.00	263.00
TAXI	120	4572.	22212.	788.00	380.00
TAXI	121	823.	23035.	847.00	321.00
TAXI	122	91.	23126.	905.00	263.00
G+M	123	8046.	31172.	576.00	888.00

TABLE A4 (CONTINUED)

## STRESS SPECTRA WITH UTILIZATION 3 FOR STUDY NO. 1

	LOAD BLOCK	NUMBER OF CYCLES PER LOAD CYCLE	NUMBER OF CYCLES AT END OF BLOCK	SIGMA MAX	SIGMA MIN
G+M	124	2377.	33549.	1006.00	858.00
G+M	125	777.	34326.	1035.00	829.00
G+M	126	366.	34492.	1065.00	799.00
G+M	127	91.	34783.	1094.00	770.00
FOGAG	128	82.	34865.	2645.00	88.00
TAXI	129	61008.	95873.	788.00	380.00
TAXI	130	45182.	141055.	847.00	321.00
TAXI	131	16400.	157455.	905.00	263.00
TAXI	132	4346.	161801.	964.00	204.00
TAXI	133	738.	162539.	1022.00	146.00
TAXI	134	82.	162721.	1088.00	88.00
G+M	135	250776.	422397.	976.00	888.00
G+M	136	76752.	499149.	1006.00	858.00
G+M	137	31998.	531047.	1035.00	829.00
G+M	138	10332.	541779.	1065.00	799.00
G+M	139	3854.	545233.	1094.00	770.00
G+M	140	328.	545561.	1124.00	740.00
G+M	141	574.	546135.	1153.00	711.00
G+M	142	246.	546781.	1182.00	681.00
G+M	143	246.	546827.	2645.00	2248.00
F1GAG	144	5.	546832.	2645.00	343.00
TAXI	145	1250.	547882.	1322.00	636.00
TAXI	146	215.	548067.	1420.00	538.00
TAXI	147	75.	548132.	1517.00	441.00
TAXI	148	5.	548137.	1615.00	343.00
G+M	149	13330.	561467.	1505.00	1323.00
G+M	150	3640.	565407.	1566.00	1262.00
G+M	151	1635.	567042.	1627.00	1201.00
G+M	152	530.	567572.	1688.00	1140.00
G+M	153	195.	567767.	1749.00	1079.00
G+M	154	20.	567787.	1810.00	1018.00
G+M	155	30.	567817.	1871.00	957.00
G+M	156	15.	567832.	1932.00	896.00
G+M	157	10.	567842.	2645.00	2248.00
F2GAG	158	26.	567868.	2645.00	168.00
TAXI	159	4845.	572712.	906.00	436.00
TAXI	160	3519.	576232.	973.00	369.00
TAXI	161	1275.	577507.	1040.00	302.00
TAXI	162	51.	577556.	1174.00	168.00
G+M	163	44880.	622438.	1252.00	1141.00
G+M	164	13260.	635698.	1294.00	1068.00
G+M	165	5508.	641206.	1344.00	1022.00
G+M	166	1785.	642091.	1390.00	976.00
G+M	167	563.	643654.	1435.00	931.00
G+M	168	51.	643705.	1481.00	885.00
G+M	169	102.	643807.	1527.00	839.00
G+M	170	51.	643858.	1573.00	793.00
G+M	171	26.	643884.	2645.00	1986.00
F3GAG	172	76.	643910.	2645.00	593.00
TAXI	173	255.	644145.	1455.00	701.00
TAXI	174	26.	644191.	1553.00	593.00
G+M	175	44906.	685097.	1552.00	1668.00
G+M	176	13260.	702257.	2109.00	1557.00
G+M	177	5508.	707165.	2213.00	1447.00
G+M	178	1785.	709650.	2329.00	1337.00
G+M	179	663.	710213.	2440.00	1226.00
G+M	180	51.	710264.	2550.00	1116.00
G+M	181	107.	710466.	2660.00	1006.00
G+M	182	51.	710517.	2771.00	895.00
G+M	183	51.	710568.	2645.00	2248.00

TABLE A5

## STRESS SPECTRA WITH UTILIZATION 4 FOR STUDY NO. 1

ONE SPECTRA REPRESENTS 333.3 HOURS

	LOAD BLOCK	NUMBER OF CYCLES PER LOAD CYCLE	NUMBER OF CYCLES AT END OF BLOCK	SIGMA MAX	SIGMA MIN
F1GAG	1	75.	75.	14237.00	263.00
TAXI	2	2030.	2105.	788.00	380.00
TAXI	3	301.	2405.	847.00	321.00
TAXI	4	75.	2481.	905.00	263.00
G+M	5	150.	2631.	1978.00	1890.00
G+M	6	150.	2781.	3582.00	3464.00
G+M	7	226.	3007.	6589.00	6501.00
G+M	8	1203.	4210.	12604.00	12515.00
G+M	9	150.	4360.	12634.00	12485.00
G+M	10	1053.	5413.	12604.00	12559.00
G+M	11	376.	5789.	12634.00	12559.00
G+M	12	150.	5939.	12662.00	12559.00
G+M	13	601.	6540.	14207.00	14119.00
G+M	14	75.	6615.	14237.00	14119.00
F2GAG	15	10.	6625.	14797.00	14119.00
G+M	16	41.	6666.	2507.00	2325.00
G+M	17	31.	6697.	4111.00	3929.00
G+M	18	31.	6728.	7118.00	6936.00
G+M	19	145.	6893.	13132.00	12950.00
G+M	20	21.	6914.	13193.00	12889.00
G+M	21	145.	7059.	13132.00	13041.00
G+M	22	52.	7111.	13193.00	13041.00
G+M	23	21.	7132.	13254.00	13041.00
G+M	24	52.	7184.	14736.00	14554.00
G+M	25	10.	7194.	14797.00	14493.00
G+M	26	21.	7215.	14736.00	14645.00
G+M	27	10.	7225.	14797.00	14645.00
TAXI	28	279.	7504.	1322.00	636.00
TAXI	29	41.	7545.	1421.00	538.00
TAXI	30	10.	7555.	1517.00	441.00
F3GAG	31	75.	7630.	14237.00	263.00
TAXI	32	2030.	8660.	788.00	380.00
TAXI	33	301.	8961.	847.00	321.00
TAXI	34	75.	10036.	905.00	263.00
G+M	35	226.	10262.	1978.00	1890.00
G+M	36	451.	10713.	3582.00	3464.00
G+M	37	75.	10788.	3512.00	3464.00
G+M	38	226.	11014.	6589.00	6501.00
G+M	39	75.	11089.	6619.00	6471.00
G+M	40	1128.	12217.	12603.00	12515.00
G+M	41	150.	12367.	12633.00	12485.00
G+M	42	1053.	13420.	12603.00	12559.00
G+M	43	376.	13796.	12633.00	12559.00
G+M	44	113.	13909.	12662.00	12559.00
G+M	45	75.	13984.	12662.00	12559.00
G+M	46	677.	14661.	14207.00	14119.00
G+M	47	75.	14736.	14237.00	14119.00
F4GAG	48	10.	14746.	14541.00	14119.00
TAXI	49	279.	15025.	1322.00	636.00
TAXI	50	41.	15066.	1421.00	538.00
TAXI	51	10.	15076.	1517.00	441.00
G+M	52	31.	15107.	2272.00	2150.00
G+M	53	31.	15138.	3476.00	3754.00
G+M	54	41.	15179.	6883.00	6761.00
G+M	55	124.	15303.	12897.00	12775.00
G+M	56	21.	15324.	12937.00	12735.00
G+M	57	87.	15407.	12897.00	12836.00
G+M	58	31.	15438.	12937.00	12836.00
G+M	59	10.	15448.	12977.00	12836.00
G+M	60	42.	15510.	14501.00	14379.00
G+M	61	10.	15520.	14541.00	14339.00
F5GAG	62	28.	15548.	12692.00	263.00
TAXI	63	756.	16304.	788.00	380.00

TABLE A5 (CONTINUED)

## STRESS SPECTRA WITH UTILIZATION 4 FOR STUDY NO. 1

	LOAD BLOCK	NUMBER OF CYCLES PER LOAD CYCLE	NUMBER OF CYCLES AT END OF BLOCK	SIGMA MAX	SIGMA MIN
TAXI	64	112.	16416.	847.00	321.00
TAXI	65	28.	16444.	905.00	263.00
G+M	66	56.	16500.	1578.00	1890.00
G+M	67	84.	16584.	3582.00	3494.00
G+M	68	84.	16668.	6589.00	6501.00
G+M	69	560.	17228.	6587.00	6545.00
G+M	70	140.	17368.	6619.00	6545.00
G+M	71	56.	17424.	6648.00	6545.00
G+M	72	112.	17536.	10551.00	10511.00
G+M	73	56.	17592.	12603.00	12515.00
G+M	74	840.	18432.	12603.00	12559.00
G+M	75	252.	18684.	12662.00	12559.00
G+M	76	84.	18768.	12662.00	12559.00
G+M	77	28.	18796.	12721.00	12559.00
F6GAG	78	2.	18798.	11311.00	441.00
TAXI	79	54.	18852.	1322.00	636.00
TAXI	80	8.	18860.	1420.00	538.00
TAXI	81	2.	18862.	1517.00	441.00
G+M	82	6.	18868.	2507.00	2325.00
G+M	83	6.	18874.	4111.00	3929.00
G+M	84	14.	18888.	7118.00	6936.00
G+M	85	2.	18890.	7179.00	6875.00
G+M	86	46.	18936.	11128.00	11037.00
G+M	87	12.	18948.	11189.00	11037.00
G+M	88	4.	18952.	11250.00	11037.00
G+M	89	2.	18954.	11311.00	11037.00
F7GAG	90	28.	18982.	8683.00	263.00
TAXI	91	756.	18982.	788.00	380.00
TAXI	92	112.	18950.	847.00	321.00
TAXI	93	28.	18978.	905.00	263.00
G+M	94	84.	19462.	1578.00	1890.00
G+M	95	84.	20046.	3582.00	3494.00
G+M	96	39.	20074.	6619.00	6471.00
G+M	97	392.	20466.	6589.00	6545.00
G+M	98	112.	20578.	6619.00	6545.00
G+M	99	28.	20606.	6648.00	6545.00
G+M	100	84.	20690.	8554.00	8506.00
G+M	101	980.	21670.	8594.00	8550.00
G+M	102	308.	21978.	8624.00	8550.00
G+M	103	84.	22062.	8653.00	8550.00
G+M	104	28.	22090.	8683.00	8550.00
F8GAG	105	2.	22092.	9306.00	636.00
TAXI	106	8.	22100.	1322.00	636.00
G+M	107	6.	22106.	2507.00	2325.00
G+M	108	6.	22112.	4111.00	3929.00
G+M	109	10.	22122.	7118.00	6936.00
G+M	110	2.	22124.	7179.00	6875.00
G+M	111	34.	22158.	7118.00	7027.00
G+M	112	8.	22166.	7179.00	7027.00
G+M	113	2.	22168.	7249.00	7027.00
G+M	114	4.	22172.	9123.00	8941.00
G+M	115	60.	22232.	9123.00	9032.00
G+M	116	18.	22250.	9184.00	9032.00
G+M	117	6.	22256.	9245.00	9032.00
G+M	118	2.	22258.	9306.00	9032.00
F9GAG	119	4.	22262.	2645.00	263.00
TAXI	120	177.	22439.	788.00	380.00
TAXI	121	32.	22471.	847.00	321.00
TAXI	122	4.	22475.	905.00	263.00
G+M	123	311.	22786.	976.00	888.00

TABLE A5 (CONTINUED)

## STRESS SPECTRA WITH UTILIZATION 4 FOR STUDY NO. 1

	LOAD BLOCK	NUMBER OF CYCLES PER LOAD CYCLE	NUMBER OF CYCLES AT END OF BLOCK	SIGMA MAX	SIGMA MIN
G+M	124	92.	22878.	1006.00	858.00
G+M	125	30.	22908.	1035.00	829.00
G+M	126	14.	22922.	1065.00	799.00
G+M	127	4.	22926.	1094.00	770.00
FCGAG	128	164.	23090.	2645.00	88.00
TAXI	129	122016.	145106.	788.00	380.00
TAXI	130	90364.	235470.	847.00	321.00
TAXI	131	32800.	268270.	905.00	263.00
TAXI	132	8692.	276962.	964.00	204.00
TAXI	133	1476.	278438.	1022.00	146.00
TAXI	134	164.	278602.	1088.00	89.00
G+M	135	519552.	798154.	976.00	888.00
G+M	136	153504.	951658.	1006.00	858.00
G+M	137	63796.	1015454.	1035.00	829.00
G+M	138	20664.	1036118.	1065.00	799.00
G+M	139	7708.	1043826.	1094.00	770.00
G+M	140	656.	1044482.	1124.00	740.00
G+M	141	1148.	1045630.	1153.00	711.00
G+M	142	492.	1046122.	1183.00	681.00
G+M	143	492.	1046614.	2645.00	2248.00
FIGAG	144	10.	1047624.	2645.00	343.00
TAXI	145	2500.	1048124.	1322.00	636.00
TAXI	146	430.	1049554.	1420.00	538.00
TAXI	147	70.	1049624.	1517.00	441.00
TAXI	148	10.	1049634.	1615.00	343.00
G+M	149	26660.	1076294.	1505.00	1223.00
G+M	150	7880.	1084174.	1566.00	1262.00
G+M	151	3270.	1087444.	1627.00	1201.00
G+M	152	1060.	1088504.	1688.00	1140.00
G+M	153	390.	1088894.	1749.00	1079.00
G+M	154	40.	1088934.	1810.00	1018.00
G+M	155	60.	1088994.	1871.00	957.00
G+M	156	30.	1089024.	1932.00	896.00
G+M	157	20.	1089044.	2645.00	2248.00
F2GAG	158	17.	1089061.	2645.00	168.00
TAXI	159	3230.	1092791.	906.00	436.00
TAXI	160	2346.	1094637.	973.00	369.00
TAXI	161	850.	1095487.	1040.00	302.00
TAXI	162	34.	1095521.	1174.00	168.00
G+M	163	29920.	1125441.	1252.00	1141.00
G+M	164	9840.	1134281.	1298.00	1068.00
G+M	165	3672.	1137953.	1344.00	1022.00
G+M	166	1100.	1138143.	1390.00	976.00
G+M	167	442.	1139585.	1435.00	931.00
G+M	168	34.	1139619.	1481.00	885.00
G+M	169	68.	1139687.	1527.00	829.00
G+M	170	34.	1139721.	1573.00	793.00
G+M	171	17.	1139738.	2645.00	1994.00
F3GAG	172	17.	1139755.	2645.00	593.00
TAXI	173	170.	1139925.	1455.00	701.00
TAXI	174	17.	1139942.	1563.00	593.00
G+M	175	29927.	1169879.	1598.00	1668.00
G+M	176	8040.	1178719.	2109.00	1557.00
G+M	177	3672.	1182391.	2219.00	1447.00
G+M	178	1190.	1183581.	2321.00	1237.00
G+M	179	442.	1184023.	2440.00	1226.00
G+M	180	34.	1184057.	2550.00	1116.00
G+M	181	69.	1184125.	2660.00	1005.00
G+M	182	34.	1184159.	2771.00	895.00
G+M	183	34.	1184193.	2645.00	2248.00

TABLE A6

## STRESS SPECTRA WITH UTILIZATION 5 FOR STUDY NO. 1

ONE SPECTRA REPRESENTS 333.3 HOURS

	LOAD BLOCK	NUMBER OF CYCLES PER LOAD CYCLE	NUMBER OF CYCLES AT END OF BLOCK	SIGMA MAX	SIGMA MIN
F1GAG	1	80.	80.	14237.00	263.00
TAXI	2	2160.	2240.	788.00	380.00
TAXI	3	320.	2560.	847.00	321.00
TAXI	4	80.	2640.	505.00	263.00
G+M	5	160.	2800.	1978.00	1890.00
G+M	6	160.	2960.	3582.00	3494.00
G+M	7	240.	3200.	6589.00	6501.00
G+M	8	1280.	4480.	12604.00	12516.00
G+M	9	160.	4640.	12634.00	12486.00
G+M	10	1120.	5760.	12604.00	12560.00
G+M	11	400.	6160.	12634.00	12560.00
G+M	12	160.	6320.	12663.00	12560.00
G+M	13	640.	6960.	14207.00	14119.00
G+M	14	80.	7040.	14237.00	14089.00
F2GAG	15	11.	7051.	14797.00	441.00
G+M	16	44.	7095.	2507.00	2325.00
G+M	17	33.	7128.	4111.00	3929.00
G+M	18	33.	7161.	7116.00	6936.00
G+M	19	176.	7337.	13132.00	12950.00
G+M	20	22.	7359.	13193.00	12889.00
G+M	21	154.	7513.	13132.00	13041.00
G+M	22	55.	7568.	13193.00	13041.00
G+M	23	22.	7590.	13254.00	13041.00
G+M	24	55.	7645.	14736.00	14554.00
G+M	25	11.	7656.	14797.00	14493.00
G+M	26	22.	7678.	14736.00	14645.00
G+M	27	11.	7689.	14797.00	14645.00
TAXI	28	297.	7946.	1322.00	636.00
TAXI	29	44.	8030.	1420.00	538.00
TAXI	30	11.	8041.	1517.00	441.00
F3GAG	31	80.	8121.	14237.00	263.00
TAXI	32	2160.	10281.	788.00	380.00
TAXI	33	320.	10601.	847.00	321.00
TAXI	34	80.	10681.	505.00	263.00
G+M	35	240.	10921.	1978.00	1890.00
G+M	36	480.	11401.	3582.00	3494.00
G+M	37	80.	11481.	3612.00	3464.00
G+M	38	240.	11721.	6589.00	6501.00
G+M	39	80.	11801.	6619.00	6471.00
G+M	40	1200.	13001.	12603.00	12515.00
G+M	41	160.	13161.	12633.00	12485.00
G+M	42	1120.	14281.	12603.00	12559.00
G+M	43	400.	14681.	12633.00	12559.00
G+M	44	120.	14801.	12662.00	12559.00
G+M	45	80.	14881.	12692.00	12559.00
G+M	46	720.	15601.	14207.00	14119.00
G+M	47	80.	15681.	14237.00	14119.00
F4GAG	48	11.	15692.	14541.00	441.00
TAXI	49	297.	15989.	1322.00	636.00
TAXI	50	44.	16033.	1420.00	538.00
TAXI	51	11.	16044.	1517.00	441.00
G+M	52	33.	16077.	2272.00	2160.00
G+M	53	33.	16110.	3872.00	3754.00
G+M	54	46.	16154.	6883.00	6781.00
G+M	55	132.	16286.	12317.00	12175.00
G+M	56	22.	16308.	12337.00	12175.00
G+M	57	88.	16396.	12867.00	12836.00
G+M	58	33.	16429.	12937.00	12836.00
G+M	59	11.	16440.	12977.00	12836.00
G+M	60	66.	16506.	14501.00	14370.00
G+M	61	11.	16517.	14541.00	14339.00
F5GAG	62	28.	16545.	12692.00	263.00
TAXI	63	756.	17301.	788.00	380.00

TABLE A6 (CONTINUED)

## STRESS SPECTRA WITH UTILIZATION 5 FOR STUDY NO. 1

	LOAD BLOCK	NUMBER OF CYCLES PER LOAD CYCLE	NUMBER OF CYCLES AT END OF BLOCK	SIGMA MAX	SIGMA MIN
TAXI	64	112.	17413.	847.00	321.00
TAXI	65	28.	17441.	505.00	263.00
G+M	66	56.	17497.	1978.00	1890.00
G+M	67	84.	17581.	3582.00	3494.00
G+M	68	84.	17665.	6589.00	6501.00
G+M	69	560.	18225.	6589.00	6545.00
G+M	70	140.	18365.	6619.00	6545.00
G+M	71	56.	18421.	6648.00	6545.00
G+M	72	112.	18523.	10569.00	10511.00
G+M	73	56.	18589.	12603.00	12515.00
G+M	74	840.	19429.	12603.00	12559.00
G+M	75	252.	19681.	12662.00	12559.00
G+M	76	84.	19765.	12652.00	12559.00
G+M	77	28.	19793.	12721.00	12559.00
FAGAG	79	2.	19795.	11311.00	441.00
TAXI	79	54.	19849.	1322.00	636.00
TAXI	80	8.	19857.	1420.00	538.00
TAXI	81	2.	19859.	1517.00	441.00
G+M	82	6.	19865.	2507.00	2325.00
G+M	83	6.	19871.	4111.00	3929.00
G+M	84	14.	19885.	7118.00	6936.00
G+M	85	2.	19887.	7173.00	6875.00
G+M	86	46.	19933.	11128.00	11037.00
G+M	87	12.	19945.	11189.00	11037.00
G+M	88	4.	19949.	11250.00	11037.00
G+M	89	2.	19951.	11311.00	11037.00
F7GAG	90	28.	19979.	8682.00	263.00
TAXI	91	756.	20735.	798.00	380.00
TAXI	92	112.	20847.	847.00	321.00
TAXI	93	28.	20875.	905.00	263.00
G+M	94	84.	20959.	1578.00	1890.00
G+M	95	84.	21043.	3582.00	3494.00
G+M	96	28.	21071.	6619.00	6471.00
G+M	97	60.	21131.	1871.00	957.00
G+M	98	392.	21523.	6589.00	6545.00
G+M	99	112.	21635.	6519.00	6545.00
G+M	100	28.	21663.	6648.00	6545.00
G+M	101	84.	21747.	8594.00	8506.00
G+M	102	980.	22727.	8564.00	8550.00
G+M	103	308.	23035.	8624.00	8550.00
G+M	104	84.	23119.	8653.00	8550.00
G+M	105	23.	23147.	8583.00	8550.00
FRGAG	106	2.	23149.	9306.00	636.00
TAXI	107	8.	23157.	1322.00	636.00
G+M	108	6.	23163.	2507.00	2325.00
G+M	109	6.	23169.	4111.00	3929.00
G+M	110	10.	23179.	7118.00	6936.00
G+M	111	2.	23181.	7171.00	6875.00
G+M	112	34.	23215.	7118.00	7027.00
G+M	113	8.	23223.	7179.00	7027.00
G+M	114	2.	23225.	7240.00	7027.00
G+M	115	4.	23229.	9123.00	8941.00
G+M	116	60.	23289.	9123.00	9032.00
G+M	117	18.	23307.	9184.00	9032.00
G+M	118	6.	23313.	9245.00	9032.00
G+M	119	2.	23315.	9306.00	9032.00
FOGAG	120	164.	23479.	2645.00	88.00
TAXI	121	22016.	45495.	788.00	380.00
TAXI	122	90364.	135659.	847.00	321.00
TAXI	123	32800.	168659.	905.00	263.00

TABLE A6 (CONTINUED)

## STRESS SPECTRA WITH UTILIZATION 5 FOR STUDY NO. 1

	LOAD BLOCK	NUMBER OF CYCLES PER LOAD CYCLE	NUMBER OF CYCLES AT END OF BLOCK	SIGMA MAX	SIGMA MIN
TAXI	124	8692.	177351.	964.00	204.00
TAXI	125	1476.	178827.	1022.00	146.00
TAXI	126	164.	178991.	1088.00	88.00
G+M	127	519552.	698543.	976.00	888.00
G+M	128	153504.	852047.	1006.00	858.00
G+M	129	63796.	915843.	1035.00	829.00
G+M	130	20664.	936507.	1065.00	799.00
G+M	131	7708.	944215.	1094.00	770.00
G+M	132	656.	944871.	1124.00	740.00
G+M	133	1148.	946019.	1153.00	711.00
G+M	134	492.	946511.	1183.00	681.00
G+M	135	492.	947003.	2645.00	2248.00
F1GAG	136	10.	947013.	2645.00	343.00
TAXI	137	250.	949513.	1322.00	636.00
TAXI	138	430.	949943.	1420.00	538.00
TAXI	139	70.	950013.	1517.00	441.00
TAXI	140	10.	950023.	1615.00	343.00
G+M	141	26660.	975683.	1505.00	1323.00
G+M	142	7880.	984563.	1566.00	1262.00
G+M	143	3270.	987823.	1627.00	1201.00
G+M	144	1060.	988893.	1688.00	1140.00
G+M	145	390.	989203.	1749.00	1079.00
G+M	146	40.	989323.	1810.00	1018.00
G+M	147	30.	989353.	1932.00	896.00
G+M	148	20.	989373.	2645.00	2248.00
F2GAG	149	13.	989386.	2645.00	168.00
TAXI	150	2541.	991527.	906.00	436.00
TAXI	151	1846.	993773.	973.00	369.00
TAXI	152	669.	994442.	1040.00	302.00
TAXI	153	27.	994669.	1174.00	168.00
G+M	154	23537.	1018006.	1252.00	1141.00
G+M	155	6954.	1024960.	1298.00	1068.00
G+M	156	2989.	1027849.	1344.00	1022.00
G+M	157	936.	1028785.	1350.00	976.00
G+M	158	348.	1029123.	1435.00	931.00
G+M	159	27.	1029160.	1481.00	885.00
G+M	160	53.	1029213.	1527.00	839.00
G+M	161	27.	1029240.	1573.00	793.00
G+M	162	13.	1029253.	2645.00	1984.00
F3GAG	163	13.	1029266.	2645.00	593.00
TAXI	164	134.	1029400.	1455.00	701.00
TAXI	165	13.	1029413.	1563.00	593.00
G+M	166	23550.	1052963.	1998.00	1668.00
G+M	167	6954.	1054917.	2109.00	1557.00
G+M	168	2889.	1062806.	2219.00	1447.00
G+M	169	936.	1063742.	2329.00	1337.00
G+M	170	348.	1064090.	2440.00	1226.00
G+M	171	27.	1064117.	2550.00	1116.00
G+M	172	53.	1064170.	2660.00	1006.00
G+M	173	27.	1064197.	2771.00	895.00
G+M	174	27.	1064224.	2645.00	2248.00

THIS PAGE IS BEST QUALITY PRACTICABLE  
FROM COPY FURNISHED TO DDC

## APPENDIX B

The segmented mission profiles are presented in Tables B-1 thru B-13. The significant flight parameters for each segment of each mission are included in the Tables. These values were used directly in the spectra development and fatigue analysis.

OEW = 103,140  
 PAYLOAD = 20,250  
 FUEL = 39,169  
 TOGW = 162,559

TABLE B1  
 BASIC FLIGHT PROFILE 1-1 (OUTBOUND)

SEG NO.	DESCRIPTION	AVERAGE		C.G. % MAC	ALTITUDE 10 <sup>3</sup> FT	AVG.		SPEED		DISTANCE		TIME HOURS
		GROSS WT.	LB FUEL			KEAS	MACH NO.	NAUTICAL MILES	STATUTE MILES			
1	TAXI & TAKEOFF CTOL	162,233	38,843	33.0	S.L.			0.0				0.0
2	CLIMB	161,502	38,112	33.0	0-1	100		1.0	1.15			.01
3		161,337	37,947	33.0	1-2.5	282		1.5	1.73			.006
4		161,172	37,782	33.0	2.5-5	280		3.0	3.45			.010
5		160,500	37,110	32.95	5-10	271		6.5	7.48			.021
6		159,550	36,160	32.9	10-20	259		17.0	19.56			.053
7		157,968	34,578	32.85	20-30	236	.6003	30.5	35.10			.086
8	CLIMB	156,403	33,013	32.80	30-34.3	212	.6379	21.6	24.86			.058
9	CRUISE	153,091	29,701	32.75	34.30	223	.6818	318.9	366.98			.809
10	DESCENT	147,078	23,688	32.50	34.3-30	231	.6800	9.4	10.82			.024
11		147,000	23,610	32.50	30-20	250	.6204	21.7	24.97			.059
12		146,800	23,410	32.50	20-10	250	.5031	20.5	23.59			.065
13		146,650	23,260	32.50	10-5	250	.4343	9.9	11.39			.035
14		146,525	23,135	32.50	5-2.5	250	.40	2.9	3.34			.018
15	DESCENT	146,470	23,080	32.50	2.5-1	250	.39	1.4	1.61			.012
16	DESCEND TO TOUCHDOWN	146,100	22,710	32.50	1-0	76		1.3	1.50			.017
17	LANDING STOL T&G	146,024	22,634	32.50	S.L.			0.0	0			0.0
18	LANDING ROLL	145,650	22,260	32.50	S.L.			0.0	0			0.0
19	CLIMB MANEUVER (+ g)	159,550	36,160			254						.244
20	" " (+ g)	159,550	36,160			254						.244
21	CRUISE MANEUVER(+ g)	153,091	29,701			223						.809
22	" " (+ g)	153,091	29,701			223						.809
23	DESCENT " (+ g)	146,650	23,260			250						.230
24	" " (+ g)	146,650	23,260									.230

OEW - 103,140  
 PAYLOAD - 20,250  
 FUEL - 39,169  
 TOW - 162,559

TABLE B2  
 BASIC FLIGHT PROFILE 1-1 (TOUCH AND GO)

SEG NO.	DESCRIPTION	AVERAGE		C.G. % MAC	ALTITUDE 10 <sup>3</sup> FT	AVG.		DISTANCE		TIME HOURS
		GROSS WT.	LB FUEL			KEAS	MPH NO.	NAUTICAL MILES	STATUTE MILES	
1	TAXI & TAKEOFF T&G	145,650	22,260	32.50	S.L			0		0
2	CLIMB	145,400	22,010	32.50	0-1	89		0.8	.92	.009
3	CRUISE	145,050	21,660	32.45	1	190	.29	14.0	16.11	0.073
4	DESCENT	144,500	21,110	32.45	1-0	72		1.3	1.50	0.018
5	LANDING CTOL	143,700	20,310	32.40	S.L			0		0
6	LANDING ROLL	143,300	19,910	32.40	S.L			0		0

OEW = 103,140  
 PAYLOAD = 20,250  
 FUEL = 39,169  
 TOW = 162,559

TABLE B3  
 BASIC FLIGHT PROFILE 1-1 (RETURN)

SEG NO.	DESCRIPTION	AVERAGE GROSS WT.	LB		C.G. % MAC	ALTITUDE 10 <sup>3</sup> FT	AVG.		SPEED KNOTS	DISTANCE		TIME HOURS
			FUEL				KEAS			NAUTICAL MILES	STATUTE MILES	
1	TAXI & TAKEOFF STOL	142,350	18,960		32.40	S.L.						0.0
2	CLIMB	142,195	18,805		32.40	0-1	100	.4401	.8		.92	.008
3		142,100	18,710		32.40	1-2.5	283	.44	1.5		1.73	.005
4		141,914	18,524		32.40	2.5-5	280	.4517	1.0		1.15	.009
5		141,354	17,964		32.40	5-10	269	.4767	5.5		6.33	.018
6		140,508	17,118		32.35	10-20	252	.5183	4.5		5.18	.045
7		139,248	15,858		32.30	20-30	286	.5996	20.5		23.59	.068
8	CLIMB	138,082	14,692		32.30	30-37	214	.6424	34.8		40.05	.080
9	CRUISE	131,000	7,610		32.20	37	206	.6793	350.1		402.88	.897
10	DESCENT	128,539	5,149		32.0	37-30	217	.6790	14.6		16.80	.037
11		128,415	5,025		32.0	30-20	250	.6235	20.2		23.25	.054
12		128,265	4,875		32.0	20-10	250	.5654	19.2		22.09	.061
13		128,102	4,718		32.0	10-5	250	.4363	9.1		10.47	.032
14		128,000	4,610		32.0	5-25	250	.405	13.6		15.65	.017
15	DESCENT	127,950	4,560		32.0	2.5-1	250	.39	3.1		3.57	.013
16	DESCENT TO TOUCHDOWN	127,400	4,010		32.0	1-0	84		3.2		3.68	.038
17	LANDING CTOL	127,112	3,722		32.0	S.L.			0			0
18	LANDING ROLL	127,112	3,722		82.0	S.L.			0			0
19	CLIMB MANEUVER (+ g)	140,508	17,118				252					.233
20	" (+ g)	140,508	17,118				252					.233
21	CRUISE " (+ g)	131,000	7,610				206					.897
22	" (+ g)	131,000	7,610				206					.897
23	DESCENT " (+ g)	128,102	4,718				250					.252
24	" (+ g)	128,102	4,718				250					.252

OEW - 103,140  
 PAYLOAD - 54,250  
 FUEL - 35,690  
 TOGW - 193,080

TABLE B4  
 BASIC FLIGHT PROFILE 1-2 (OUTBOUND)

SEG NO.	DESCRIPTION	AVERAGE		C.G. % MAC	ALTITUDE 10 <sup>3</sup> FT	AVG. SPEED		DISTANCE		TIME HOURS
		GROSS WT.	LB FUEL			KEAS	MACH NO.	NAUTICAL MILES	STATUTE MILES	
1	TAXI & TAKEOFF CTOL	192,700	35,310	26.60	S.L.			0		0
2	CLIMB	192,050	34,660	26.55	0-1	115		1.5	1.73	.013
3		191,600	34,210	26.50	1-2.5	290		2.0	2.30	.007
4		191,324	33,994	26.45	2.5-5	287		4.0	4.60	.013
5		190,750	33,360	26.40	5-10	277		8.5	9.78	.027
6		189,450	32,060	26.35	10-20	260		22.8	25.24	.070
7		187,450	30,060	26.25	20-30	240		46.0	52.94	.128
8	CLIMB									
9	CRUISE	182,100	24,710	25.90	30.	243	.68	208.4	239.82	.520
10	DESCENT									
11		178,625	21,295	25.70	30-20	250	.63	23.0	26.47	.061
12		178,514	21,124		20-10	250	.51	28.2	32.45	.070
13		178,300	20,910		10-5	250	.43	10.7	12.31	.038
14		178,000	20,810		5-2.5	250	.40	5.1	5.87	.020
15	DESCENT	178,125	20,735		2.5-1	250	.39	5.0	5.75	.019
16	DESCENT TO TOUCHDOWN	177,900	20,510		1-0	87		1.3	1.50	.015
17	LANDING CTOL T&S	177,500	20,110		S.L.			0		0
18	LANDING ROLL	177,300	19,910	25.70	S.L.			0		0
19	CLIMB MANEUVER (+ g)	190,750	33,360			277				.258
20	" (+ g)	190,750	33,360			277				.258
21	CRUISE " (+ g)	182,100	24,710			243				.520
22	" (+ g)	182,100	24,710			243				.520
23	DESCENT " (+ g)	178,300	20,910			250				.223
24	" (+ g)	178,300	20,910			250				.223

TABLE B5  
BASIC FLIGHT PROFILE 1-2 (RETURN)

OEW - 103,140  
PAYLOAD - 55,250  
FUEL - 35,690  
TOGW - 193,080

SEG NO.	DESCRIPTION	AVERAGE		C.G. % MAC	ALTITUDE 10 <sup>3</sup> FT	AVG.		SPEED MACH NO.	DISTANCE		TIME HOURS
		GROSS WT.	FUEL LB			KEAS			NAUTICAL MILES	STATUTE MILES	
1	TAKEOFF CTOL	177,000	19,610	25.70	S.L.				0		0
2	CLIMB	176,500	19,110	25.6	0-1	109			1.2	1.38	.011
3		176,000	18,610	25.6	1-2.5	287	.45		2.1	2.42	.006
4		175,600	18,490	25.6	2.5-5	284	.46		3.0	3.45	.011
5		175,300	17,810	25.5	5-10	276	.48		3.0	9.21	.025
6		174,200	16,810	25.4	10-20	252	.53		19.0	21.86	.060
7		172,500	15,110	25.3	20-30	238	.59		38.0	43.73	.105
8	CLIMB	170,600	13,410	25.2	30-32	220	.64		11.9	13.69	.033
9	CRUISE	167,540	10,150	25.0	32	233	.68		283.9	326.70	.504
10	DESCENT	164,325	6,925	24.8	32-30	237	.68		4.7	5.41	.012
11		164,241	6,851	24.8	30-20	250	.62		22.7	26.12	.073
12		164,072	6,682	24.7	20-10	250	.51		21.5	24.74	.068
13		163,895	6,505	24.7	10-5	250	.44		10.4	11.97	.037
14		163,770	6,380	24.7	5-2.5	250	.40		5.1	5.87	.019
15	DESCENT	163,700	6,310	24.7	2.5-1	250	.39		3.3	3.80	.014
16	DESCENT TO TOUCHDOWN	163,300	5,910	24.7	1-0	91			3.1	3.57	.034
17	LANDING CTOL	162,850	5,460	24.6	S.L.				0		0
18	LANDING ROLL	162,700	5,310	24.6	S.L.				0		0
19	CLIMB MANEUVER (+ 9)	175,300				276					.251
20	" (+ 9)	175,300				276					.251
21	CRUISE (+ 9)	167,340				233					.504
22	" (+ 9)	167,540				233					.504
23	DESCENT (+ 9)	163,895				250					.257
24	" (+ 9)	163,895				250					.257

OEW = 103,140  
 PAYLOAD = 20,250  
 FUEL = 43,010  
 TOGW = 166,400

TABLE B6  
TRAINING FLIGHT PROFILE 2-1 (OUTBOUND)

SEG NO.	DESCRIPTION	AVERAGE		C.G. % MAC	ALTITUDE 10 <sup>3</sup> FT	AVG.		SPEED MACH NO.	NAUTICAL MILES	DISTANCE		TIME HOURS
		GROSS WT.	LB FUEL			KEAS				STATUTE MILES		
1	TAXI & TAKEOFF CTOL	166,000	42,610	33.1	S.L.							
2	CLIMB	165,500	42,110	33.1	0-1	110			1.1			.010
3	▲	165,200	41,810	33.1	1-2.5	288		.44	1.7			.006
4		165,000	41,610	33.1	2.5-5	283		.4561	3.1			.011
5	▼	164,450	41,060	33.05	5-10	274		.47	6.8			.022
6	CLIMB	163,750	40,360	33.05	10-15	263		.50	7.9			.024
7												
8												
9	CRUISE	160,070	36,680	32.95	15	273		.5485	106.5			.309
10												
11												
12	DESCENT	159,065	35,675	32.90	15-10	250		.4786	10.5			.035
13	▲	158,940	35,550		10-5	250		.4344	10.2			.036
14		158,825	35,435		5-25	250		.3956	5.0			.019
15	▼	158,750	35,360		2.5-1	250		.39	3.0			.012
16	DESCENT TO TOUCHDOWN	158,540	35,150		1-0	81			1.3			.016
17	LANDING STOL	158,100	35,710		S.L.				0			0
18	LANDING ROLL	157,650	34,260	32.90	S.L.				0			0
19	CLIMB MANEUVER (+ g)	164,450	41,060			274						.073
20	" " (+ g)	164,450				274						.073
21	CRUISE " (+ g)	160,070	36,680			273						.309
22	" " (+ g)	160,070	36,680			273						.309
23	DESCENT " (+ g)	158,940	35,550			250						.118
24	" " (+ g)	158,940	35,550			250						.118

OEW - 103,140  
 PAYLOAD - 20,250  
 FUEL -  
 TOGW - 166,400

TABLE B7  
 TRAINING FLIGHT PROFILE 2-1 (6 TOUCH AND GO'S)

SEG NO.	DESCRIPTION	AVERAGE		LB FUEL	C.G. % MAC	ALTITUDE 10 <sup>3</sup> FT	AVG.		SPEED		DISTANCE		TIME HOURS
		GROSS WT.					KEAS	MACH NO.	NAUTICAL MILES	STATUTE MILES			
1	TAXI & TAKEOFF STOL	152,466		29,076	32.7	S.L.							
2	CLIMB	152,095		28,705	↑	0-1	100			5.4	6.21		.054
3	CRUISE	151,266		27,876		1	182		.28	85.2	98.05		.444
4	DESCENT	150,857		27,467		1-0	76			7.8	8.98		.102
5	LANDING STOL	150,437		27,047	↓	S.L.				0			0
6	LANDING ROLL	150,437		27,047	32.7	S.L.				0			0

OEW - 103,140  
 PAYLOAD - 20,250  
 FUEL -  
 TOGW - 166,400

TABLE B8  
TRAINING FLIGHT PROFILE 2-1 (RETURN)

SEG NO.	DESCRIPTION	AVERAGE		C.G. % MAC	ALTITUDE 10 <sup>3</sup> FT	AVG. SPEED		DISTANCE		TIME HOURS
		GROSS WT.	LB FUEL			KEAS	MACH NO.	NAUTICAL MILES	STATUTE MILES	
1	TAXI & TAKEOFF	142,900	19,510	32.4	S.L.			0		
2	CLIMB	142,400	19,010	32.4	0-1	100		.8	.92	.008
3		142,000	18,610	32.4	1-2.5	280	.45	2.1	2.42	.007
4		141,900	18,510	32.35	2.5-5	280	.45	1.9	2.19	.007
5	CLIMB	141,500	18,110	32.35	5-10	272	.46	5.2	5.98	.017
6										
7										
8										
9	CRUISE	137,869	14,479	32.25	10	259	.47	109	125.43	.361
10										
11										
12										
13	DESCENT	136,538	13,148	32.2	10-5	250		9.4	10.82	.034
14		136,425	13,035		5-2.5	250		4.7	5.41	.018
15		136,350	12,960		2.5-1	250		2.9	3.34	.011
16	DESCENT	136,000	12,610		1-0	84		3.1	3.57	.037
17	LANDING	135,650	21,260		S.L.			0		0
18	LANDING ROLL	135,500	12,110	32.2	S.L.			0		0
19	CLIMB MANEUVER (+ g)	141,900	18,510			280				.039
20	" " (+ g)	141,900	18,510			280				.039
21	CRUISE " (+ g)	137,869	14,479			259				.361
22	" " (+ g)	137,869				259				.361
23	DESCENT " (+ g)	136,425	13,035			250				.100
24	" " (+ g)	136,425	13,035			250				.100

OEW - 103,140  
 PAYLOAD - 54,250  
 FUEL - 44,125  
 TOGW - 201,515

TABLE B9  
 TRAINING FLIGHT PROFILE 2-2 (OUTBOUND)

SEG NO.	DESCRIPTION	AVERAGE		C.G. % MAC	ALTITUDE 10 <sup>3</sup> FT	AVG.		SPEED MACH NO.	DISTANCE		TIME HOURS
		GROSS WT.	LB FUEL			KEAS			NAUTICAL MILES	STATUTE MILES	
1	TAXI & TAKEOFF	201,100	43,710	27.0	S.L.						
2	CLIMB	200,350	42,960	26.95	0-1	114			1.6	1.84	.014
3		199,900	42,510	26.9	1-2.5	290		.45	2.4	2.76	.008
4		199,724	42,334	26.9	2.5-5	288		.46	4.0	4.60	.013
5		199,000	41,610	26.9	5-10	280		.48	9.0	10.36	.029
6	CLIMB	198,100	40,710	26.85	10-15	268		.51	10.8	12.43	.034
7											
8											
9	CRUISE	195,928	38,538	26.6	15	262		.52	77.5	89.18	.215
10											
11											
12	DESCENT	194,171	36,781	26.5	15-10	250		.4786	11.2	12.89	.037
13		194,038	36,648	26.5	10-5	250		.4344	10.9	12.54	.039
14		193,925	36,535	26.5	5-2.5	250		.40	5.4	6.21	.020
15		193,850	36,460	26.5	2.5-1	250		.39	3.3	3.80	.013
16	DESCENT	193,600	36,210	26.45	1-0	93			1.3	1.50	.014
17	LANDING CTOL	193,200	35,810	26.45	S.L.				0		0
18	LANDING ROLL	192,933	35,543	26.45	S.L.				0		0
19	CLIMB MANEUVER (+ g)	199,000	41,610			280					.098
20	" " (+ g)	199,000	41,510			280					.098
21	CRUISE " (+ g)	195,928	38,538			262					.215
22	" " (+ g)	195,928	38,538			262					.215
23	DESCENT " (+ g)	193,850	36,460			250					.123
24	" " (+ g)	193,850	36,460			250					.123

OEW - 103,140  
 PAYLOAD - 54,250  
 FUEL - 44,125  
 TOGW - 201,515

TABLE B10  
 TRAINING FLIGHT PROFILE 2-2 (6 TOUCH AND GO'S)

SEG NO.	DESCRIPTION	AVERAGE		C.G. % MAC	ALTITUDE 10 <sup>3</sup> FT	AVG.		SPEED MACH NO.	DISTANCE		TIME HOURS
		GROSS WT.	L8 FUEL			KEAS			NAUTICAL MILES	STATUTE MILES	
1	TAXI & TAKEOFF CTOL	186,650	29,260	26.2	S.L.				0		0
2	CLIMB	186,100	28,710	↑	0-1	117			8.4	9.67	.172
3	CRUISE	185,350	27,960		1	216			97.2	111.85	.444
4	DESCENT	185,650	27,260		1-0	87			7.8	8.98	.090
5	LANDING STOL T&G	184,250	26,860	↓	S.L.				0		0
6	LANDING ROLL	184,000	16,610	26.2	S.L.				0		0

OEW - 103,140  
 PAYLOAD - 54,250  
 FUEL - 201,515  
 TOGW - 201,515

TABLE B11  
 TRAINING FLIGHT PROFILE 2-2 (RETURN)

SEG NO.	DESCRIPTION	AVERAGE		LB FUEL	C.G. % MAC	ALTITUDE 10 <sup>3</sup> FT	AVG.		SPEED		DISTANCE		TIME HOURS
		GROSS WT.					KEAS	MACH NO.	NAUTICAL MILES	STATUTE MILES			
1	TAXI & TAKEOFF	178,000		20,610	25.65	S.L.					0		0
2	CLIMB	177,500		20,110	25.65	0-1	109			1.2	1.38		.011
3	▲	177,100		19,710	25.65	1-2.5	287	.45		2.0	2.30		.007
4	▼	176,877		19,487	25.60	2.5-5	285	.46		3.3	3.80		.011
5	CLIMB	176,300		18,910		5-10	274	.48		7.4	8.52		.024
6													
7													
8													
9	CRUISE	177,500		20,110	25.65	10	287	.52		102.6	118.07		.305
10													
11													
12													
13	DESCENT	171,081		13,691	25.25	10-5	250	.43		10.5	12.08		.037
14	▲	170,950		13,560	▲	5-2.5	250	.40		5.2	5.98		.020
15	▼	170,900		13,510		2.5-1	250	.39		3.1	3.57		.022
16	DESCENT	170,500		13,110		1-0	94			3.1	3.57		.033
17	LANDING	170,000		12,610	▼	S.L.				0			0
18	LANDING ROLL	169,900		12,510	25.25	S.L.				0			0
19	CLIMB MANEUVER (+ g)	176,877		19,487			285						.053
20	- " (+ g)	176,877		19,487			285						.053
21	CRUISE - (+ g)	177,500		20,110			287						.305
22	- " (+ g)	177,500		20,110			287						.305
23	DESCENT - (+ g)	170,900		13,510			250						.112
24	- " (+ g)	170,900		13,510			250						.112

OEW - 103,140  
 PAYLOAD - 27,000  
 FUEL - 39,860  
 TOGW - 170,000

TABLE B12  
 LOW-ALTITUDE RESUPPLY FLIGHT PROFILE 3-1

SEG NO.	DESCRIPTION	AVERAGE		C.G. % MAC	ALTITUDE 10 <sup>3</sup> FT	AVG.		SPEED MACH NO.	DISTANCE		TIME HOURS
		GROSS WT.	FUEL LB			KEAS			NAUTICAL MILES	STATUTE MILES	
1	TAXI & TAKEOFF CTOL	169,324	39,184	31.35	S.L.						
2	CLIMB	169,000	38,860	31.30	0-.5	100			1.1	1.27	.011
3	CRUISE	164,800	34,660	31.25	.5	300		.4618	144.2	165.94	.473
4	DESCENT	160,600	30,460	31.10	5-0	81			1.3	1.50	.016
5	LANDING CTOL	160,200	30,060	31.10	S.L.				0		0
6	LANDING & TAKEOFF STOL	159,573	29,433	31.0	S.L.				0		0
7	CLIMB	159,000	28,860	31.0	0-.5	100			1.0	1.15	.010
8	CRUISE	154,803	24,663	30.85	.5	300		.4618	144.2	165.94	.473
9	DESCENT	150,600	20,460	30.70	5-0	76			1.3	1.50	.017
10	LANDING STOL	150,200	20,060	30.70	S.L.				0		0
11	LANDING & TAKEOFF ROLL STOL	149,500	19,360	30.60	S.L.				0		0
12	CLIMB	149,025	18,885	30.60	0-.5	100			.9	1.04	.009
13	CRUISE	144,967	14,827	30.40	.5	300		.4618	144.1	165.83	.473
14	DESCENT	140,800	10,660	30.25	5-0	72			1.3	1.50	.018
15	LANDING STOL	140,400	10,260	30.25	S.L.				0		0
16	LANDING & TAKEOFF ROLL STOL	139,800	9,660	30.20	S.L.				0		0
17	CLIMB	139,300	9,160	30.15	0-.5	110			.8	.92	.008
18	CRUISE	135,471	5,330	30.0	.5	300		.4618	138.3	159.15	.454
19	DESCENT	131,500	1,360	29.8	5-0	82			3.1	3.57	.038
20	LANDING STOL	131,100	960	29.8	S.L.				0		0
21	LANDING ROLL	130,936	796	29.8	S.L.				0		0

OEW = 103,140  
 PAYLOAD = 62,000  
 FUEL = 51,540  
 TOGW = 216,680

TABLE B13  
 LOW-ALTITUDE RE SUPPLY FLIGHT PROFILE 3-2

SEG NO.	DESCRIPTION	AVERAGE		C.G. % MAC	ALTITUDE 10 <sup>3</sup> FT	AVG.		DISTANCE		TIME HOURS
		GROSS WT.	FUEL LB			KEAS	MACH NO.	NAUTICAL MILES	STATUTE MILES	
1	TAXI & TAKEOFF CTOL	216,000	50,850	26.3	S.L.					
2	CLIMB	215,550	50,360	26.3	0-.5	119		1.9	2.19	.016
3	CRUISE	210,998	45,858	26.1	.5	300	.4618	138.2	159.04	.454
4	DESCENT	206,400	41,260	26.0	.5-0	100		3.1	3.57	.031
5	LANDING CTOL	205,800	40,660	26.0	S.L.			0		0
6	LANDING & TAKEOFF CTOL	205,200	40,060	26.0	S.L.			0		0
7	CLIMB	204,500	39,360	25.9	0-.5	121		1.7	1.96	.014
8	CRUISE	200,120	349,80	25.5	.5	300	.4618	138.4	159.27	.455
9	DESCENT	195,600	30,460	25.3	.5-0	100		3.1	3.57	.031
10	LANDING CTOL	195,000	29,860	25.3	S.L.			0		0
11	LANDING & TAKEOFF CTOL	194,400	29,260	25.3	S.L.			0		0
12	CLIMB	193,900	28,760	25.25	0-.5	115		1.5	1.73	.013
13	CRUISE	189,525	24,385	25.00	.5	300	.4618	138.6	159.50	.455
14	DESCENT	185,100	19,960	24.6	.5-0	97		3.1	3.57	.032
15	LANDING CTOL	184,400	19,260	24.6	S.L.			0		0
16	LANDING & TAKEOFF CTOL	184,000	18,860	24.5	S.L.			0		0
17	CLIMB	183,500	18,360	24.45	0-.5	108		1.3	1.50	.012
18	CRUISE	179,000	14,060	24.20	.5	300	.4618	138.6	159.50	.455
19	DESCENT	174,900	9,760	23.9	.5-0	94		3.1	3.57	.033
20	LANDING	174,400	9,260	23.9	S.L.			0		0
21	LANDING ROLL	174,180	9,040	23.9	S.L.			0		0

## APPENDIX C

The following shear and moment curves are the external loads that were applied to the idealized computer model to generate internal structural member loads. Figures C1 and C2 identify the ultimate static value for each fuselage station which has the most positive and most negative value. Figures C3 through C26 are the shear and moment curves for each individual unit fatigue condition. Figures C27 through C34 are the shear and moment curves for each individual ultimate static condition.

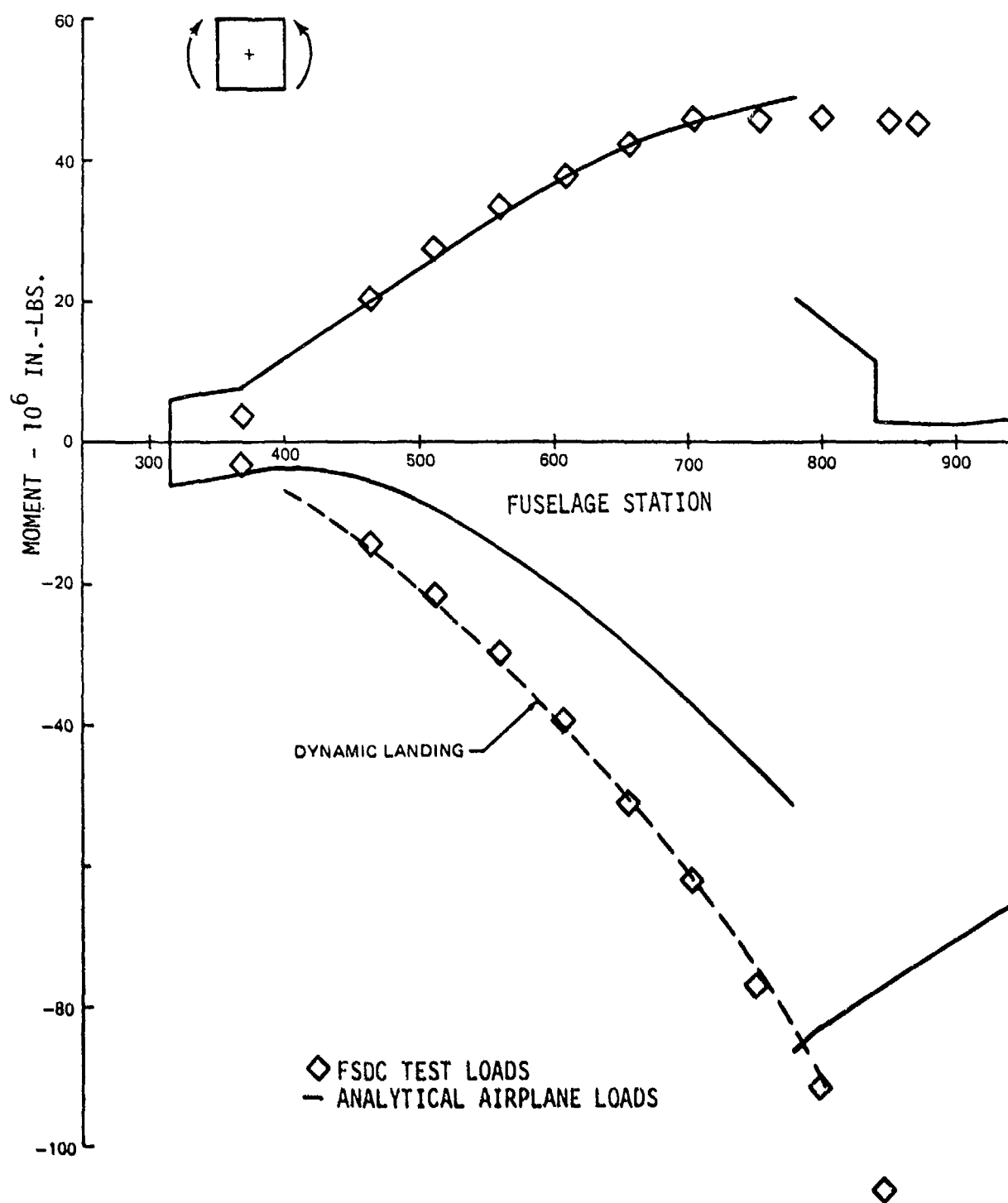


FIGURE C1. VERTICAL BENDING MOMENT - PABST MAX-MIN ULTIMATE

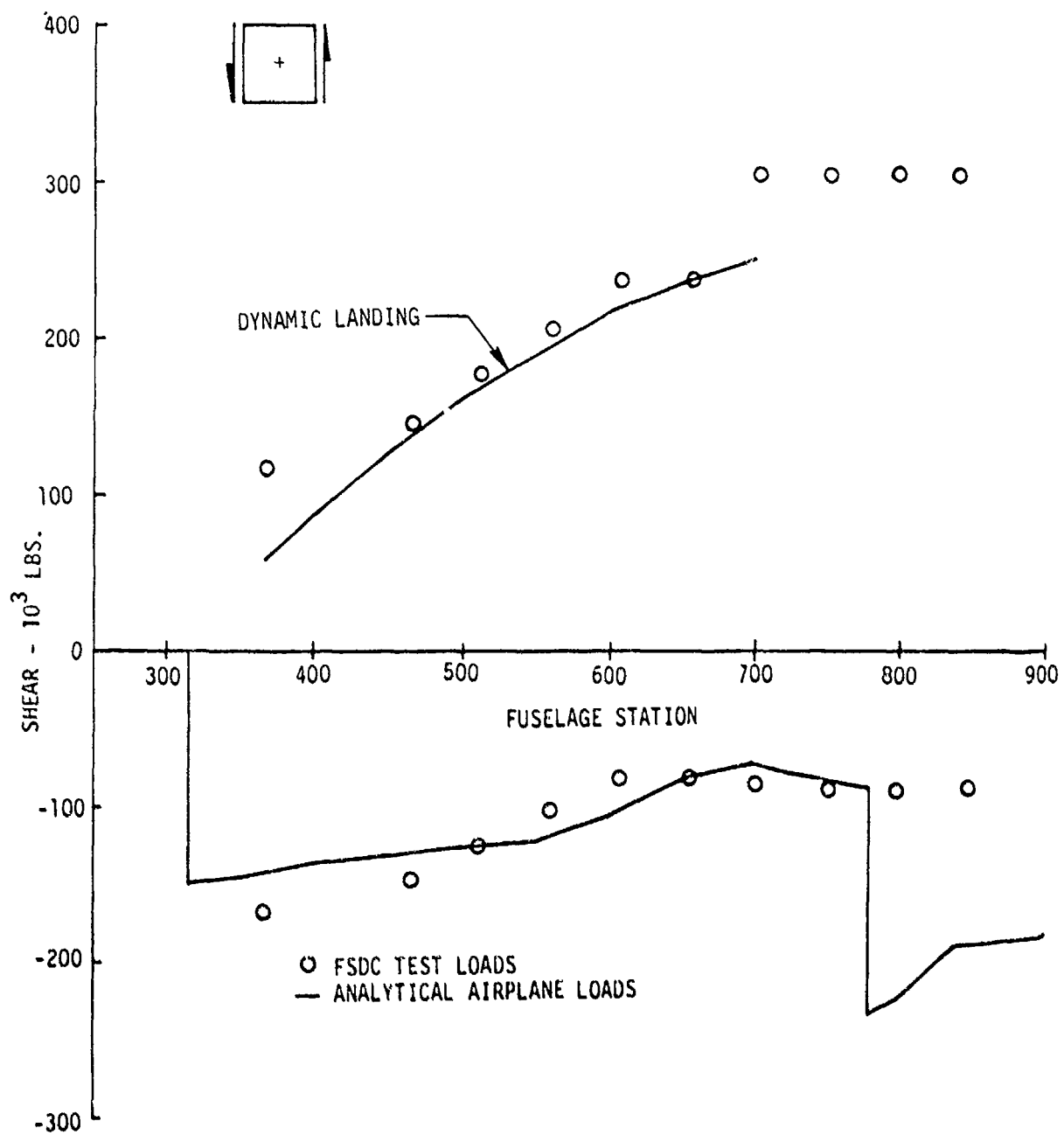


FIGURE C2. VERTICAL SHEAR - PABST MAX-MIN ULTIMATE

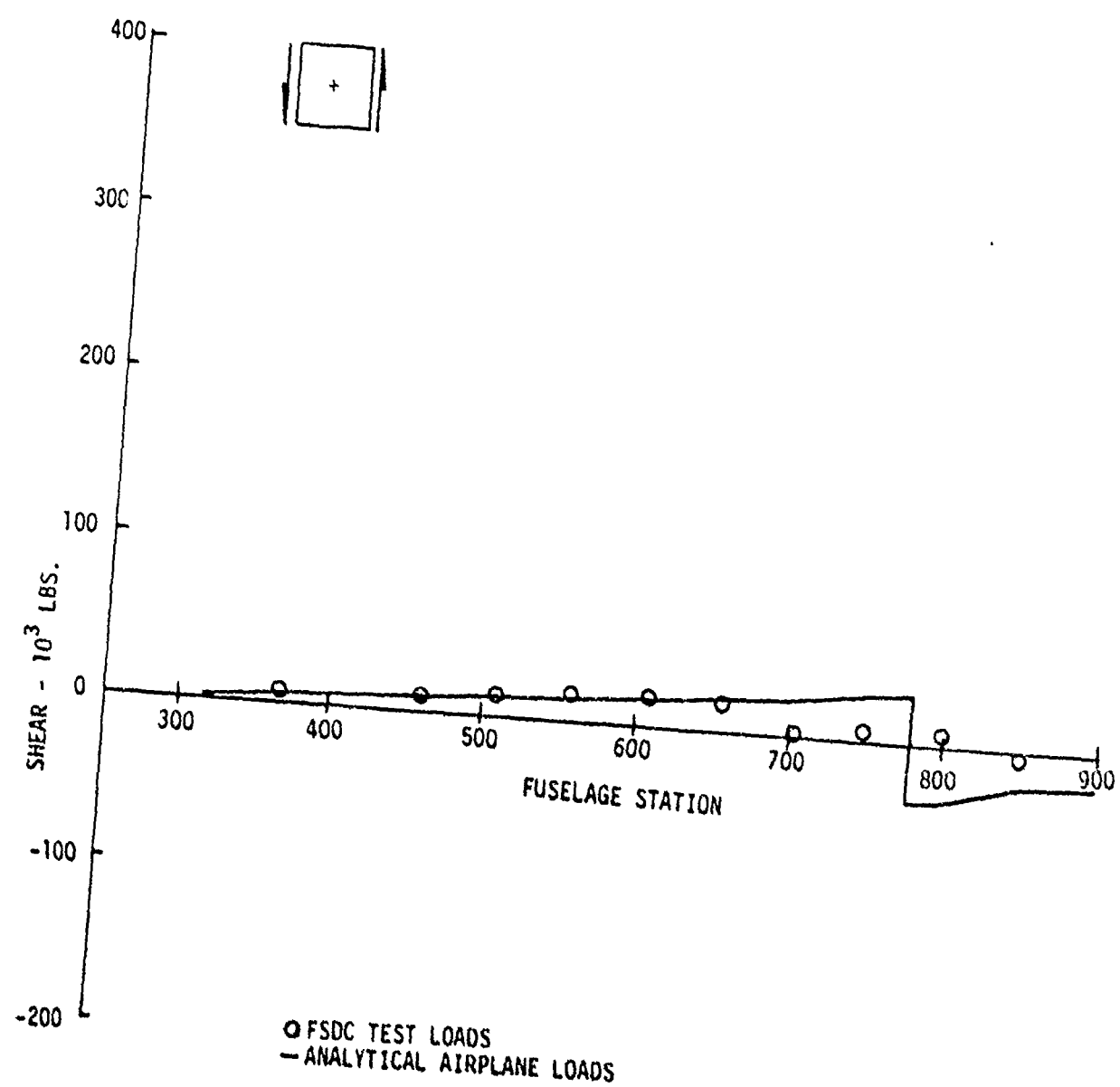


FIGURE C3. VERTICAL SHEAR - CONDITION 15 FG (2) FATIGUE CONDITION (LIMIT)

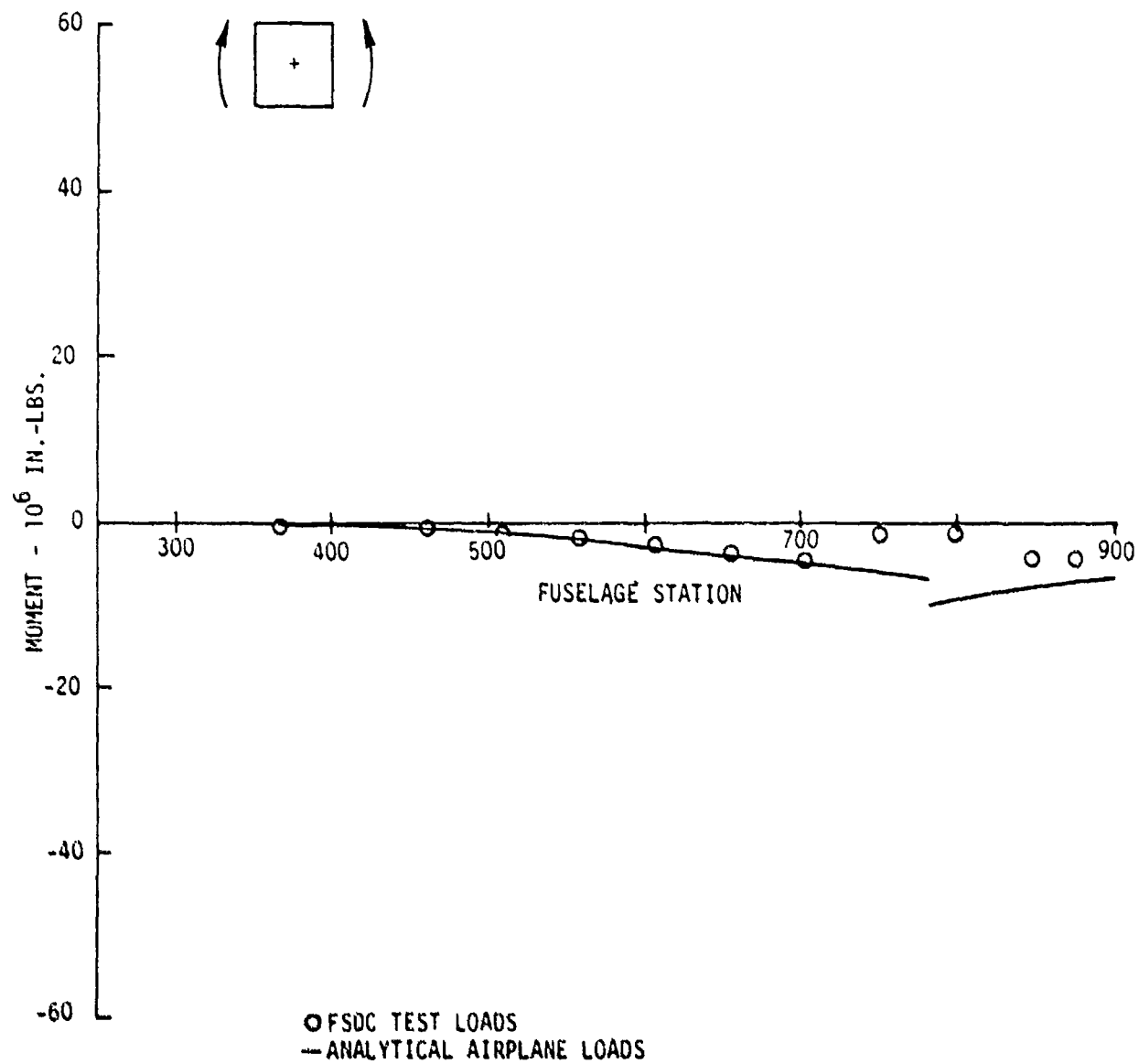


FIGURE C4. VERTICAL BENDING MOMENT - CONDITION 15 FG (2)  
FATIGUE CONDITION (LIMIT)

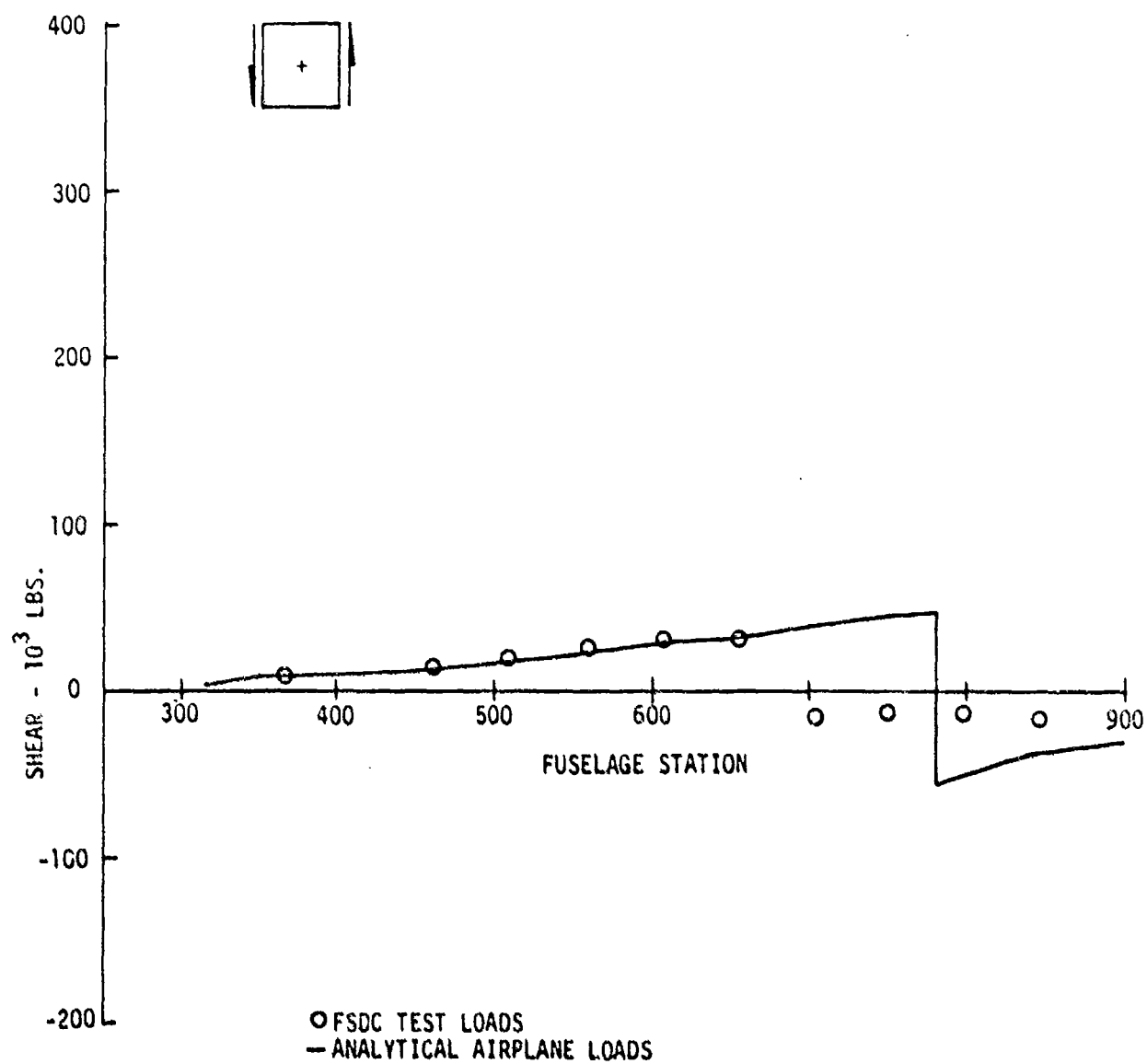


FIGURE C5. VERTICAL SHEAR - CONDITION 16 FG (3) FATIGUE CONDITION (LIMIT)

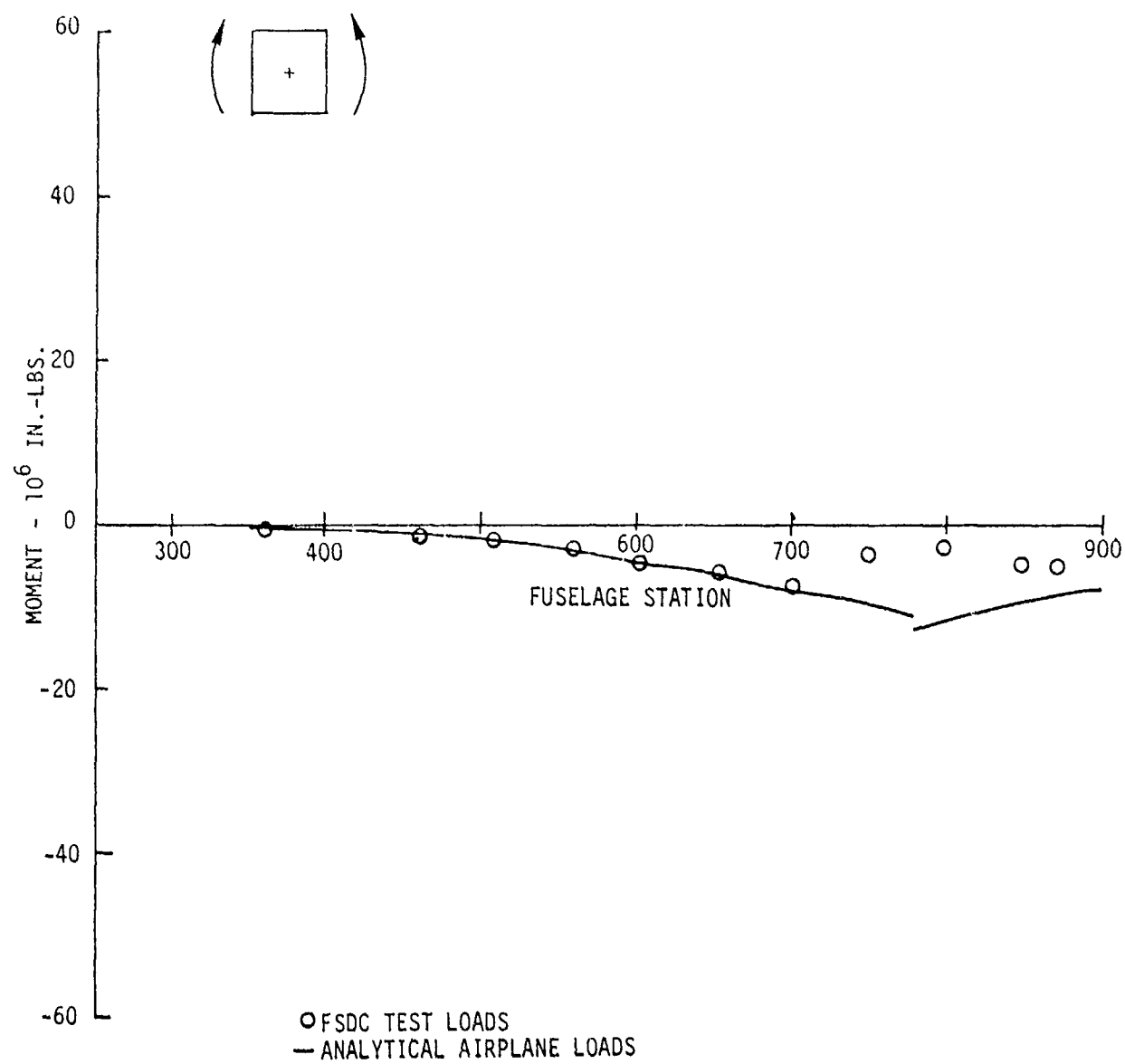


FIGURE C6. VERTICAL BENDING MOMENT — CONDITION 16 FG (3) CONDITION (LIMIT)

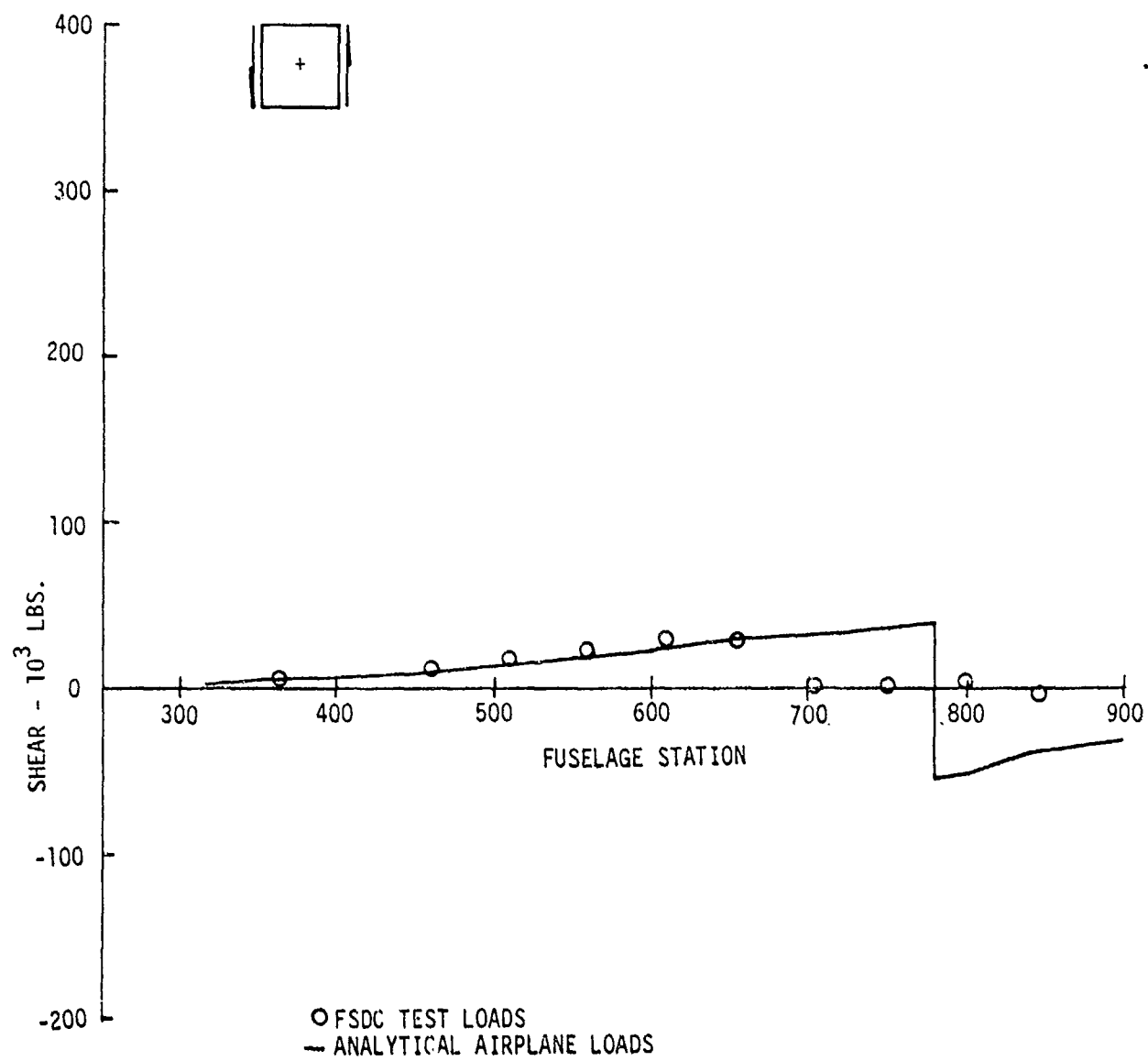


FIGURE C7. VERTICAL SHEAR - CONDITION 19 FG (4) FATIGUE CONDITION (LIMIT)

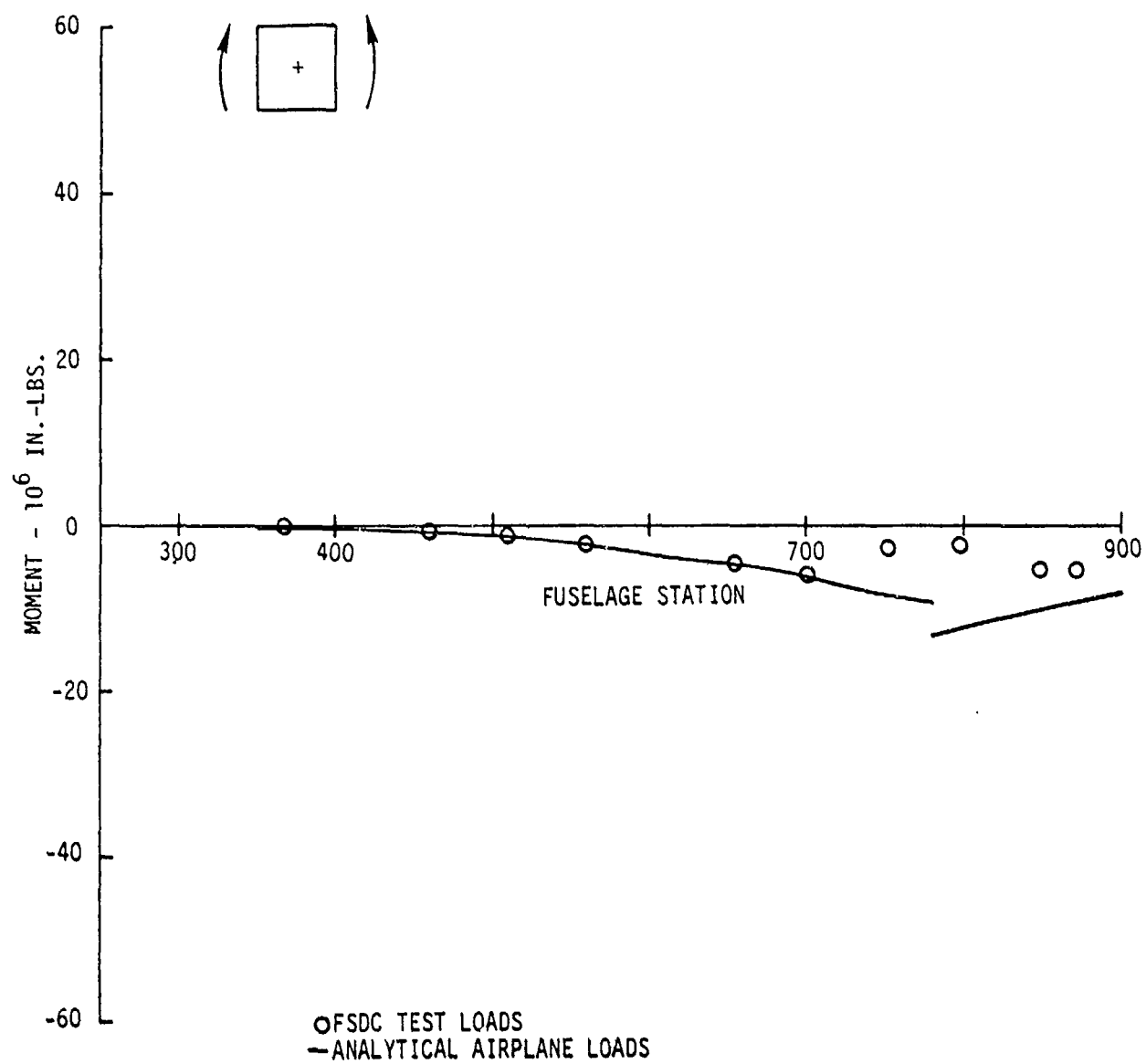


FIGURE C8. VERTICAL BENDING MOMENT - CONDITION 19 FG (4) FATIGUE CONDITION (LIMIT)

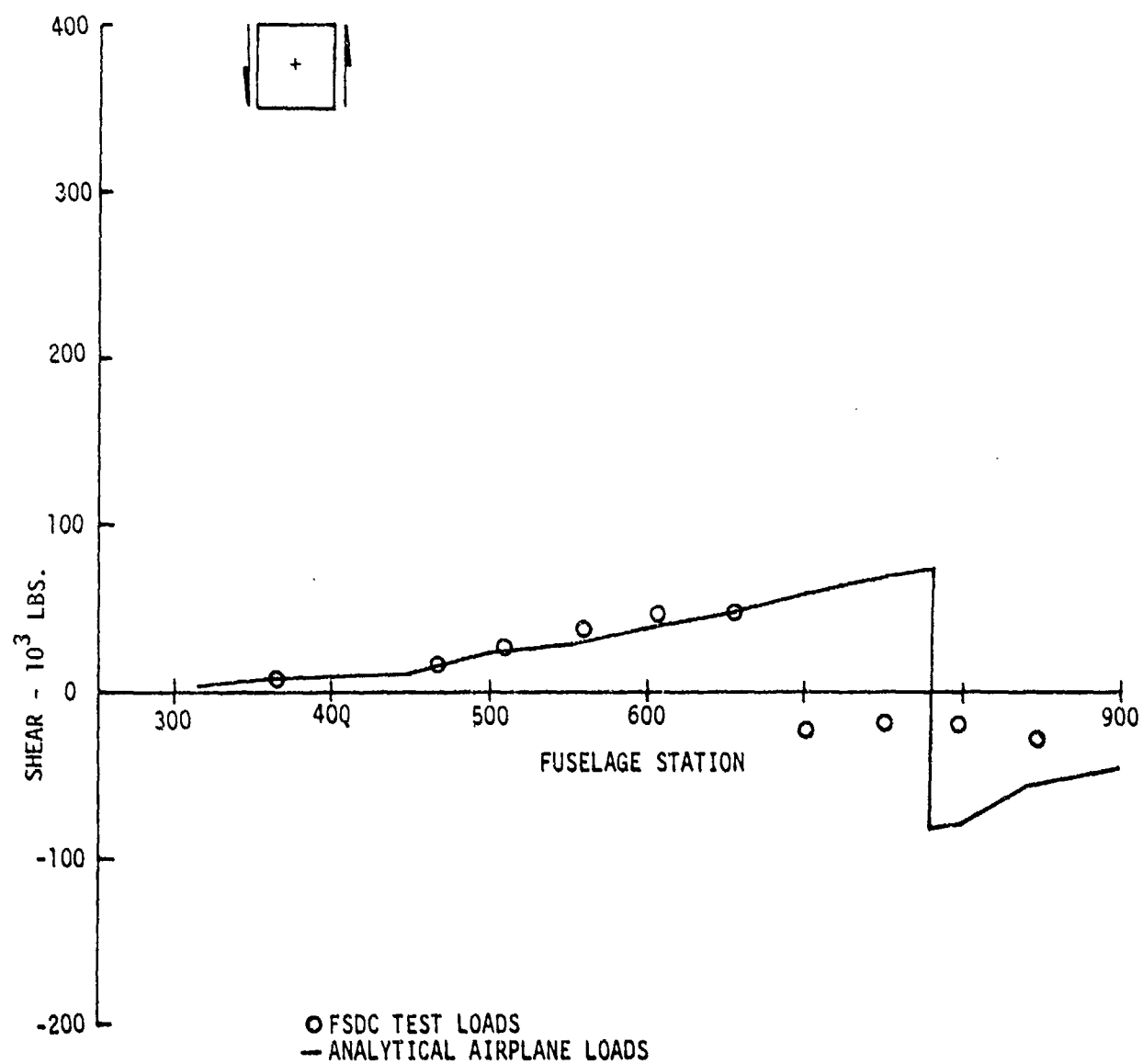


FIGURE C9. VERTICAL SHEAR - CONDITION 20 FG (5) FATIGUE CONDITION (LIMIT)

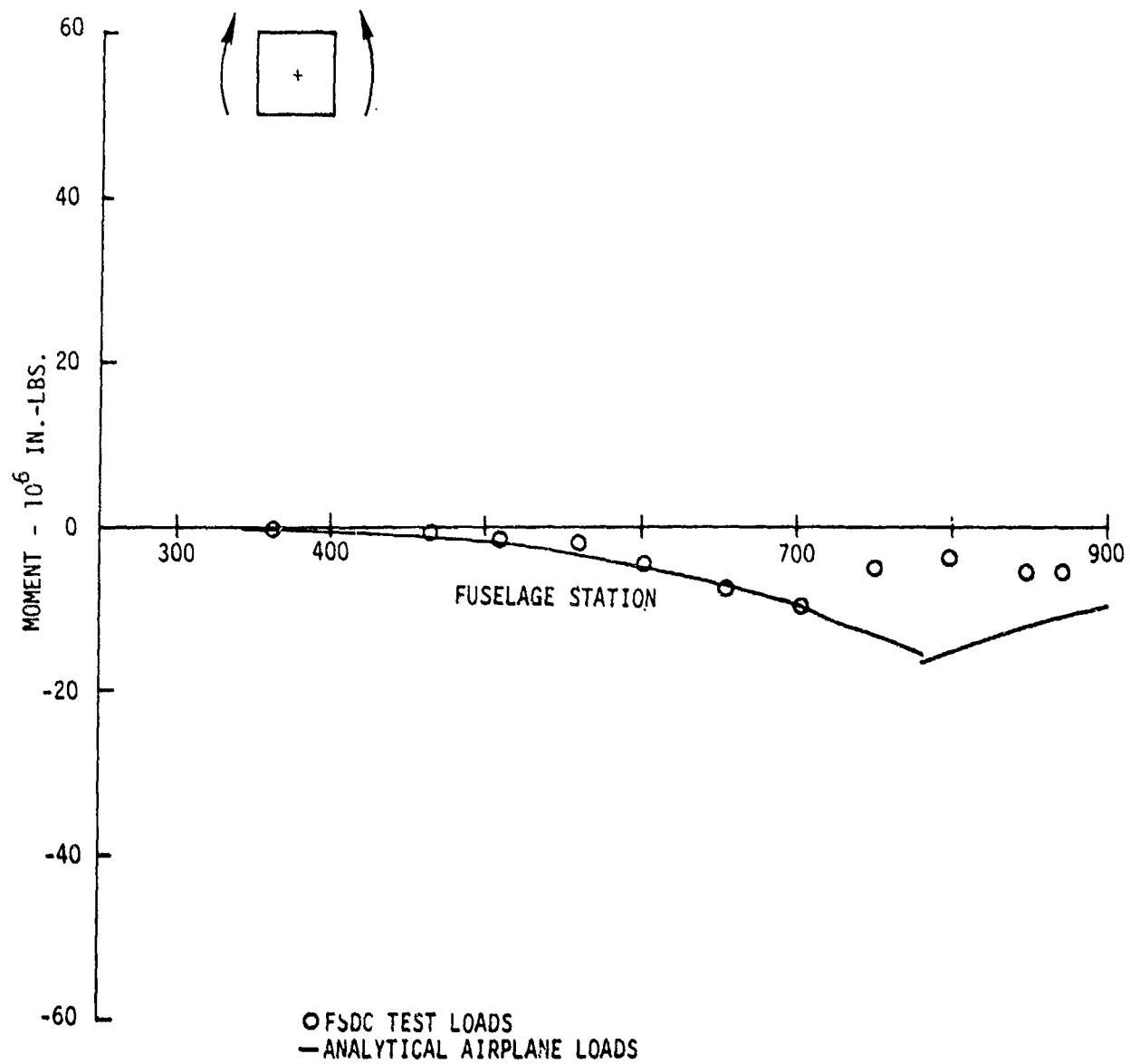


FIGURE C10. VERTICAL BENDING MOMENT - CONDITION 20 FG (5) FATIGUE CONDITION (LIMIT)

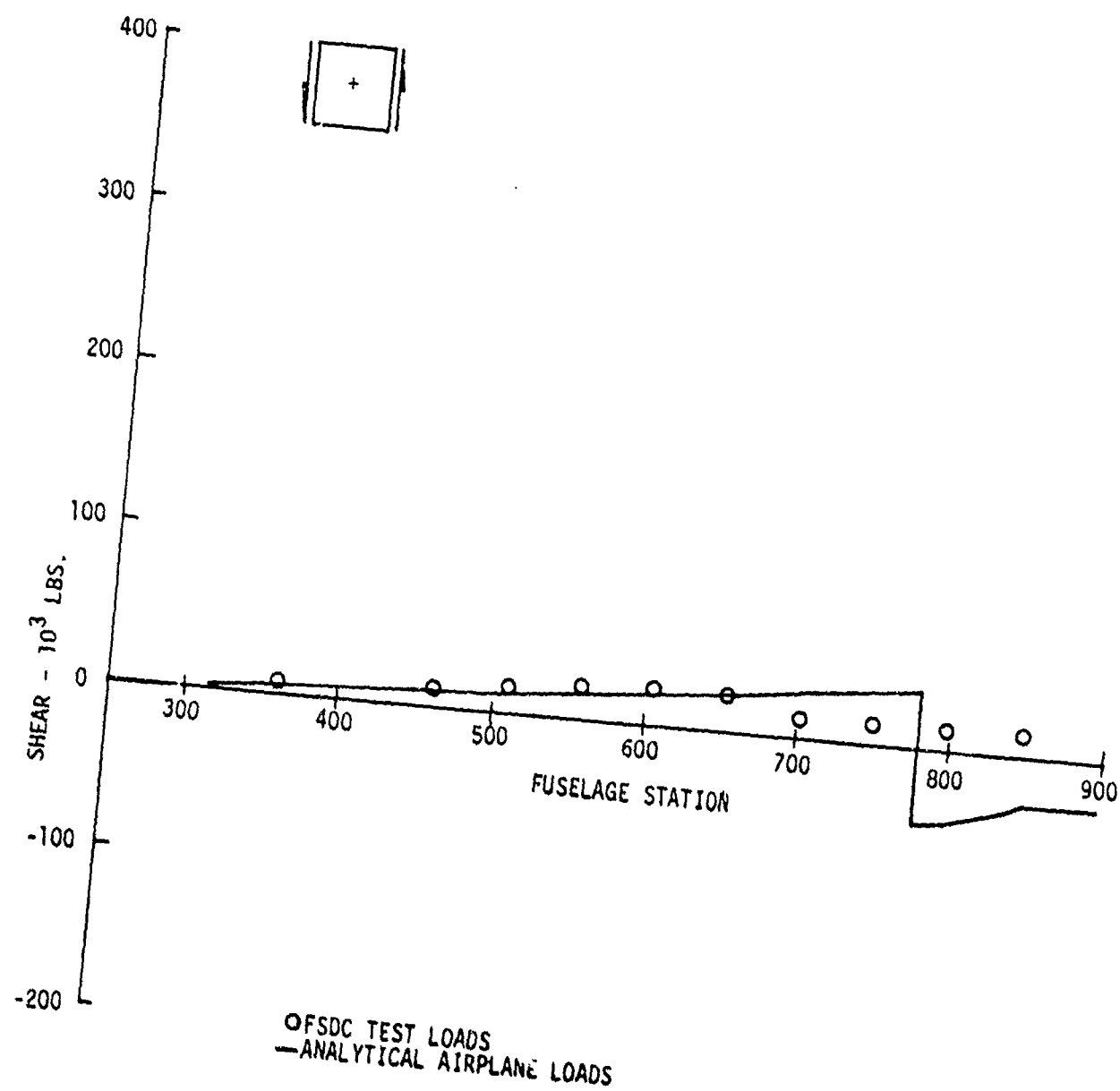


FIGURE C11. VERTICAL SHEAR - CONDITION 27 FG (8) FATIGUE CONDITION (LIMIT)

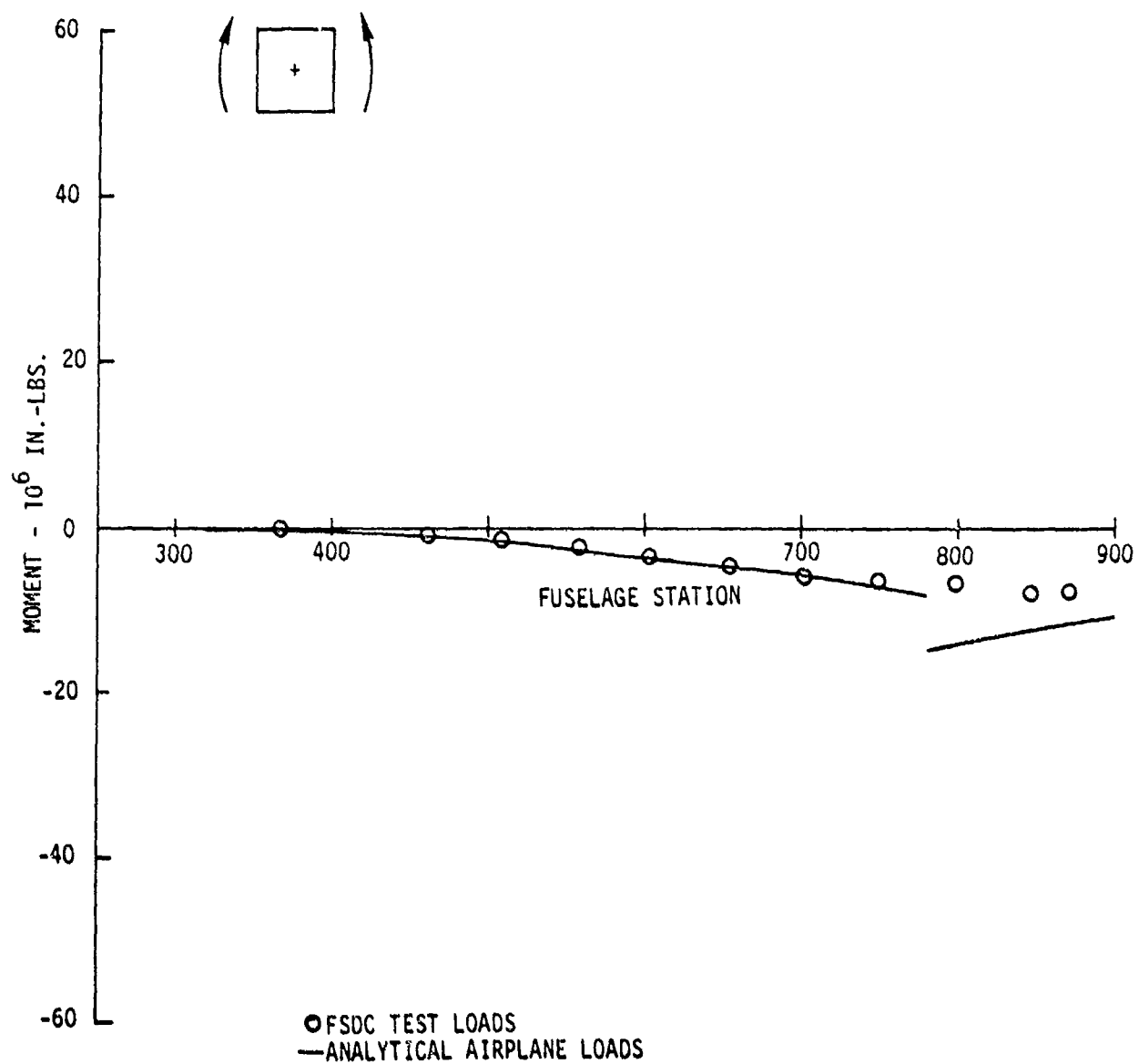


FIGURE C12. VERTICAL BENDING MOMENT - CONDITION 27 FG (6) FATIGUE CONDITION (LIMIT)

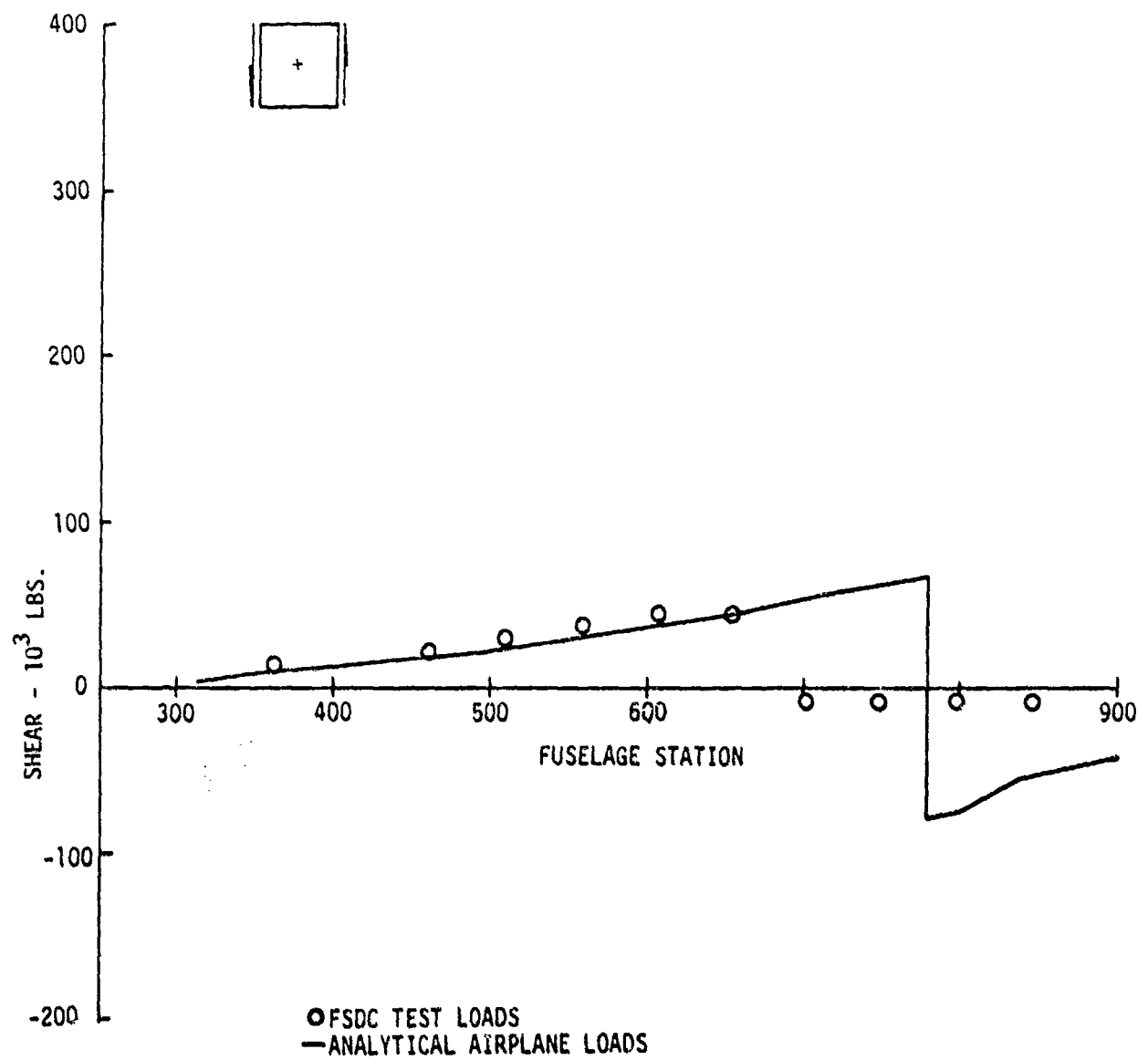


FIGURE C13. VERTICAL SHEAR - CONDITION 28 FG (7) FATIGUE CONDITION (LIMIT)

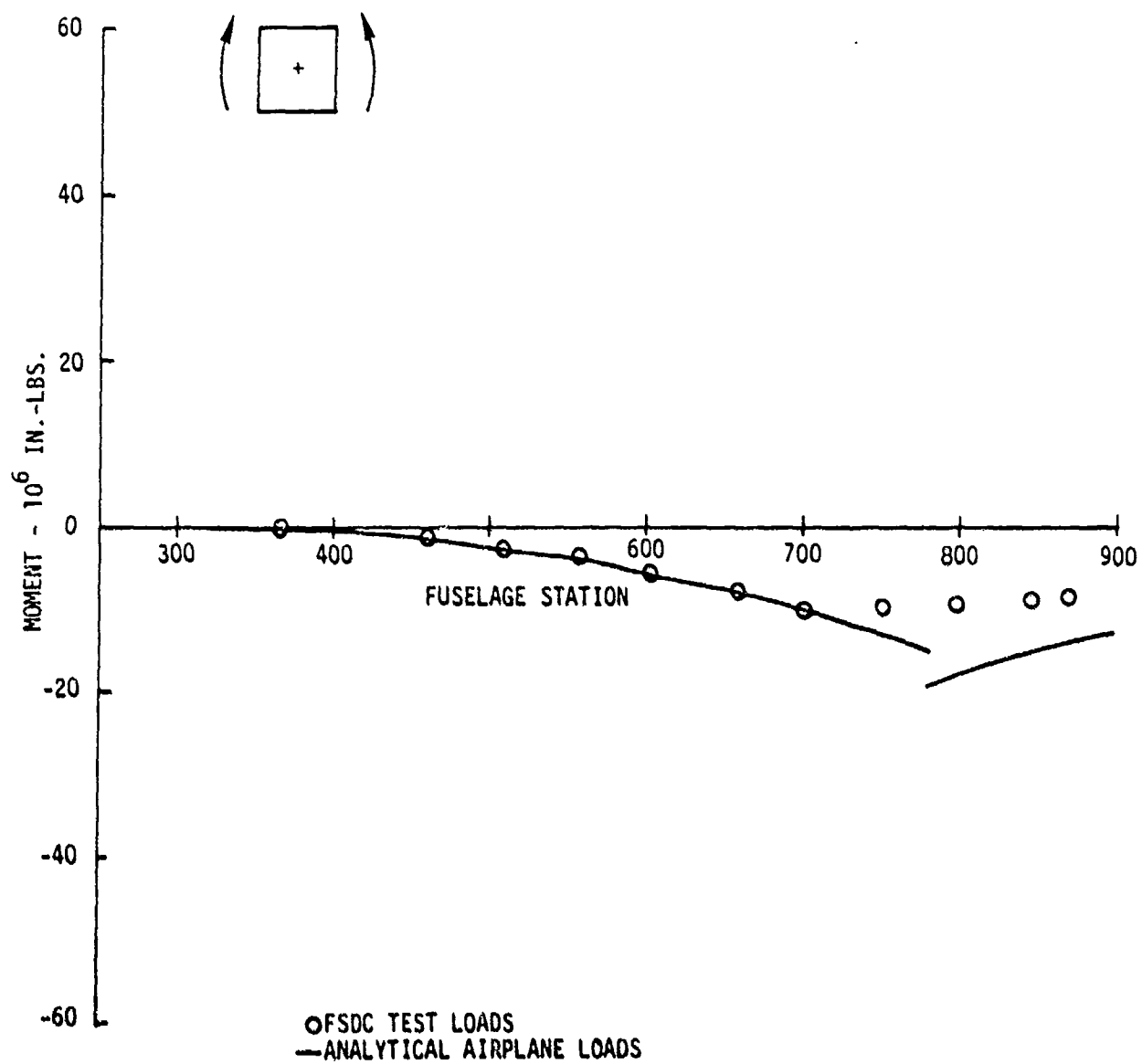


FIGURE C14. VERTICAL BENDING MOMENT - CONDITION 28 FG (7) FATIGUE CONDITION (LIMIT)

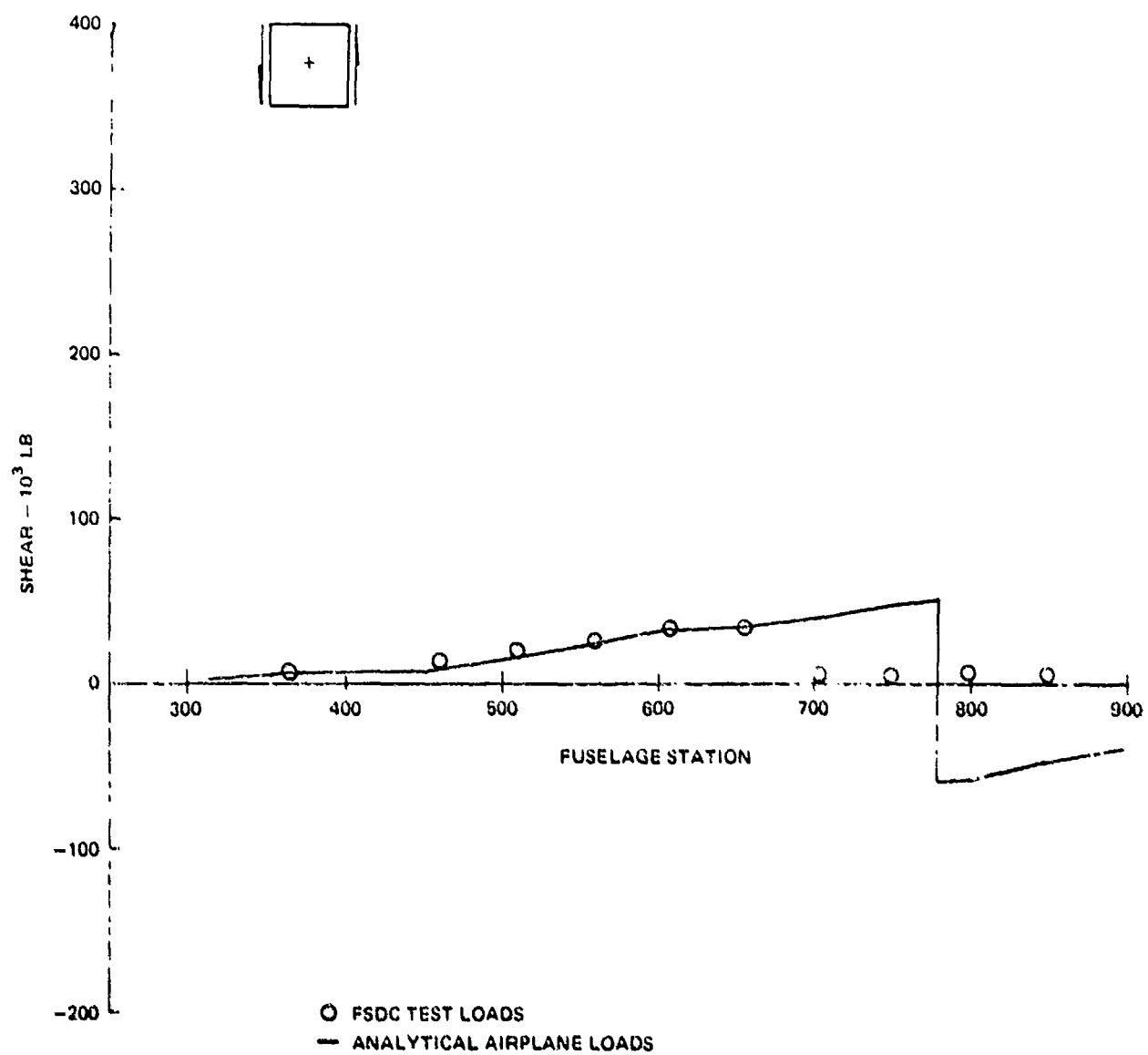


FIGURE C15. VERTICAL SHEAR-CONDITION 39FG (8) FATIGUE CONDITION (LIMIT)

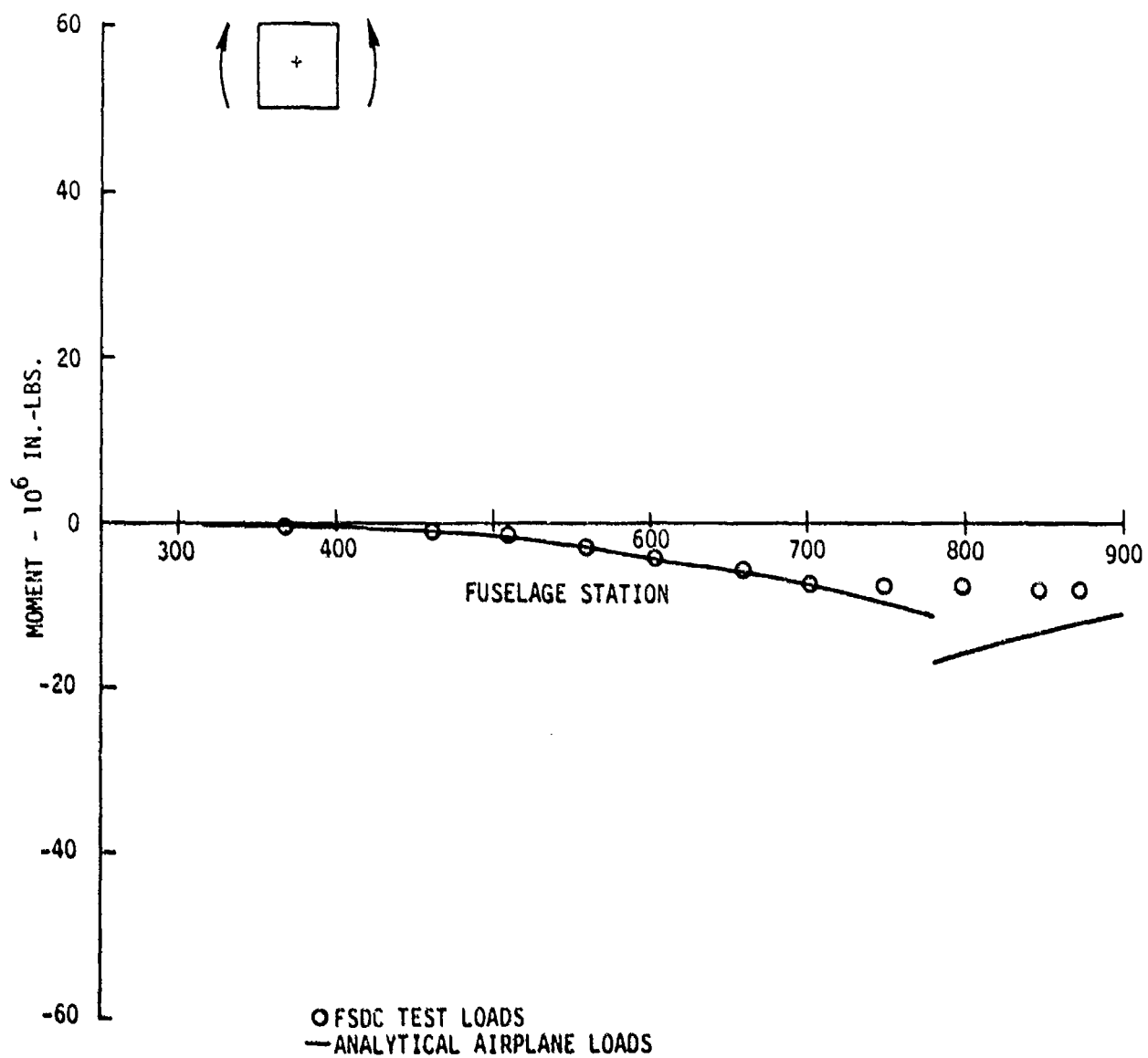


FIGURE C16. VERTICAL BENDING MOMENT - CONDITION 39 FG (8) FATIGUE CONDITION (LIMIT)

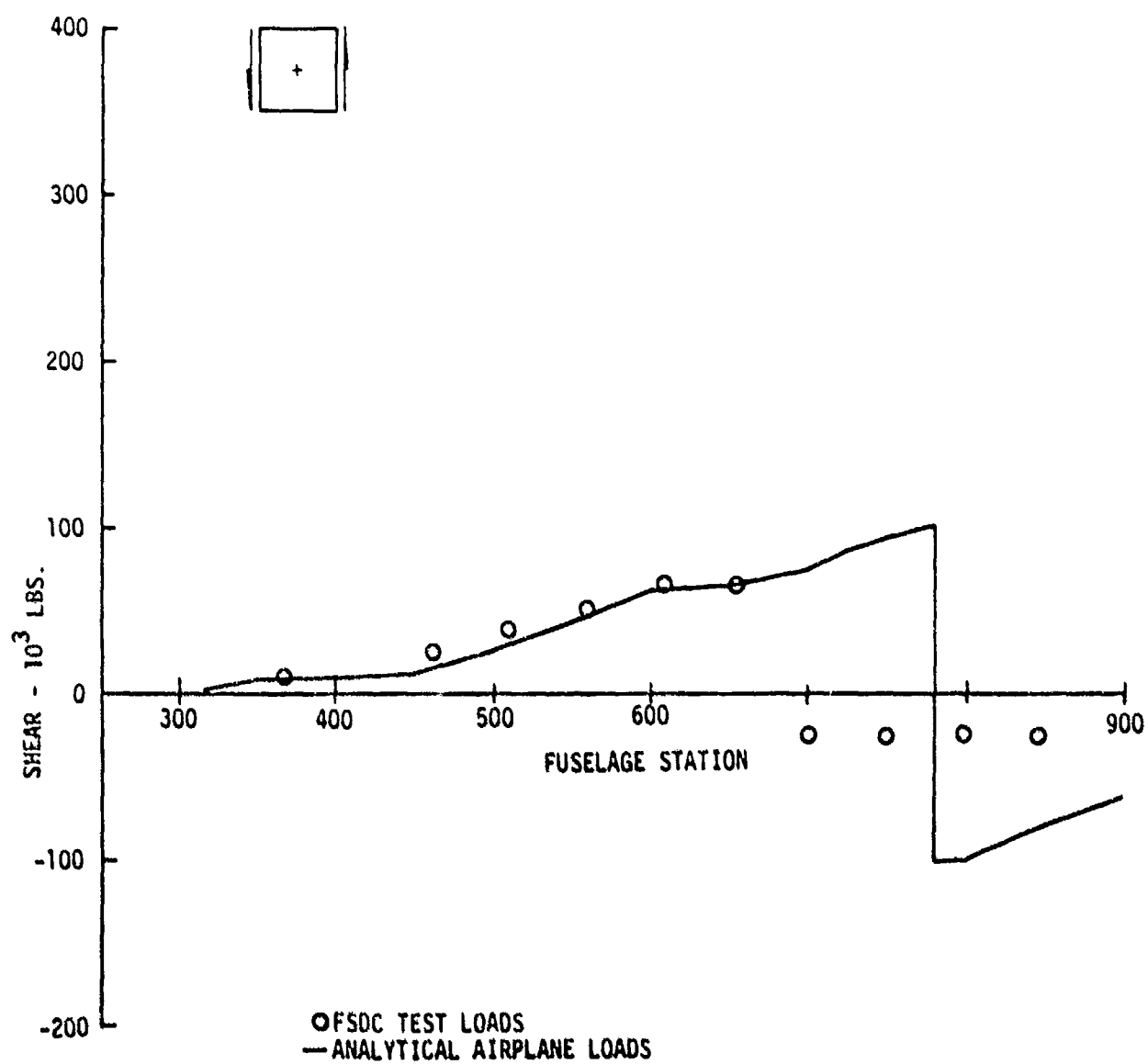


FIGURE C17. VERTICAL SHEAR -- CONDITION 40 FG (9) FATIGUE CONDITION (LIMIT)

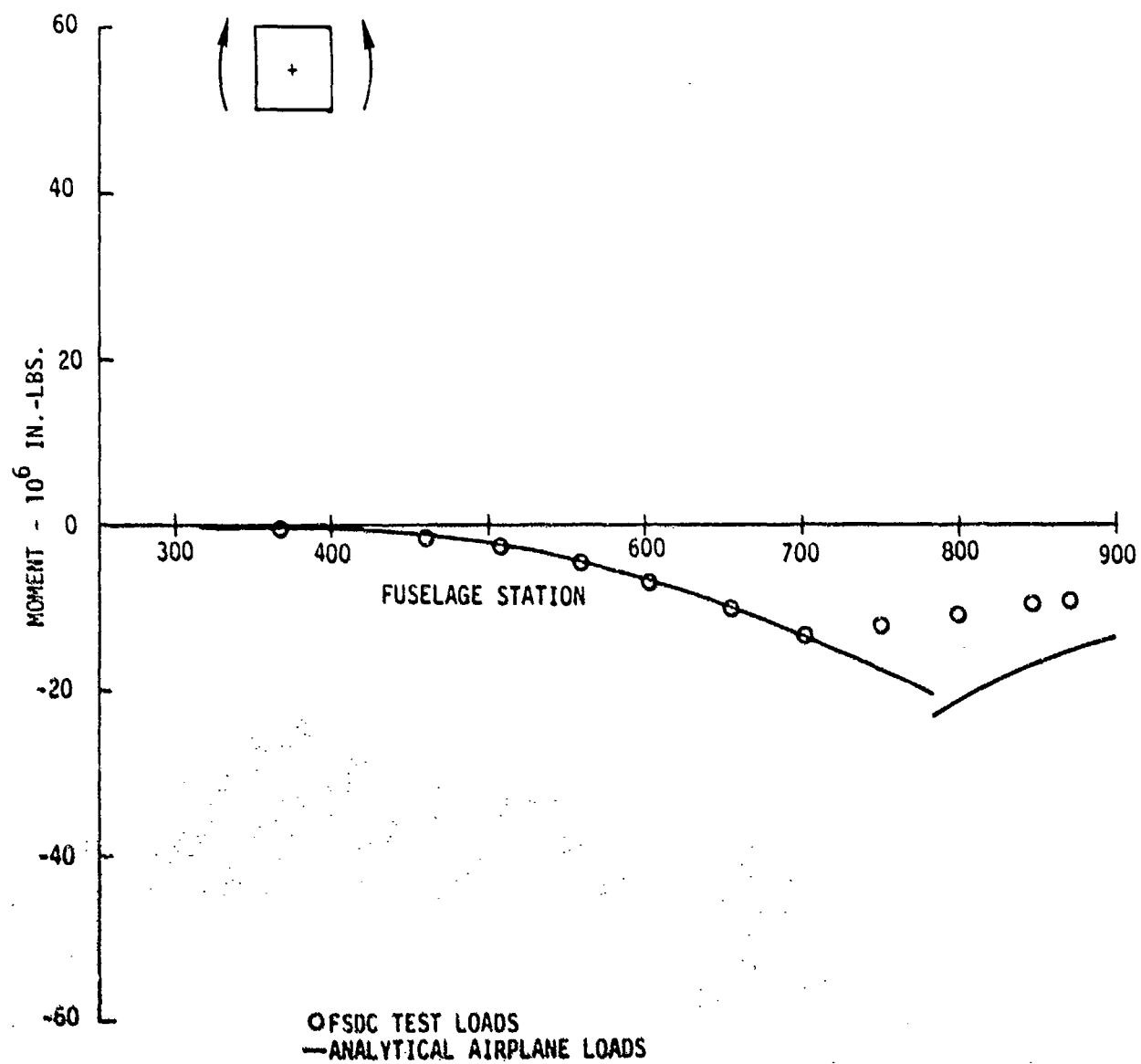


FIGURE C18. VERTICAL BENDING MOMENT - CONDITION 40 FG (9) FATIGUE CONDITION (LIMIT)

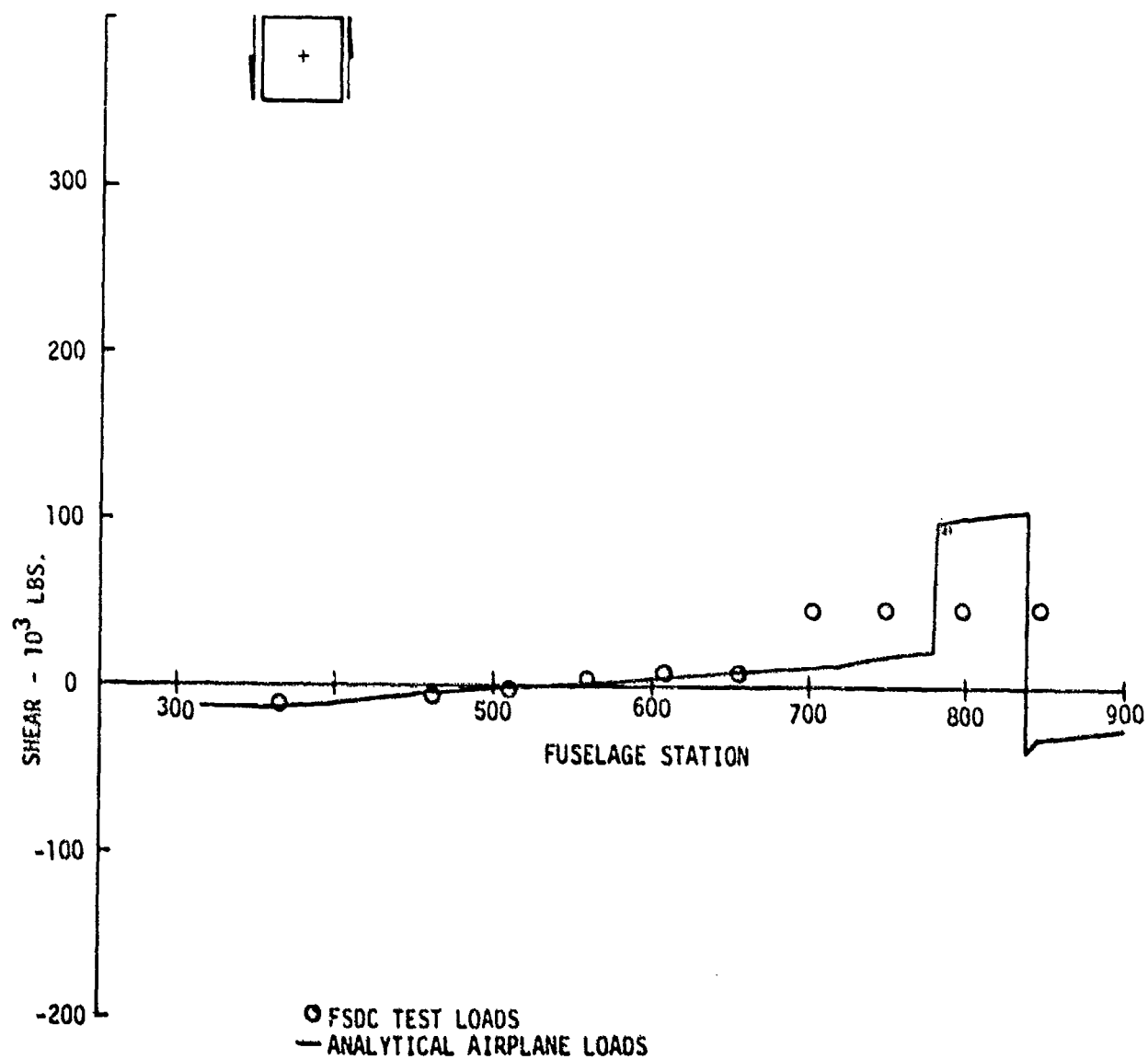


FIGURE C19. VERTICAL SHEAR - CONDITION 1 FG (10) FATIGUE CONDITION (LIMIT)

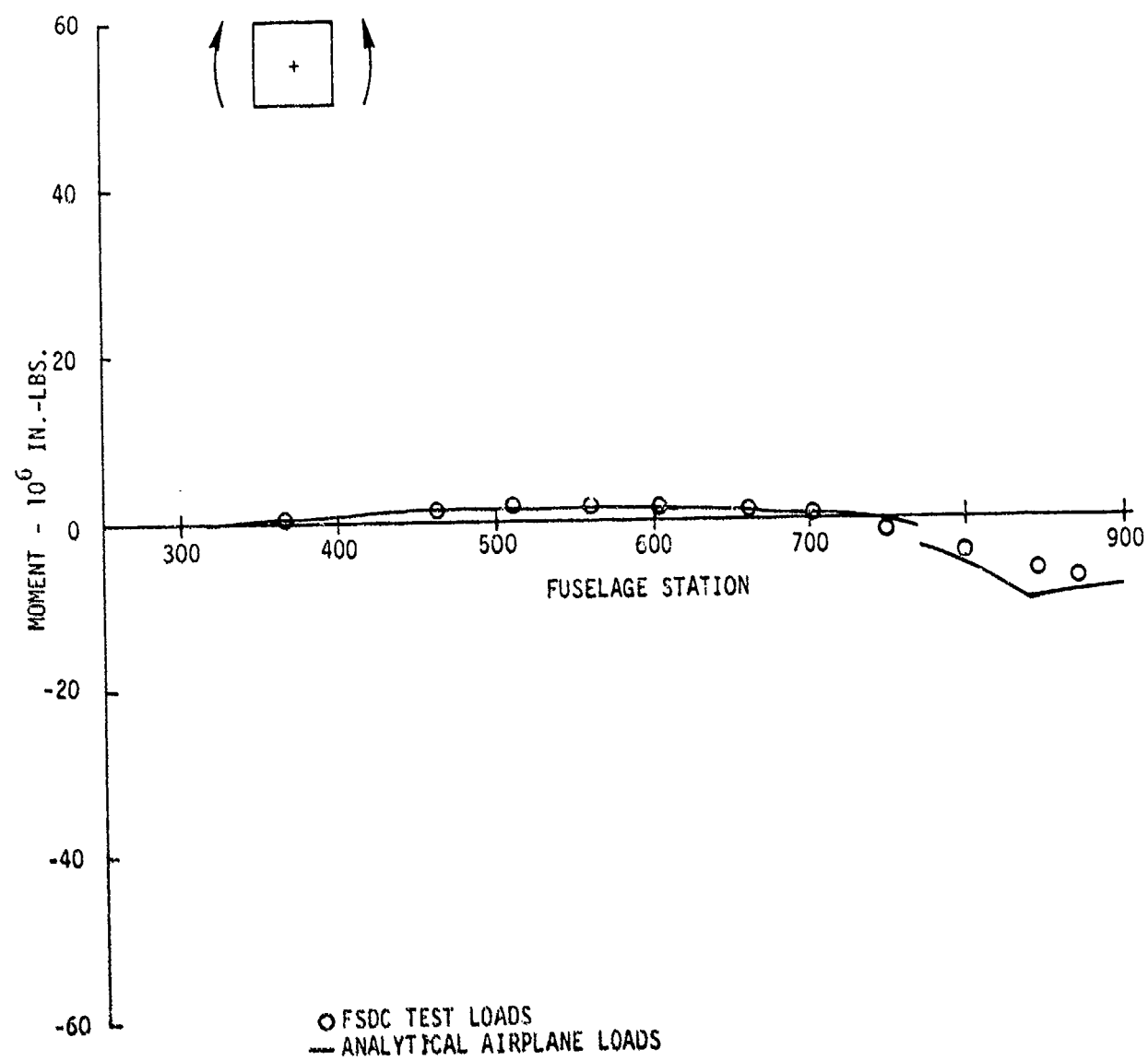


FIGURE C20. VERTICAL BENDING MOMENT -- CONDITION 1 FG (10) FATIGUE CONDITION (LIMIT)

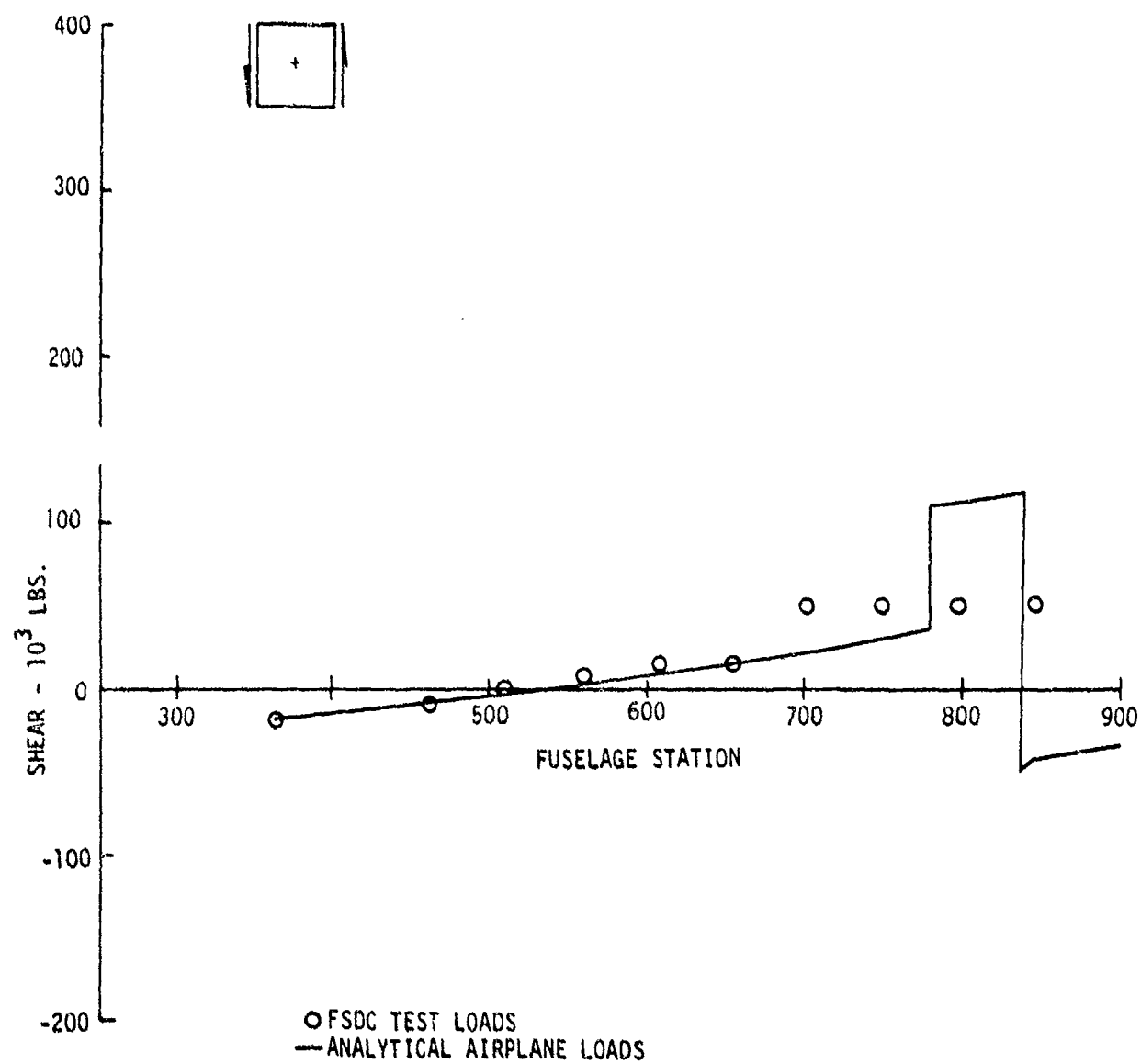


FIGURE C21. VERTICAL SHEAR - CONDITION 3 FG (11) FATIGUE CONDITION (LIMIT)

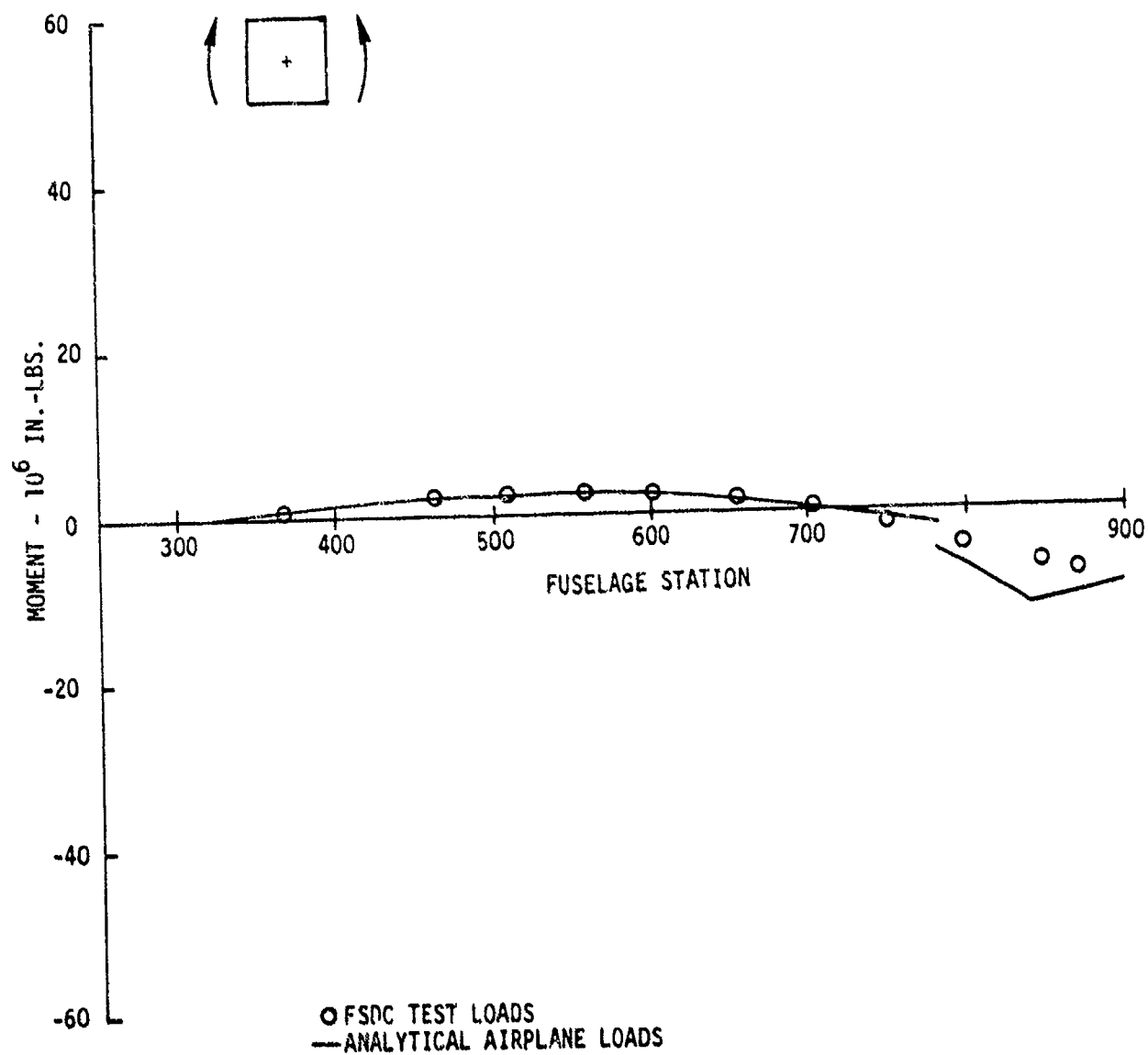


FIGURE C22. VERTICAL BENDING MOMENT -- CONDITION 3 FG (11) FATIGUE CONDITION (LIMIT)

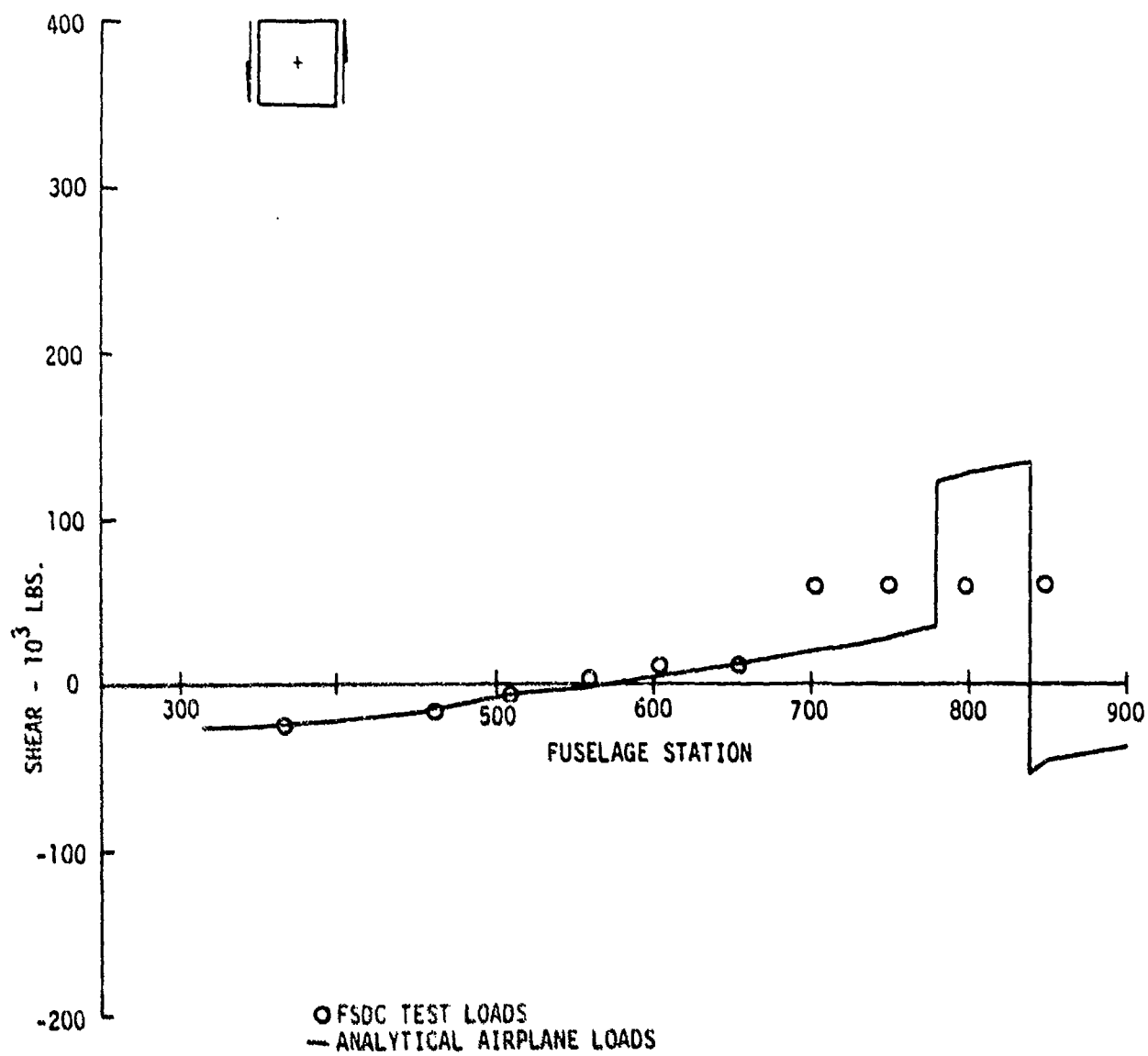


FIGURE C23. VERTICAL SHEAR - CONDITION 11 FG (12) FATIGUE CONDITION (LIMIT)

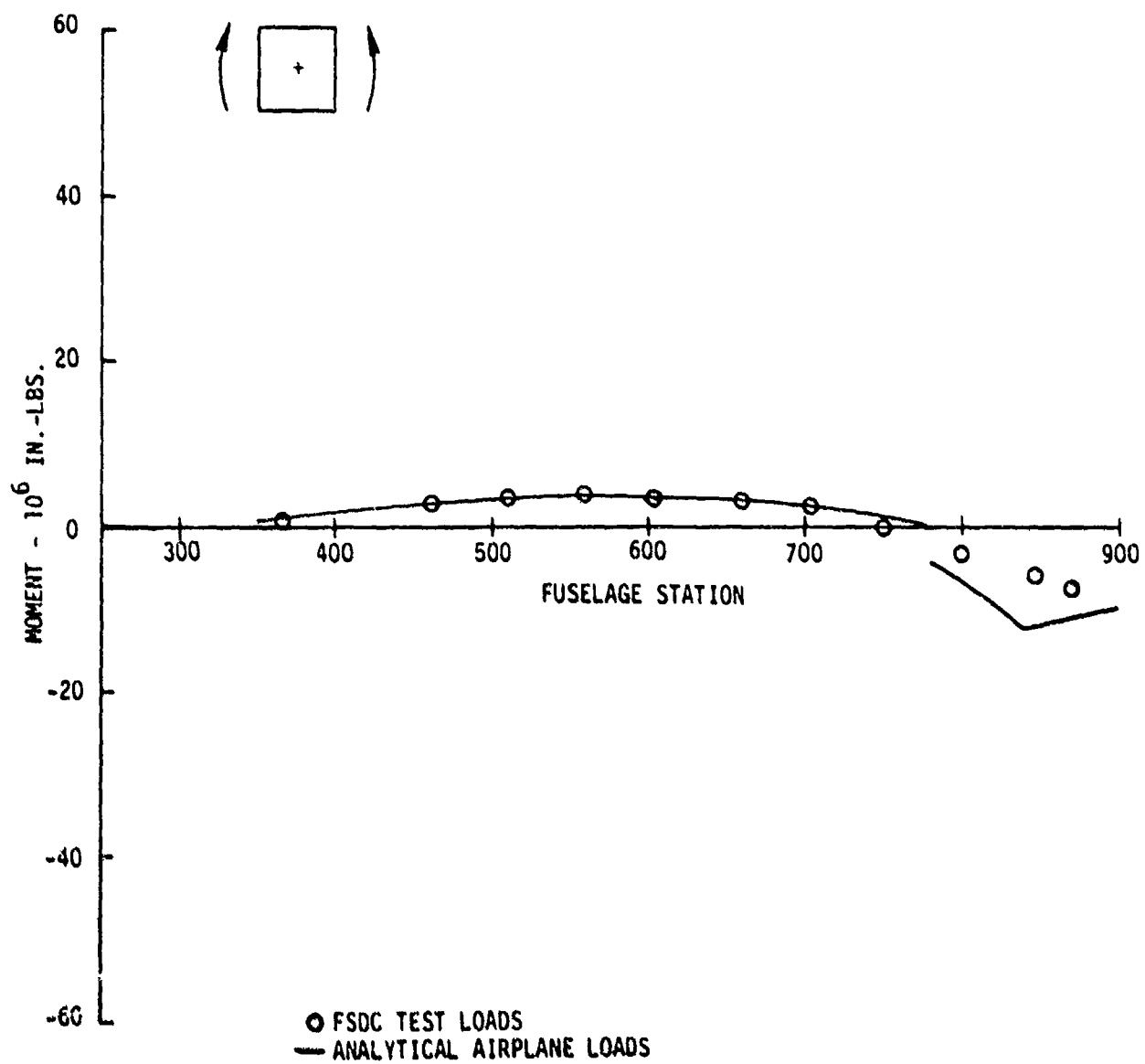


FIGURE C24. VERTICAL BENDING MOMENT - CONDITION 11 FG (12) FATIGUE CONDITION (LIMIT)

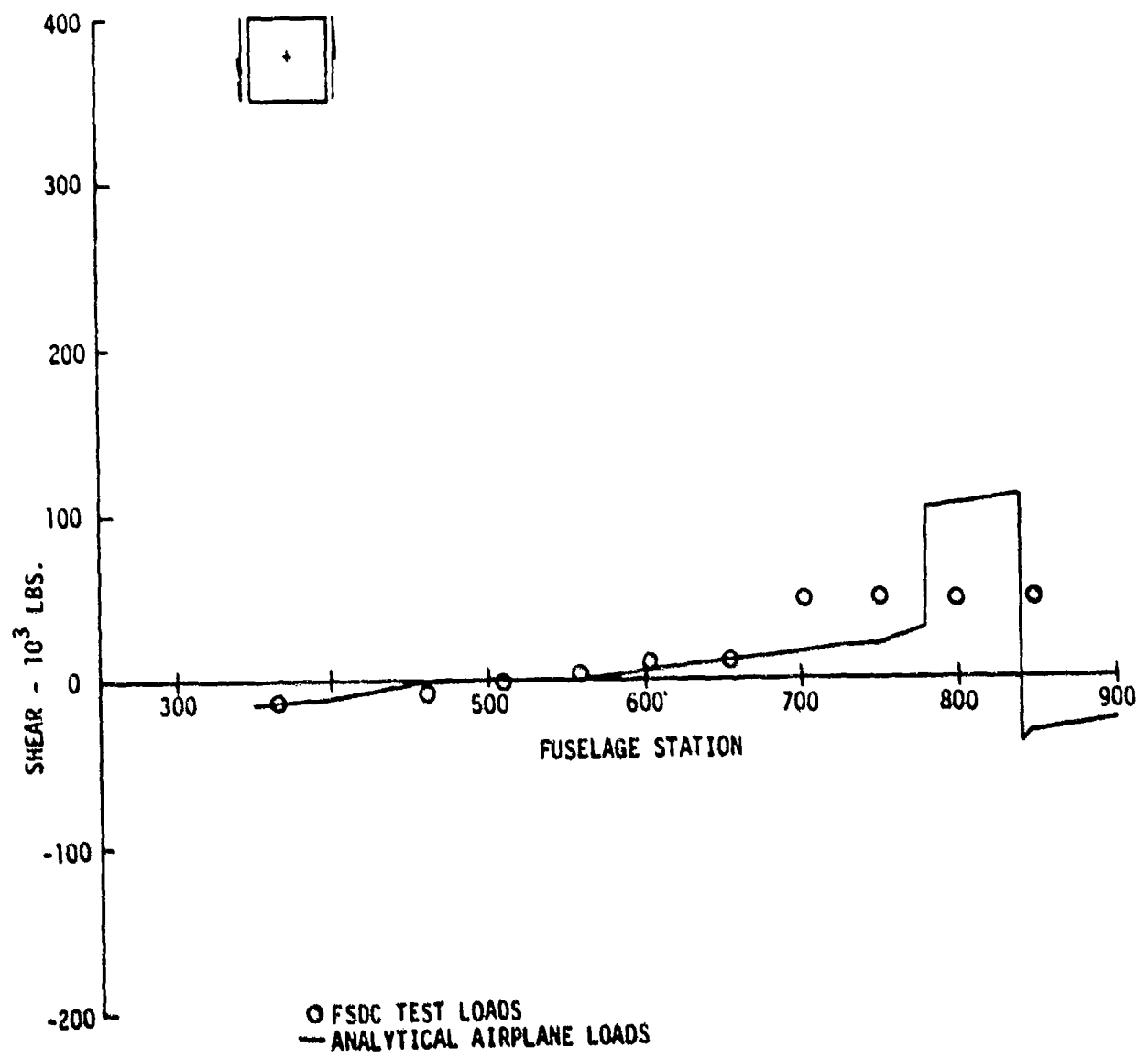


FIGURE C25. VERTICAL SHEAR - CONDITION 7 FG (13) FATIGUE CONDITION (LIMIT)

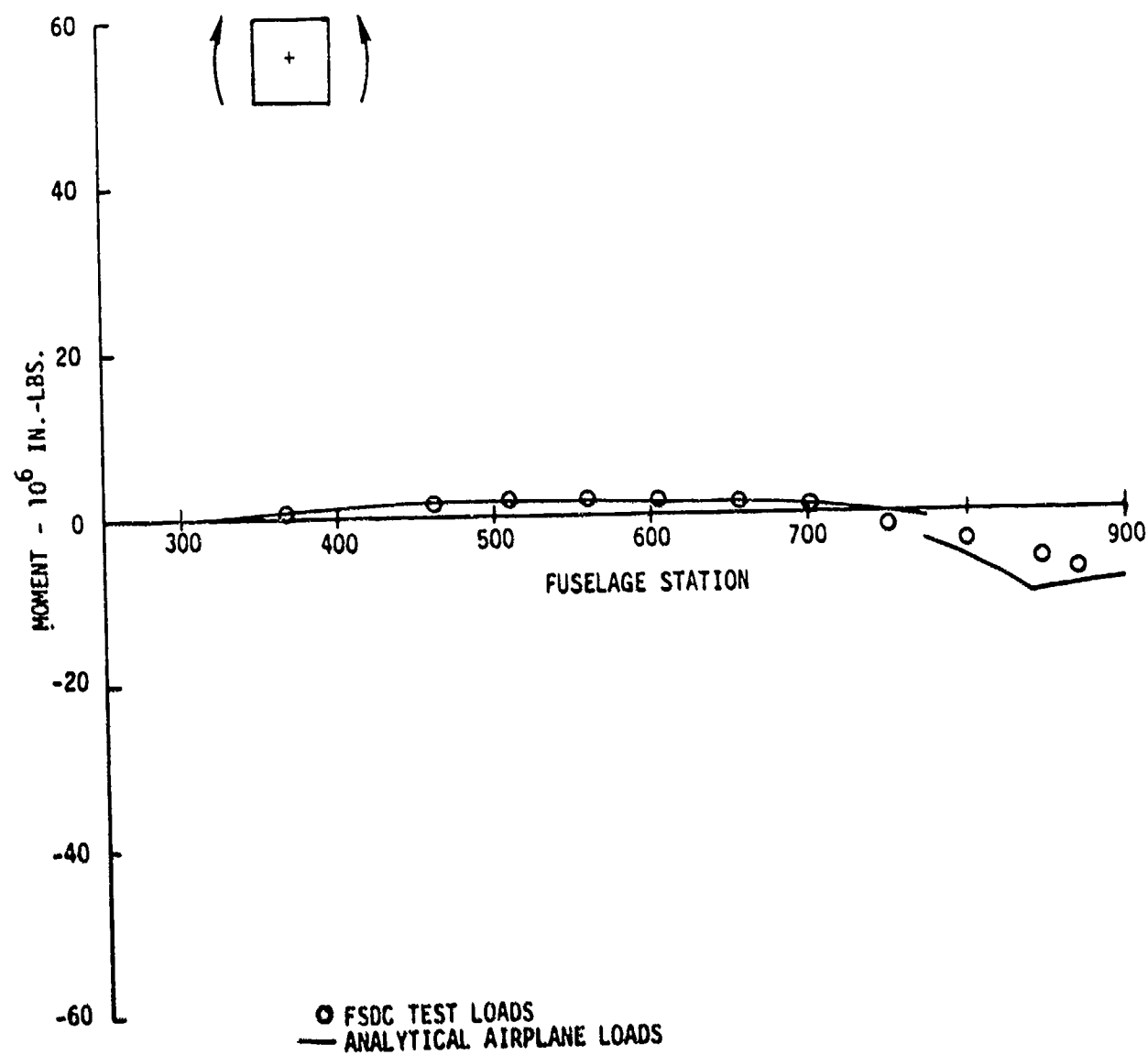


FIGURE C28. VERTICAL BENDING MOMENT – CONDITION 7 FG (13) FATIGUE CONDITION (LIMIT)

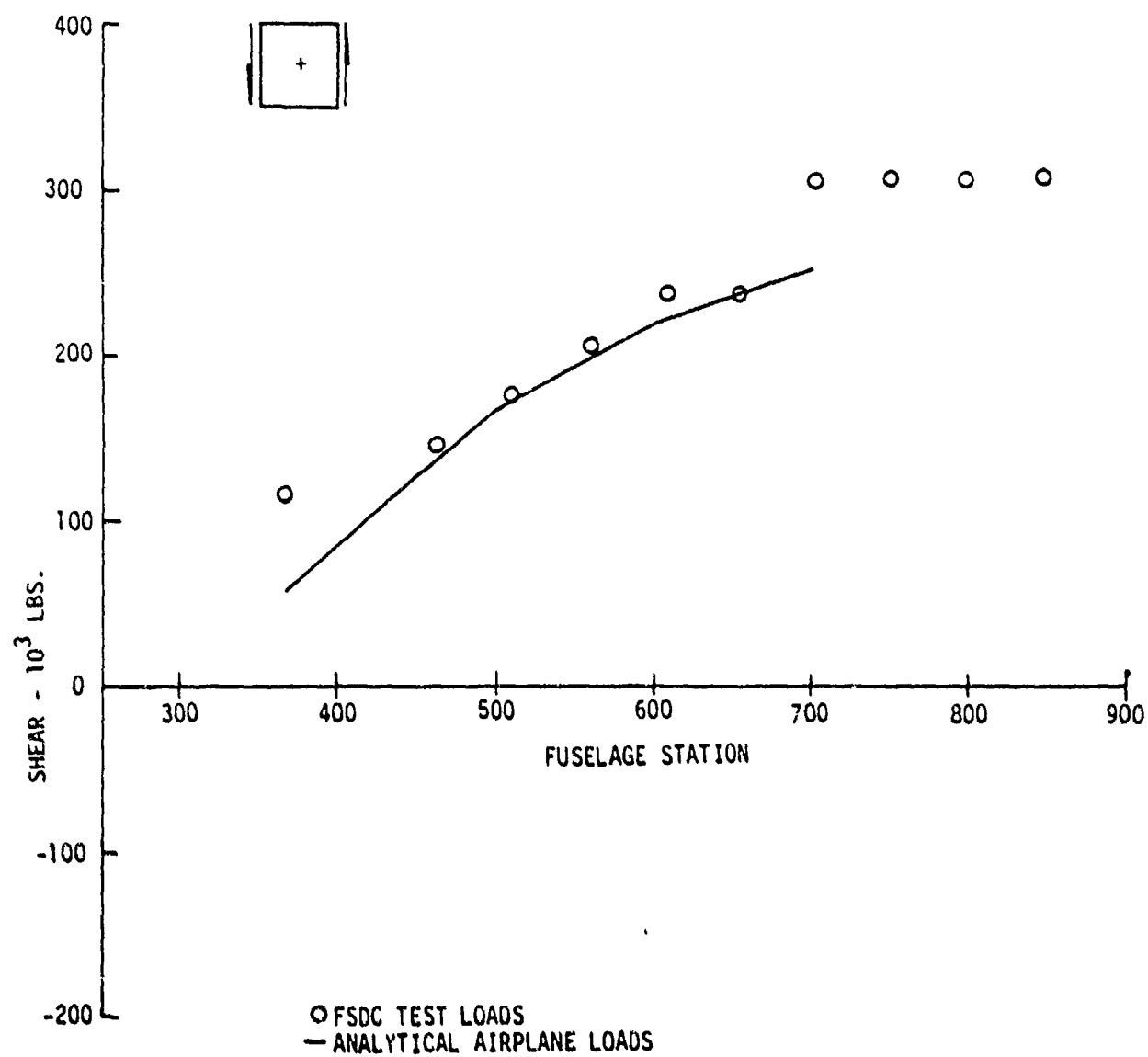


FIGURE C27. VERTICAL SHEAR - CONDITION F525.119 (14) ULTIMATE

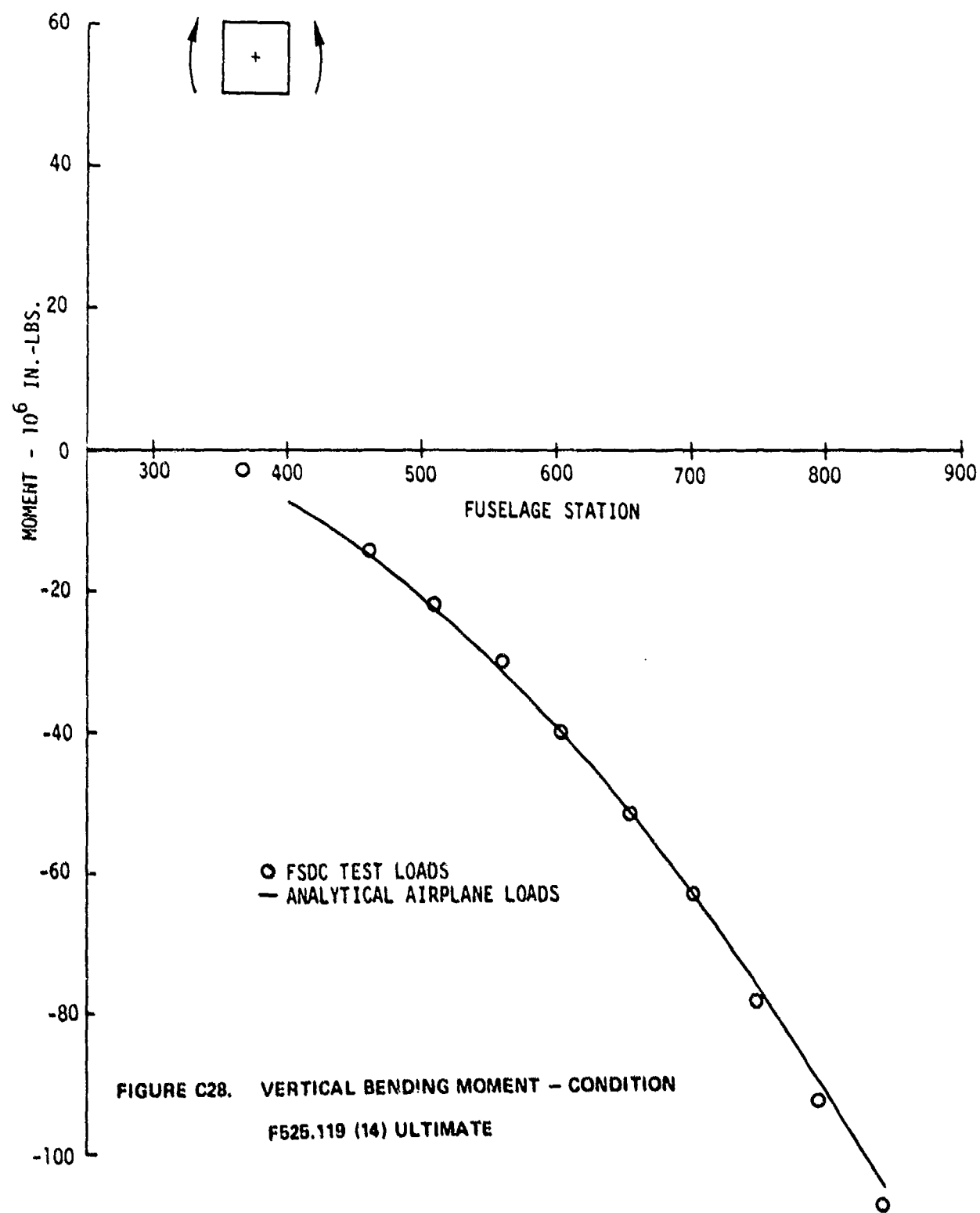


FIGURE C28. VERTICAL BENDING MOMENT - CONDITION  
F525.119 (14) ULTIMATE

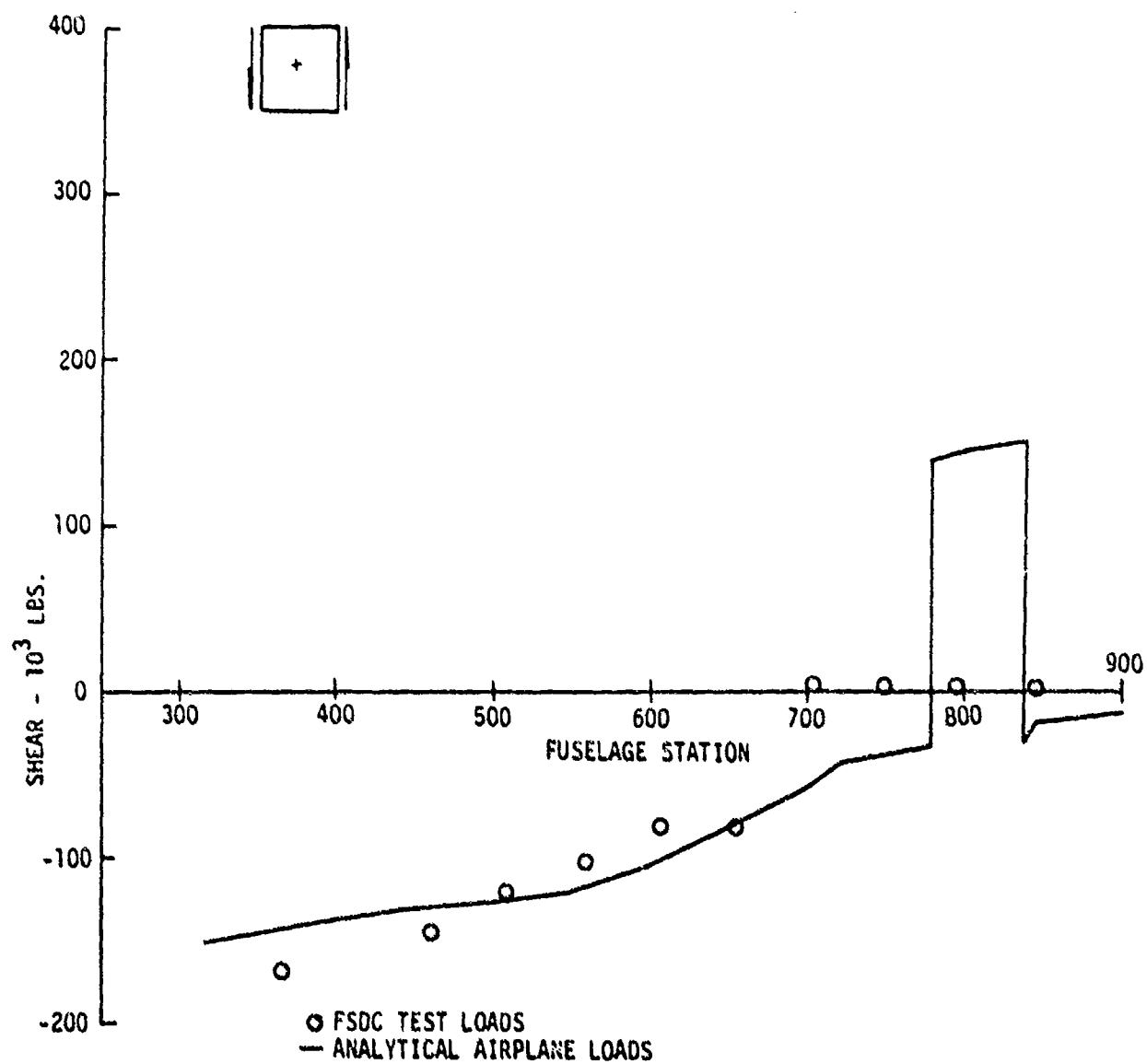


FIGURE C29. VERTICAL SHEAR CONDITION 2262 GD (15) ULTIMATE

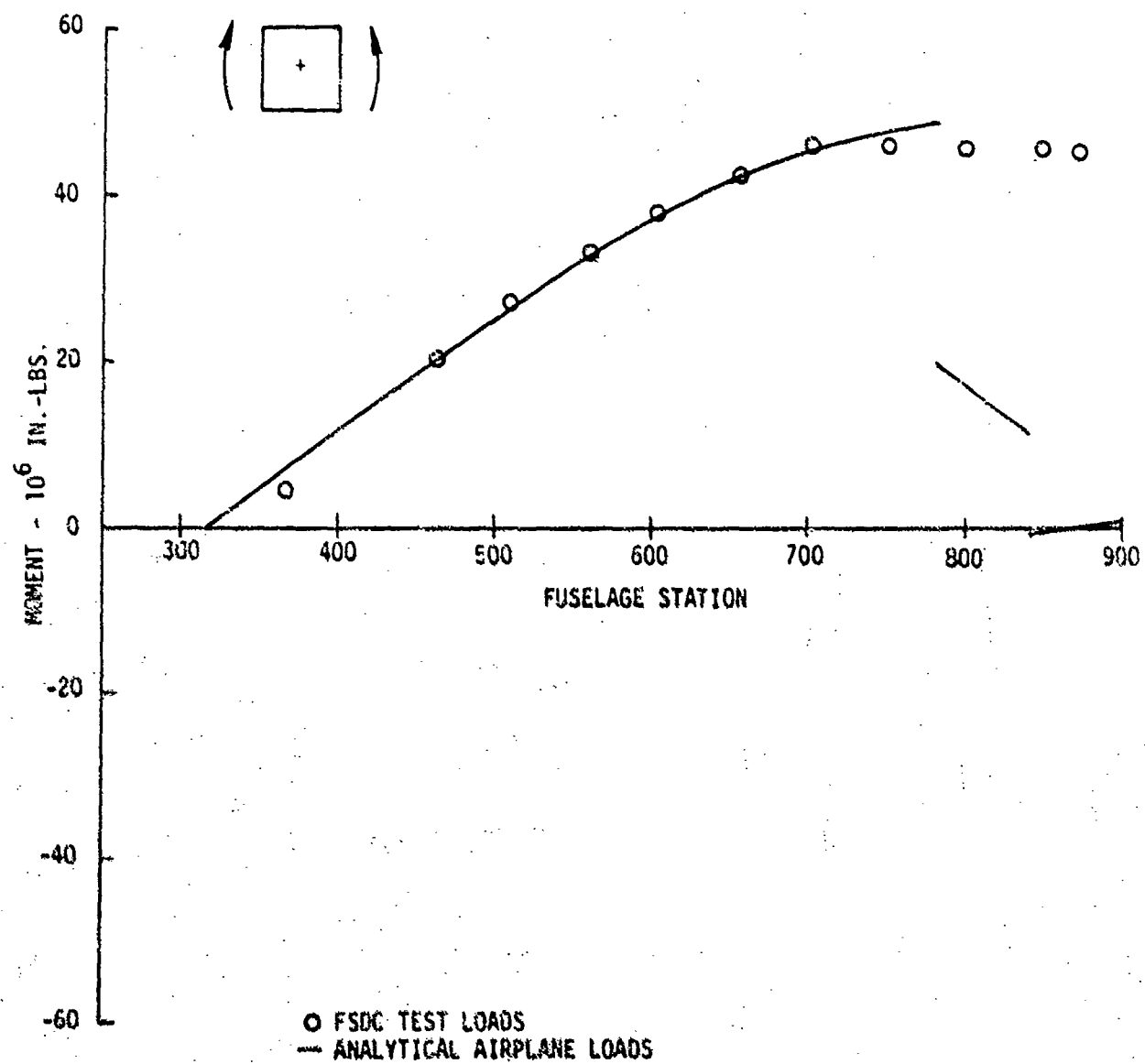


FIGURE C30. VERTICAL BENDING MOMENT - CONDITION 2262 GD (15) ULTIMATE

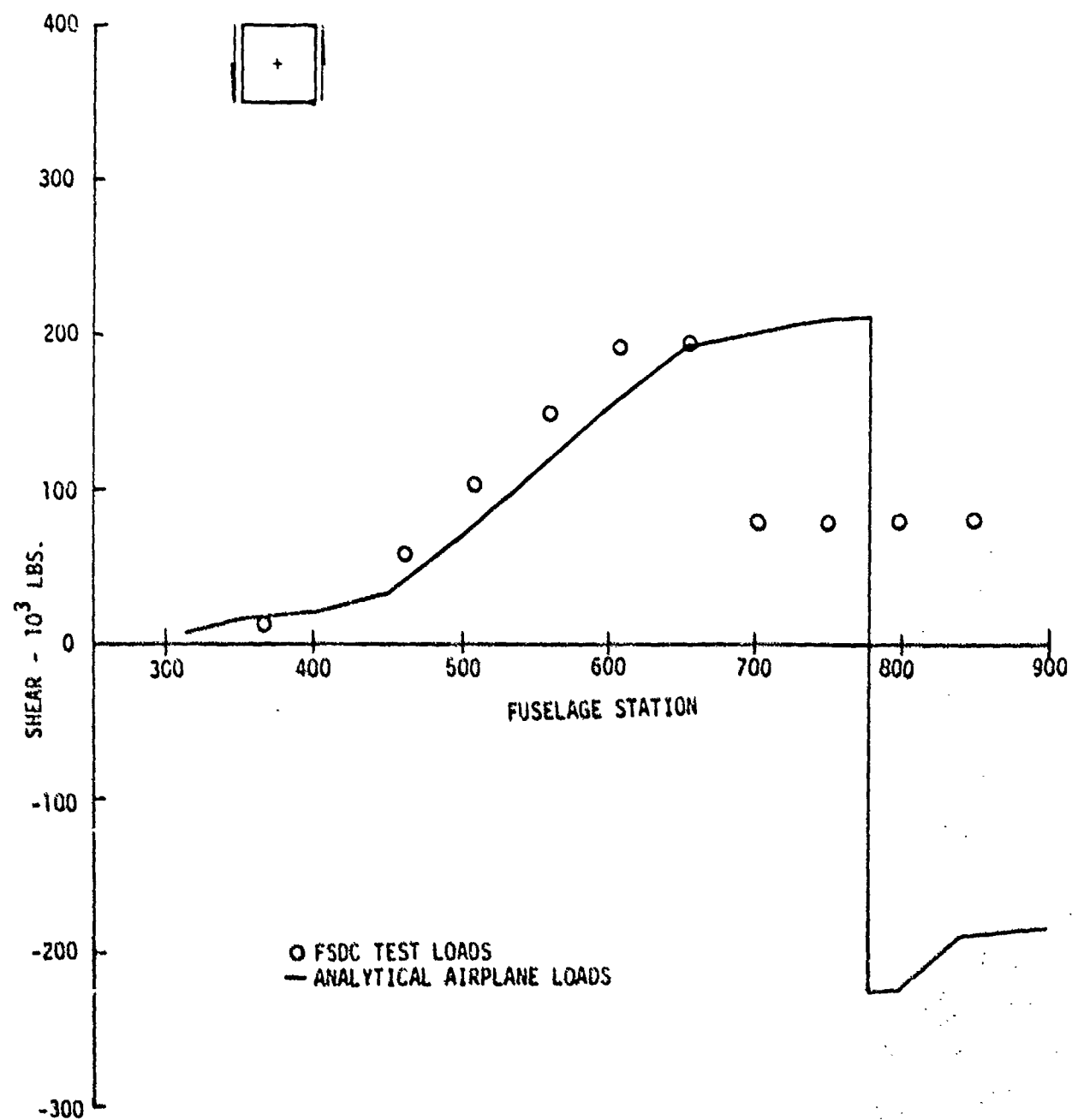


FIGURE C31. VERTICAL SHEAR - CONDITION 2513 VH (16 AND 17) ULTIMATE

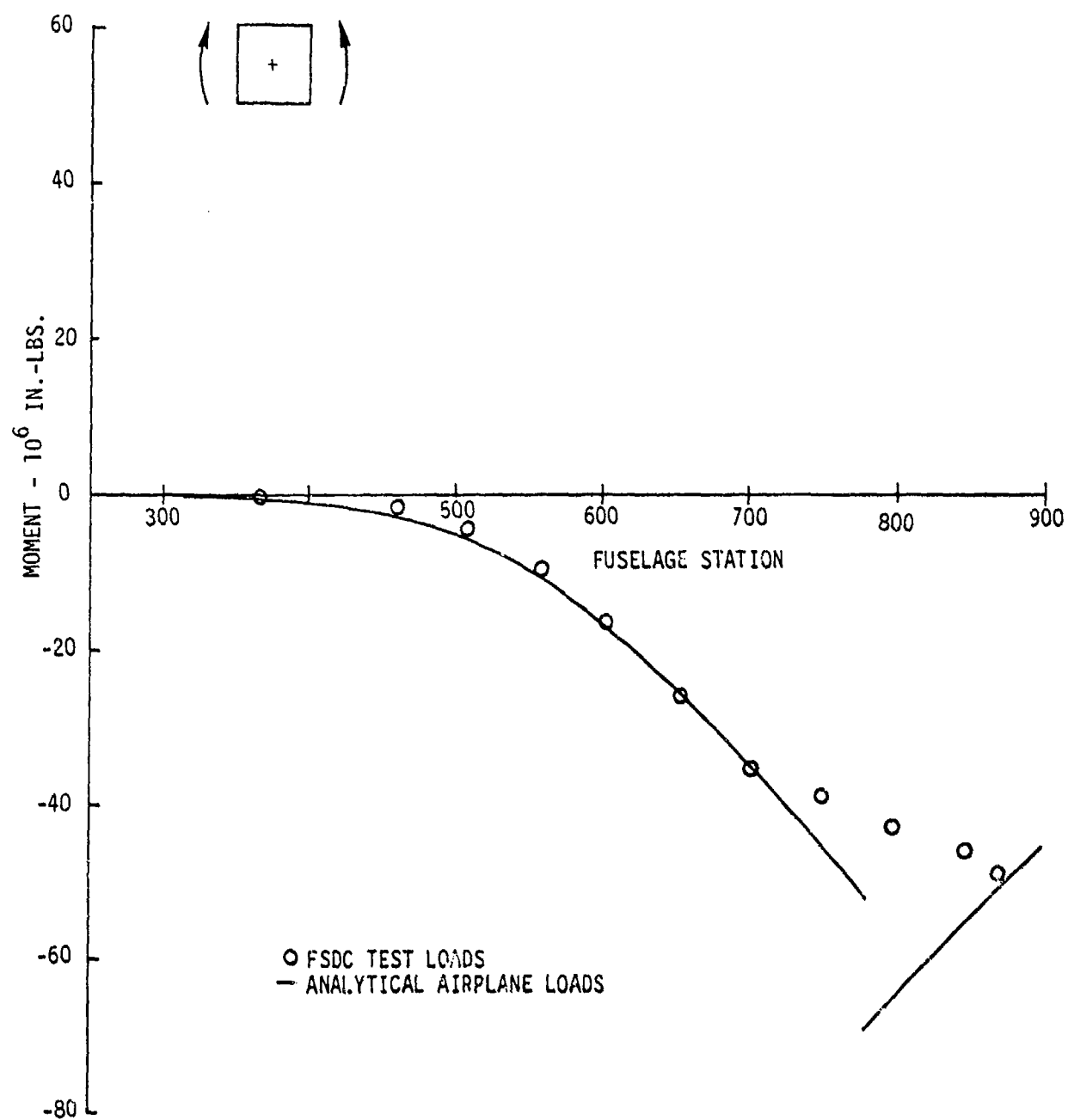


FIGURE C32. VERTICAL BENDING MOMENT - CONDITION 2513 VH (16 AND 17) ULTIMATE

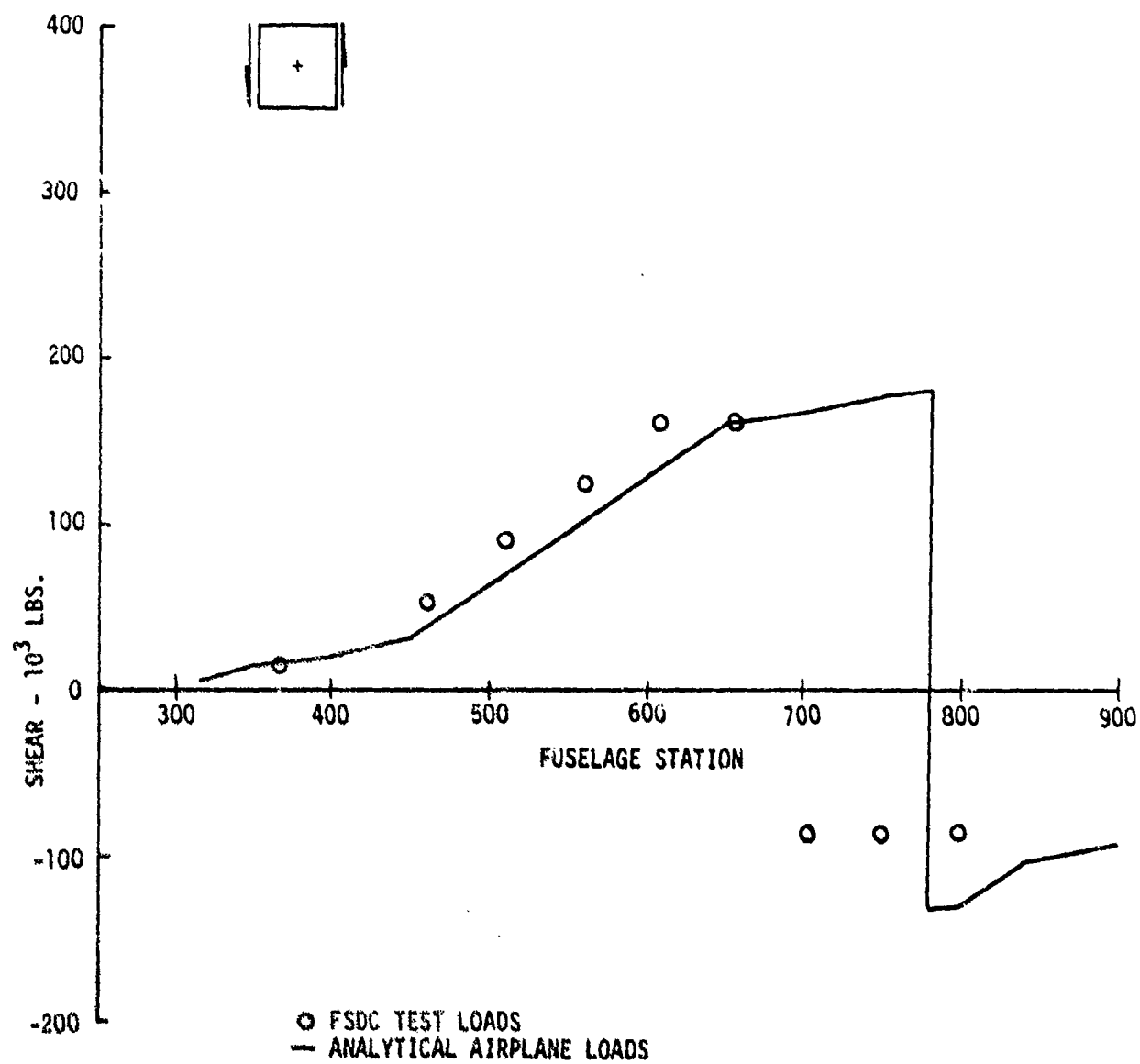


FIGURE C33. VERTICAL SHEAR - CONDITION 2059 BM (18 AND 19) ULTIMATE

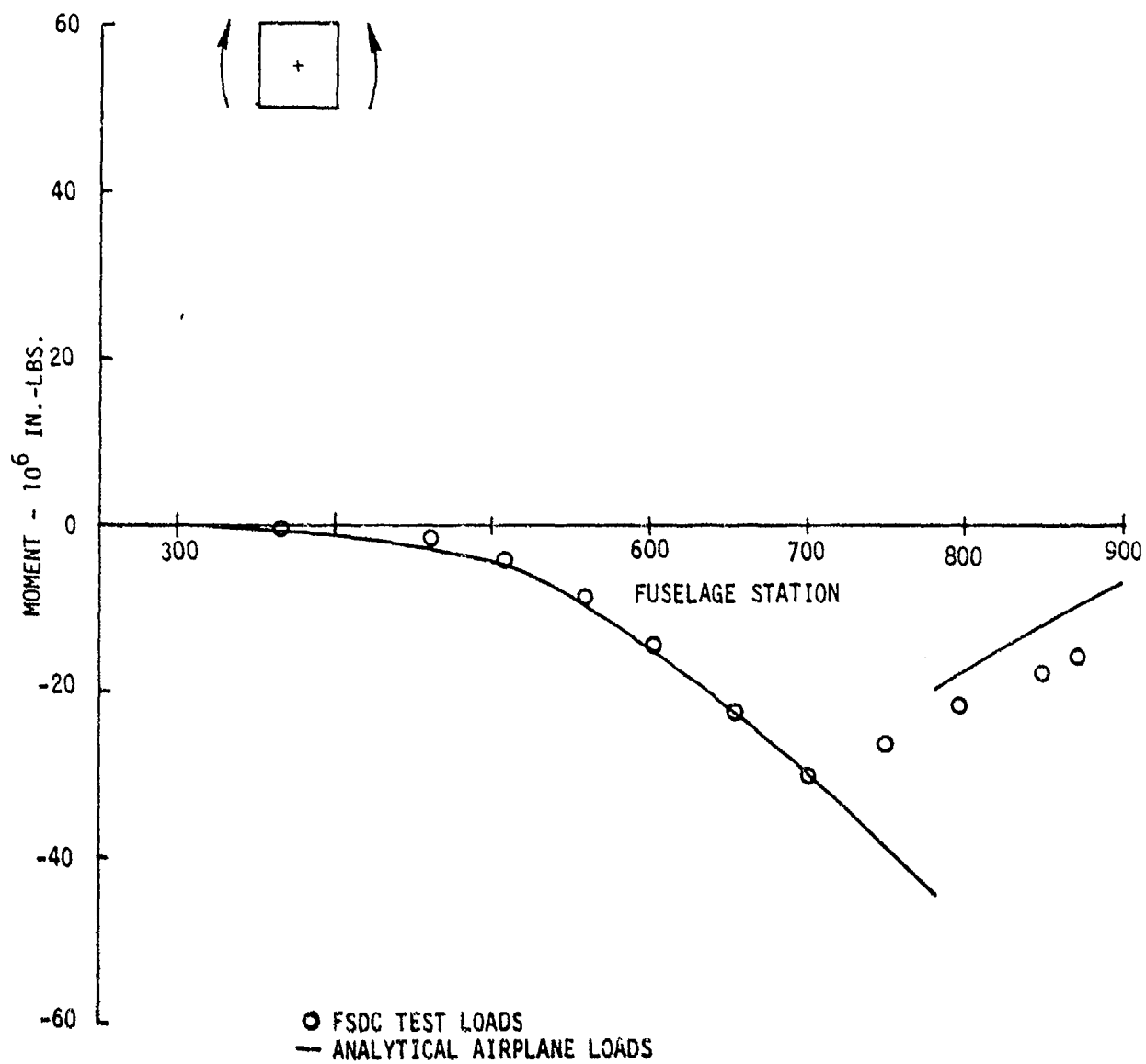


FIGURE C34. VERTICAL BENDING MOMENT - CONDITION 2059 BM (18 AND 19) ULTIMATE

## REFERENCES

1. "Primary Adhesively Bonded Structure Technology (PABST) Phase Ib: Preliminary Design," (Douglas Aircraft Company), Air Force Flight Dynamics Laboratory Technical Report No. AFFDL-TR-76-141, December 1976.
2. Wilhem, D.P., "Fracture Mechanics Guidelines for Aircraft Applications." Air Force Flight Dynamics Laboratory Technical Report AFFDL-TR-69-III. February 1970.
3. Liu, A.F., "Stress Intensity Factor for a Corner Flaw." Engineering Fracture Mechanics. Pergamon Press. 1972. Vol. 4, P. 176.
4. Engle, Robert M., Jr., "CRACKS, A FORTRAN IV Digital Computer Program for Crack Propagation Analysis." Air Force Flight Dynamics Laboratory Technical Report AFFDL-TR-70-107, October 1970. Page 7.
5. Swift, T., "The Effects of Fastener Flexibility and Stiffener Geometry on the Stress Intensity in Stiffened Cracked Sheet." Prospects of Fracture Mechanics, Noordhoff International Publishing Co., Leyden, Netherlands, 1975.
6. Kuhn, P., "Notch Effects on Fatigue and Static Strength." Current Aeronautical Fatigue Problems; Proceedings of a Symposium, Rome, Italy, April 23-25, 1963. Edited by J. Schijve, J. R. Heath-Smith, and E. R. Welbourne. Oxford. Pergamon Press, Ltd., 1965, pages 229-264.
7. Erdogan, F., Tuncel, O. and Paris, P., "An Experimental Investigation of the Crack Tip Stress Intensity Factors in Plates Under Cylindrical Bending." Transactions of the ASME. Journal of Basic Engineering. December 1962. Vol. 84, No. 4. Pages 542-546.
8. Anon., "Damage Tolerant Design Handbook." Battelle Columbus Laboratories Metals and Ceramics Information Center Report MCIC - HB-01. Parts 1 and 2. December 1972.

#### REFERENCES (cont)

9. C. M. Hudson, "Effect of Stress Ratios on Fatigue-Crack Growth in 7075-T6 and 2024-T3 Aluminum-Alloy Specimens," NASA Report TN D-5390 1969.
10. Anon., "Metallic Materials and Elements for Aerospace Vehicle Structures." Military Standardization Handbook MIL-HDBK-5B, Change Notice 2, 31 August 1973, page 3-217.
11. Mehr, P. L., "ALCOA 7475 Sheet and Plate," ALCOA Application Engineering Division, New Kensington, Pa., 2nd Ed., Oct. 1973, page 19.
12. Hart-Smith, L.J., "Adhesive Bond Stresses and Strains at Discontinuities and Cracks in Bonded Structures," Trans. ASME Journal Eng. Matl & Tech., Vol. 100, No. 1, pp 16-24, January 1978.